Modelling of lymphocyte migration in the peripheral lymphoid tissue

A thesis submitted for the degree of

Doctor of Philosophy

of the Australian National University

by

Wichat Srikusalanukul

Developmental Physiology Group
Division of Molecular Medicine
John Curtin School of Medical Research
The Australian National University
Canberra, Australia

May 1999

For my mum

Statement of originality

The work described in this thesis is original and was carried out by myself under the supervision of Dr P J McCullagh in the Division of Molecular Medicine at the John Curtin School of Medical Research, Australian National University. With the exception of the analysis of model parameters in Chapter 6, which were performed on the basis of a collaborative work with Dr Maria Durisova of the Institute of Experimental Pharmacology, Slovak Academy of Sciences, all of the contents of this thesis are the original work of the author and have neither been presented nor are currently being presented for any other degree.

WICHAT SRIKUSALANUKUL

Acknowledgments

Many people have been involved and contributed to the success of this study. First of all, I would like to express my great gratitude to ANU and JCSMR for providing me an ANU PhD scholarship which allowed me to pursue my enthusiasm about the model applications in bio-medicine, and to my supervisor, Dr Peter McCullagh, for his kind patience and invaluable support throughout the four years since starting my course.

Also I would like to thank Prof Stjepan Marcelja (Department of Applied Mathematics, Research School Physical Sciences and Engineering, ANU) for his help at the initial stage of my course, Dr Max Simpson-Morgan for his help in setting up an automated collection system for lymph, Dr Ross Odell (Graduate School of Biomedical Engineering, University of New South Wales) and Dr Goeff Aldis (School of Mathematics and Statistics, University College, Australian Defence Force Academy) for their advice about compartmental models, and especially Dr Franky De Bruyne (Department of Systems Engineering, Research School Information Sciences and Engineering, ANU) for his advisory role in Chapter 5 (Prediction models), Dr Maria Durisova (Institute of Experimental Pharmacology, Slovak Academy of Sciences) and Dr Ladislav Dedik (Slovak University of Technology) for their supervision of Chapter 6 (Structured models).

I want to thank all of my laboratory colleagues, Mr Bernie Barancewicz, Mrs Karen King, Ms Sandra Veness and all of the staff in Wing F, who were full of help in all matters involved with my experiments, Ms Ruth Hagan and Ms Michelle Stevens for their help in reading manuscripts, and Mr Geoffrey Osborne and Ms Sabin Gruninger (Flow Cytometry Unit, JCSMR) for their help with the flow cytometry study, Dr Elizabeth Washington and Dr Wayne Kimpton (Department of Veterinary Preclinical Sciences, University of Melbourne) for their help in monoclonal staining and wonderful hospitality during my visit in 1996.

I owe special thanks and love to my family in Thailand and S.Korea and especially to my wife, Ms Sunkyung Shynn, and my children, for their durable support. Special thanks also goes to my sister, Ms Wiwan Srikusalanukul, who came from Thailand to help us deal with some intense situations during the last few weeks of the preparation of this thesis.

Most of all, to my mum, who was waiting for my return.

Abstract

Lymphocyte recirculation and migration is one of the most essential components of the immune system as it allows lymphocytes to recognise, to interact with and to respond to antigen in any site of the body. Lymphocyte migration through peripheral lymphoid tissue, plays a greater part in antigen recognition by the immune system than traffic through the major lymphatic vessels, but its regulation is still poorly understood.

To understand the kinetics of lymphocyte migration within lymphoid tissue and to construct suitable models to explain it, a sheep model was chosen for the present study. The efferent lymphatic ducts draining a peripheral lymph node, either the popliteal or the prescapular lymph node, were cannulated. Lymphocytes were collected and labelled with a selected fluorescent dye, then injected back into the blood circulation and monitored in both blood and lymph by means of flow cytometry.

Theoretical models have been increasingly recognised by biomedical researchers as having applications to biomedical problems. Three different approaches, namely compartmental models, prediction error models and structured models, have been explored to describe the dynamics of lymphocyte migration within lymphoid tissues under normal conditions. The information obtained from each individual model has shown some degree of variation from the others. This will assist in providing more comprehensive descriptions of the entire complicated events of lymphocyte migration. Even though several modelling approaches often used in medical and physiological modelling will be introduced a completely true model has yet to be attained.

At the end of this thesis, the conclusion will be drawn that these models represent only the first step in understanding and explaining lymphocyte migration in a lymph node (system). The contents of this thesis represent only a starting point in trying to quantify and model lymphocyte migration under normal physiological conditions. However, the information given in this thesis should help to contribute to the future development of lymphocyte migration in both biomedical and modelling studies.

Table of contents

Chapter 1/ Introduction

As this thesis deals with the application of mathematical principles of analysis to a biological problem, its introduction falls into two parts. The first of these gives an account of the history and background to lymphocyte recirculation and of the significance of this phenomenon for the immune response. Essential features of the anatomy and physiology of lymphocyte migration that are relevant to attempts at its mathematical modelling will be outlined. General reviews of previous attempts to apply theoretical models to describe lymphocyte recirculation and migration will also be included. The second part of the introduction considers the fundamental principles and methodology of modelling that are relevant to the contents of this thesis. It is unavoidable that both biological and mathematical aspects of the subject have necessarily to be considered in detail. However it is also necessary that data and calculations be presented in a manner that is accessible to readers from both of these backgrounds. To facilitate this, terminology relating to both biology and modelling contexts will be clarified when first used.

Part I: Biological backgrounds

1.1 The contribution of lymphocytes to the functioning of the immune system

In everyday life, the body is continually exposed to many ***pathogens*** (ie ***micro-organisms*** that are capable of producing diseases), such as viruses, bacteria and parasites. The consequences for the body of diseases caused by micro-organisms can vary from very mild to irreversible damage to parts of, or to the whole body. Fortunately, the damage to the body produced by infectious diseases is commonly mitigated by the response of the immune system. The ***immune system*** is able to distinguish non-self entities, such as ***pathogenic micro-organisms***[1], and to mount responses against them. A variety of mechanisms underpin immune responses, but in general, they are mediated by a

[1] ***Pathogenic micro-organisms*** can potentially cause diseases or harmfulness to the body.

class of cells known as ***leucocytes*** (eg ***white blood cells***, ***WBC***). The most important type of leucocyte for mounting immune responses is the ***lymphocyte***. These cells play a crucial role in immune responses because they continually move through the body and have the capacity to monitor for signs of the entry of any micro-organisms expressing foreign ***antigens***[2].

1.2 Physiology and anatomy of lymph nodes

1.2.1 Lymphoid tissues and lymphatic systems

From an anatomical perspective, the immune system can be considered to comprise two main components. One of these is a circulating (or recirculating) component of mobile cells (eg lymphocytes). ***Recirculating lymphocytes*** will be fully described in the next section of this chapter. The other component of the immune system is fixed ***lymphoid tissue*** through which migrating cells transit. Lymphoid tissues have been subdivided into ***primary and secondary types***. The distinguishing feature is that ***cellular proliferation and differentiation*** occurs in primary tissues independently of any exposure to antigen, whilst it is necessary for both processes to be driven by antigen in secondary tissues. Primary lymphoid tissues include the ***thymus*** and ***bone marrow***. In these tissues, lymphocytes differentiate from ***stem cells***, and mature before emigration. The thymus is the primary lymphoid tissue for ***T lymphocytes*** in all species that have been studied. ***B lymphocytes*** originate from the bone marrow of mice and, in the chick, from a structure unique to avian species, the ***bursa of Fabricius***. The origin of B lymphocytes in mammalian species other than the mouse has yet to be formally defined, although evidence is accumulating to suggest that, in the sheep, the gut associated lymphoid tissue functions as an avian bursa equivalent. After ***emigrating*** from primary lymphoid tissues, lymphocytes enter the blood and lymph circulation system to reach secondary lymphoid tissues, such as the ***spleen*** and ***lymph nodes***.

The ***lymphatic system*** is a network comprising lymphatic vessels, lymphoid tissues and special organs (such as the spleen and lymph nodes). This lymphatic network extends throughout almost all organs and tissues of the body in a distribution similar to that of the blood circulation network. The term ***central lymphatic system*** will be used to refer to the central parts of the lymphatic

[2] A substance, usually a protein, that causes the immune reaction and production of ***antibody*** which is a variety of protein essential to the immune response and produced by some special tissues in the body to react with a specific foreign molecule or antigen.

system, especially to the great lymphatic vessels such as the ***thoracic duct***[3] in mammals. The term ***peripheral lymphatic system*** will be used to describe the regional parts of the lymphatic system that includes many minor lymphatic vessels. These vessels are responsible for returning lymph from all parts of the body to the central system.

There are many routes (eg skin, gut and respiratory system) by which potentially pathogenic micro-organisms may enter the body but, irrespective of the route, they will soon encounter lymphocytes in the draining regional lymph nodes. The special structure of (secondary) lymphoid tissues provides an optimal environment in which continually circulating lymphocytes can interact with each other, with other types of cell such as ***antigen-presenting cells*** and with antigens (of micro-organisms) carried via lymphatic vessels. For this reason, lymphocyte recirculation and migration within the peripheral lymphatic system may be expected to provide a more comprehensive description of the participation of lymphatics and lymphoid tissues in the immune response than can be obtained from studies performed in the central lymphatic system. Figure 1.1 demonstrates the route of foreign antigen delivery to the lymph node via afferent lymph vessels. Most immune reactions occur in the lymphoid tissues.

Figure 1.1: The pathway of lymphocyte recirculation

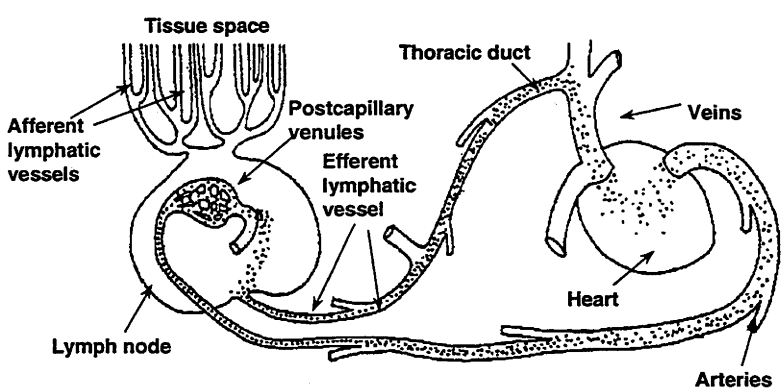

Lymphocytes escape from the arterial blood circulation to the lymphatic system (in the lymphoid tissue) and then return to venous blood system.

Foreign antigens are drained to a lymph node via afferent lymphatic vessels and react with several types of cells within lymphoid tissues.

[3] The common lymphatic vessel that receives lymph from almost all of the lymphatic vessels in the body and returns it to the blood circulation via a major venous vessel the ***superior vena cava.***

1.2.2 Anatomy and organisation of lymphoid tissue in lymph nodes

Lymph nodes are the most plentiful type of secondary lymphoid tissue. They are encapsulated round kidney or bean-shaped organs composed of lymphoid tissue. They very often appear in groups or chains rather than singly. In a typical lymph node, the concave side represents the ***hilum***, where arterial vessels and nerves enter and veins leave the organ. Lymph enters the lymph node through ***afferent lymphatic vessels***, which pass through the convex margin of the organ. The ***efferent lymphatic vessels*** transport lymph away from the node (Figure 1.2).

A highly packed collagen fibre capsule encloses the entire outer surface of the lymph node and is generally thickened at the hilum. A number of collagen fibres, called ***trabeculae***, originate from the inner surface of the capsule and extend to the interior of the lymph node. The trabeculae divide the lymphoid tissue into several segments with each segment consisting of the outer and inner portions termed the ***cortex*** and ***medulla*** respectively.

Figure 1.2: Cross section of lymph node

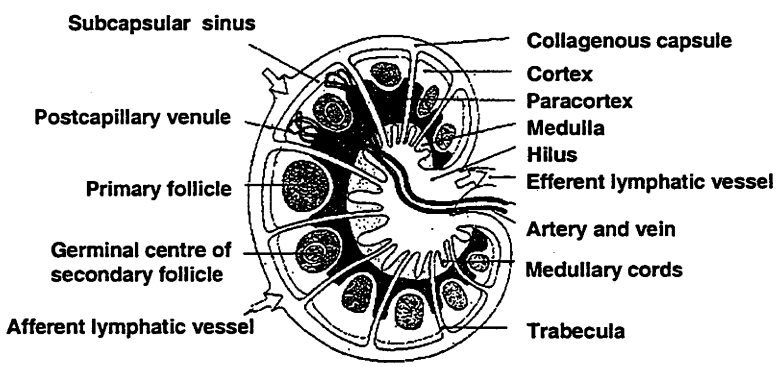

Diagram depicting the schematic structure of a lymph node. Full details are given in section 1.2.2.

The cortex contains a number of ***follicles*** of aggregated lymphocytes. Furthermore, there are lymphocyte aggregations that extend to the medullary region and form solid cords termed ***medullary cords***. Within the follicles during certain stages of the immune response, vigorous ***mitosis***[4] results in the

[4] A type of cell division results in the formation of two genetically identical cells.

production of lymphocytes. In some of the inner areas of the cortex, the ***paracortex***, numerous ***postcapillary venules (PCV)***[5] can be identified. In some species, the ***endothelium*** of these venules is characterised by a peculiar thick or cuboidal appearance[6]. These special endothelial venules play a most important role in lymphocyte migration by allowing lymphocytes to adhere and start their migration processes from the blood (see more in section 1.3 in this chapter).

Histologically, there are two main components of lymph node tissue. One of these is the scaffolding, formed by a mesh of ***reticular fibres***. This mesh, which is synthesised by ***reticular cells***, supports the whole structure of the lymph node. The second or cellular component in lymph node tissue consists principally of lymphocytes with a small number of ***macrophages***[7]. The cell component is considered to be a mobile component through which unbound cells can migrate along the ***interstitial matrices***[8] within spaces between this reticular mesh. Interaction with foreign antigens, which is one of the first components of the defence mechanisms of the immune response, starts as lymphocytes traverse this mesh. Lymphoid tissues also contain a network of blood vessels and sinuses which provide abundant pathways for lymphocytes to recirculate from the blood stream to the lymphatic system.

1.3 Lymphocyte recirculation and its functions

1.3.1 Life history of lymphocytes and the discovery of lymphocyte recirculation

Studies on the life history of lymphocytes were undertaken as early as the 1920's. At that time, it was believed that the lymphocytes in blood were short-lived cells. Several controversial hypotheses were advanced to explain the short life span that lymphocytes in the blood circulation were considered to have. First, it was postulated that lymphocytes were excreted (by gut) from the blood circulation (Bunting and Huston, 1921) or destroyed in some tissues or organs such as lymph nodes (Ehrich, 1946) or even skin (Andrew and Andrew, 1949). Second, it was suggested that lymphocytes could transform into other cell types in the blood circulation (Bloom, 1937; Rebuck and Crowley, 1955). Third, the

[5] In living tissues, blood is transported along the arterial blood system and passed through the venous blood system via a network of very tiny vessels, the ***capillary vessels***. The ***postcapillary venules*** are tiny venous vessels that gather blood from the capillary network.
[6] Normal ***endothelial cells*** (cells that line blood vessels) have a flat and thin configuration.
[7] Another type of leucocyte which has the capacity to phacocytose (ie engulf and break down) foreign materials and debris.
[8] The matrix is the intercellular fluid-like substance that acts as a medium through which mobile cells can migrate.

possibility was raised that lymphocytes may recirculate from the blood circulation to other tissues and later reappear again in the blood.

The first hypothesis failed to identify consistently the postulated sites of lymphocyte destruction or excretion as there was inadequate experimental evidence from those studies (Ehrich, 1946; Andrew and Andrew, 1949) to support it. A number of studies (Ebert *et al.*, 1940; Medawar, 1940) were adopted in attempts to prove the occurrence of lymphocyte transformation to other cell types These studies produced some morphological evidence for lymphocyte transformation, but failed to obtain any functional evidence. In addition, these studies were generally based on observation of single living lymphocytes and their relevance for a mixed lymphocyte population such as that which occurs in lymph nodes was questionable.

It had been proposed for a long time by some researchers that lymphocytes continually recirculate between blood and the lymphatic system. A study in rabbits demonstrated that animals, which were allowed to bleed, had a low level of lymphocytes in their blood (Sjövall, 1936). The continuous drainage of lymph (from the main lymphatic duct entering the blood circulation) in rats resulted in a fall in the number of lymphocytes passing through the duct after 24 hours of drainage (Mann and Higgins, 1950). However, it was subsequently demonstrated that this fall could be prevented by re-infusion of the drained lymph into the blood circulation (Gowans, 1957). Confirmation of the concept of lymphocyte recirculation was provided by the observations of Gowans (Gowans, 1959). He demonstrated that, in rats, lymphocytes labelled with radioisotope recirculated from blood to lymph after an intravenous infusion of those cells. This experiment, in demonstrating ***lymphocyte recirculation***, opened a new era of lymphocyte and immunological studies. Lymphocyte recirculation entails the continuous recirculation of mature lymphocytes from the blood stream to the lymphoid tissues, and some specific organs, and their eventual return back to the blood stream via the main lymphatic duct, ie thoracic duct (Figure 1.1).

1.3.2 The discovery of sites and routes of lymphocyte migration

Whilst the ability of lymphocyte to recirculate between blood and lymph was discovered in 1959 by Gowans, the site at which this occurred was not identified at that time. Circulating lymphocytes travel via the blood circulation network and reach secondary lymphoid tissues. It was recognised that lymph nodes contain postcapillary venules (PCV) lined by peculiar-shaped endothelial cells. These distinctive venules are highly localised in the paracortical regions of the lymph

node. In some mammalian species, such as rodents, these special venules are called ***high endothelial venules (HEV)*** as they are characterised by the presence of high cuboidal endothelial cells. The unusual morphology of these endothelial cells led to the early suggestion that the HEV were the major sites at which lymphocyte migration was taking place.

The fate of lymphocytes in lymphoid tissues remained speculative until the demonstration of the exact route of lymphocyte recirculation by Gowans and Knight (Gowans and Knight, 1964). This study revealed that, after intravenous infusion of radioisotopically labelled lymphocytes, numbers of labelled small lymphocytes were localised around the walls of postcapillary venules whilst others had penetrated across the endothelial walls into surrounding lymphoid tissues. Moreover, this study also indicated the direction of migration of lymphocytes. The cells were travelling out from postcapillary venules rather than entering them. It was concluded that, under normal physiological conditions, a large-scale migration of lymphocytes from the blood circulation into lymphoid tissue occurred across the wall of these specialised postcapillary venules (Gowans and Knight, 1964). This finding focussed attention on interaction between lymphocytes and endothelium.

Even though the site of lymphocyte recirculation (ie at the postcapillary venules) was discovered, the exact route of lymphocyte migration through the endothelial wall remained in doubt. The original electron microscope study (of the postcapillary venule wall in rats) suggested that small lymphocytes cross the endothelial wall by entering directly into the endothelial cells and passing through their cytoplasm (Marchesi and Gowans, 1964). Subsequently, a very careful statistical study of electron microscopic data on lymphocyte migration in the early 1970's (Schoefl, 1972)revealed that lymphocytes migrate via the inter-endothelial space, not through endothelial cells as suggested by Marchesi and Gowans. In addition, it was observed that endothelial cells were soft and extremely pliable, ie non-rigid, which may be a special feature facilitating the function of these cells. This may be necessary to provide a suitable environment for lymphocytes to emigrate through the inter-endothelial spaces (Schoefl, 1972).

A later technique (Stamper and Woodruff, 1976) to study lymphocyte-endothelial interaction utilised an *in vitro* model that allowed visualisation of interactions between lymphocytes and specialised venules. In this technique, the lymph node was sectioned at a thickness of 8 μm and layered with a suspension of lymphocytes under a controlled environment. This facilitated adhesion of

lymphocytes to endothelial cells. This technique has continued to be valuable in studying lymphocyte-endothelial cell interaction.

1.3.3 Role of lymphocyte-endothelial cell interaction

Recognition of the role of HEV suggested that lymphocyte migration in lymphoid tissues is a selective process which could involve multiple and complex sequences of ***receptor-ligand***[9] interactions (Springer, 1990; Abernethy and Hay, 1992; Imhof and Dunon, 1995). A large number of families of adhesion molecules are considered likely to play a vital role in mediating the processes underlying those interactions. A three-stage model of ***neutrophil***[10] migration from the blood circulation through surrounding tissues has been proposed as part of the process of inflammation (Springer, 1994; Mackay, 1995). Lymphocyte migration through peripheral HEV is likely to require stages that are analogous to those involved in the neutrophil model. The proposed stages are:

1. **Tethering and rolling stage**: Lymphocytes are delivered from the main arterial vessel and finally reach the postcapillary venules. Because of the hemodynamic characteristics of blood vessels, lymphocytes tend to collide[11] with the inner wall of blood vessels where there is a high shear stress (Lawrence and Springer, 1991; Zhao *et al.*, 1995). Without any additional mechanism, it is unlikely that lymphocytes could attach to the wall of those vessels. However special mechanisms enable lymphocytes to slow down and so have more chance to proceed to the following stage. During this stage, a family of adhesion molecules, namely ***selectins***, has been proved to have an important role for mediating the initial tethering and, subsequently, the rolling stage (Lawrence and Springer, 1991). The rolling of lymphocytes along the surface of endothelial cells is explained by an unstable molecular bond established between the tips of the ***microvilli***[12] of lymphocytes (where selectins occur) and the surface of endothelial cells (where the selectin ligands are expressed) lining the inner wall of postcapillary venules. The selectin family comprises P-selectin, E-selectin and L-selectin. These can be expressed in several different tissues. However, only L-selectin plays an important role in lymphocyte recirculation to peripheral lymph nodes under

[9] A reaction between two specific molecules that generally causes a linkage bond between those molecules.
[10] ***Neutrophil*** is the most common type of leucocyte and plays an essential role in the response to an invasion of pathogens and in inflammatory processes.
[11] In the initial stage, lymphocytes are delivered along blood circulatory trees by intra-vascular pressure. Random and repeated collisions occur between lymphocytes and the vessel wall before the lymphocyte-endothelial cell interaction occurs.
[12] Many tiny projections of lymphocyte surfaces.

conditions (Bradley *et al.*, 1994; Lepault *et al.*, 1994; Bradley *et al.*, 1998), while P and E-selectin have a more important role in inflamed environments. L-selectin is expressed by almost all lymphocytes (ie except memory lymphocytes) while its ligands are expressed on the surface of endothelial cells at the postcapillary venules. The term "***homing receptor***" has often been used for L-selectin following the original description by Gallatin of its role in the initial attachment of lymphocytes to the HEV in lymph nodes (Gallatin *et al.*, 1983).

2. **Activation stage:** After the first stage, tethering and rolling successfully brings lymphocytes into proximity with the endothelial surface. At this stage, the ***G-protein-coupled receptors*** expressed on the surface of lymphocytes interact with ***chemokines***[13] that are released from the endothelial cells lining the vessel wall. The reactions between G-protein-coupled receptors and chemokines bring lymphocytes in the direction of the site of chemokine production.

3. **Adhesion and strengthening:** Following the activation stage, another family of adhesion molecules on the surface of lymphocytes, namely the ***integrins***, is activated. Subsequently, the activated integrins establish a stronger bond with integrin ligands (namely, ***Immunoglobulin Superfamily Members on Endothelium, IgSF***) expressed on the surface of endothelial cells. The movement of migrating lymphocytes out of the postcapillary venules (ie ***diapedesis***) via inter-endothelial spaces occurs after this stage.

There are some minor differences in other models of lymphocyte adhesion and emigration (Butcher, 1991; Shimizu *et al.*, 1992; Tanaka *et al.*, 1993) in the way events occurring in each stage are classified. However, the basis of lymphocyte-endothelial reactions and the families of adhesion molecules principally involved in these reactions, such as selectins and integrins, still remain very similar to the three-stage model.

Even though recirculating lymphocytes have been randomly travelling along blood circulatory networks, there is still continual rearrangement of recirculating lymphocytes in tissues around the body. This rearrangement may be due to the different patterns of lymphocyte migration in different tissues and to the varieties of lymphocyte subtypes entering and leaving those tissues. The non-random migration of lymphocytes has been observed in many studies, providing clear

[13] Small polypeptides (ie protein), synthesised by some specific cells, which attract leucocytes in a certain direction.

evidence of the existence of tissue-specific migratory preferences in lymphocyte recirculation (Mackay *et al.*, 1988; Kimpton *et al.*, 1990; Mackay *et al.*, 1992; Washington *et al.*, 1994). The term "homing" has been often used to describe this preferential migratory property. The highly preferential recruitment of lymphocytes from blood to various specific tissues reflects a mechanism that can recognise the relationship between specific lymphocyte subsets and those specific tissues. This mechanism must operate at the site of lymphocyte migration (ie between lymphocyte surfaces and endothelial walls) which is specific for certain lymphocyte subtypes and the tissues. Moreover, this mechanism can also discriminate the differences between lymphoid and non-lymphoid tissues. Thus, rearrangement of lymphocyte subsets within recirculating lymphocyte populations could take place. The information available about lymphocyte-endothelial interaction provides comprehensive explanations of why some lymphocyte subtypes prefer to recirculate back to their tissues of origin.

1.3.4 The tempo of migration of lymphocytes in lymphoid tissues

At present, the fate of a lymphocyte, after having successfully attached to an endothelial cell, migrated through the inter-endothelial space and penetrated the underlying basement membrane to the parenchyma of the lymph node, remains substantially unknown. Interaction of lymphocytes with various cells lying in lymphoid tissues and the mechanisms regulating lymphocyte transit through different micro-architectural components of the node, such as T and B cell segregation areas, have not been well established. The interaction of adhesion molecules on the lymphocyte surface with endothelial cells could not, on its own, explain these kinetics. Nor has the arrangement of the reticular mesh in lymphoid tissue provided an explanation of how the predominant areas of lymphocyte segregation are established. There must be other physical and immunological attributes of migrating lymphocytes that contribute to variations in the kinetics of their migration. Further molecular studies of the mechanisms of interaction of cellular and extracellular components in lymphoid tissues may provide information about the duration of residence of migrating lymphocytes within the node, the movement of lymphocytes within the node and the role of these in lymphocyte function and the factors which determine when they leave the node.

1.3.5 The immunological significance of lymphocyte recirculation

During the period in which the existence of lymphocyte recirculation was being experimentally demonstrated, independent investigation of the immunological

capacity of lymphocytes led to the hypothesis, and its experimental demonstration, that one lymphocyte (and its descendants) produced only a single antibody (Burnet, 1959). It was obvious that this proposition would require the existence of a very large number of lymphocytes if an animal were to be able to react against all possible antigens. Furthermore, as indicated above, the immune response must be initiated promptly in response to any microbial invasion if it is to limit and minimise the damage of that invasion. If a full range of lymphocyte reactivities was to be continuously available in lymphoid tissue draining every region of the body, it is likely that each regional lymph node would necessarily be very large. However, a biologically economical alternative, which became feasible with the demonstration of lymphocyte recirculation, was that a full range of reactivities could be accessible to every lymph node as a result of the frequent passage of the entire lymphocyte population through all of the lymphoid tissue.

An additional limitation to the operation of the immune system, in the absence of lymphocyte recirculation, could be the restriction of immunological memory to that regional lymphoid tissue that had been exposed to any specific antigen rather than its dissemination (ie spreading) throughout the lymphoid tissue of the entire body. For example, in the absence of lymphocyte recirculation, immunisation would have to utilise the intravenous route if it was to confer systemic immune protection. However, the role of lymphocyte recirculation in providing lymphocytes to most tissues and organs and the systemic dissemination of specific immune memory has been recognised as critical for functioning of the immune system.

1.3.6 The diversity of lymphocytes and the contribution of this to immunological functions

The concept that lymphocyte recirculation underpins the immune response was initially based on the assumption that lymphocytes presented a ***homogeneous*** population (ie a single population, all the cells of which had similar functional capacity). However, the discovery by Mitchell and Miller in the early 1970s (Miller and Mitchell, 1969) of the interaction of T and B lymphocytes in the mounting of immune responses rendered this assumption invalid. Since then an increasingly wide range of lymphocyte ***phenotypes***[14] have been recognised. Accompanying this finding of diversity of phenotypes, a variety of functional capacities have been recognised as attributable to different lymphocyte populations. Whilst comprehensive demonstration of specific functional associations with specific

[14] ***Phenotypes*** represent the complete characteristics of the expressed features of a living organism or a group of living organisms.

lymphocyte phenotypes has not been achieved, it is not unreasonable to anticipate that some phenotypes provide an indication of particular functional capacities on the part of lymphocytes expressing them. In view of the relationship between lymphocyte immune function and migratory capacity, it is also reasonable to anticipate that some phenotypes may be associated with differences in migratory property. In other words, it would be surprising if some correlation did not also exist between lymphocyte phenotypes and their migratory behaviour.

1.4 Objectives of the present study

Lymphocyte migration through peripheral lymphoid tissue, as distinct from traffic through the major lymphatic vessels, plays a most important part in antigen recognition by the immune system, but its regulation is still poorly understood. The main objectives of this study are

1. To undertake experiments to provide data on the kinetics of lymphocyte migration within lymphoid tissue under normal physiological conditions, which can then be subjected to detailed analysis. This process of data collection involves a large number of details including experimental design, animal selection, surgical operation and techniques, lymph cell manipulation and fluorescent labelling, experimental maintenance and data sampling.

2. To interpret information obtained from experimental data and construct suitable theoretical models capable of describing the kinetics of lymphocyte migration. The models should be precise and should contain information sufficient to explain most of the relevant biological events behind lymphocyte migration.

3. To simulate or predict some unusual situations of lymphocyte migration from knowledge of current models.

1.5 General review on studies of lymphocyte recirculation

1.5.1 Animal models in studies of lymphocyte recirculation

Studies of lymphocyte recirculation and migration have utilised a variety of techniques. Lymphocyte recirculation and migration itself is undoubtedly a complicated dynamic immunological and physiological process involving many participating tissues and organs. Studies of lymphocyte migration have generally

been undertaken as ***in vivo*** experiments (ie experiments undertaken in a living organism) since any experimental protocol to mimic this process ***in vitro*** (ie experiments undertaken in laboratory apparatus) would be very difficult to envisage. Thus, selection of an appropriate animal model is one of the preliminary stages before proceeding to plan experiments in any detail.

Small animal models utilising rodents have quite often been used for studies of lymphocyte recirculation employing the technique of thoracic duct cannulation to gain access to the lymphatic system (Ford and Simmonds, 1972; Sprent, 1973; Sprent and Basten, 1973; Fossum *et al.*, 1983; Smith and Ford, 1983; Westermann *et al.*, 1994). In such experiments, because of the limitations of the surgical technique, only the central components of the lymphatic system (ie thoracic duct) could be accessed to provide experimental data. Furthermore, a large number of lymphocytes were deliberately drained from experimental animals as a consequence of the high flux of normal lymphocyte transit through the thoracic duct. Thus, the data obtained from those studies were limited to a series of single-point observations which could be made within a few days before the occurrence of an abrupt fall in the number of lymphocytes in the circulation, due to the thoracic duct drainage. As has been previously mentioned in section 1.2 of this chapter, many crucial parts of the immune response occur at the peripheral lymphatic system level (ie in peripheral lymphoid tissue) rather than in the central lymphatic system, from which data has generally been obtained in studies using small animal models. Such data do not necessarily describe the underlying pattern of lymphocyte migration through lymphoid tissue. Alternatively, a large number of lymphocyte recirculation experiments in small animal models have been directed particularly to study of the molecular mechanisms of lymphocyte adhesion to the endothelium rather than to the migration process as a whole (Bradley *et al.*, 1994; Bradley *et al.*, 1998).

In contrast, large animal models such as those based on the sheep, provide the opportunity for accessible surgical interventions by use of peripheral lymphatic cannulation techniques. The techniques for collection of lymph from peripheral lymphatic vessels of sheep were originally documented by Morris and his colleagues (Hall and Morris, 1962). The number of lymphocytes drained out of the animal throughout the experiment by these techniques is relatively small compared with the whole lymphocyte pool of the animal. Consequently, studies in large animal models are likely to be more physiologically relevant than those in small animals. The cannulation technique in large animal models permits sampling of either central or peripheral components of the lymphatic system with minimal disruption of surrounding tissues, blood circulation and the lymphatic

system itself. The sampling procedure can be repeatedly performed via a chronic cannulation using an indwelling catheter or polyvinyl chloride tube. This approach minimises direct physical contacts with animals that might otherwise interfere with the experiment. The surgical techniques developed for studies of lymphocyte recirculation and migration in sheep models have been fully developed and reported not only for single lymph nodes but also in many visceral organs (Chin and Hay, 1980; Chin and Cahill, 1984; Mackay *et al.*, 1988; Washington *et al.*, 1994; Mackay *et al.*, 1996). They also have been adopted for use in foetal lambs (Kimpton *et al.*, 1989; Kimpton *et al.*, 1990).

1.5.2 Theoretical models in studies of lymphocyte recirculation

A large number of studies of lymphocyte recirculation and migration have been reported using both small and large animal models (Sprent, 1973; Sprent and Basten, 1973; Issekutz *et al.*, 1980; Reynolds *et al.*, 1982; Fossum *et al.*, 1983; Smith and Ford, 1983; Borgs and Hay, 1986). Such studies concentrated either on the localisation of labelled lymphocytes in particular visceral organs or on the tempo of labelled lymphocyte reappearance in particular lymphatic vessels. However, there appear to have been very few interactive studies in which mathematical analysis of data on lymphocyte migration was applied to generate further experimentation to test its predictions. Mathematical analysis of lymphocyte migration has been undertaken on a very limited scale. Furthermore, the few studies that have been undertaken have entailed no more than retrospective examination of data from earlier experimental studies that was originally collected without the specific purpose of mathematical analysis in mind (Ottaway, 1981; Farooqi and Mohler, 1989; Stekel, 1997; Stekel *et al.*, 1997; Stekel, 1998).

In an early attempt to explain lymphocyte migration by means of mathematical expression, Ottaway (Ottaway, 1981) used a simple kinetic model of differential equations to explain the localisation of radioisotope-labelled lymphocytes in various tissues after an intravenous infusion of those cells. Data obtained from an earlier study in rats (Smith *et al.*, 1980) were used. According to this study, three fundamental steps were required to explain the tissue localisation of labelled lymphocytes. First, lymphocytes were delivered from the central part of the blood circulation to the periphery, ie a delivery step. The tissue perfusion fraction was calculated (or retrieved from the literature) from the proportion of blood volume delivered to that tissue divided by the ***cardiac output***[15] during a

[15] The ***cardiac output*** is the volume of blood expelled from the ventricles (ie lower chambers) of heart in a certain time interval (ie a unit of volume/ time).

fixed time period. Then, the number of lymphocytes delivered to that tissue was calculated by multiplication of the cardiac output by the concentration of lymphocytes in blood and the tissue perfusion fraction. In the second step, lymphocytes arrived and attached to the tissues. This step implied an ability on the part of lymphocytes to attach to a specific tissue. In this paper, the authors used the term "uptake". The number of lymphocytes in this step was calculated from the number of lymphocytes in step 1 (the delivery step) multiplied by an uptake constant fraction. Third, after lymphocytes having successfully entered the tissues, the number of lymphocytes leaving was determined by the product of the total number of lymphocytes residing in that tissue at that time and a constant fraction. A differential equation was initially constructed to explain each individual event of these three steps and finally all equations were solved to obtain parameters of interest. However, many assumptions were made and considerable data from the literature was required to achieve solutions in this study.

Farooqi and Mohler (Farooqi and Mohler, 1989) successfully constructed four different types of mathematical models, namely linear time-invariant, linear time-variant, linear time-invariant with time delay and non-linear, from data obtained from a previous lymphocyte recirculation study in rats (Smith and Ford, 1983). In Smith and Ford's study, radioisotopically labelled lymphocytes were intravenously introduced into rats and the distribution of those lymphocytes was subsequently determined in several tissues and organs, such as venous blood, lungs, spleen, liver, lymph nodes etc. The basic model comprised 12 compartments representing 12 individual tissues and organs. In each type of model, a set of differential equations was individually constructed according to the properties of that type. All unknown parameters in those equations were simultaneously solved by extensive mathematical manipulations. The models obtained from this study mimicked the actual data with varying degrees of success in each individual tissue or organ. To summarise their results, the fit of the time-delay model was better than that of the other two linear models, but was not as good as the more complicated non-linear model.

A recent study has revealed another approach in the application of simple one dimensional dispersion equations to explain lymphocyte migration in lymphoid tissue and spleen (Stekel *et al.*, 1997). Compared with the complicated models of Farooqi (Farooqi and Mohler, 1989), this model consists of three major compartments, namely blood, spleen and lymphoid tissue. In this study, blood is considered to be homogenous and well mixed with respect to circulating lymphocytes. In contrast, spleen and lymphoid tissues are considered as one-

dimensional tube-like organs, through which lymphocytes can migrate. There are two-way connections between the blood and another two compartments, ie the spleen and the lymphoid compartment. Thus a simple first order kinetic equation was used to explain the dynamics of lymphocyte movements in the blood while more complicated convection equations (ie partial differential equations) were used to explain those in spleen and lymphoid tissue. Some additional values were quoted from the literature, such as the mean transit time of lymphocytes through spleen and lymphoid tissue. The simulated results from this model fitted quite well with the experimental results of lymphocyte recirculation from a previous lymphocyte recirculation study undertaken in rats (Westermann *et al.*, 1988).

The modified version of Stekel's model has been significantly improved by adding some elements to the original compartments of the previous model (Stekel, 1997; Stekel, 1998). The elements added to the modified model were intended to mimic the real physiological mechanism of lymphocyte migration. For the purposes of this modification, lymphocytes were regarded as either mobile or bound (to the ***follicular dendritic cells***[16]) while they are migrating within spleen and lymphoid tissues. However, the basic structure of the mathematical equations that appeared in this modified version was still identical with that of the original model.

[16] A type of antigen-presenting cell which reacts with several types of lymphocytes to facilitate recognition and response to the presence of foreign antigens.

Part II: Modelling fundamentals and methodology

1.6 Modelling: From engineering to medicine

In most engineering processes, such as in an oil refinery plant or a car engine, (theoretical or mathematical) models which explain the whole process play an essential role in controlling and designing the most efficient operation to obtain the optimal benefit under certain restrictive conditions (eg expense, fuel consumption, chemical interactions). Apart from the initial purpose of engineering requirements, modelling has been undertaken for an increasing number of applications. Understanding the complexities of a whole process, optimising its cost-benefit, controlling manufacturing procedures, and conducting inexpensive and less complicated simulated experiments under various conditions are some of the initial purposes for which models have been constructed.

With the rapid advance of computation technology and improved understanding of model capabilities, the concept of theoretical models is no longer limited to engineering. Appropriate models can, for example, be applied to economical and ecological processes and particularly, of relevance to this thesis, to biomedical processes. In biology and medicine, the application of modelling methods is increasingly utilised by researchers to obtain a greater understanding of the nature and real behaviour of the chaotic processes in their fields of interest. Mathematical models have been reported in studies of glucose and ***insulin***[17] metabolism in diabetic patients, and have been used to achieve a more steady level of their blood glucose (Boroujerdi *et al.*, 1995; Parker *et al.*, 1999). In ***renal*** (ie kidney) failure patients, ***haemodialysis***[18] is still one of the treatments of choice. Knowledge of ***urea*** (ie one of waste products synthesised in body) and ***sodium***[19] kinetics models (Grandi *et al.*, 1995; Ursino and Innocenti, 1997) have improved the quality of haemodialysis treatment. Consequently, this knowledge should lead to new, alternative and more efficient treatments (Akcahuseyin *et al.*, 1998) and, ultimately, help to improve the quality of life of those patients. In several heart diseases (such as heart failure), mathematical models (Baykal *et al.*, 1997; Woodruff *et al.*, 1997) have shown remarkable benefits in diagnosis, estimation of heart function and planning for drug treatment of those particular heart conditions. There are still numerous applications of modelling in medically

[17] A hormone, released from endocrine cells in the pancreas of mammal species, controls the level of blood glucose. Failure of control of blood glucose is a feature of ***diabetes***.
[18] A medical treatment that removes waste products (such as ***urea***) from the body, especially, of patients suffering from insufficient kidney function.
[19] ***Sodium***, one of the most important elements found in the body, is involved mainly in controlling acid-base and water balance of the body.

related fields, for example in studies of drug kinetics (ie ***pharmacokinetics***) (Martonen, 1993; Young and Hsiao, 1994; Rippley and Stokes, 1995), the mechanism of muscle contractions (Wexler *et al.*, 1997), of eyes movement (Rey and Galiana, 1991), of respiratory ventilation and of its effect on sleeping disorders (Modarreszadeh *et al.*, 1995;Lai and Bruce, 1997) and so on.

1.7 Systems and signals

Before proceeding further with this section, it is necessary to introduce some terms that will often be quoted in the following sections. The term ***system*** can be defined in several different ways (Marmerelis and Marmarelis, 1978; Ljung, 1987). Generally, a system is an arbitrary object that contains within it a set of connecting and interacting ***elements***. For example, considering a car as a system, it is obvious that there are many parts of the engine simultaneously working and interacting together to generate the driving force for the engine. Another example would be an audio system that consists of the interconnecting of a receiver, a disc player, speakers and so on.

Systems may be loosely classified into certain different types depending on the physical properties used to explain them, such as mechanical systems (eg a car engine) and electrical systems (eg a dryer). In biological and medical fields, a particular biological tissue or organ can also be treated as a system. For example, a mammalian retina contains numerous neurone networks. The retina itself can be considered as a system of which the elements are its interacting neurones.

A ***signal*** is an observable (ie measurable) quantity changing in time. By defining a boundary to a system, signals entering that system can be classified as ***inputs*** while those leaving can be termed ***outputs***. The terms input and output are frequently referred to as ***stimuli*** (to the system) and ***responses*** (from the system) respectively. Furthermore, a ***disturbance*** (or ***noise***) is another signal that is considered to be undesirable but also unavoidable. In all the processes of a system, the measured or observed quantities are always perturbed by a disturbance signal. In biomedical experiments, many uncontrollable conditions (ie the surrounding magnetic field in certain types of brain studies) contribute to the disturbance signal. Figure 1.3 illustrates diagrammatically a system with one input and one output. Such a system is defined as a system with ***a Single Input and a Single Output (SISO)*** which is the prototype of the systems[20]examined

[20] In general, most if not all, systems contains multi-inputs-multi-outputs (MIMO). The system to be focussed in this thesis is a SISO system.

throughout this thesis. In Figure 1.3, a rectangle (ie a box) and arrows respectively, represent the system and signals (input, output, and disturbance). The direction of the arrow indicates the direction of the signal, whether leaving from or coming to the system.

Figure 1.3: The SISO system and SISO system with disturbance

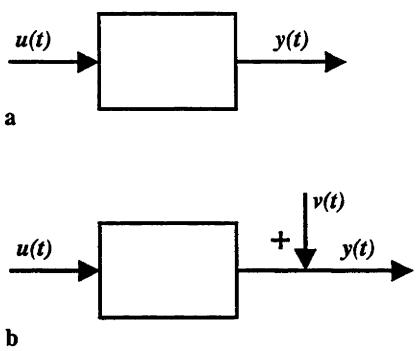

A SISO system: a system with a single input, $u(t)$, and a single output, $y(t)$.

A SISO system with a disturbance, $v(t)$.

By introducing a stimulus (input) to a system, that system will respond by producing a response (output). Again, in a car engine, the fuel consumption rate and the driving force can be considered as an input and an output respectively. Similarly, in a biological system such as the mammalian retina, the introduction of electrical stimuli to the retina will produce (recordable) neurone action (ie electrical) potential as a response. The relationship between the stimulus and the response of any system is unique and specific for that system.

1.8 Categorisation of systems

Having introduced the concept of a system and an input-output signal in section 1.7, systems can be classified into several categories depending on their properties. The ***deterministic system*** describes a system which works with an exact relationship between inputs and outputs without any uncertainty, ie one can assume (or predict) the future value of the deterministic system with good accuracy if the input and system characteristics are known. On the other hand, the ***stochastic system*** operates with uncertainty. However, it can be described with statistical (probability) concepts. For example, the coordinates of a stone thrown into the air could be precisely predicted (provide there is no disturbance from wind or other influences), while the future value of the stock market cannot

be accurately predicted. The first and second situations exemplify deterministic and stochastic systems respectively.

A ***static system*** is a system in which change of output is instantaneously linked to some change of input, ie the output of the static system depends only on the present input, not on the previous input. In contrast to this, the output of the ***dynamic system*** could be varied since it depends on previous inputs. Again, the initial force applied to a thrown stone determines its height in the air as this follows a static system. But in the case of the stock market, which is an example of a dynamic system, previous and present information have to be considered in judging the movement of the market (at the present time).

A system can be considered as a ***linear system*** if it obeys the ***principle of superposition***[21] while it can be considered as a ***non-linear system*** if it does not. The terms ***continuous (time)***[22]and ***discrete (time)***[23]***system*** are used to describe, respectively, the continuity and discontinuity of system signals in the time scale. A system is said to be a ***time-invariant system*** if a shift in time of the input signal causes an identical shift in the time of the output signal. It can be said to be a ***time varying system*** if this time shift property does not exist in that system. A time-invariant system is sometimes called a ***shift-invariant system***.

Systems which possess the properties of linearity and time-invariance, ie ***linear time-invariant systems (LTI systems)*** are an important class of systems because they are easily characterised by their ***unit impulse responses***[24] (more detail will be given in Chapter 5-Prediction error models). The theory of LTI systems is the foundation for constructing many daily life necessities. Many systems, for example communication and control systems, can be modelled as LTI systems. LTI systems are relatively easy to manipulate mathematically. LTI

---

[21] ***The principle of superposition*** describes the linear relationship between the input and output. For example, giving the input x_1 to the system will create the output y_1 while giving the input x_2 to the system will create the output y_2. Thus, giving the input x_1+x_2 to the system would produce the output y_1+y_2 (ie ***additivity property of superposition principles***). Furthermore, given that C is an arbitrary constant, giving the input Cx_1 to the system would produce the output Cy_1 (ie ***homogeneity property of superposition principles***).

[22] ***A continuous signal*** can be written by a form of continuous mathematical equation. For example, given an equation $y(t) = 0.3t - 0.01$ for $t \in [0, +\infty]$, then $y(t)$ can be considered as a continuous signal in a range of t from 0 to plus infinity.

[23] ***A discrete signal*** can not be written in the form of continuous mathematical equations. A discrete data (or signal) can be obtained by the discretization of a continuous signal.

[24] The ***unit impulse input*** $\delta(t)$, also called the ***delta function*** or the ***Dirac function***, contains the property of $\int_{-\infty}^{\infty} \delta(t)dt = 1$. The response from applying the unit impulse input to a system is called the ***unit impulse response***.

systems can be employed and provide powerful tools for analysis and design in many applications. Thus, from this point until the end of this thesis, all systems will be defined as LTI systems, unless otherwise indicated.

1.9 Functional and physical identification of systems

It may be appropriate to regard a model as a tool that can describe or answer questions about the system without having to do an experiment. Very often, a theoretical model may be described as a mathematical model since the main component of these models always consists of a set of mathematical equations describing the relationships among the observed quantities (ie distances, flows, voltages and so on). Generally, almost all systems may be represented by one or more mathematical model(s). However, the ultimate aim of modelling is to obtain a suitable model which is accurate both in the modelling context and in its description of the crucial characteristics of the system under study.

The selection of sources of information can have a remarkable influence on modelling. The information required to build a model can come from two main sources. The first source is prior information available from the literature and from current knowledge of that particular system. It is a very common practice in the modelling of physiological systems for the system under study to be assumed (or sometimes known) to be based on this type of information. Mathematical equations can be subsequently constructed to describe hypothesised models. However, the parameters of those mathematical equations would still be unknown. ***Parameter estimation*** is normally undertaken to obtain the best goodness of fit (ie least error) between mathematical equations representing those hypothesised models and the actual data. It is obvious that this approach is not a systematic approach and is solely dependent on skills and backgrounds of the modellers.

The second source is fresh information derived solely from observations or experimentation on the system. There is a common tendency not only for biomedical scientists but also for almost all scientists in all fields to perceive an experiment in terms of cause-effect, or stimulus-response, relationships. These relationships are often established by applying an external stimulus to the system under study, followed by close observation of its response during a certain period of time depending on the nature of that particular system. By using the results of a stimulus-response experiment, the characteristics of a system may be described without knowing any prior information (ie internal structure) about that system. This approach, which is based on the description of response to any

individual stimulus, is called ***functional identification of the system.*** A system in which functional identification has been undertaken is often referred to as a ***black box*** system since information (eg components or elements) inside the box is unavailable. This approach considers the whole system rather than all the details of interacting elements. Using this approach, only information about the stimulus-response relationship of that system is required, not any prior information about the structure of the system. For example, in the present study of the lymph node system, the prior information includes items such as blood flow to the lymph node, the total number of lymphocytes residing in the node, etc.

However, most biomedical scientists prefer to interpret information in the light of their field of expertise. It follows that any interpretation will completely reflect the prior knowledge of the interpreters. In the case of medical researchers, it is likely that reliance will be placed on the structure of the system, eg the histology and anatomy of that system. As the functional identification of a system is not concerned with the detailed components of that system, results normally relate to the whole response of the system rather than to individual responses from each of the system components. Common questions that often arise are how to interpret the result of functional identification or how to discover the interaction of various components inside the studied system. These questions lead to another approach. In order to reveal the components inside the black box, it is necessary first to perform a stimulus-response test for the whole black box. Then, a model that comprises its internal structural details can be constructed by using all the knowledge derived from results of the stimulus-response test (sometimes together with available prior information and/ or additional necessary assumptions). This process is termed ***physical identification of the system.*** Theoretically, this process can be done by breaking a "black box" system down into its various components, and then performing a set of tests to obtain responses from points within the box itself. Practically, however there is often a considerable barrier to breaking a system into its components and doing a stimulus-response test for each individual component under conditions applying in intact biological environments (especially in the case of an ***in vivo***[25] experiment).

Without either or both of priori information or assumptions, stimulus-response experiments alone could not precisely reveal all of the information about components which are hidden in the system. Nevertheless, a well-designed

[25] An **in vivo** experiment means an experiment performed in a living animal (or organism). A closely related term is **in vitro** experiment, which means an experiment performed using laboratory apparatus. Any experiment can include either one of these or both.

stimulus-response experiment, with additional information, can provide a guide (ie hypothesis) to the construction of a physical model.

1.10 An attempt to construct a theoretical model of lymphocyte migration from novel data specially collected for this purpose

Lymphocyte migration through peripheral lymphoid tissue represents an important part of the function of the immune system, but it is still poorly understood. Under normal conditions, it has been estimated that about one-fourth of the blood lymphocytes that arrive at postcapillary venules will successfully migrate through the inter-endothelial space into lymph node tissues. The remaining blood lymphocytes return to the central blood vessels through the venous system. Furthermore, the majority of lymphocytes appearing in the efferent lymph are derived from the blood. It has been calculated that approximately 5% of the lymphocytes in lymph are derived from cell division in the lymph node or from entry into it via afferent lymph vessels (Hall and Morris, 1962; Hall and Morris, 1965b). Any changes in the blood-borne lymphocyte population would be expected to have an effect on the lymphocyte population in efferent lymph if the calculation that approximately 95% of this is derived directly from the circulating blood is accurate. This information has influenced the experimental design of the present study. An experimental protocol that can demonstrate the relationship between the lymphocyte profile (ie concentration) in both blood and lymph simultaneously would be more advantageous for any attempt at modelling. To achieve this, the injection of labelled lymphocytes into the blood circulation and the monitoring of those cells in both blood and lymph has been used to track labelled lymphocytes. This was followed by construction of mathematical models to describe the kinetics of lymphocyte migration within lymph node tissue.

As the present study was intended to concentrate on the events involved in lymphocyte migration, the sheep model was selected because of its advantages compared with in vitro or small animal models which have been described in section 1.5.1. A major goal of this thesis was to compare alternative approaches to modelling the events of lymphocyte migration in lymphoid tissue. From their starting point, these experiments were planned to obtain enough informative data to construct suitable models while avoiding physiological assumptions whenever possible. This modelling approach was considered to have substantial advantages compared with modelling from retrospective data. In the latter situation, informative data may be unavailable since the original experiments were directed to achieve other goals. There are three main approaches followed

in this thesis. A compartmental model is an example of a classical biological model, which still requires many assumptions and availability of physiological values from other known sources. In fact, all of the published models previously developed to describe lymphocyte migration and summarised above in this section are purely compartmental analysis-based models. The second approach will be to model in the time domain using the technique of system identification. This is a new trend in modelling which has not been used very much by biological scientists. The third approach will be an attempt to combine two modelling techniques, namely the frequency and time domain analysis together, to give a clear picture of lymphocyte migration.

In lymphocyte migration experiments, compromise between the aims of the experiment and constraints imposed by the modelling procedures is required at several points. Almost all of the experimental procedures will be performed in the laboratory with experimental animals. Physiological data collection in lymphocyte studies is subject to possible complications introduced by dealing with animal and lymphocyte preparations. There are ethical constraints inherent in long-term experiments with conscious animals. The process of sampling and data collection is likely to require a few weeks from the start for each individual experiment. Furthermore, continuation of this process requires ongoing, manual input to keep the experiment progressing smoothly. Failure of maintenance or any technical interruption may cause an involuntary cessation of the experiment.

Unlike studies in some other biomedical fields, for example the neurosciences, data on lymphocyte recirculation can not be acquired continuously in a short period of time by using computer-aided devices. The results of lymphocyte migration experiments require more time to collect and process to obtain a unique discrete data pattern. This is a significant distinguishing feature compared with the short time scale of experiments in neurological sciences (which might take only a few seconds to a few minutes to collect the sample). Data acquired from those studies can include a great number of data points within a short experimental time, depending on the speed of sampling frequency and the ability of recording devices used in those studies.

Finally lymphocyte migration experiments present a set of uneven-discrete data which extend over an experimental period of about 10 days. This introduces a further difficulty in processing the actual data since the basic principle of the signal may have to be determined as a pre-requisite to proceeding to further stages of analysis. Firstly, signals should be in an appropriate pattern to be characterised as evenly discrete data. Secondly, the number of items of data

should be sufficient to satisfy the modelling procedure. Clearly, if the data set is small, there will be a tendency to have a large variation (error) in the models. To achieve those requirements, the actual data must be processed (ie interpolated) by using a ***linear interpolation***[26] algorithm to get a constant sampling interval.

1.11 Thesis structure: Multiple approaches

The contents of each chapter of this thesis are intended to provide a complete account of the subject matter of that individual chapter. The following are the outlines of each chapter.

- Chapter 2: Experimental procedures. This chapter gives all the experimental details including those relating to the techniques used in experiments. Some experimental pitfalls will be identified and commented upon.

- Chapter 3: Experimental results. All data will be summarised and presented. Discussion based on observations from that data will be undertaken and compared with previous studies. A preliminary attempt to analyse the outcomes of data will also be included.

- In Chapter 4, Compartmental analysis, one of the classical approaches applied in many biomedical fields will be introduced. The compartmental model can be considered as a solely ***physical model*** (ie a model with its componential configuration) since it requires a considerable amount of known sources and assumptions (namely relevant studies of histo-anatomy, histo-physiology and immunology) for construction of model components. A set of mathematical equations (mainly differential equations) will be used to describe the hypothesised compartmental model. The identification of unknown parameters appearing in those mathematical equations will be undertaken so as to give the best fitting criteria.

- Chapter 5 will deal with the concept of functional identification of a system (through stimulus-response experiments) in the time domain. In contrast with the approaches adopted in Chapter 4, the physical model in this approach is totally unknown. The analysis is focused on its stimulus-

[26] There are several methods of ***interpolation***. The more complicated the interpolating method, then the greater the chance that the original information will be changed. In this case, a linear interpolation would be one of the simplest ways that can ensure the actual data still remained unaltered after the interpolation process.

response relationship without making any assumptions about the structure of the system.

- Chapter 6 will examine a structured model approach[27], leading to another step in modelling. This approach combines a concept of two approaches (ie functional and physical identification of systems) together. Again, the physical model in this approach is totally unknown and the analysis is focused on its stimulus-response relationship without giving any prior information. First, the functional system will be identified in the frequency domain. Given the information obtained from the frequency domain analysis, the informative characteristics of the system will be determined as a guide to the construction of a structured model. Any assumptions made in this chapter on model structure will be optimised by incorporating more information from the experimental data itself.

At the end of this thesis, the conclusion will be drawn that these models represent only the first step in understanding and explaining the events of lymphocyte migration in a lymph node (system). The contents of this thesis represent only a starting point in trying to quantify and model lymphocyte migration under normal physiological conditions. Even though several modelling approaches, often used in medical and physiological modelling, will be introduced and compared, a completely true model still has yet to be attained. In the context of modelling, reference to a "suitable model", is more appropriate. More information obtained in the future should contribute to an improvement of the preliminary model(s) presented in this thesis.

[27] A structured model approach is named by its final objective of obtaining a structured model. This approach, in fact, combines the functional and the physical identification of systems together.

Chapter 2/
Experimental procedures

Animals

Merino ewes, 3-5 years old, of approximately 25-35 kg weight, were randomly selected from local flocks, transported to a holding room and kept in metabolic cages. The cages allowed animals to lie and stand freely, but not to turn around. Two separate containers placed at the front of the cages provided free access to water and food (ie lucerne chaff). A wire mesh floor allowed urine and feces to pass through a chute which funneled into a container at the rear of the cage. The food and water, and experimental room were maintained on a daily basis. Animals were kept caged for at least 3 days prior to surgery to allow them to accustom themselves to the experimental laboratory environments.

Pre operative preparations and anaesthesia

Sheep were starved for food and water for a period of at least 12 hours prior to surgery. ***Thiopentone sodium*** (Jurox Pty Ltd, NSW, Australia) at a dose of 4 mg per 1 kg of animal weight was injected via an external jugular vein to induce anaesthesia. A size 9.0 cuffed ***endotracheal tube*** (Rusch, Germany) was introduced into the trachea of the sheep to maintain its airway during surgery. A gas mixture of 1-3% ***halothane*** (Fluothane, ICI Australia operations Pty Ltd, Australia) and 100% oxygen was administrated via the endotracheal tube from a Boyle' s ***anaesthetic apparatus*** (British Oxygen Company). Surgery was normally undertaken in the morning and lasted for about 1-2 hours depending on the complexity of operation. The operation time, from when sheep were fully anaesthetised until the end of anaesthesia, was approximately 1.5-2.5 hours for each operation.

Under full anaesthesia, wool covering the operative area was removed using an animal clipper with a fine comb blade. The skin was scrubbed thoroughly with 7.5% w/v ***aqueous povidone-iodine*** (Betadine Surgical Scrub, ICI Pharmaceuticals, VIC, Australia) followed by application of a wash of 70% ***ethanol*** containing a mixture of 5 w/v% ***chlorohexidine gluconate*** and 4 w/v%

isopropyl alcohol (Hibitane, Faulding Pharmaceuticals, Australia). Sterile drapes were used to cover all the non-sterile fields leaving only the operative area exposed. All instruments, tubing and catheters used in the operating theatre were sterilised under strictly controlled conditions.

Cannulation of efferent lymphatic vessels

Initially, the desired efferent lymphatic vessel was located and the direction of lymph flow was identified. If more than one lymphatic vessel was found, the largest one was chosen to be cannulated while the others were tied off. The efferent vessel was carefully dissected to remove all surrounding fat and tissues and ligated with 3 metric silk (Davis and Greck, Australia) at the distal end of the efferent vessel as far from the node as possible. A second, loose, ligature was placed around the vessel about 1-2 cm below the first ligature to provide sufficient length for cannulation. An appropriate size of ***polyvinyl chloride tube*** (Dural Plastic and Engineering, Dural, NSW, Australia) was chosen and preliminary adjustment undertaken to ensure satisfactory alignment of it with the lymphatic vessel. A minute incision was made in the wall of the efferent vessel in the prepared region with ***Noyes-iris scissors*** (Kaiser's, WA, Australia). To provide a free flow of lymph through the cannula, the opened tip of the cannula was positioned to avoid it lying against either lymphatic valves or the inner wall of the efferent vessel. An ***aneurysm needle*** was used to break any lymphatic valves along the efferent vessel that might have interrupted attempts at cannula insertion and obstructed the lymph flow.

The cannula was slowly inserted into the lymphatic vessel until its tip passed through the point of the second ligature. Then the second ligature was firmly tied. Additional ligatures were sometimes required to maintain the alignment of the cannula and ensure there were no obstructions. At the final step, the flow of lymph was checked to ensure that it was running freely before the wound was closed. Generally after wound closure, an obstruction of the cannula, lying underneath the skin, could not be remedied without general anaesthesia for re-operation on the animal. Powdered ***Benzyl penicillin sodium*** (CSL limited, VIC, Australia) was applied to the wound. The skin was closed with ***Michel wound clips*** (Medicon Instrumente, Germany) without any suture to muscles or aponeurosis. The external cannula was secured to the skin by sutures with 1 metric silk (Davis and Greck, Australia). Efferent lymph was allowed to drain freely under internal pressure within the lymphatic vessel.

Surgical approach to the efferent vessel of the popliteal lymph node

The operation described by Hall and Morris (Hall and Morris, 1962) was carried out with anaesthetised animals placed on either side with the fore leg of the same side as the operative field secured back towards the hind limbs. An injection of 0.5-1 ml 1% ***Evans blue*** (Searle diagnostic, England) was given in the draining area of the ***popliteal lymph node*** (ie the area above the hock) to make the efferent lymphatic vessel more visible. An incision was made through the skin and subcutaneous tissue beginning about 2 to 3 cm below a point midway between the ***trochanter major*** and the ***sciatic tuberosity***, and continued down the leg for 5 to 10 cm. The ***aponeurosis*** between the posterior head of the ***biceps femoris*** and the ***semitendinosus muscles*** was incised. ***Wound retractors*** were used to expose the operative field. Muscular branches of the posterior femoral vessels were separately ligated with 3 metric silk (Davis and Greck, Australia). The efferent vessel from the popliteal lymph node, lying posteromedially to those vessels, was identified by blunt dissection. A 0.8mm/1.2 mm (inner/outer diameter) polyvinyl chloride tube (SV55, Dural Plastic and Engineering, Dural, NSW, Australia) was used to cannulate the lymphatic vessels using previously described techniques.

Surgical approach to the efferent vessel of the prescapular lymph node

The operation described by Pederson and Morris (Pederson and Morris, 1970) was carried out with anaesthetised animals placed on their backs with their fore legs securely tied backward to make the operative field more accessible. An injection of 0.5-1 ml 1% Evans blue in the draining area of the ***prescapular lymph node*** (ie the area caudal to the shoulder joint) was undertaken to make the efferent lymphatic vessel of the prescapular lymph node more visible. An incision was made through the skin and underlying tissues starting at a point about 5 cm cranial to the shoulder joint and extending cranially for about 10 cm along the ventral edge of the ***brachiocephalic muscle***. Blunt dissection through the subcutaneous tissues exposed the ventral edge of the brachiocephalic muscle. The efferent vessel, located on the reflected medial surface of the muscle, was identified by blunt dissection. A 1.0 mm/1.5 mm (inner/outer diameter) polyvinyl chloride tube (SV70, Dural Plastic and Engineering, Dural, NSW, Australia) was used to cannulate the lymphatic vessels by techniques previously described.

Catheterisation of the external jugular vein

The technique of ***percutaneous vascular catheterisation***, described by Seldinger (Seldinger, 1953), has been used in this experiment. It allows catheter entry into an area without an incision as a needle is used to introduce the catheter. Thus it minimises injuries to surrounding tissues. A 14-gauge needle was introduced through the wall of the ***external jugular vein***, followed by the advanced portion of a wire guide. The needle was withdrawn while the wire guide was in place. A 16-gauge catheter (15 cm length with J-tip wire guide, Cook Veterinary Products, Australia) was introduced into the vessel with a twist motion along the wire guide. The wire guide was removed and the catheter was secured to the skin of the sheep by multiple sutures with 1 metric silk (Davis and Greck, Australia). Normal saline solution was used to flush the catheter and blood was drawn to ensure that there was a free flow within the catheter.

Post operative maintenance

General anaesthesia was normally terminated at the time of skin closure. Sheep were allowed to recover from the influence of general anaesthesia in the operating theatre. Then they were moved to metabolic cages (Figure 2.1) for full recovery. The endotracheal tubes were left in place during the recovery period to prevent any possible airway aspiration and removed after post-operative evaluation.

Before commencing surgery, all tubing and connectors in the laboratory (where sheep were to be placed) were set up, and cleaned thoroughly by infusion of 70% ethanol for at least an hour, followed by infusion of sterile normal saline solution. To prevent clot formation in draining lymph, a sterile solution of ***Ethylene Diamine Tetra Acetic acid***, ***EDTA*** (Sigma Chemical Co., MO, USA, code E-5134) at a concentration of 100 mg/ml was continuously infused by a peristaltic pump (Model P-3, Pharmacia Fine Chemicals, Sweden) and mixed with draining efferent lymph via a three way glass connector to achieve a final concentration in the lymph of approximately 2mg/ml (Figure 2.1). A sterile mixture of 0.9% ***normal saline solution*** and ***heparin*** (CSL limited, VIC, Australia) at a final concentration of 50 units/ml was continuously infused by a peristaltic pump (Model P-3, Pharmacia Fine Chemicals, Sweden) at a rate of approximately 10 ml/hr through the indwelling intravenous catheter to prevent blood clot formation at the tip of the catheter (Figure 2.1).

The tubing and connectors used to carry efferent lymph were frequently checked and flushed with sterile 0.9% normal saline solution to prevent accumulation of sediment. All infusion solutions and laboratory instruments exposed to either blood or lymph (such as the collecting bottles, plastic tubes and all connectors) were kept in conditions that were as sterile as possible.

Figure 2.1: Experimental diagram

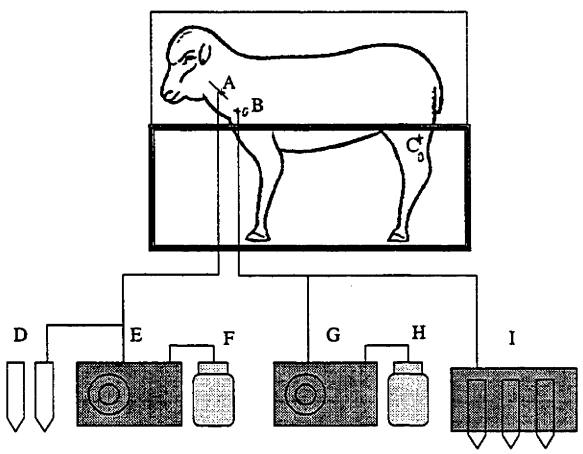

The sheep was kept in a metabolic cage. The indwelling catheter was inserted into the external jugular vein (A). Blood sampling was performed manually (D). The peristaltic pump (E) was used to deliver a continuous infusion of heparinised normal saline solution (F) to prevent blood clot formation.

A cannula was inserted into the efferent lymphatic vessel of either the prescapular lymph node (B) or the popliteal lymph node (C). Using a peristaltic pump (G), the efferent lymph was mixed with EDTA (H) and allowed to drain freely along the tubing and finally into the plastic containers. Lymph sampling frequency was controlled by a programmable fraction collector (I).

Collection of lymphocytes

Animals were allowed a few days after the operation for full recovery before starting an experiment. In the present study, a considerable number of lymphocytes were required for the infusion step. It had been previously reported that there were no significant kinetic differences between lymphocytes collected over either a 4 hour or a 16 hour period (Reynolds *et al.*, 1988). Thus overnight lymph (ie about 12-18 hours) from the cannulated efferent lymph vessel was collected in ***polypropylene bottles*** (Falcon, Becton Dickinson, USA) with a continuous infusion of EDTA solution under sterile conditions. Furthermore, it was noticed in the present experiment that, during collection, maintenance of lymph at a cooler temperature improved lymphocyte viability compared with those collected at room temperature (no data shown). During collection, the temperature of the lymph was cooled down to approximately 10°-15°C by placing collecting bottles in a container partly filled with ice. The temperature of the lymph was kept as stable as possible until sufficient lymph had been collected to proceed to the next stage.

Fluorochrome labelling of lymphocytes

Lymphocytes were labelled with fluorescent dye under sterile conditions as follows.

1. The number of lymphocytes in the overnight lymph collection was counted. A minimal number of about 10^9 lymphocytes was required at the beginning of labelling.
2. Lymphocytes were washed and resuspended 3 times in ***Phosphate Buffered Saline*** (***PBS***). For each spin, the ***centrifuge*** (Model TJ-6, Beckman Instruments Inc, CA, USA) was set at 1500 rpm (about 500 g) for 5 minutes. Cell-free lymph was retained for the next step. The final concentration of the lymphocyte suspension was adjusted to approximately $5x10^7$cells/ ml.
3. ***5-(and-6)-carboxyfluorescein diacetate, succinimidyl ester, (CFSE)*** (Molecular Probes Inc., USA) was mixed with the lymphocyte suspension at a concentration of 3-5 µM per $5x10^7$ lymphocytes.
4. The mixture of CFSE and lymphocytes was incubated in a warm bath at 37°C for 15 minutes and occasionally mixed gently to ensure an evenly distributed reaction in the container.
5. A volume of cell-free lymph (equal to the volume of the mixture of CFSE and lymphocytes) was added to stop the reaction. Lymphocytes were washed and resuspended 3 times in Phosphate Buffered Saline (PBS). Ten ml of cell free lymph was used for the final suspension. Small numbers of labelled lymphocytes were taken for a pre-infusion study. Low lymphocyte viability (ie more than 10% damaged lymphocytes as a consequence of labelling processes) or the low quality of CFSE staining (ie less than 90% CFSE staining) were indications for discarding a specimen.

Infusion of labelled lymphocytes

CFSE labelled lymphocytes (generally about 1-2 $x10^9$ cells) were infused back into donor animals via the indwelling intravenous catheter as a bolus within a minute followed by 10-20 ml of normal saline to flush any lymphocytes adherent to the tubing. This infusion technique is considered to represent a bolus as previously discussed in Chapter 1. Zero time was counted as the starting time of the infusion. To establish a basic routine, all infusions of labelled lymphocytes were performed at 10 am on the day on which an experiment started.

Blood sampling

For each blood sample, approximately 3-5 ml of venous blood was manually drawn from the indwelling venous catheter into a 5 ml sterile plastic syringe (Terumo Medical Corp., USA) containing 0.5 ml of 2% EDTA. Heparinised normal saline was used to flush the remaining blood in the tubing after sampling. The frequency of blood sampling was greater during the first few hours and decreased after that. In most experiments, blood sampling was undertaken at 2, 5, 10, 20, 30 minutes, and 1, 2, 3, 4, 6, 12 and 24 hours after infusion, and thereafter every 24 hours until the end of the experiment (ie about 7 to 12 days depending on the conditions of each individual animal and experiment).

Blood samples taken during the day (ie between 8 am - 4 pm) were processed to the stage of lymphocyte preparation (and monoclonal staining in sub-population studies) on the same day whilst ones taken during the night (ie between 4 pm - 8 am) were kept overnight in a 37°C warm bath and processed to the stage of lymphocyte preparation on the following day.

Lymph sampling

In most experiments, the efferent lymph (well mixed with 2% EDTA) was allowed to drain freely and collected into 15 ml plastic containers using a ***fraction collector*** (Model FC203, Gilson Co., WI, USA) programmed to collect the lymph every 2 to 8 hours (Figure 2.1). A period of about 15-30 minutes was required for collection of each sample of efferent lymph, depending on the lymph flow rates in individual animals at the time of experiment. The volume of draining efferent lymph was recorded and the lymphocyte concentration was counted using a ***haemocytometer*** every 12-24 hours to determine the total number of lymphocytes drained from the efferent lymph during that period.

Lymph samples collected during the day (ie between 8 am - 4 pm) were processed to the stage of lymphocyte preparation (and monoclonal staining in sub-population studies) on the same day whilst ones collected during the night (ie between 4 pm-8am) were kept overnight in a 4°C refrigerator and processed to the stage of lymphocyte preparation on the following day.

Preparation of lymphocytes

Lymphocytes from lymph samples can be directly prepared from the collected efferent lymph because the majority of cells in lymph are lymphocytes. Lymph

was washed three times in 4°C ***Phosphate Buffered Saline*** with 2% ***Bovine Serum Albumin*** (Sigma Chemical Co., MO, USA, code A-6793), 2mg/ml ***EDTA*** and 0.1% ***Azide*** (Sodium azide, Sigma Chemical Co., MO, USA, code S-2002) ***(PBS/BSA/EDTA/Az)*** and resuspended by centrifugation (Model TJ-6, Beckman Instruments Inc, CA, USA) set at 1500 rpm (about 500 g) for 5 minutes.

However, in the preparation of blood samples, it was necessary to destroy red blood cells (RBC) by a lysis technique. The lysis mixture containing 0.83% ***ammonium chloride*** (Ajax Chemicals Ltd, Australia) and 0.17 M ***Tris buffer*** (Tris [hydroxymethyl]- aminomethane, Sigma Chemical Co., MO, USA, code T-1378) at a ratio of 9:1 was warmed to a temperature of 37°C (ie in a water bath for about 15 minutes). Subsequently, blood was added to this lysis mixture in a ratio of 4:1. To ensure complete lysis of RBC, the mixture of blood and lysis solution was well mixed and left for a few minutes before its first resuspension, followed by three washes and resuspensions similar to the procedure used for the preparation of lymphocytes from lymph samples. The final suspension contained a mixture of granulocytes and lymphocytes, but no red blood cells.

In whole population studies, lymphocytes were fixed in 3% ***formaldehyde*** (Methanol free, 10% Ultrapure, Polyscineces Inc., PA, USA) and kept in a light free environment at 4°C (ie in an ordinary refrigerator) until flow cytometry analysis. For additional sub-population studies, lymphocytes were exposed to specific monoclonal antibodies before flow cytometry analysis.

Monoclonal staining

All monoclonal antibodies used in the present study were obtained from the Centre for Animal Biotechnology (School of Veterinary Science, The University of Melbourne, Victoria, Australia) and have been previously reported (Washington *et al.*, 1988; Abernethy *et al.*, 1990; Kimpton *et al.*, 1990). These monoclonal antibodies included SBU-T1 (25.91), SBU-T4 Pool (44.38+44.97), SBU-T8 (24.96) and SBU-p220 (20.96) for recognition of CD5, CD4, CD8 and CD45R respectively. The concentrations of monoclonal antibodies used in the present experiment were varied from 1:20-1:80 depending on each type of monoclonal antibody and the specific batch. The following are the steps of monoclonal staining:

1. Fifty µl solution of monoclonal antibody was added to each selected well of a (V-shaped bottom) 96-well plate (Corning Costar Corp., USA). This amount of monoclonal antibody is sufficient for 1-2 x 10^6 cells/ well.

2. Approximately 2 x 10^6 cells (ie about 50 µl of cell suspension) were added to each well. The plate was sealed with a plastic sticker and the whole plate was incubated at 4°C for 30 minutes on a continuous shaker.
3. The whole plate was spun using a centrifuge (Model TJ-6, Beckman Instruments Inc, CA, USA) at 1000 rpm (about 200 g) for 2 minutes. It was then washed and resuspended three times in 150 µl PBS/BSA/EDTA/Az solution.
4. After addition of 50 µl of 1:400 ***Anti-mouse immunoglobulin R-Phycoerythrin conjugated, PE*** (Silenus Laboratories, Australia, code DDAPE), each plate was sealed and incubated at 4°C for another 30 minutes on a continuous shaker.
5. Step 3 was repeated. Stained cells could be analysed (by flow cytometer) immediately after this step or alternatively fixed in ***3% formaldehyde*** (Methanol free, Ultrapure, Polyscineces Inc) and kept in a light free environment at 4°C for a few days, before flow cytometry analysis. In the present experiment, all samples were fixed, kept at 4°C in resealed plates and analysed within 7 days of fixation.

Flow cytometry study

All flow cytometry studies were conducted at The John Curtin School of Medical Research using the FACScan flow cytometer (Fluorescence Activated Cell Analyser, Becton Dickinson, San Jose, CA, USA). The FACScan equipped with an argon ion laser operating at 15 mW power and 488 nm wavelength was used for excitation of all fluorochromes. The standard configuration for spectral discrimination of fluorescence emission contains three ranges of 530/30, 575/20 and 670 LP nm for FL1, FL2 and FL3 detectors respectively.

All flow cytometry experiments were classified into pre and post infusion categories. All samples were gated on both forward light scatter and 90° light scatter to exclude any other cells, debris and cell clumps. The number of cells required was approximately 20,000-50,000 for each sample. All flow cytometry studies were undertaken within a week of the cells being fixed.

Pre infusion study: This included

1. A final concentration of 10 µg/ml of ***Propidium Iodide (PI)*** was used to stain lymphocytes before and after labelling with CFSE to determine their viability. FL3 detector was used to detect the emission of PI and a histogram of light

scatter versus log integrated red fluorescence was used for data acquisition and storage.

2. The efficiency of CFSE labelling of lymphocytes was determined. The FL1 detector was used to detect the emission of CFSE and a histogram of light scatter versus log integrated green fluorescence was used for data acquisition and storage.
3. In sub-population studies, the percentages of lymphocyte sub-populations (stained with PE, Anti-mouse immunoglobulin R-Phycoerythrin conjugated, Silenus Laboratories, Australia, code DDAPE) of interest (CD4, CD8, CD5 and CD45R) among the CFSE labelled lymphocytes was determined as a percentage of the infused population. FL1 and FL2 detectors were used to detect the emission of CFSE and PE. A dot plot of log integrated green fluorescence and log integrated red fluorescence was used for data acquisition and storage.

Post infusion study: Lymphocytes were prepared from samples obtained from the selected draining efferent lymph and blood as previously described.
The flow cytometry studies at this stage included

1. In whole population studies, the percentage of the CFSE labelled lymphocytes was measured using the same technique for determination of the efficiency of CFSE labelling previously described in step 2 of the pre-infusion study.
2. In sub-population studies, the percentages of sub-populations of interest (CD4, CD8, CD5 and CD45R) among the CFSE labelled lymphocytes were determined using the same technique as previously described in step 3 of the pre-infusion study.

Acquired data were saved and, subsequently, analysed to obtain more information by a computer package (CellQuest Version 3.1f, Becton Dickinson, San Jose, CA, USA). All dot plots and histograms used in the analysis step were similar to ones used in the acquisition step.

Statistical Analysis

All statistical analysis in this thesis, unless defined otherwise, was undertaken using an Analysis of Variance (ANOVA) of the SPSS program (SPSS Inc., USA), where a p-value of less or equal to 0.05 was considered statistically significant.

Chapter 3/
Experimental results

3.1 Introduction

The present study was intended to describe the characteristics of lymphocyte migration in lymphoid tissue and, in doing this, to acquire results suitable for mathematical modelling. Lymph was collected overnight from the prescapular or popliteal efferent lymphatic vessels of sheep, labelled with the fluorescent dye CFSE, and intravenously infused back into the donor. The time of infusion has been recorded as time zero. The experimental time represents the total time elapsing from time zero until the end of an experiment. The efficiency of fluorescent dye (CFSE) labelling of lymphocytes, the viability of lymphocytes before and after labelling and the percentages of labelled lymphocytes in both blood and efferent lymph were determined by flow cytometry.

All experiments should be considered as whole population studies (to be presented in section 3.2 of this chapter) because the labelled autologous lymphocytes, which were transfused to each sheep, had not been separated any specific lymphocyte subsets. However, in recognition of the phenotypic heterogeneity of the cell components of lymph, some studies of the migration of lymphocyte subsets within the transfused whole population were performed to detect any differences between the migratory capacities of the major lymphocyte subsets. The technique of monoclonal staining was used to determine the percentages of the major lymphocyte subsets. Because the fluorescent dye used for monoclonal staining (PE) can be distinguished from the one used for labelling (CFSE) by flow cytometry, detection of labelled cells and monoclonal antibody-stained cells could be performed simultaneously on each sample. This was done in some experiments. The results of lymphocyte subset studies will be presented in section 3.3 of this chapter. Full details of experimental procedures have already been described in Chapter 2.

Although the experiments to be reported in this chapter were undertaken over a 24-month period, no significant differences were observed between the results of experiments undertaken at different times during this period. Furthermore, there

has not been any report from other laboratories of seasonal influences producing variations in lymphocyte recirculation. Throughout these experiments, sheep were maintained in a laboratory room at a controlled temperature (about 15°-20° C) and a regulated day and night cycle of light. The total period required for accumulation of all of the data was approximately 2-2.5 years. The results obtained in approximately half of the experiments were not analysed and have not been recorded in this section, because data collection was incomplete owing to premature interruption of flow in the lymphatic cannula or because of instrumental breakdown affecting lymph collection. However, there was nothing to suggest that omission of data because of technical failure is likely to have resulted in biased selection of data for analysis. The results of 21 individual experiments using 16 animals have been included in this thesis. All experimental details are summarised in Table 3.1.The results from some experiments will be re-summarised and analysed separately in Chapters 4, 5 and 6.

On the assumption that a crucial event in lymphocyte recirculation may be transportation of lymphocytes from blood to lymphoid tissue, the arterial blood may be more representative of the level of lymphocytes entering the postcapillary venules than the venous blood would be. In one lymphocyte recirculation study in sheep, some small, but significant, differences were reported between the concentrations of some lymphocyte subpopulations in arterial and venous blood from the mesenteric artery and vein (McGeown and Crockard, 1993). However, lymphocyte sampling from venous blood (ie the jugular vein) was utilised in the present study as repeated arterial sampling was found to be technically impractical. Several attempts were made to insert indwelling catheters in the femoral artery. However, due to the high pressure in that artery and movement of the animal's legs, dislodgment of arterial catheters became a major problem. A complete set of data from femoral artery sampling was not achieved in any experiment. Moreover, it was reasonable to assume that the time required for mixing of lymphocytes within the blood circulation is likely to be of the order of minutes (Bjerknes *et al.*, 1986; Borgs and Hay, 1986) whereas the time scale of lymphocyte migration has been reported to be of the order of days (Trevella and Morris, 1980; Reynolds *et al.*, 1982; Chin and Cahill, 1984). Thus, the use of venous rather than arterial samples in the present study was appropriate and more practical. The external jugular vein was selected as the site for insertion of the indwelling catheter on account of its appropriate size and ready surgical accessibility. Additionally, it is located in the same operative field, in which most operations were undertaken (ie cannulation of the efferent lymphatic vessels from the prescapular lymph node). This reduced the duration of each operation in addition to simplifying the procedure.

Table 3.1: Summary of all experiments

Animal[a]	Time[b]	Lymphocyte subset[c]				Whole[d]	Dose[e]	Viability[f]	LFlow[g]
		CD4	CD5	CD8	CD45R				
B481	136					+	3.95	96.30	19.93
B687	167					+	1.08	97.92	18.21
B445(1)	124					+	1.99	99.45	14.10
B445(2)	100					+	1.52	99.57	16.28
B882	72					+	1.69	99.67	21.75
B857(1)	240	+		+		+	1.33	89.13	13.46
B857(2)	120	+		+		+	0.52	88.50	12.17
R021(1)	72	+		+		+	0.92	90.14	16.36
B045	72	+		+		+	0.55	99.33	10.12
R021(2)	96	+		+		+	0.59	99.65	13.84
R153(1)	142					+	0.62	90.03	N/A
R153(2)	168					+	1.53	99.67	N/A
R401	240					+	1.61	98.99	13.78
R705	360		+		+	+	1.92	99.40	15.30
R632	240		+		+	+	1.80	99.70	15.36
R634	120		+		+	+	1.54	99.53	15.42
R798	240		+		+	+	1.64	99.34	14.78
R797	168	+	+			+	2.52	99.36	21.54
R890	216	+	+			+	0.60	97.88	8.70
Y044(1)	240					+	1.08	99.57	11.26
Y044(2)	192					+	1.40	98.21	12.15
Mean	167.86	7/21	6/21	5/21	4/21	21/21	1.44	97.21	14.97
± SD	± 74.62						± 0.79	± 3.95	± 3.55

[a]**Animals** are coded according to their tagged numbers. (1) and (2) denote two separate experiments which were undertaken in the same animal using lymph nodes on different sides. Lymph was obtained from an efferent lymphatic vessel of a prescapular lymph node of all animals, except in R153(1) and (2) lymph of which was obtained from an efferent lymphatic vessel of the popliteal lymph node. [b]**Time** is the total number of hours in the actual experimental data. [c]**The percentage of a lymphocyte subset** as determined in an experiment is denoted by an addition sign. [d]**Whole** denotes whole population studies. [e]**Dose** is the number of labelled lymphocytes infused in each experiment ($x10^9$). [f]**Viability** denotes the percentages of lymphocytes surviving after the labelling process. Viability tests were performed immediately before infusion. [g]**LFlow** is the mean number of lymphocytes draining from the efferent lymphatic vessel in 1 hour ($x10^7$ cells/ hr).

Even though it is possible to collect lymphocytes from lymphatic vessels in a number of locations in sheep, the efferent lymphatic vessels from popliteal and prescapular lymph node have commonly been selected. In each location, there is a single and isolated lymph node (ie not groups or chains of nodes). Furthermore, the efferent vessels from these nodes are easily identified and surgically accessed. In particular, the efferent vessel of the prescapular node lies superficially under the skin. The technique of efferent lymph vessel cannulation has been well described and widely reported. It offers the best opportunity to obtain information about lymph in an intact physiological environment. Operations requiring the insertion of polyvinyl chloride tubes into lymphatic vessels are not major as the exposed operative site is relatively small and does not involve major organs. Thus, the risk of post-operative complications (apart from those associated with general anaesthesia) is low.

Lymphocytes derived from the efferent vessel of either the prescapular or the popliteal lymph node were used in the present study. These cells are mainly small lymphocytes (ie mature lymphocytes) which are already fully capable of recirculating and migrating through the body (Abernethy *et al.*, 1990). For this reason they were considered to be more appropriate cells with which to initiate this study than the many stages of maturing lymphocytes residing in the lymphoid tissues.

In all experiments, the bolus infusion method (ie a rapid infusion in a short time period) was used to introduce the labelled lymphocytes into the venous blood via an indwelling catheter. This method was selected primarily in order to avoid the need for excessive lymphocyte manipulation, with the consequent risk of contamination and damage. The bolus infusion method has been criticised as unphysiological compared with slower infusion methods. However, no significant differences between these two infusion methods were reported in a trial lymphocyte recirculation study in sheep (Hall *et al.*, 1976).

The techniques that would be required if a slower infusion method had been selected, such as the use of a mechanical pump, are prone to increase physical damage to labelled lymphocytes. Even through labelled lymphocytes were resuspended in cell free lymph after the final step of labelling, this may not represent an authentic *in vivo* environment. Consequently, any prolongation of the infusion time would be liable to increase the death rate of lymphocytes in a laboratory environment and could permit deterioration of the fluorescent intensity of labelled lymphocytes. Furthermore, the use of a pump could not necessarily guarantee a steady rate of entry of cells into the circulation. It has been observed

occasionally in the present study that aggregations or clumps of lymphocytes were attached along the inner wall of tubing and connectors.

The experimental time for all 21 experiments was 167.86 ± 74.62 hours (mean ± standard deviation, SD). The time of termination of an experiment was determined either by the accumulation of sufficient data (which generally required approximately 7-10 days after infusion) or by an abrupt decrease in the number of lymphocytes in efferent lymph. In other word, the experiment was performed under conditions of a steady level of lymphocyte output from efferent lymph. Consequently, the variation in number of lymphocytes draining in efferent lymph between individual experiments was small (data not shown). The overall mean number of lymphocytes draining from the efferent lymphatic vessel for 19 experiments was 14.97 ± 3.55x10^7 cells per hour. The number of labelled lymphocytes infused in an experiment averaged 1.44 ± 0.79x10^9. Before each infusion, about 5x10^6 labelled lymphocytes were examined by flow cytometry to demonstrate the labelling efficiency with the fluorescent dye (CFSE) of those lymphocytes and their subsequent viability (PI test). The labelling efficiency with the fluorescent dye was shown to range from 95 to 99% in most experiments (ie more than 95% of lymphocytes take up the CFSE, data not shown). There were no significant differences between the viability of lymphocytes before and after labelling (data not shown). The viability of lymphocytes after labelling was in the range of 88.50% to 99.70% in most experiments with a mean value of 97.21 ± 3.95%.

This high level of viability confirms both the minimal toxicity of the CFSE (Weston and Parish, 1992) and the low incidence of damage to labelled lymphocytes during manipulation. Consequently, the subsequent kinetics of migration of those lymphocytes could reasonably be expected to reflect the overall kinetics of intact recirculating lymphocytes. The viability of labelled lymphocytes, which reappeared in the efferent lymph after infusion, was not tested. However, viable lymphocytes were selected at the time of flow cytometry (ie by the use of their different cell morphology to exclude all other cells). This was based on the principle that "all other cells" including dead cells and debris would show a different pattern in a plot of lymphocytes in between the forward and 90° light scatter (see more detail in Chapter 2- Flow cytometry study).

CFSE is an ideal dye for long-term *in vivo* migration studies as it establishes a strong covalent bond with the intracellular macromolecules of lymphocytes, so extending its retention time within the cells (Weston and Parish, 1992). There was no evidence either from the present study or from previous reports to

suggest any likelihood of re-utilisation of CFSE released from labelled lymphocytes after re-infusion. Lymphocyte division results in a halving reduction of fluorescent intensity for each division (Lyons and Parish, 1994), but there was no suggestion of such a reduction in the present study.

The experiments described in this chapter were intended to provide data to be used for subsequent modelling of cell migration. Since the modelling procedures to be described in subsequent chapters required a certain minimum amount of information, any experiments which failed (ie which were involuntarily terminated) before 72 hours after lymphocyte infusion will be ignored. In most experiments (19 out of 21), the site of cannulation, both for collection of lymphocytes to be suitably labelled and reinfused, and for the retrieval of labelled, recirculating lymphocytes, was the prescapular efferent lymphatic vessel. Only 2 experiments (R153(1) and R153(2)) were undertaken using the popliteal efferent lymphatic.

In all experiments, labelled lymphocytes were treated as a single population (non-specific phenotype). All of these experiments can be categorised as whole population studies. However, there is some evidence that the surface antigens presented may affect the migration kinetics of recirculating lymphocytes (Washington *et al.*, 1988; Abernethy *et al.*, 1990; Abernethy *et al.*, 1991). For this reason, some expanded studies (11 out of 21 experiments) were undertaken using separated lymphocyte subsets to determine whether any differences in migration kinetics were identifiable between lymphocyte subsets. Lymphocyte subsets, including CD4, CD5, CD8 and CD45R, were detected by additional monoclonal staining techniques as described in Chapter 2.

All flow cytometry studies were undertaken using the standard laser beam and configurations of the FACScan flow cytometer (Fluorescence Activated Cell Analyser, Becton Dickinson, San Jose, CA, USA). The number of cells required was approximately 20,000-50,000 for each sample. In this section, typical results (data from R634) of flow cytometry are demonstrated (Figure 3.1). More detail of flow cytometry studies was given in Chapter 2.

Figure 3.1: Analysis of flow cytometry

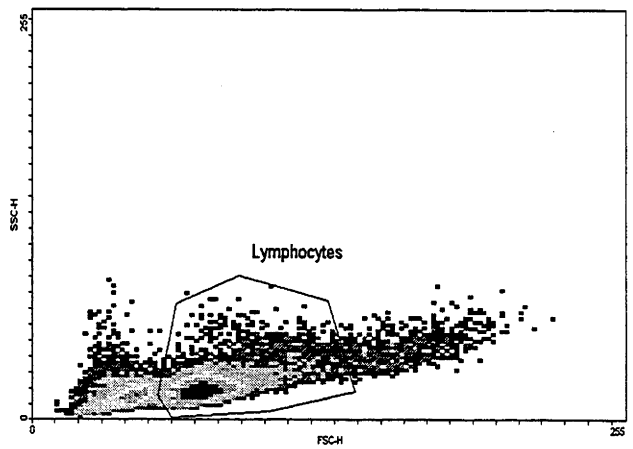

All samples are gated for lymphocyte populations on both forward light scatter (FSC-H) and 90° light scatter (SSC-H) to exclude any other cells, debris and cell clumps.

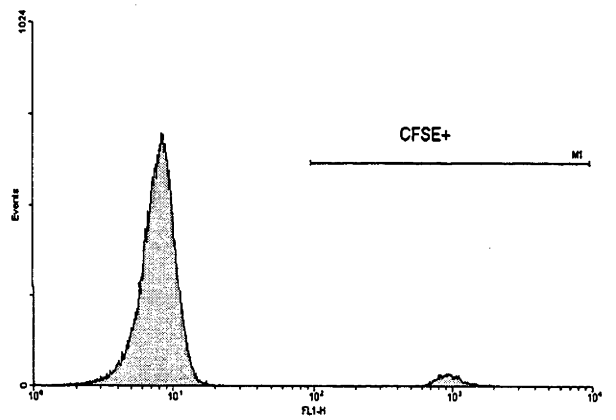

The histogram illustrates the number of events versus the level of CFSE expression in the FL1 detector (log integrated green fluorescence). The majority of cells are non-CFSE labelled (ie control lymphocytes) The CFSE labelled lymphocytes fall in the range of fluorescence intensities designated by the marker region M1.

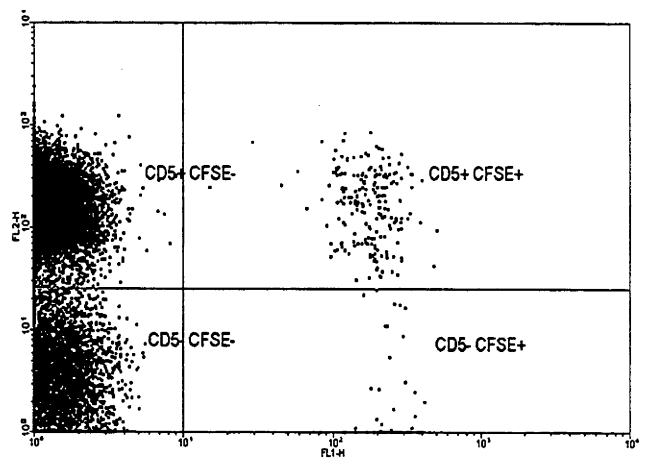

In subset studies, the dot plot of FL1 (log integrated green fluorescence) and FL2 (log integrated red fluorescence) were used to display the relative levels of CFSE and PE respectively. A quadrant was set based on the negative control to allow quantitation of the numbers of lymphocyte subsets according to the properties of fluorochrome(s) binding to each lymphocyte.

3.2 Results of whole population studies

In this section, lymphocyte samples were examined to determine their percentages of labelled cells. The labelled lymphocytes used in the present study were assumed to represent the whole recirculating lymphocyte population. Observations of the level of labelled lymphocytes were made on both blood and efferent lymph and, are summarised, compared with some previous studies and presented in sections 3.2.1 and 3.2.2 respectively.

3.2.1 The disappearance of labelled lymphocytes from venous blood

Information obtained by blood sampling is invaluable for many types of dynamic studies because it can be undertaken without interrupting the normal physiological function of the blood circulation. Almost all transportation processes (ie of oxygen, drugs, cells and so on) occurring in living tissues or organs are, directly or indirectly, dependent upon the blood circulatory system. Venous blood has often been selected for sampling, not only for lymphocyte recirculation studies but also for a substantial number of biomedical studies, on account of its accessibility as mentioned in section 3.1. In lymphocyte recirculation studies, after a bolus infusion of labelled lymphocytes, the frequency of labelled lymphocytes in blood always follows a declining pattern. The term disappearance is used to describe this declining pattern.

Observations from previous studies

In a previous study of lymphocyte recirculation in rats (Smith and Ford, 1983), lymphocytes obtained from the thoracic duct were collected, radioisotopically labelled, and intravenously reinfused into rats. The level of labelled lymphocytes (ie expressed as percentages of radioactivity recovered compared with the initial infused activity per organ or tissue) was determined in venous blood, and in several tissues and organs at sequential time points after infusion. The first, instantaneous venous blood sampling was performed immediately after infusion, followed by further samplings at 1, 5, 30 and 60 minutes during the first hour. A few minutes after infusion, labelled lymphocytes had been distributed to a number of tissues and organs throughout the body. The major sites in which lymphocytes appeared were lungs, spleen, liver, lymph nodes and bone marrow. The rapidity of lymphocyte recirculation from blood to several sites in the body was established by the results of this study. For example, very rapid transportation of labelled lymphocytes from blood to lungs and liver was observed. The radioactivity level of labelled lymphocytes, expressed as a

percentage of dose infused was about 40% in blood, 40% in the lungs and 13% in the liver 1 minute after infusion. Subsequently, high levels of labelled lymphocytes were observed in blood, lungs and liver for the first few minutes after which they fell exponentially to reach a relatively stable level by 60 minutes. On the other hand, the level of labelled lymphocytes attained a peak value of about 40% in the spleen by 30-60 minutes after infusion.

Findings of the disappearance of labelled lymphocytes from venous blood similar to those obtained in rats have been reported in lymphocyte recirculation studies in sheep (Frost *et al.*, 1975; Hall *et al.*, 1976; Borgs and Hay, 1986; Witherden *et al.*, 1990). The highest level of labelled lymphocytes in blood was observed during the first hour after an intravenous infusion of labelled lymphocytes. This was followed by a rapid decline during the first 12 hours, and a slower decline in the next 12 hours to reach a more stable level by 24 hours. The levels of labelled lymphocyte subsets (CD4, CD5 and Gamma-delta) in blood were observed to decrease by 80% of their initial levels over the first 3 hours (Witherden *et al.*, 1990). Additionally, it has been suggested that about 70-80% of labelled lymphocytes disappear from the blood almost immediately after they are infused (Hall *et al.*, 1976). However, none of these studies reported in greater detail on the pattern of disappearance of labelled lymphocytes during the period immediately after infusion (especially during the first hour) as described in rats by Smith & Ford (Smith and Ford, 1983).

Observations from the present study

In the present study, the percentages of labelled lymphocytes in venous blood were observed by repetitive venous blood sampling. In most experiments, these observations were made at 2, 5, 10, 20, 30 minutes, 1, 2, 3, 4, 6, 12 and 24 hours after infusion, and thereafter every 24 hours until the end of the experiment. Figure 3.2(a) illustrates a typical pattern of disappearance of labelled lymphocytes from the venous blood of one experimental animal (R705). All actual data of individual experiments are given in Figure 3.5A-3.5W at the end of this section. In all experiments, the highest percentages of labelled lymphocytes in venous blood occurred during the first hour after infusion. This was followed by a rapid decrease in the percentage of labelled lymphocytes in venous blood during the first 12 hours leading to attainment of a relatively steady state after 24 hours. Fluctuations in the levels of labelled lymphocytes beyond 24 hours were invariably minor, resulting in a plateau pattern. In almost all experiments, the percentages of labelled lymphocytes in the blood remained relatively constant at a non-zero level until the end of the observation period.

Figure 3.2: The disappearance of labelled lymphocytes from venous blood

a

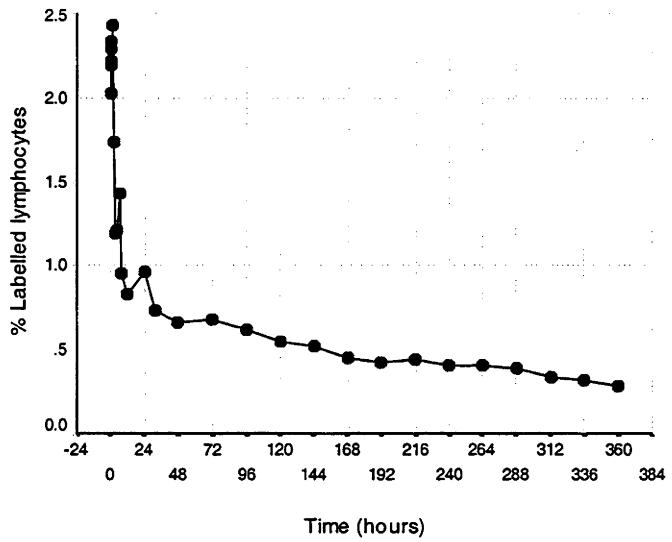

Figure 3.2 (a) demonstrates a typical pattern of disappearance of labelled lymphocytes in the venous blood along the time scale (in hours). Time zero is the starting time at which labelled lymphocytes were infused. This data was derived from R705.

b

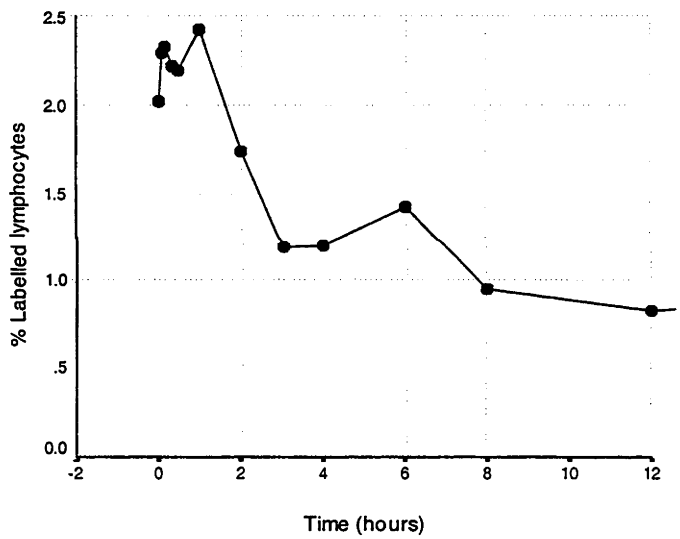

Figure 3.2 (b) is the enlargement of Figure 3.2(a) during the first 12 hours. The moderate variation of labelled lymphocytes is clearly observed in the first 60 minutes. The highest level of labelled lymphocytes is observed at 1 hour, together with a small rise in level at 6 hours after infusion.

Closer examination of the pattern of labelled cells in the blood during the first 12 hours (Figure 3.2(b)) revealed considerable fluctuation in the percentages of labelled lymphocytes in the first few hours. This was especially noticeable during the first 60 minutes. In most experiments, the percentages of labelled lymphocytes observed at either 4 or 6 hours were slightly in excess of the levels during the previous 1 to 4 hours (Figure 3.2(a) and 3.2(b)).

The disappearance pattern of labelled lymphocytes from venous blood observed in the present study was very similar to those of previous studies in sheep (Frost *et al.*, 1975; Hall *et al.*, 1976) but slightly different in time scale compared with

those in rats (Smith and Ford, 1983; Westermann *et al.*, 1988). Data on percentages of labelled lymphocytes in blood were selected from 8 different experiments and normalised to the maximal value of 1. Figure 3.3 (upper panel), illustrates a simultaneous scatter plot of all normalised data and their least square means (illustrated in a surface plot). The figure reveals a trend of disappearance of labelled lymphocytes from the blood identical with that previously described.

In 13 out of a total of 21 experiments (ie in about half of all experiments), the highest percentages of labelled lymphocytes in the blood were attained by 2 minutes after infusion (ie at the time of taking the first blood sample). However, in 8 experiments out of the total, the highest percentages of labelled lymphocytes were not observed at 2 minutes but at another time, between 5 minutes and 1 hour after infusion. For example in Figure 3.2(b), ie sheep R705, the highest percentage of labelled lymphocytes (ie 2.428 %) was observed at 1 hour. Nevertheless, the highest percentages of labelled lymphocytes did not occur later than 1 hour in any experiment. As previously mentioned, the level of labelled lymphocytes in the blood at the end of the observation period remained above zero in most experiments. However this was not the case for R021(2) (Figure 3.5K upper panel). In this experiment, the percentage of labelled lymphocytes in the blood dropped to a value close to zero within 72 hours.

In the first few minutes after infusion, labelled lymphocytes were re-assorted and distributed to several tissues. The unstable period that is indicated by large fluctuations and rapid decrease in the percentages of labelled lymphocytes in the first 24 hours may be explained as a transitional stage during which labelled lymphocytes newly introduced into the blood circulation are being redistributed in a variety of tissues. In most experiments, the occurrence of the highest percentages of labelled lymphocytes in the venous blood at 2 minutes implies that the labelled lymphocytes were very rapidly mixed and redistributed in the blood circulation. According to data from studies in rats (Smith and Ford, 1983), the variations in occurrence of the highest percentages of labelled lymphocytes in the venous blood, observed within the first hour, may be due to a rapid return of a large number of recirculating lymphocytes from lungs and liver.

The increase in percentage of labelled lymphocytes observed at 4-6 hours is unlikely to represent an experimental error for several reasons. In the first place, the pattern was similar in most experiments. Secondly, this finding was observed not only in the present study but also in that of Smith and Ford (Smith and Ford, 1983). It was also evident in the application of a theoretical model of lymphocyte

recirculation (Stekel *et al.*, 1997; Stekel, 1998). The explanation for increase in percentage of labelled lymphocytes at 4-6 hours is likely to be similar to that for variation in the occurrence of the highest percentages of labelled lymphocytes in the venous blood during the first hour. The influence of return to the blood circulation of a large number of labelled lymphocytes (ie up to 40%) residing in the spleen during the first few hours is believed to be responsible (Smith and Ford, 1983).

The findings in the present study indicated that lymphocyte recirculation to the blood is a rapid event. Both the variation in occurrence of the highest percentages of labelled lymphocytes in venous blood in the first hour and the increase in percentage of labelled lymphocytes observed at 4-6 hours have been attributed to lymphocyte recirculation from lung and liver, and spleen. If labelled lymphocytes were unable to recirculate back to the blood circulation, the percentages of these cells in the blood should follow an exponential decay pattern and not increase at any time after infusion. Furthermore, the relatively stable level of labelled lymphocytes in blood after 24 hours (as reflected in a smoother pattern compared with earlier measurements) implies that most re-assortment and re-distribution of labelled lymphocytes has already occurred during the first 24 hours.

An unusual decrease in the of level of labelled lymphocyte in the blood of one sheep (R021(2), Figure 3.5K-upper panel) suggests that a large proportion of the labelled lymphocytes disappeared from the blood circulation faster than was normally observed in the other experiments. The possibility that a large number of labelled lymphocytes had died during the experiment appears doubtful. The viability of labelled lymphocytes prior to infusion was 99.65%. No satisfactory explanation for this result is apparent.

Figure 3.3: The scatter plots of normalised blood and lymph data (upper and lower panel respectively) and the surface plots of their least square means.

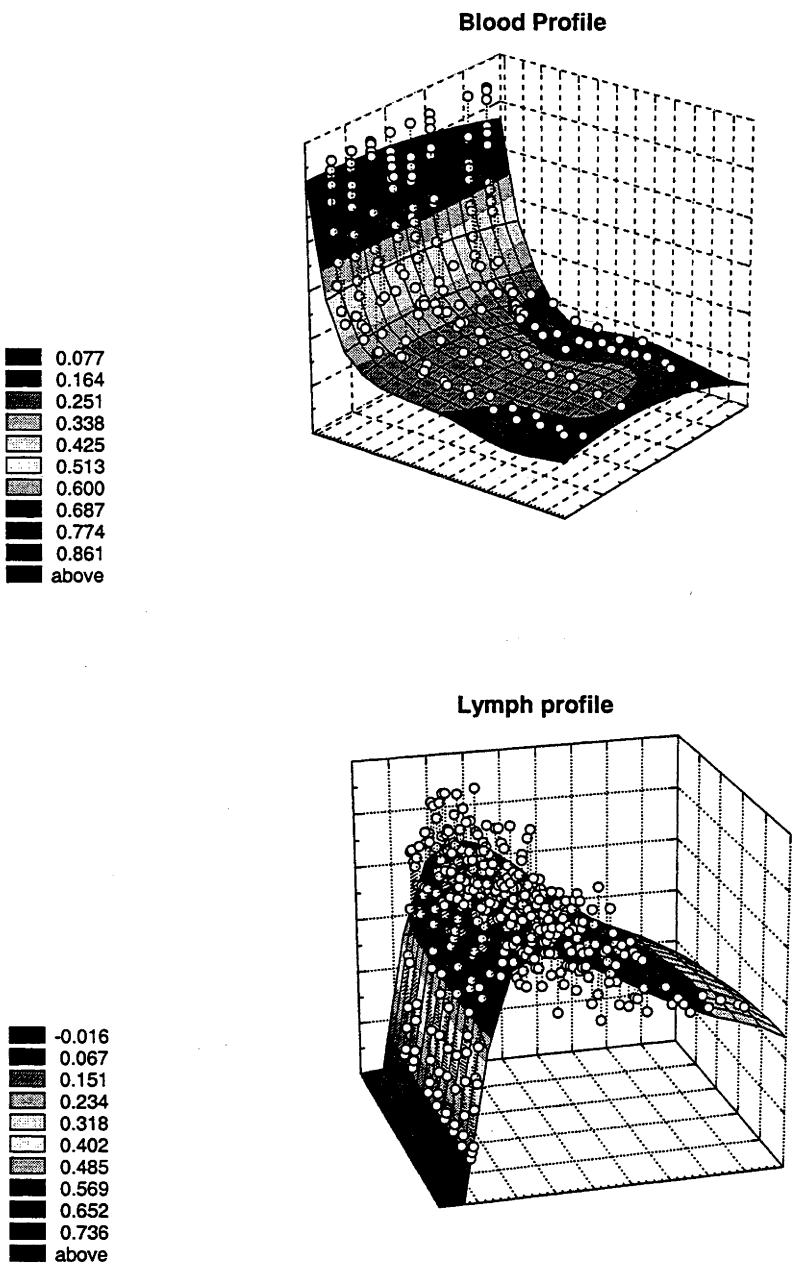

3.2.2 The appearance of labelled lymphocytes in efferent lymph

A general feature of lymphocyte recirculation studies is that, after introduction of a certain number of labelled lymphocytes, the levels of those labelled lymphocytes in the lymphatic vessel(s) under study are monitored at sequential time points. The level of labelled lymphocytes in lymph in such experiments always starts from an unobservable or a very small value during the first hour after infusion and gradually rises to a certain level over the course of a few days.

Observations from previous studies

In a lymphocyte recirculation study in rats (Ford and Simmonds, 1972), the appearance of radioactively labelled lymphocytes in the thoracic duct was monitored after intravenous infusion of these cells. An automatic fraction collector was used to collect two-hourly fractions of lymph for a total of 36 hours. Labelled lymphocytes were first detected, albeit at a very low level, in the first 2 hours. The level rapidly increased from 2 to 8 hours, reached a maximal peak around 12 to 18 hours, then fell abruptly from 18 to 24 hours and continued to fall more gradually after 36 hours. The findings of this study were very similar to those of other studies in rats (Smith and Ford, 1983; Westermann *et al.*, 1988).

The tempo of lymphocyte appearance in the efferent lymph from a sheep peripheral lymph node, after intravenous infusion of labelled lymphocytes, has been described in a number of lymphocyte recirculation studies (Hall *et al.*, 1976; Trevella and Morris, 1980; Chin and Cahill, 1984). In one experiment of Frost *et al* (Frost *et al.*, 1975), the efferent lymph was collected by a fraction collector every 20 minutes over the first 60 hours following an infusion of radioisotopically labelled lymphocytes. It was reported that labelled cells first appeared 3 hours after infusion. Subsequently, the level of labelled lymphocytes increased steadily over the next 24 hours before reaching a peak at 27-36 hours and progressively falling over the following 48-72 hours (Frost *et al.*, 1975). Similar patterns of lymphocyte appearance in the efferent lymph have been observed, with minor variations of timing, in the other studies (Issekutz *et al.*, 1980; Trevella and Morris, 1980; Reynolds *et al.*, 1982; Chin and Cahill, 1984).

Observations from the present study

In most of the experiments in the present study, after the labelled lymphocytes were intravenously infused and efferent lymph was freely drained into 15 ml plastic containers. No additional anti-coagulant was required in containers as 2%

EDTA was continuously infused to mix with the draining lymph. In most experiments (12 out of 21 experiments), lymph was collected by an automatic fraction collector every two hours for the first 48 hours and every four hours thereafter. For each sample, a minimum lymph volume of about 5 ml was required for examination. Lymph draining between samplings was discarded and kept in a large container (with a volume of 600 ml) for the purpose of total volume and cell count calculation. The period required for collection of each sample of efferent lymph was about 15-30 minutes depending on the lymph flow rates in individual animals at the time. Lymph data in the present study will be regarded as instantaneously collected data.

The first reappearance of labelled lymphocytes was recognised in the 2 hour sample of efferent lymph in most experiments (16 out of 21). However the percentages of labelled lymphocytes detected in that (ie the 2 hour sample of efferent lymph) were very small (ie of the order of 0.001 to 0.01%). A gradual increase in the percentage of labelled lymphocytes was observed in all experiments. The highest percentages of labelled lymphocytes occurred at some time between 24 and 72 hours in most experiments. A typical pattern of appearance of labelled lymphocyte in efferent lymph obtained from R705 is demonstrated in Figure 3.4 (a). All actual data from individual experiments will be given in Figure 3.5A-3.5W at the end of this section. The rate of increase in percentage of labelled lymphocytes was highest between 4 to12 hours as reflected in a very steep slope. The rate of increase gradually declined to zero at the time of occurrence of the highest percentages of labelled lymphocytes (ie peak). After this peak, the percentage of labelled lymphocytes slowly declined at a relatively stable rate until the end of the experiment (Figure 3.4 (a)). The percentage level at the end of the observation period in most experiments remained in excess of half of the observed maximum. For example, in Figure 3.4(a), of which the experimental time was 360 hours, the percentages of labelled lymphocytes in efferent lymph at the end of the experiment dropped to slightly in excess of half of its highest level by around 36 hours.

Data on percentages of labelled lymphocytes in efferent lymph were selected from 8 different experiments and normalised to the maximal value of 1. Figure 3.3 (lower panel), illustrates a simultaneous scatter plot of all normalised data and their least square means (illustrated in a surface plot). The figure reveals a trend of appearance of labelled lymphocytes in efferent lymph identical with that previously described.

Figure 3.4: The appearance of labelled lymphocytes in efferent lymph

a

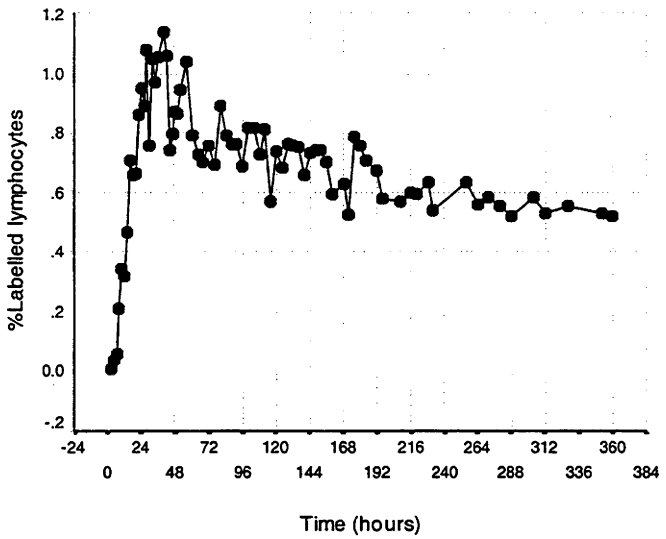

Figure 3.4 (a) demonstrates a typical pattern of appearance of labelled lymphocytes in the efferent lymph over a time scale (in hours). Time zero is the starting time at which the labelled lymphocytes were infused. This result was obtained with R705.

b

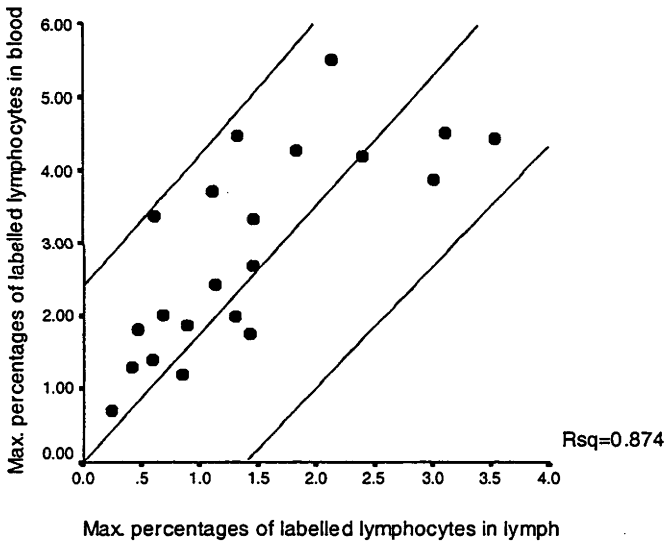

Figure 3.4 (b) demonstrates a linear regression plot between the maximal percentages of labelled lymphocytes found in blood and lymph samples. It implies a good linear relationship with an R squared value of 0.8263. Data from 8 different experiments are used in this plot. The middle line denotes the mean linear regression line; the two outer lines denote the 95% confidence interval.

In some experiments, the techniques for collecting the efferent lymph varied slightly from those described in the first paragraph of this section. For example, in B481 and B687, efferent lymph was collected in a plastic bottle fixed to the skin of sheep. Bottles containing efferent lymph were manually changed after a period of 2 to12 hours depending on the time of the day. In B857(1), B857(2), B045, R021(2), R153(1) and R153(2)), efferent lymph was collected by an automatic fraction collector every four hours throughout the entire experiment. Apart from these variations in efferent lymph collections, the pattern of appearance of labelled lymphocytes in efferent lymph in most experiments remained as previously described. The highest percentages of labelled

lymphocytes were still observed at some time between 24 and 72 hours. The time of observation of the first appearance of labelled lymphocytes in efferent lymph was subject to some slight variations in accord with variation in sampling technique.

The occurrence of a peak percentage of labelled lymphocyte could not be clearly observed in 6 (B481, B445(1), B445(2), B882, R021(1) and B045) out of 21 experiments (lower panels of Figure 3.5A, 3.5 C, 3.5D, 3.5E, 3.5H, and 3.5J respectively). In most experiments that generated sufficient data (ie had a long experimental time), the occurrence of the peak percentage of labelled lymphocytes was generally readily detected. Uncertainty about the occurrence of a peak of labelled lymphocytes in some experiments, such as those using sheep B882, R021(1) and B045, (lower panels of Figure 3.5E, 3.5 H and 3.5J respectively) was attributable to a relative shortage of data collected. However, this was not the case in some other experiments, such as those using sheep B481, B445(1) and B445(2) (Lower panels of Figure 3.5A, 3.5 C and 3.5D respectively), in which the period of lymph collection was 136, 124 and 100 hours respectively. In these experiments, it nevertheless remained difficult to identify the occurrence of the highest level. There might have been some relationship between the disappearance pattern from blood and the visibility of peak percentages of labelled lymphocytes in the efferent lymph. However, simple observation did not permit the formulation of any conclusions on such a relationship at this stage.

The percentages of labelled lymphocytes in the efferent lymph of sheep R021(2) (lower panel of Figure 3.5K) dropped almost to zero 96 hours after infusion. This was quite an unusual feature. These findings in efferent lymph corresponded well with those in the blood of this sheep, which contained relatively low percentages of labelled lymphocytes, as described in the previous section.

A closed relationship between the maximum percentages of labelled lymphocytes in the blood and efferent lymph has been observed from the results of the present study. To quantify this observation and define the relationship, a simple linear regression analysis was performed. The maximum percentages of labelled lymphocytes in lymph corresponded well with those in blood with the R squared value of 0.874, ie fairly fitted with a linear regression (Figure 3.4 (b)). Such a finding may support the proposal of a linear system for the lymph node previously described in Chapter 1. In other words, an increase in number (or percentages if a fixed blood volume is assumed) of recirculating lymphocytes in

the blood may linearly increase the number (or percentage) of appearance of labelled lymphocytes in the efferent lymph.

Figure 3.5A-3.5W summarise all actual data obtained from individual experiments. The percentages of CFSE labelled lymphocytes (and some major subsets) in blood (upper panels) and efferent lymph (lower panels) have been plotted on the y-axis along with the experimental time (hours) on the x-axis. Closed circles represent the CFSE labelled lymphocytes whilst opened triangles, squares, circles and inverted triangles represent CD4, CD5, CD8 and CD45R lymphocyte subsets respectively.

Figure 3.5A: Experimental data from B481

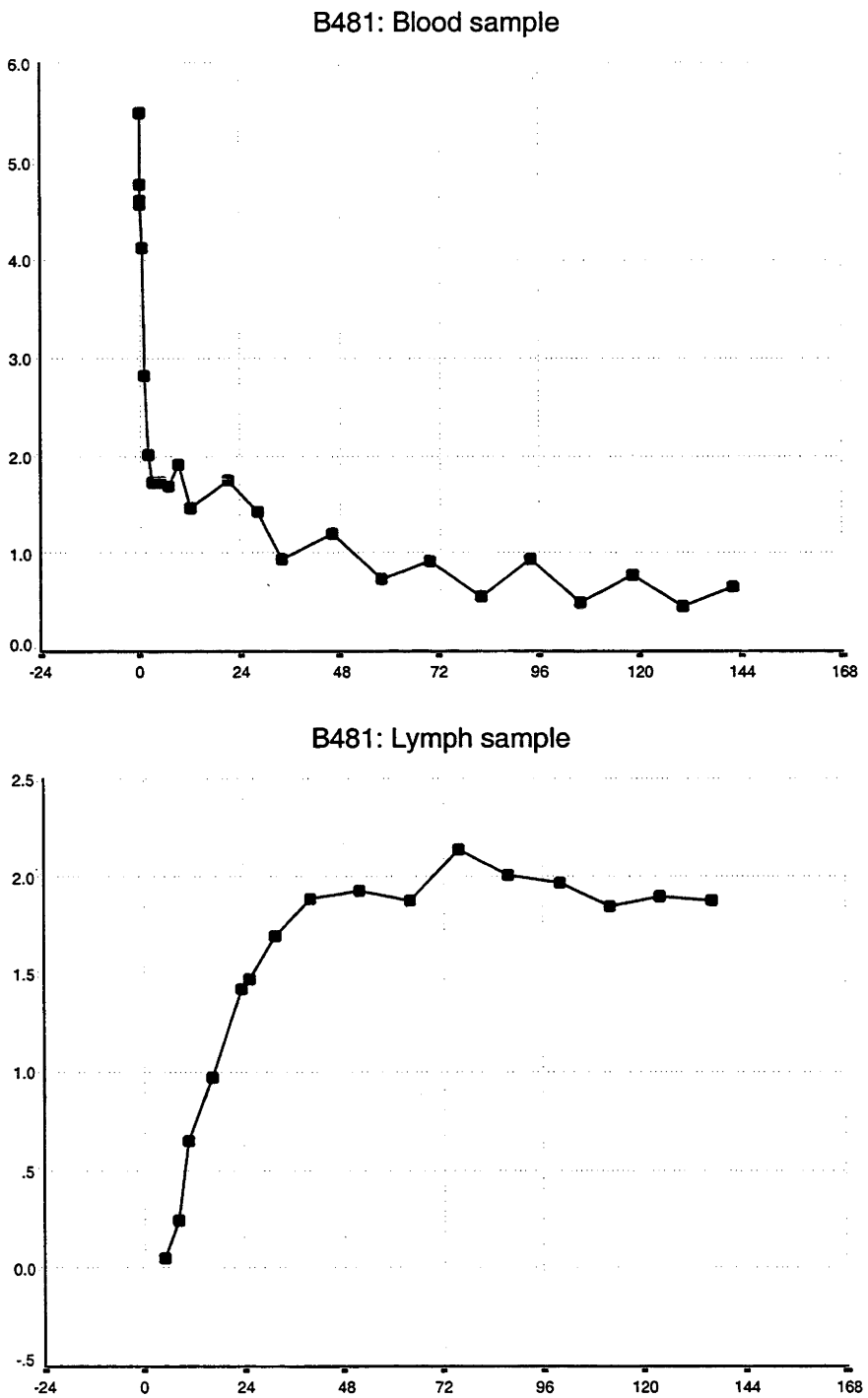

Figure 3.5B: Experimental data from B687

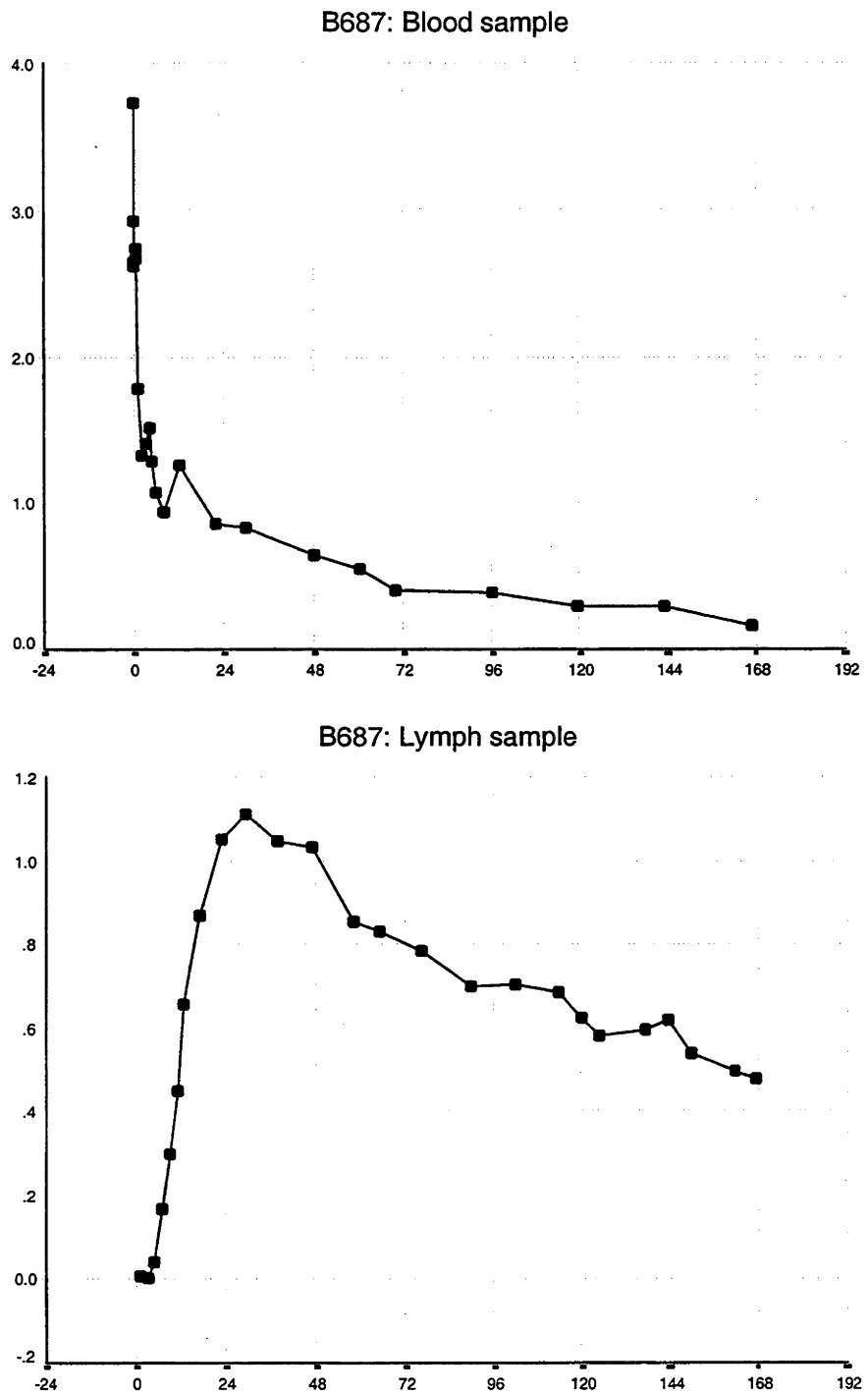

Figure 3.5C: Experimental data from B445(1)

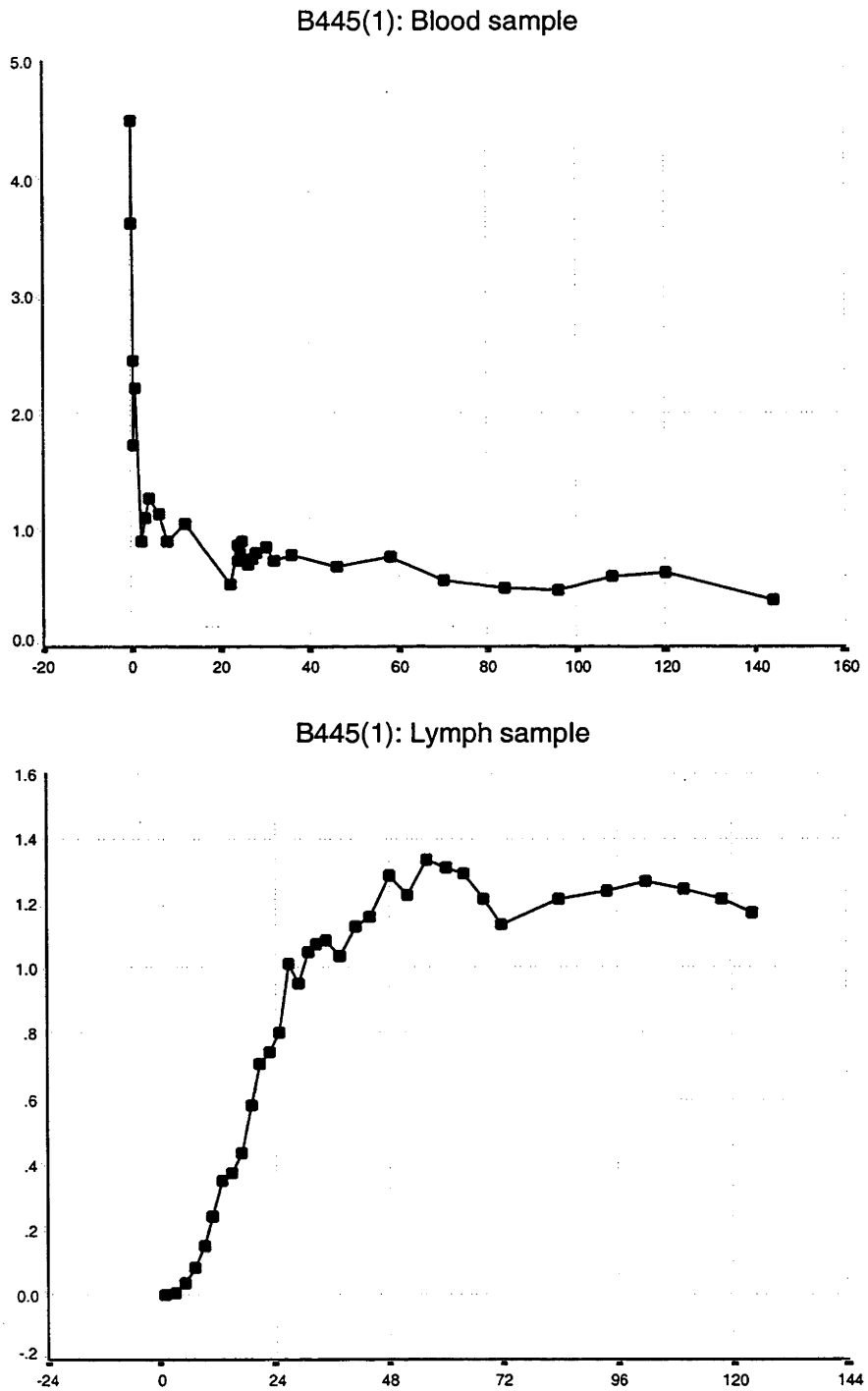

Figure 3.5D: Experimental data from B445(2)

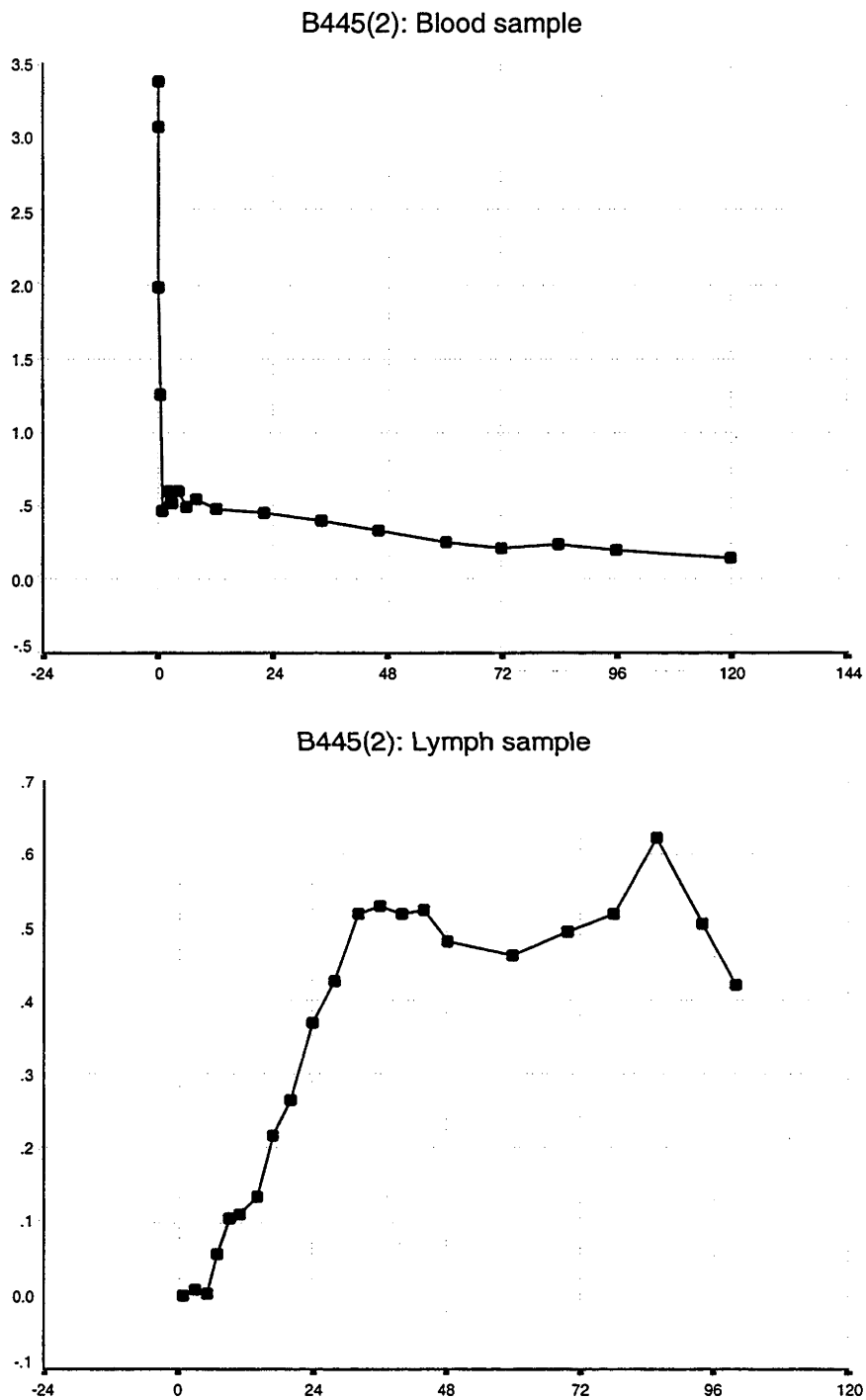

Figure 3.5E: Experimental data from B882

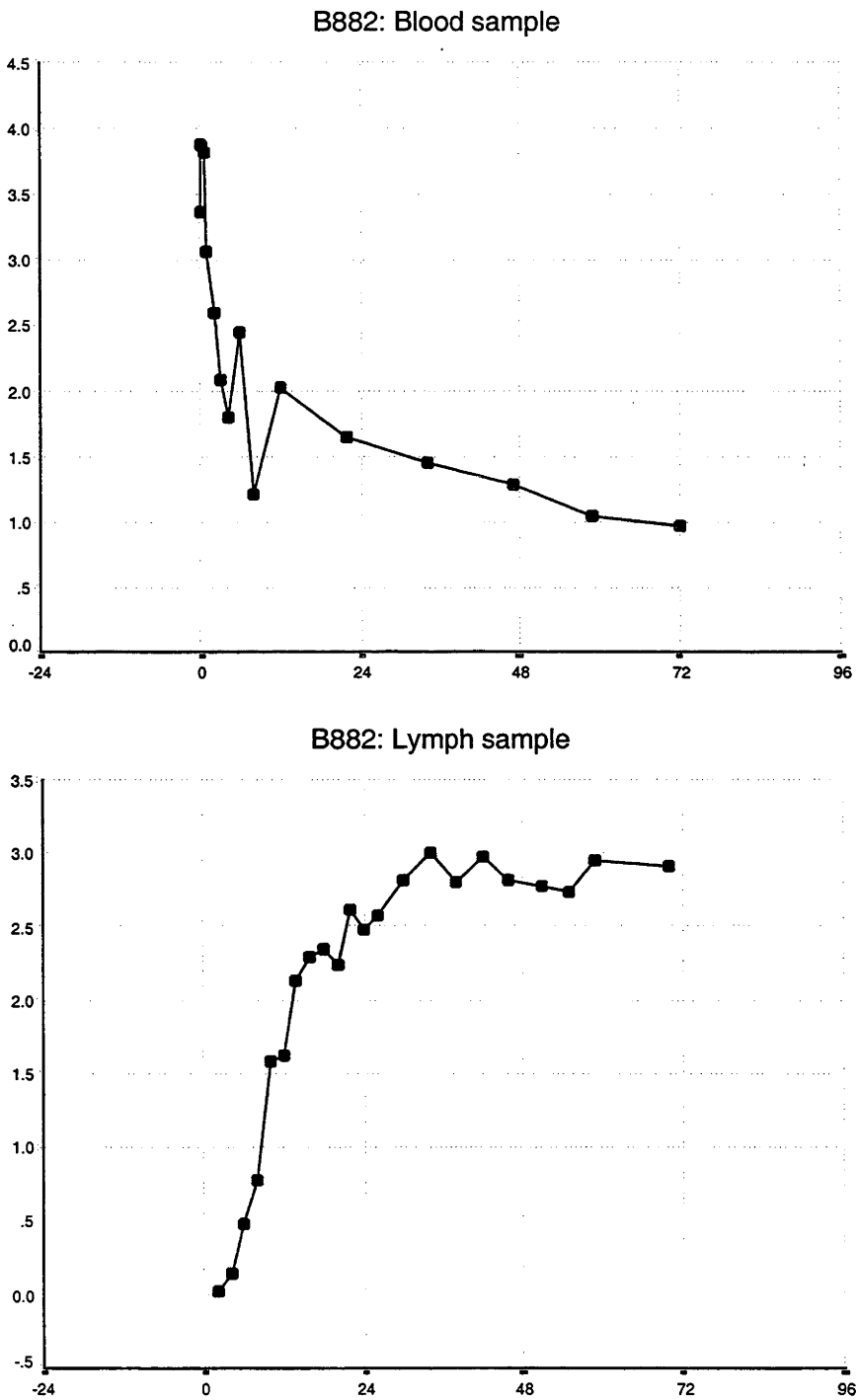

Figure 3.5F: Experimental data from B857(1)

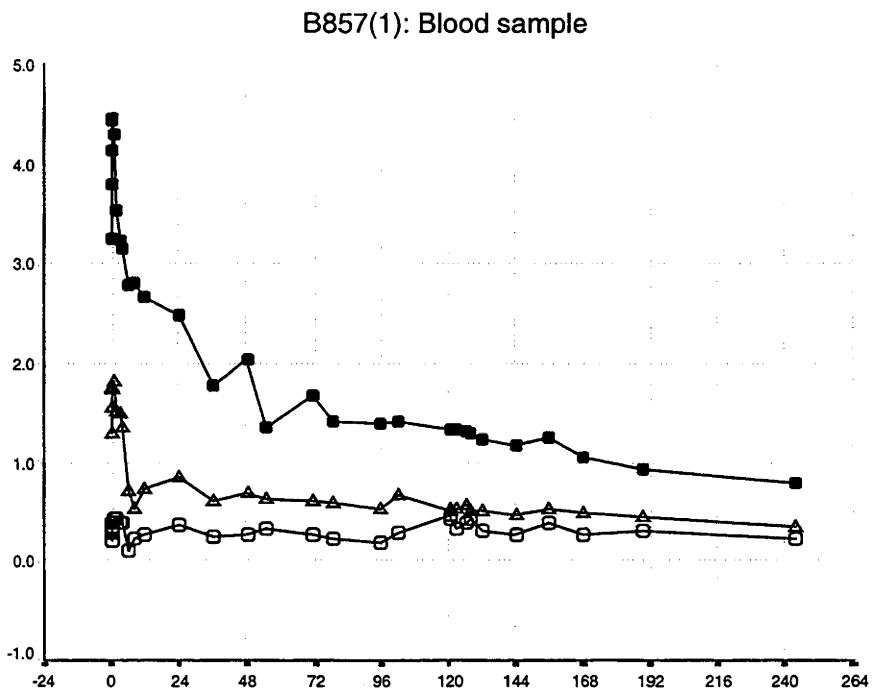

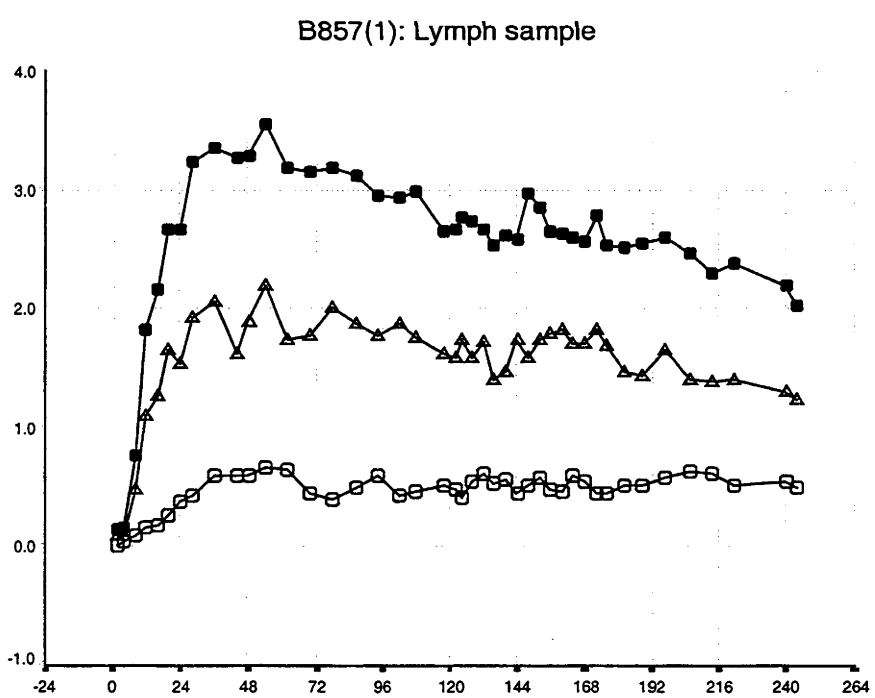

Figure 3.5G: Experimental data from B857(2)

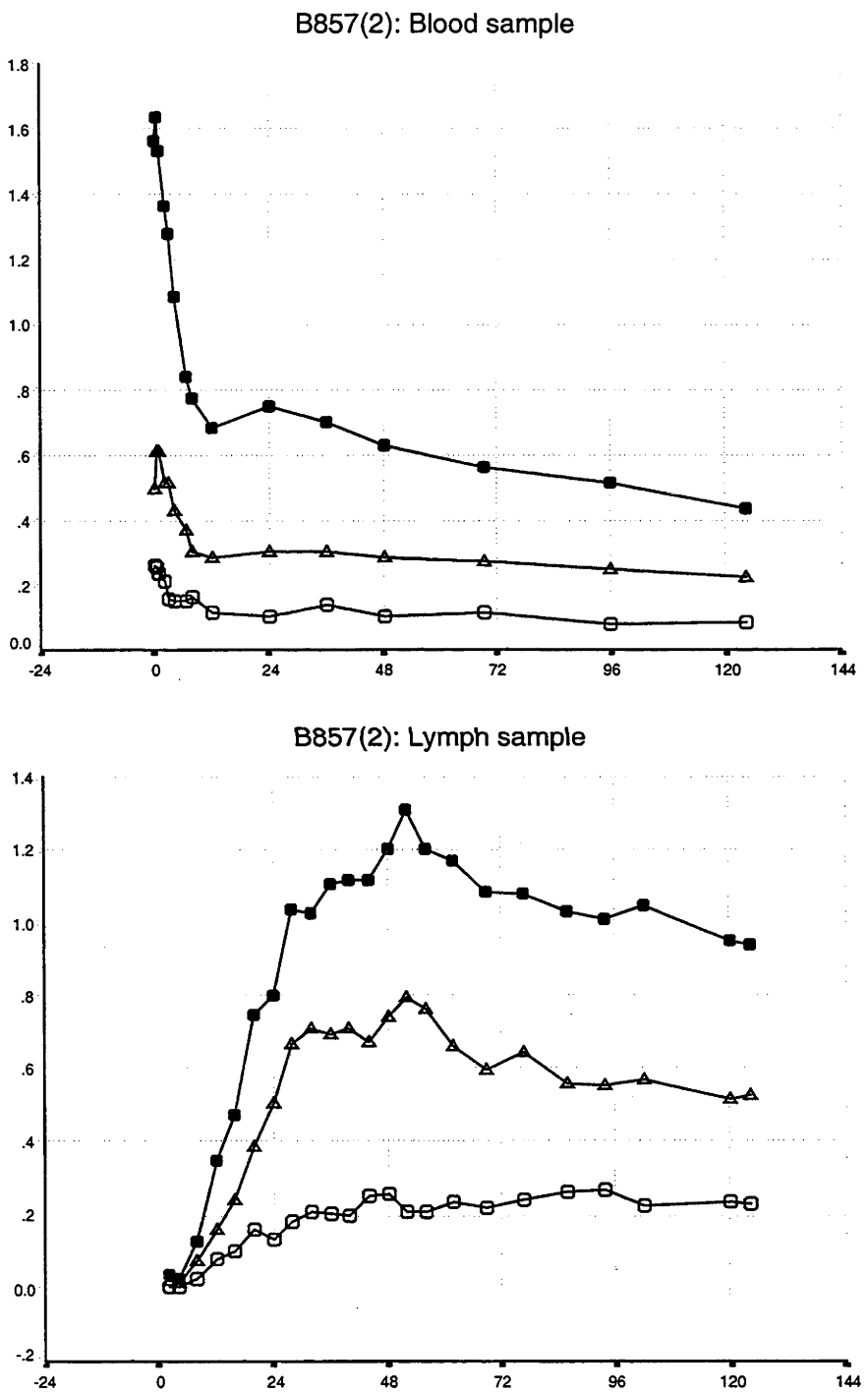

Figure 3.5H: Experimental data from R021(1)

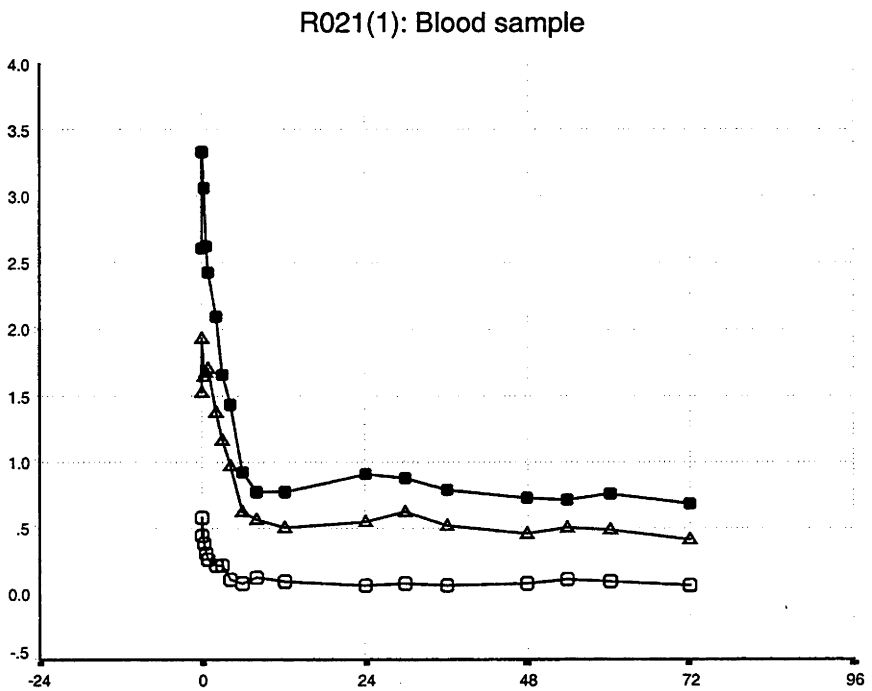

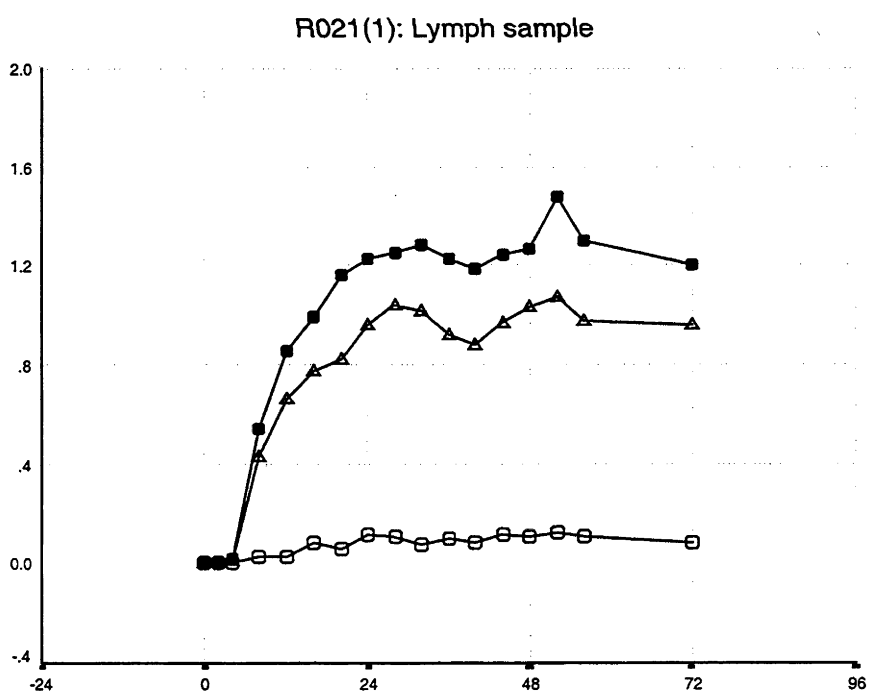

Figure 3.5J: Experimental data from B045

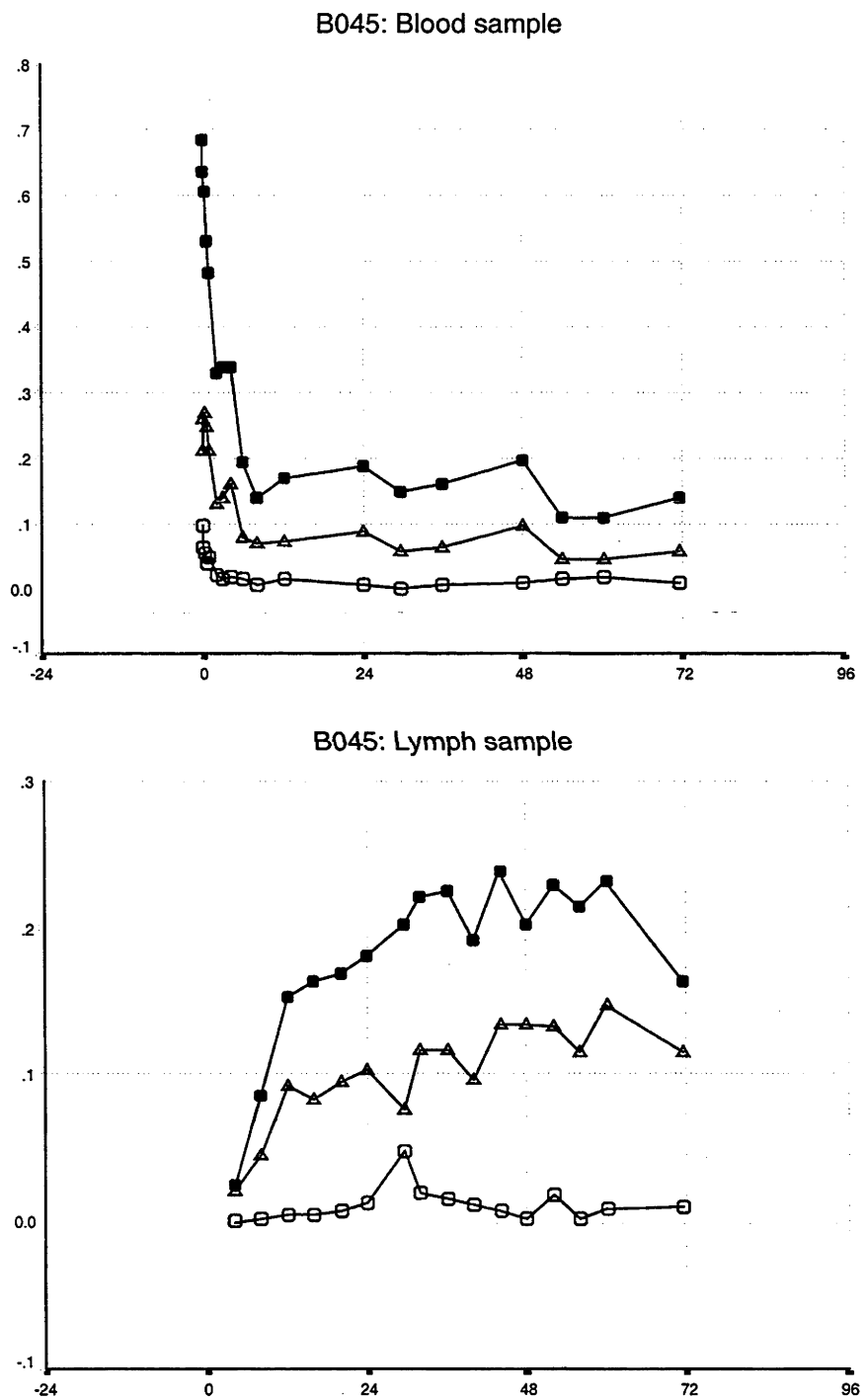

Figure 3.5K: Experimental data from R021(2)

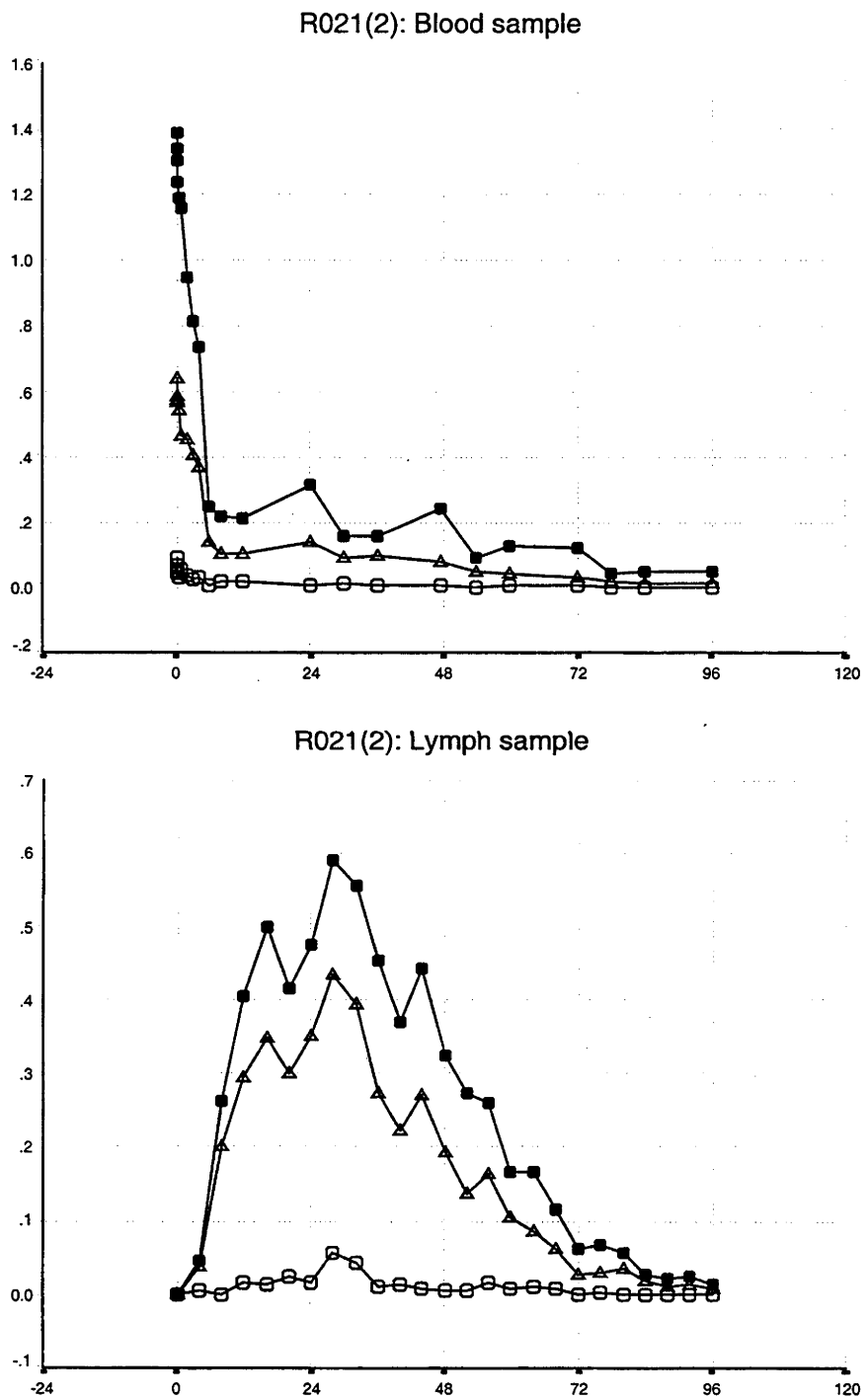

Figure 3.5L: Experimental data from R153(1)

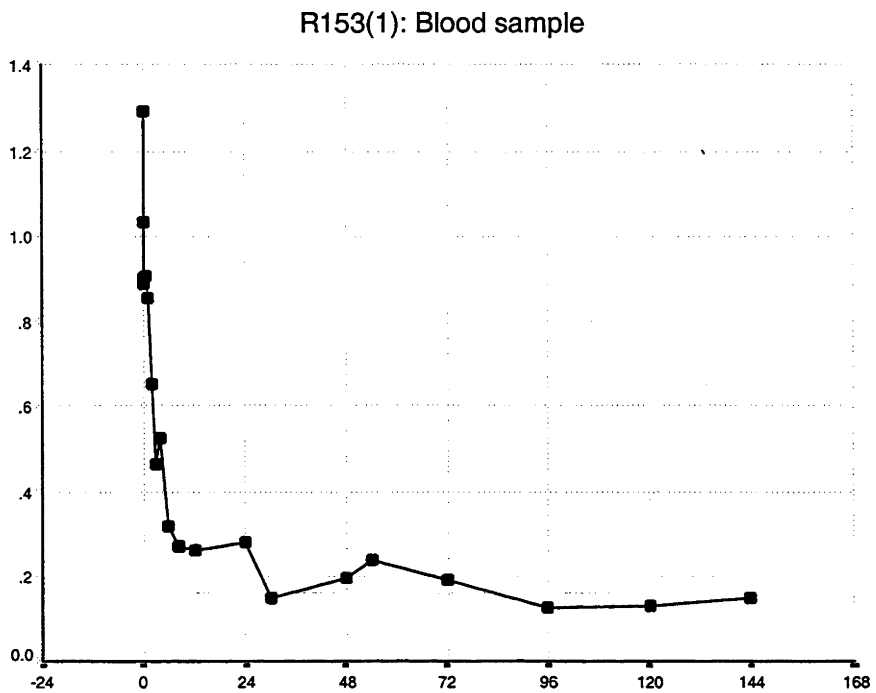

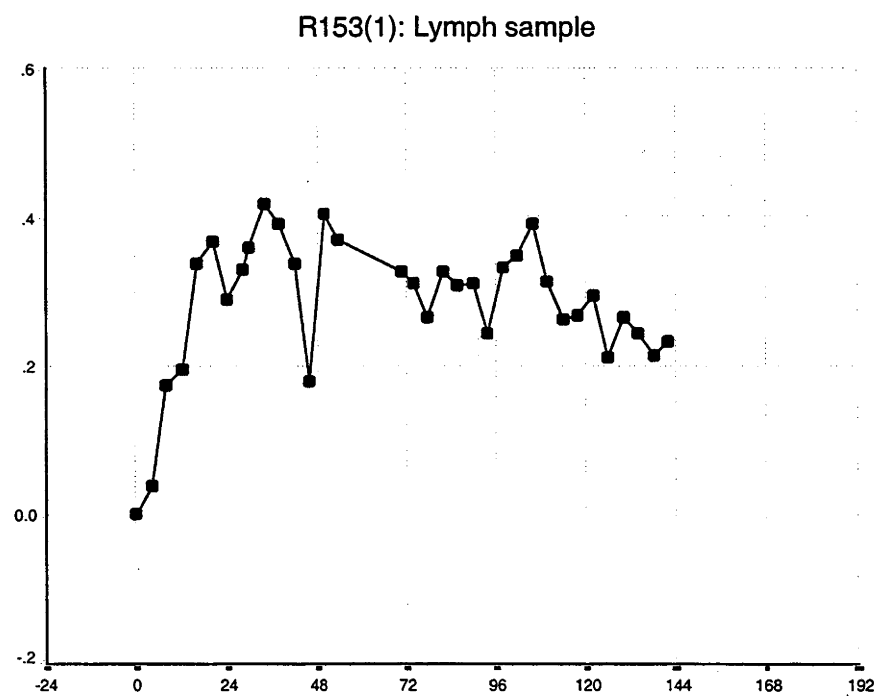

Figure 3.5M: Experimental data from R153(2)

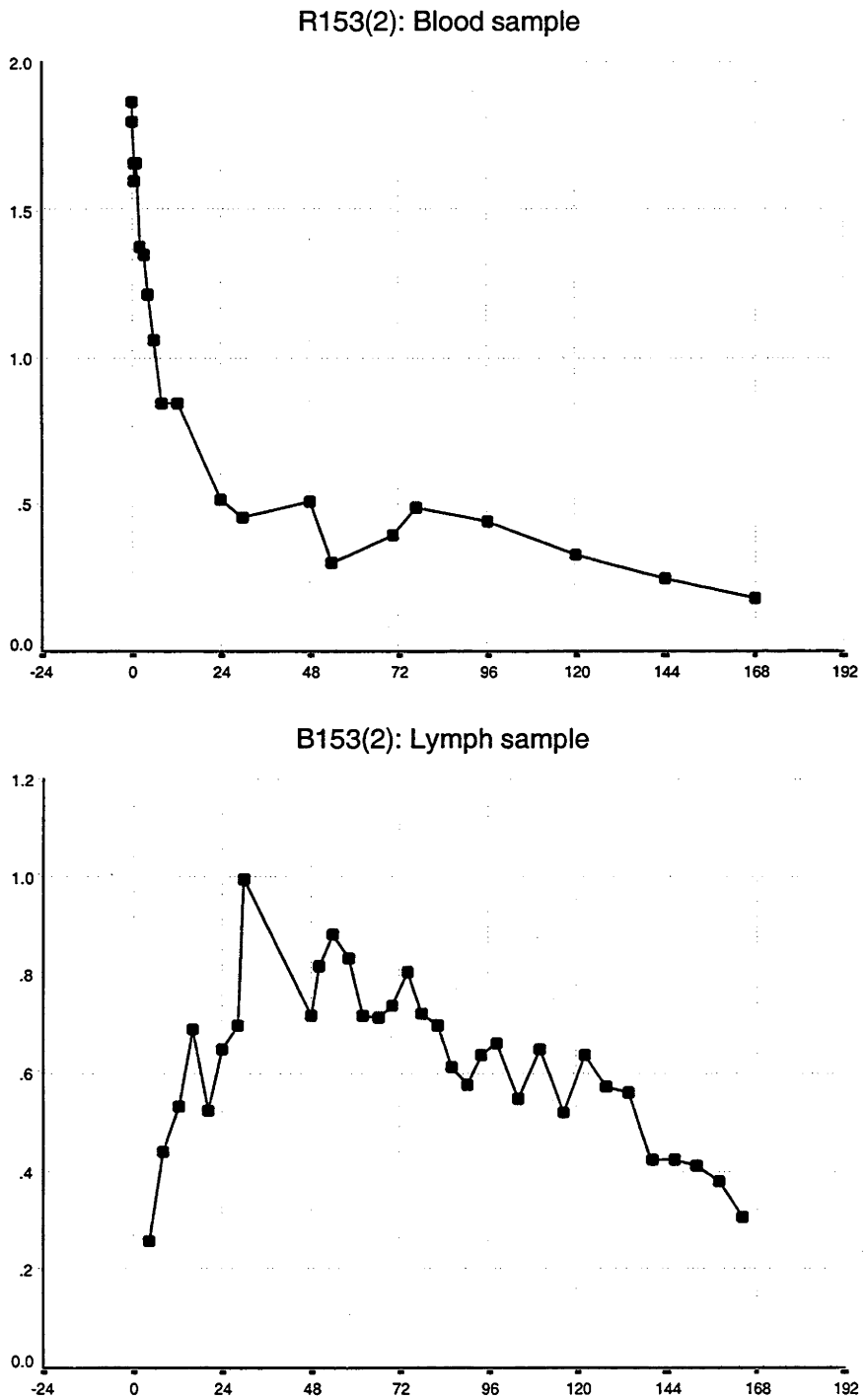

Figure 3.5N: Experimental data from R401

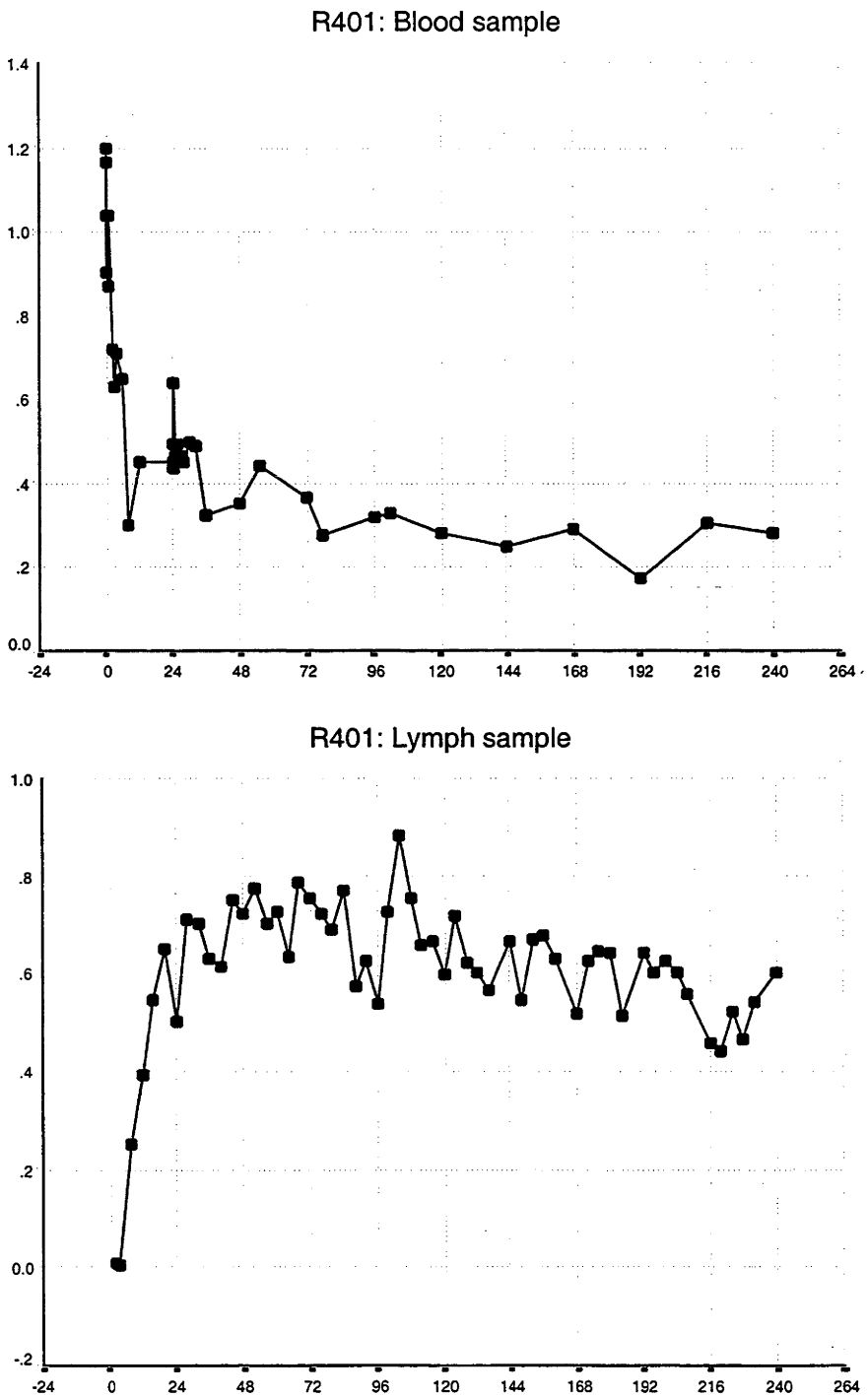

Figure 3.5P: Experimental data from R705

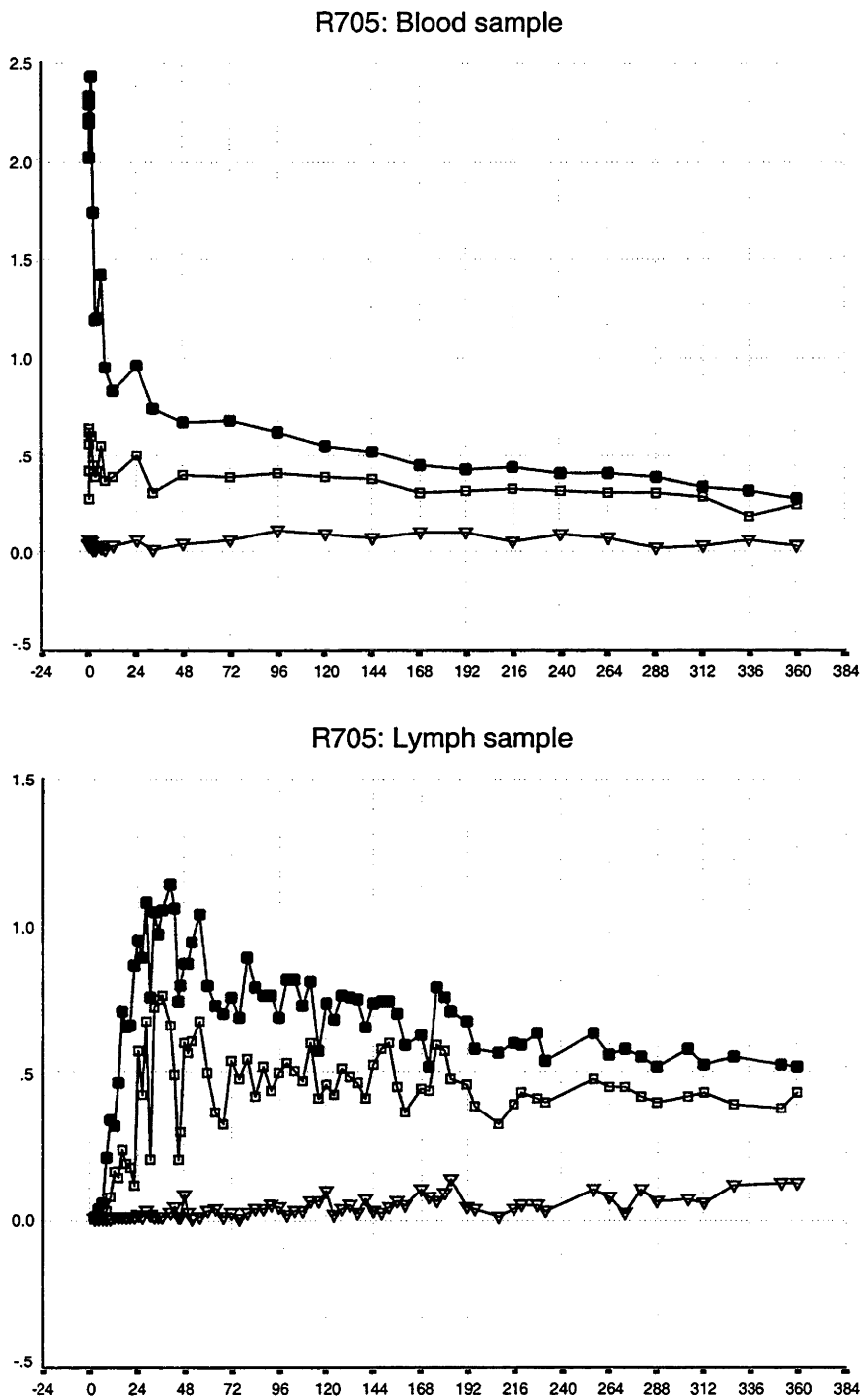

Figure 3.5Q: Experimental data from R632

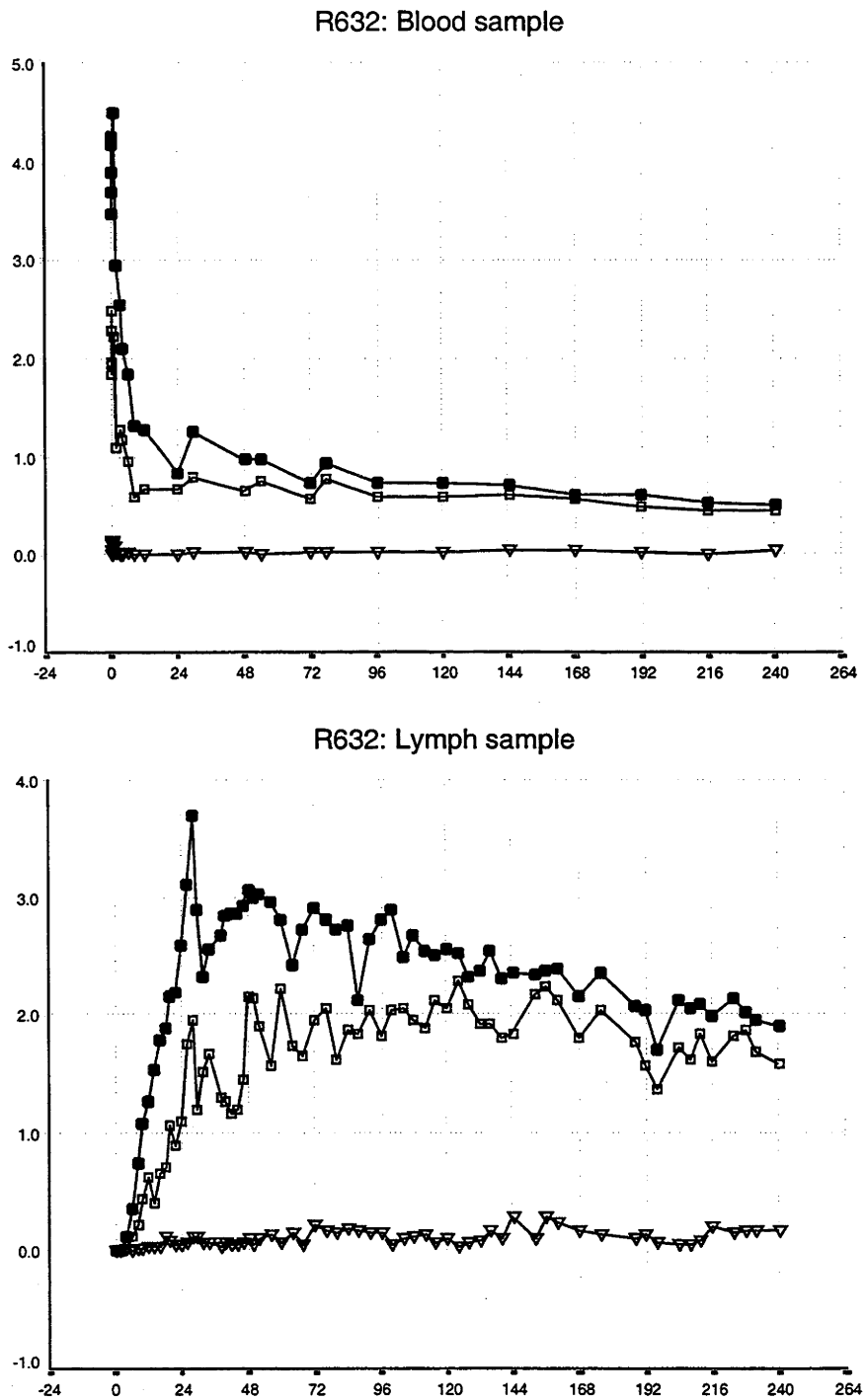

Figure 3.5R: Experimental data from R634

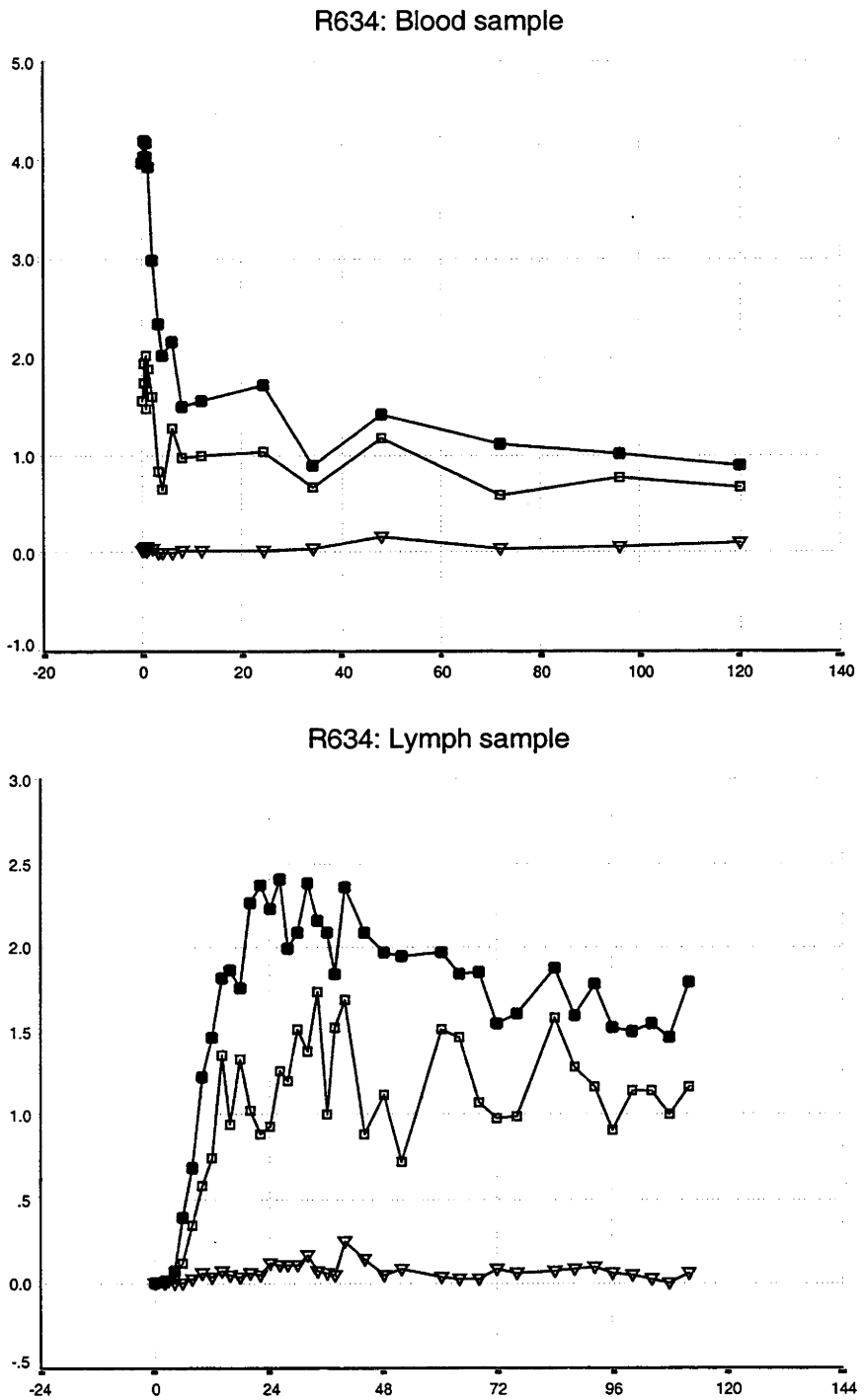

Figure 3.5S: Experimental data from R798

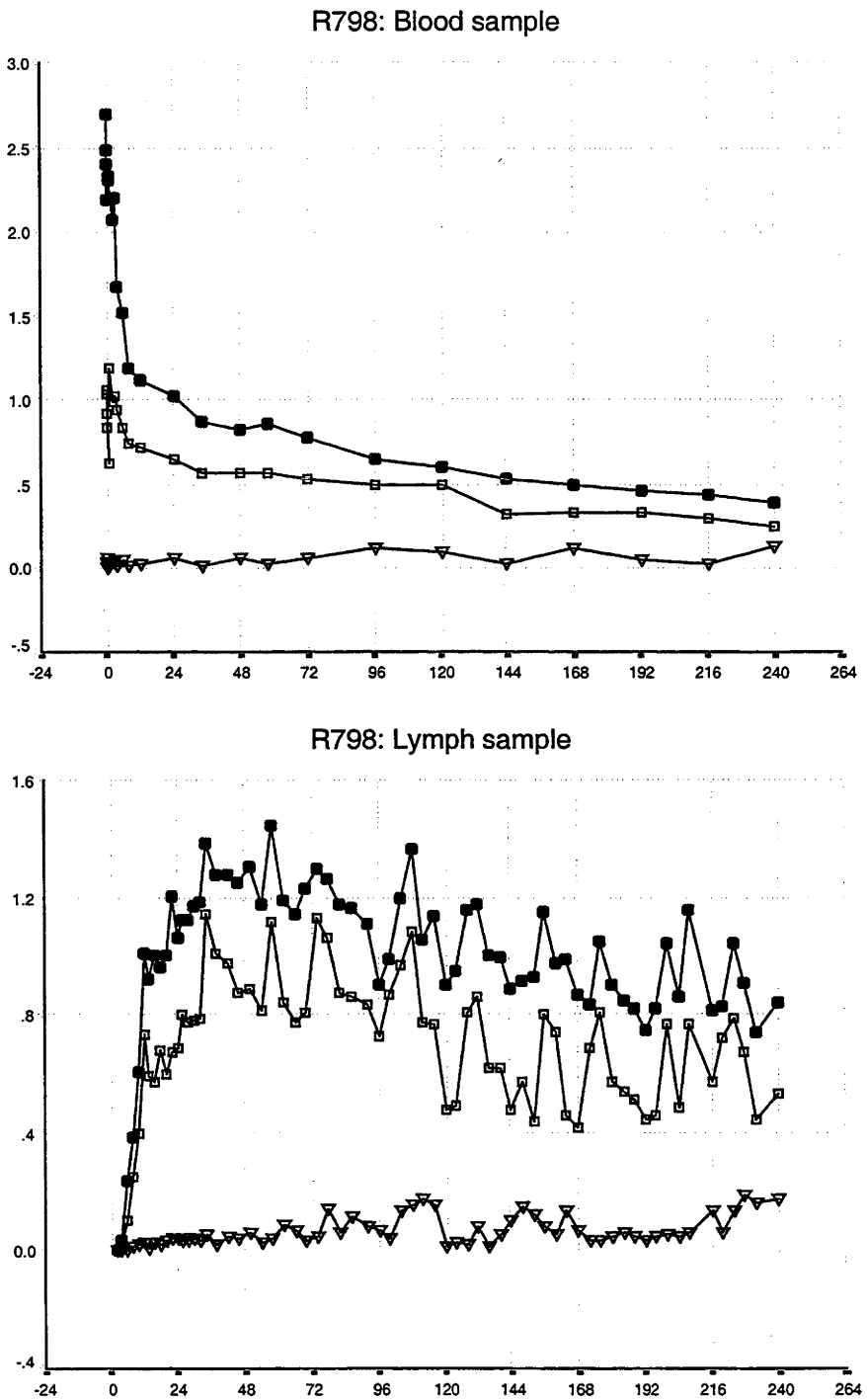

Figure 3.5T: Experimental data from R797

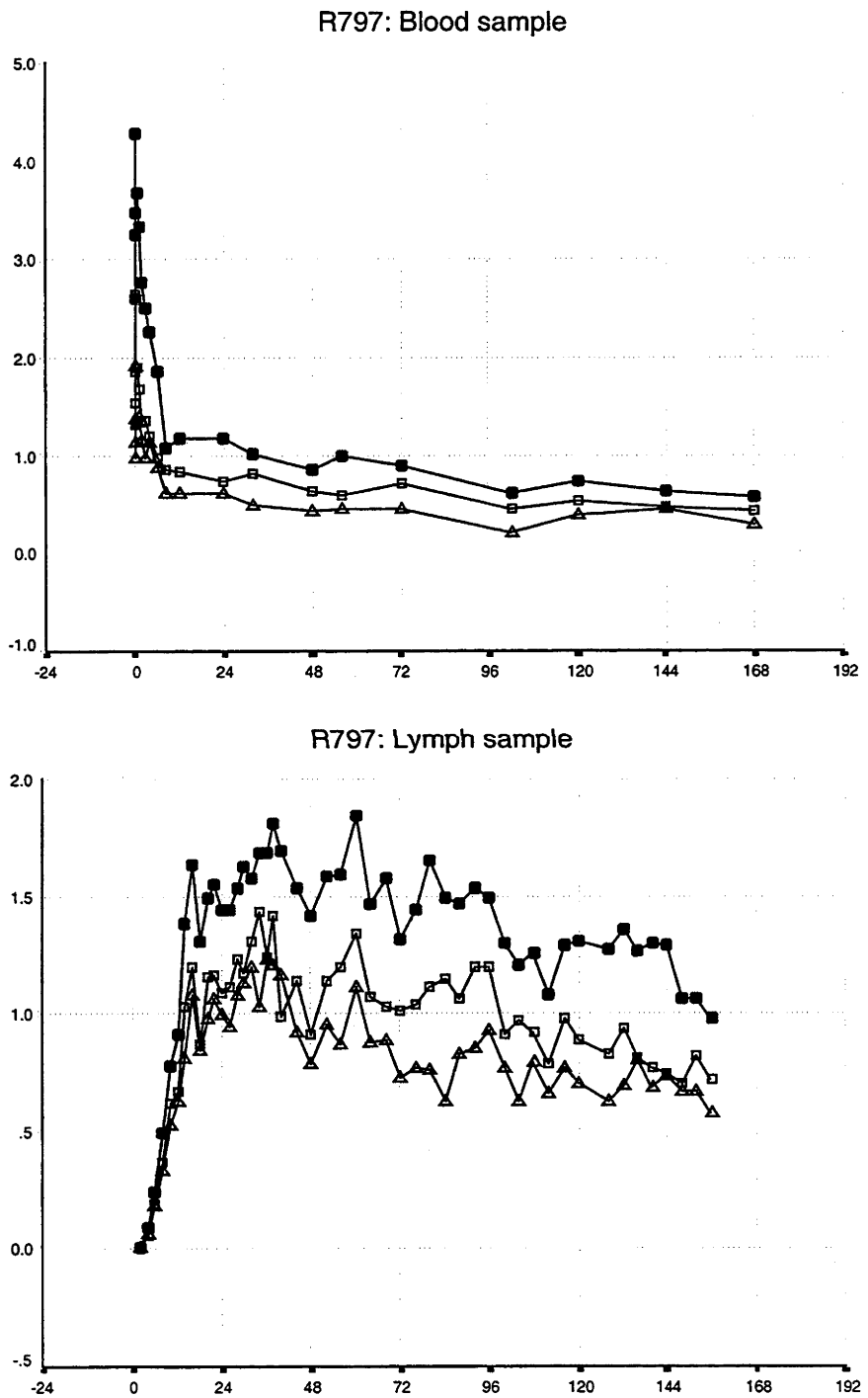

Figure 3.5U: Experimental data from R890

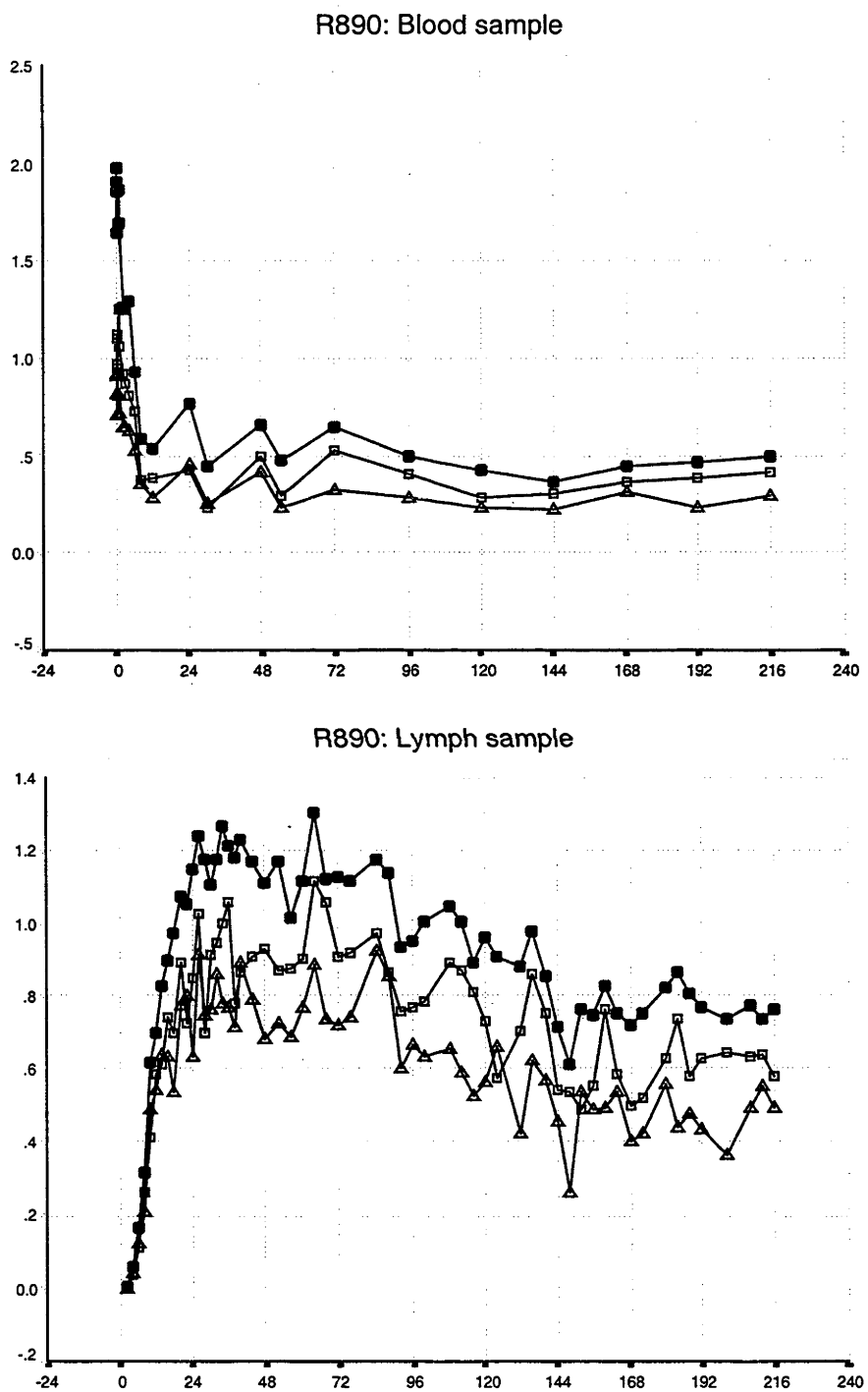

Figure 3.5V: Experimental data from Y044(1)

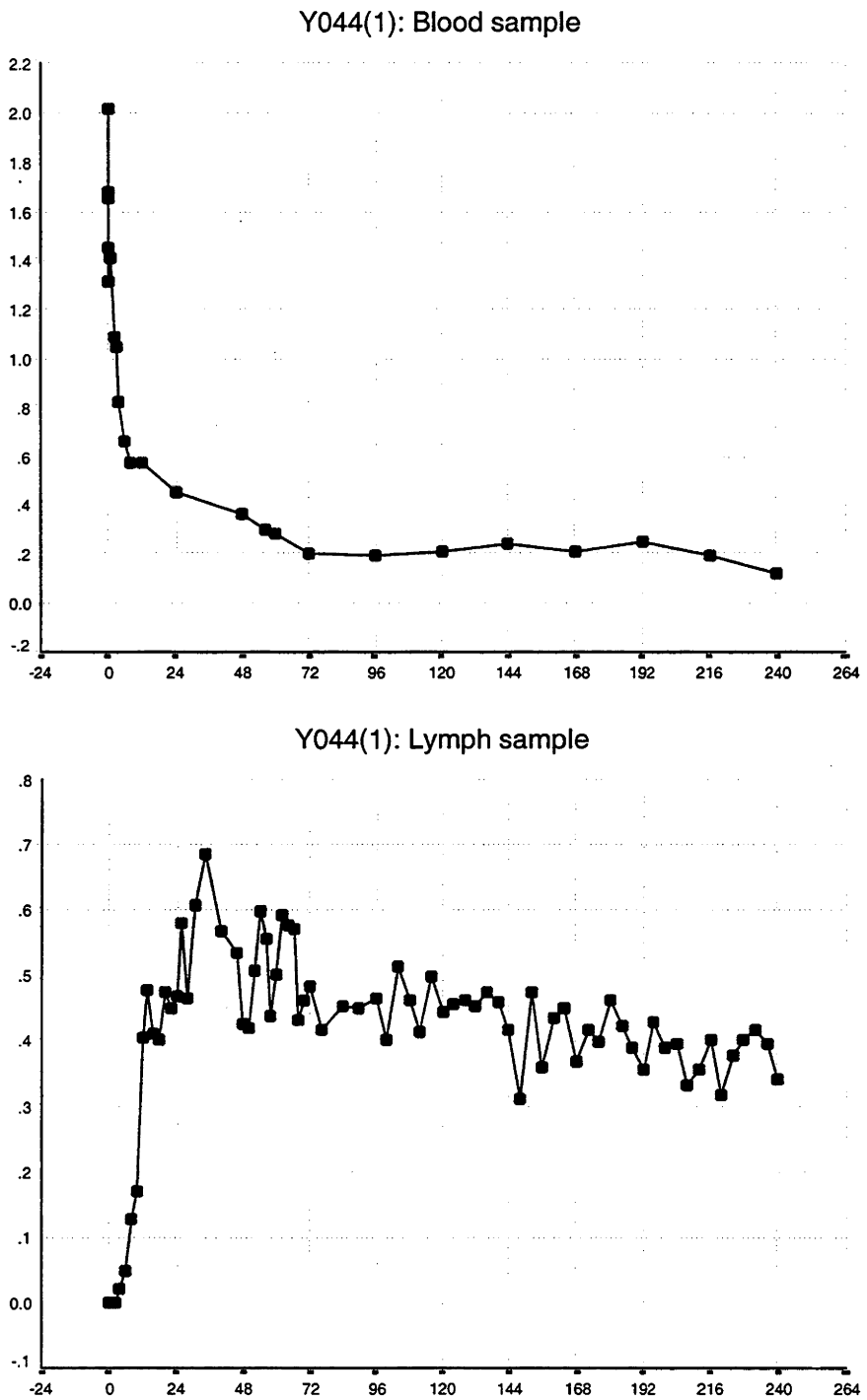

Figure 3.5W: Experimental data from Y044(2)

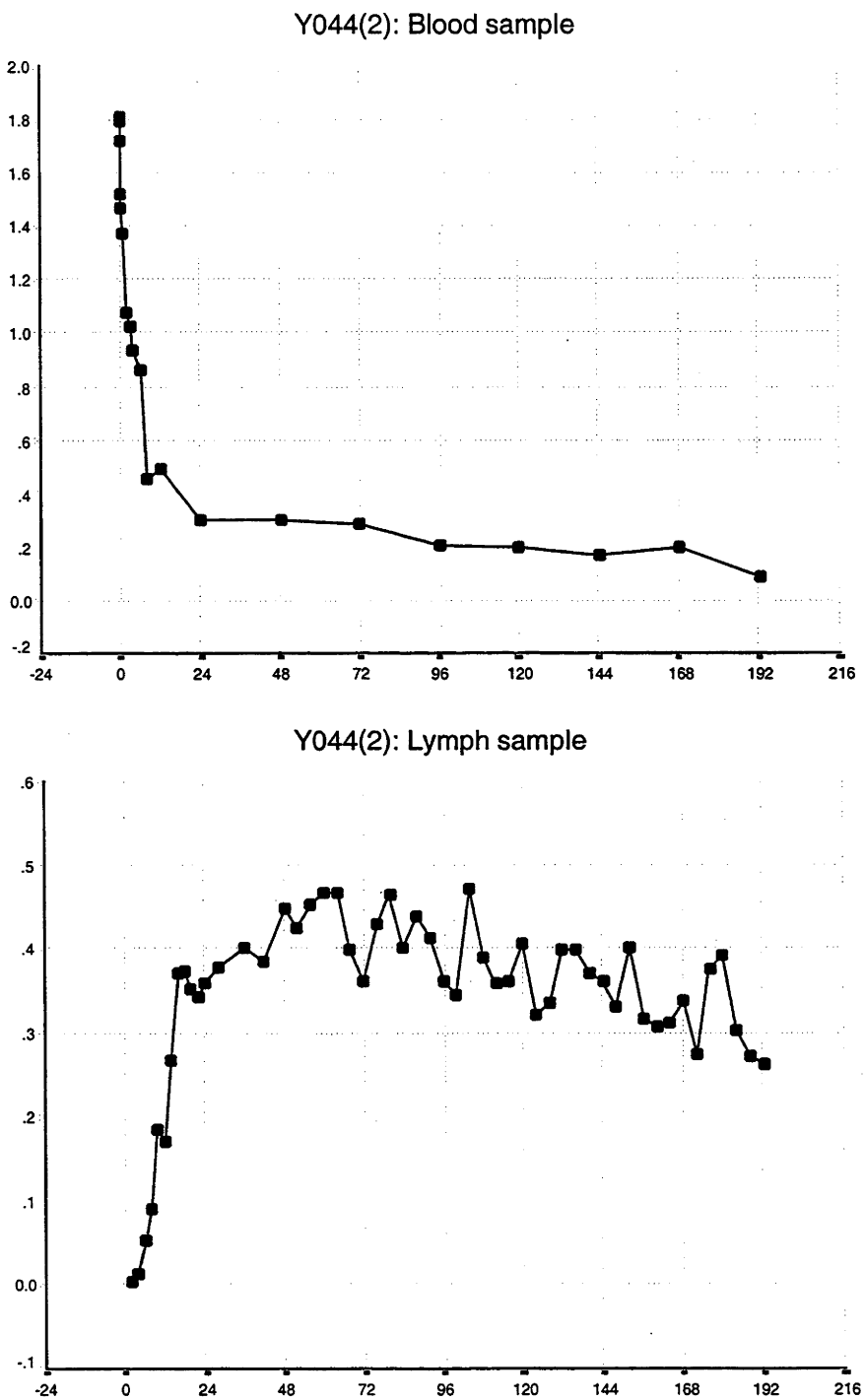

3.3 Results of lymphocyte subset studies

Having observed lymphocyte migration at the whole population level in the previous section, it was appropriate to take account of phenotype heterogeneity among the cells in a population of lymphocytes. Since the early 1970s, following the work of Mitchell and Miller (Miller and Mitchell, 1969), it has been known that lymphocytes in the lymph are not a homogenous population. A large number of lymphocyte subsets have since been identified. The present study aimed to detect any differences between the migratory capacities of several major lymphocyte subsets. It was anticipated that an understanding of the migratory characteristics of those selected major subsets would be of advantage in modelling (to be presented in the following chapter). If different lymphocyte subpopulations migrate in a different fashion, it would be necessary to take account of this in attempting to produce an accurate model representing the migration of the whole lymphocyte population.

In this section, lymphocytes collected from the efferent lymph were labelled (with CFSE) and infused back into the sheep. All (lymphocyte) samples collected from blood and efferent lymph were examined to determine the percentages of expression of several lymphocyte phenotypes, namely CD4, CD5, CD8 and CD45R, in both the labelled and unlabelled cell populations. The technique of monoclonal antibody staining to identify lymphocyte subsets expressing specific phenotypes was applied to each lymphocyte sample. After this, flow cytometry (FACScan) was performed to determine the percentages of each subset in each population (ie labelled and unlabelled). The full details of this technique have been described in Chapter 2. These subset studies were successfully undertaken in 11 experiments using lymphocytes from a total of 9 different animals. However, two pairs of experiments (ie R857(1) and R857(2), R021(1) and R021(2)) were undertaken simultaneously in the same animals (ie R857 and R021 respectively). Thus the results to be presented in this section will be summarised according to the animal identification numbers (Table 3.1).

3.3.1 Distribution of lymphocyte subsets in the blood and efferent lymph in individual animals

The distribution of lymphocyte subsets in the blood and prescapular efferent lymph of sheep have been previously reported (Washington *et al.*, 1988). In that study, lymphocyte samples (from blood and prescapular efferent lymph) were taken from sheep a few days after operation but labelled lymphocytes were not introduced into the animal under study. The distribution of lymphocyte subsets

observed in that study would be expected to provide an indication of the distribution of phenotypes to be expected within unlabelled populations in the present study. Washington *et al* found that the percentages of lymphocytes expressing CD5 and CD4 in prescapular efferent lymph were always significantly higher than the percentages of CD5 and CD4 lymphocytes in blood. On the other hand, the percentage of CD8 lymphocytes in blood was slightly higher than that in prescapular efferent lymph in one individual animal, but there were no significant differences between the frequency of these cells in blood and lymph in the whole group of animals. In summary, the mean percentages of CD4, CD5 and CD8 (± standard deviations) found in blood were 24 ± 3, 59 ± 2 and 13 ± 2, and in prescapular efferent lymph 55 ± 3, 76 ±2 and 9 ±1 respectively. A similar distribution of these lymphocyte subsets, in both blood and prescapular efferent lymph, had been reported in earlier studies in sheep (Mackay *et al.*, 1986; Abernethy *et al.*, 1990).

Figure 3.6A-3.6J present all of the raw data obtained from individual animals during this study. The percentages of lymphocyte subsets in blood (upper panels) and efferent lymph (lower panels) have been plotted on the Y axis along with the experimental time (hours) on the X-axis. Closed and opened marks represent the (CFSE) labelled and unlabelled lymphocyte populations whilst triangles, squares, circles and inverted triangles represent CD4, CD5, CD8 and CD45R lymphocyte subsets respectively.

In the CD4, CD8 and CD45R subsets of lymphocytes, the percentages of labelled populations found in both blood and efferent lymph in any one animal were relatively uniform. In other words, there were no obvious differences between the percentages of those subsets (either found in blood or efferent lymph) throughout the whole experiment in the same animal. In contrast, there were some differences between the percentages of CD5-expressing cells in labelled populations during the experiments. For example, in sheep R705, R632 and R634 (Figure 3.6D, 3.6E and 3.6F respectively), the percentages of CD5 lymphocytes (in the labelled population, closed squares) were about 20-30% in efferent lymph in the first few hours of the experiment. After this, these percentages gradually rose to reach a stable level (approximately 60%-80%) at around 120-144 hours. Nevertheless, the percentages of CD5 lymphocytes found in the efferent lymph corresponded well with those found in blood.

Figure 3.6A: Percentages of lymphocyte subsets in B857

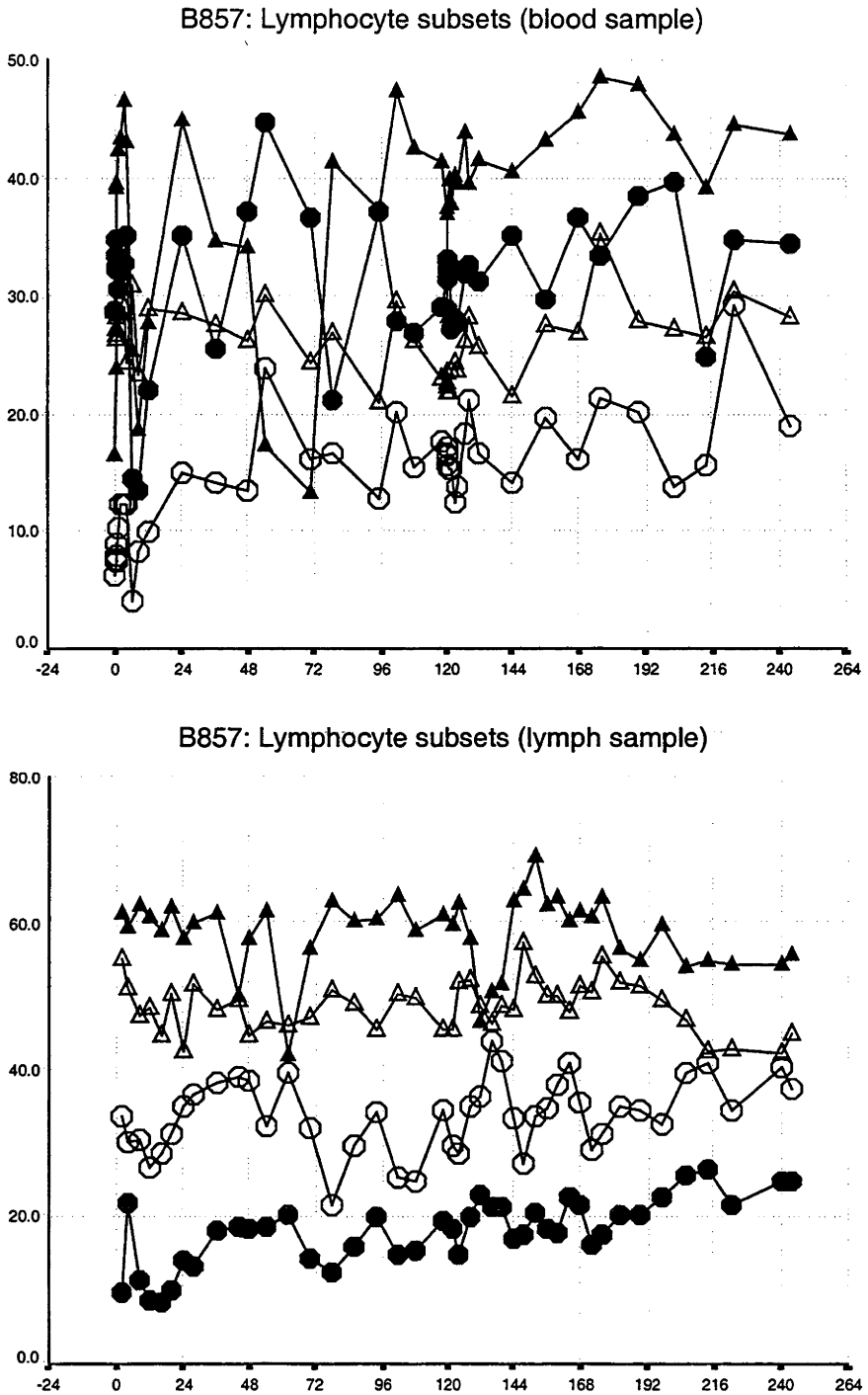

Figure 3.6B: Percentages of lymphocyte subsets in R021.

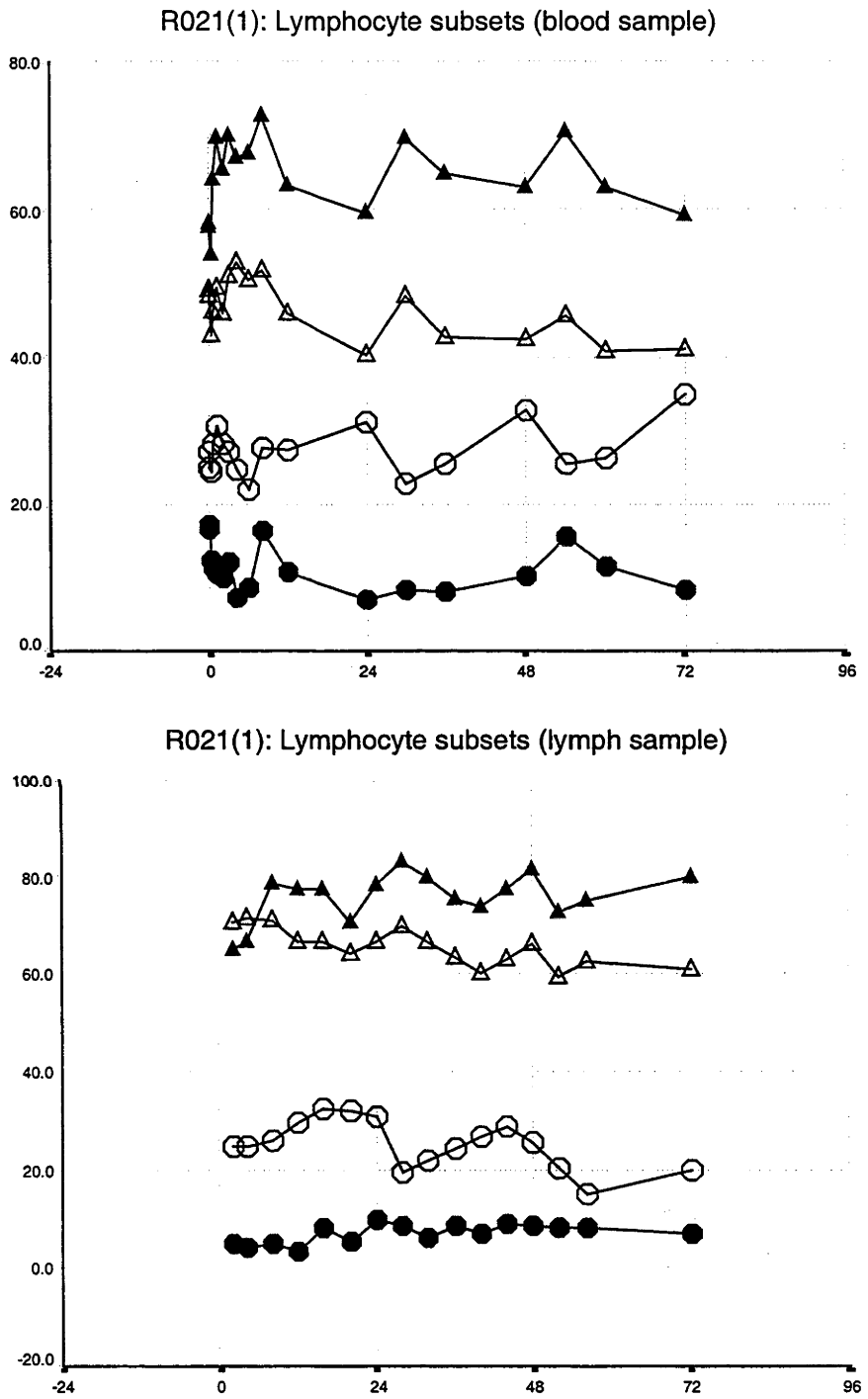

Figure 3.6C: Percentages of lymphocyte subsets in B045.

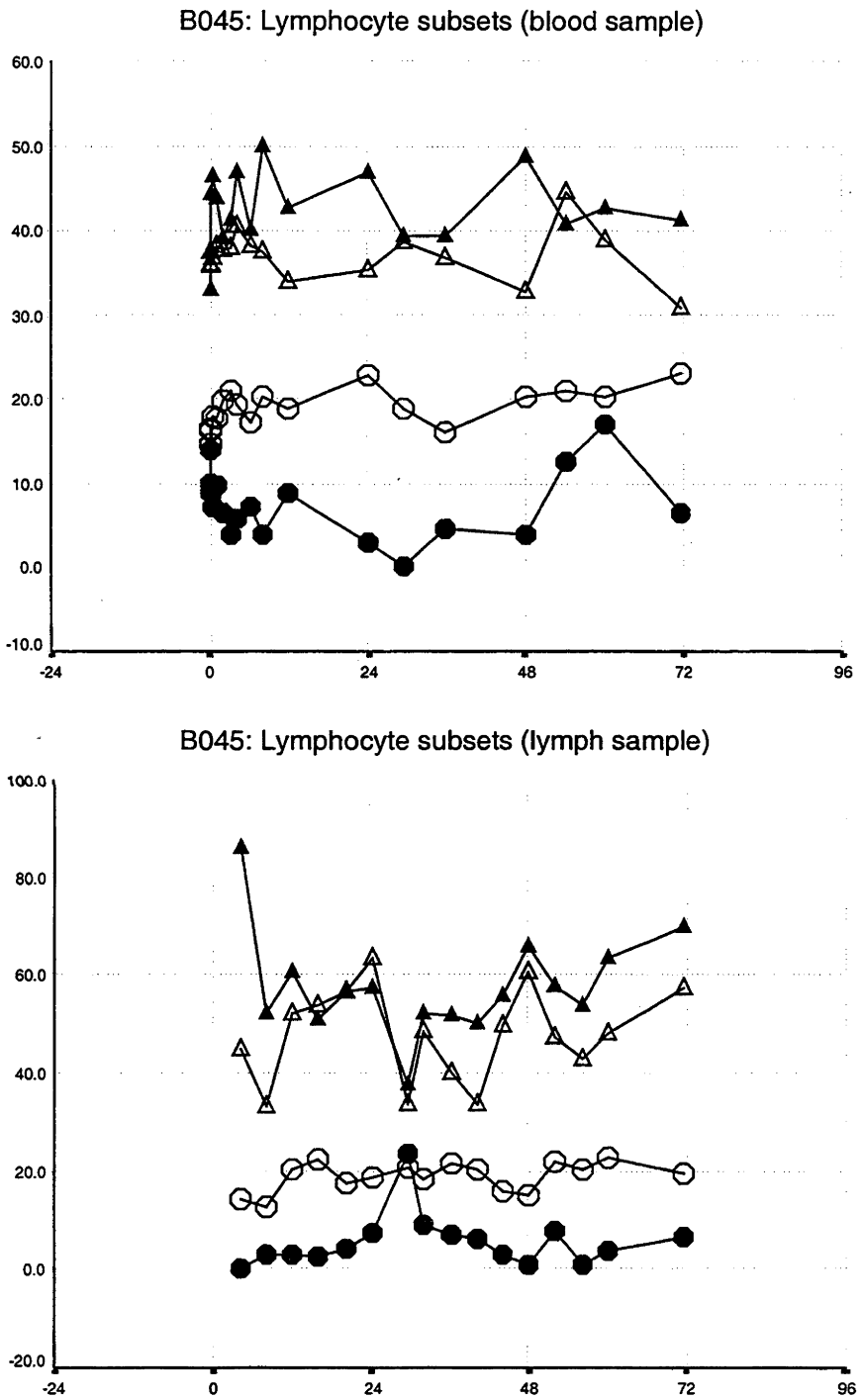

Figure 3.6D: Percentages of lymphocyte subsets in R705.

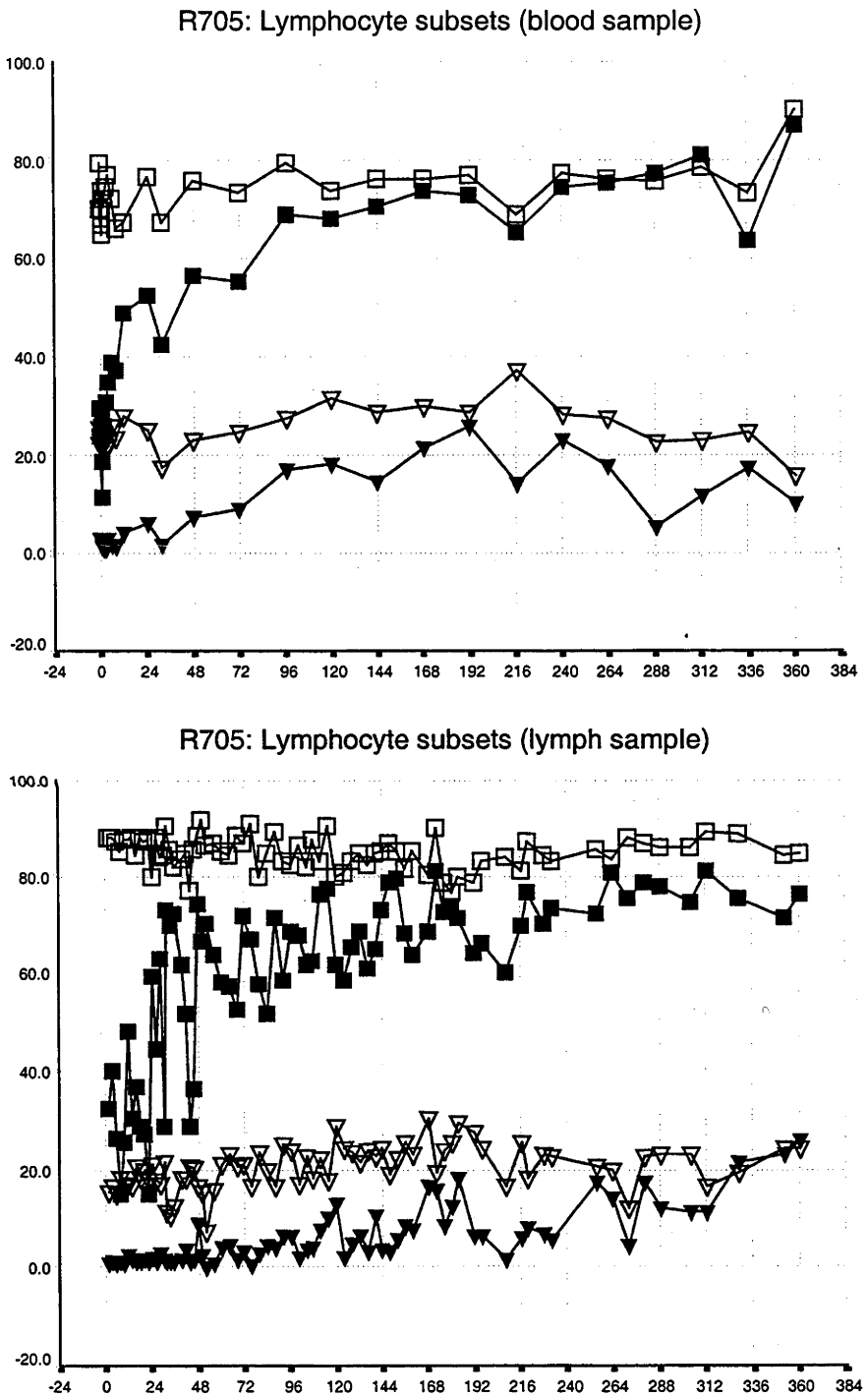

Figure 3.6E: Percentages of lymphocyte subsets in R632.

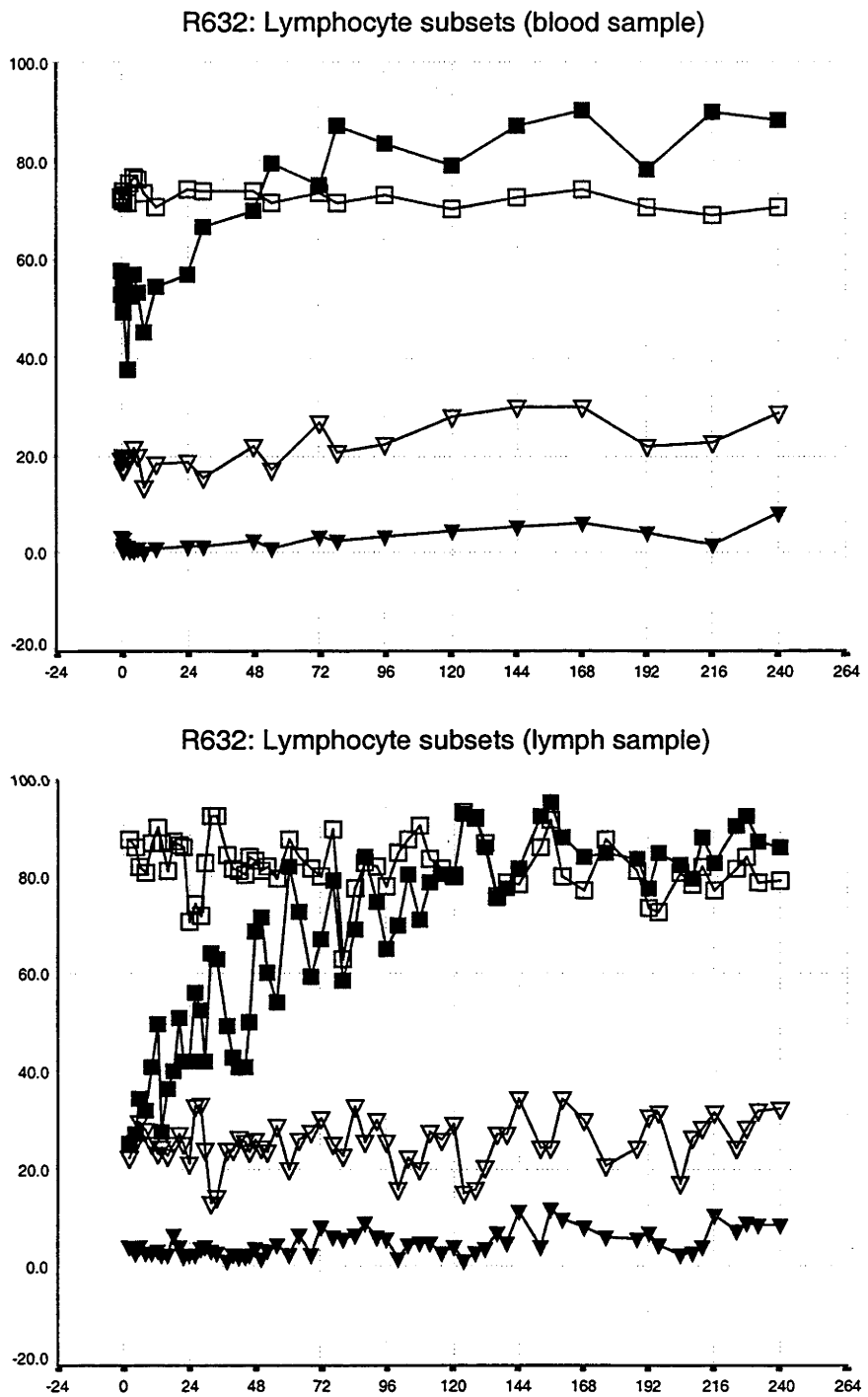

Figure 3.6F: Percentages of lymphocyte subsets in R634.

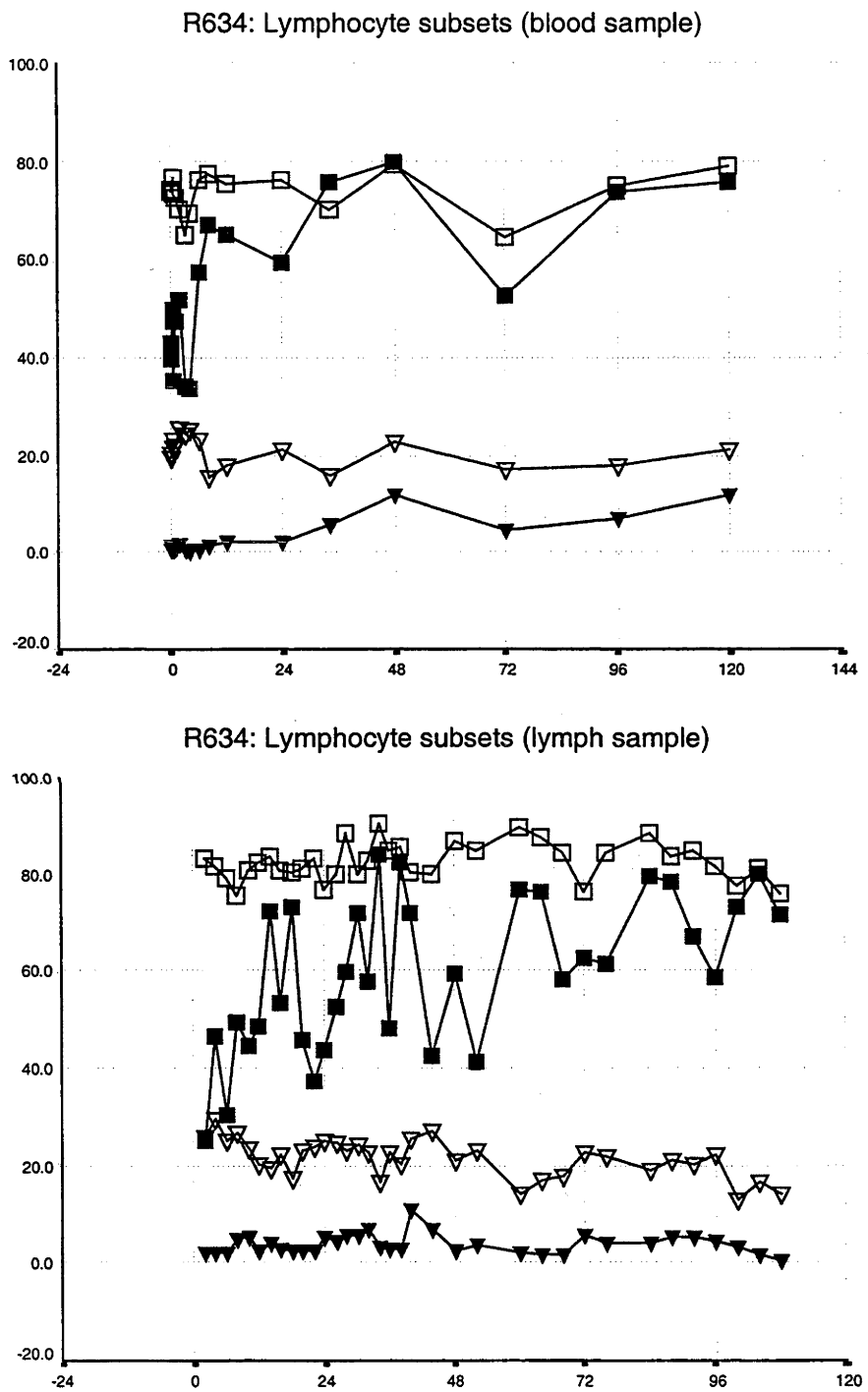

Figure 3.6G: Percentages of lymphocyte subsets in R798.

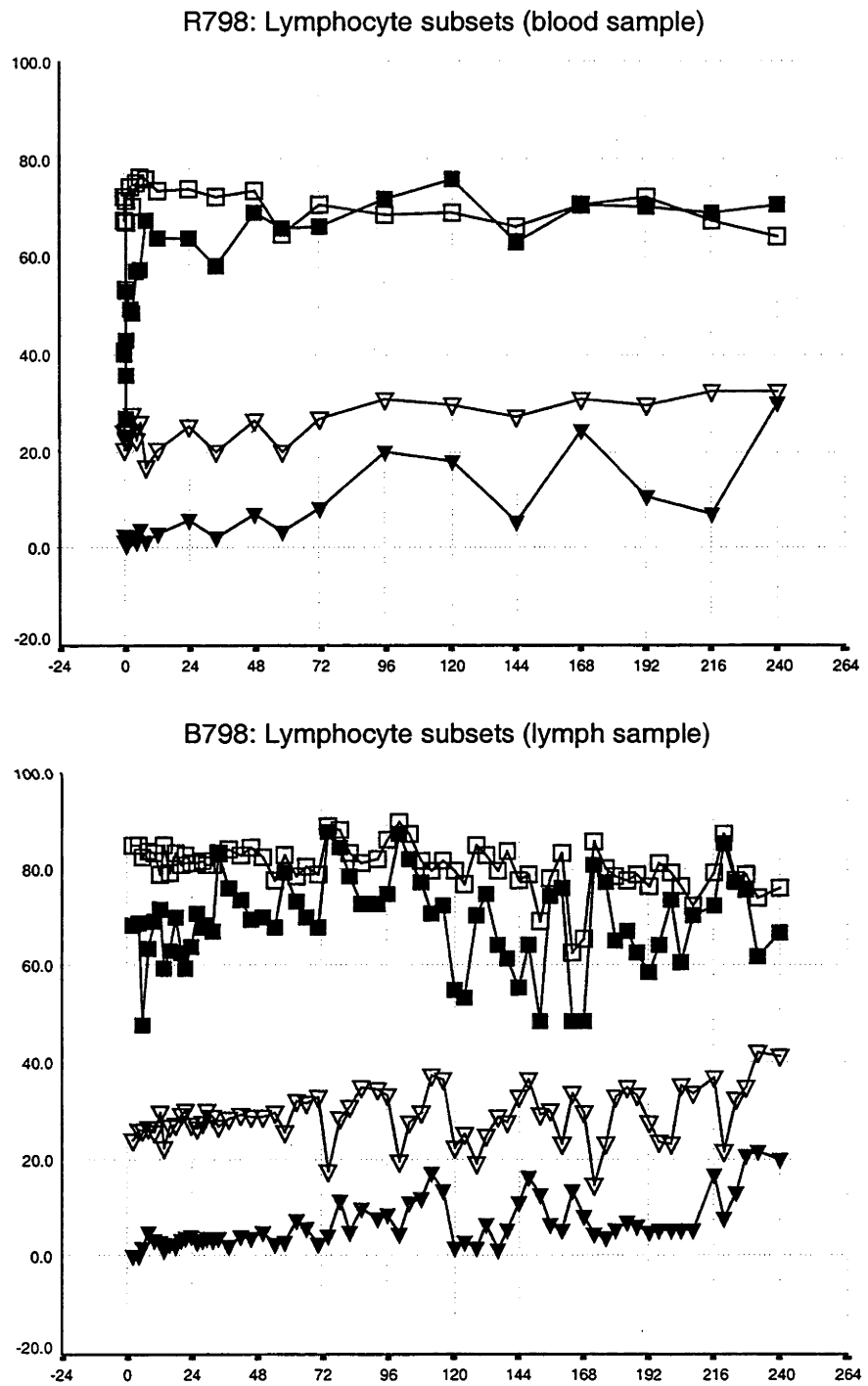

Figure 3.6H: Percentages of lymphocyte subsets in R797.

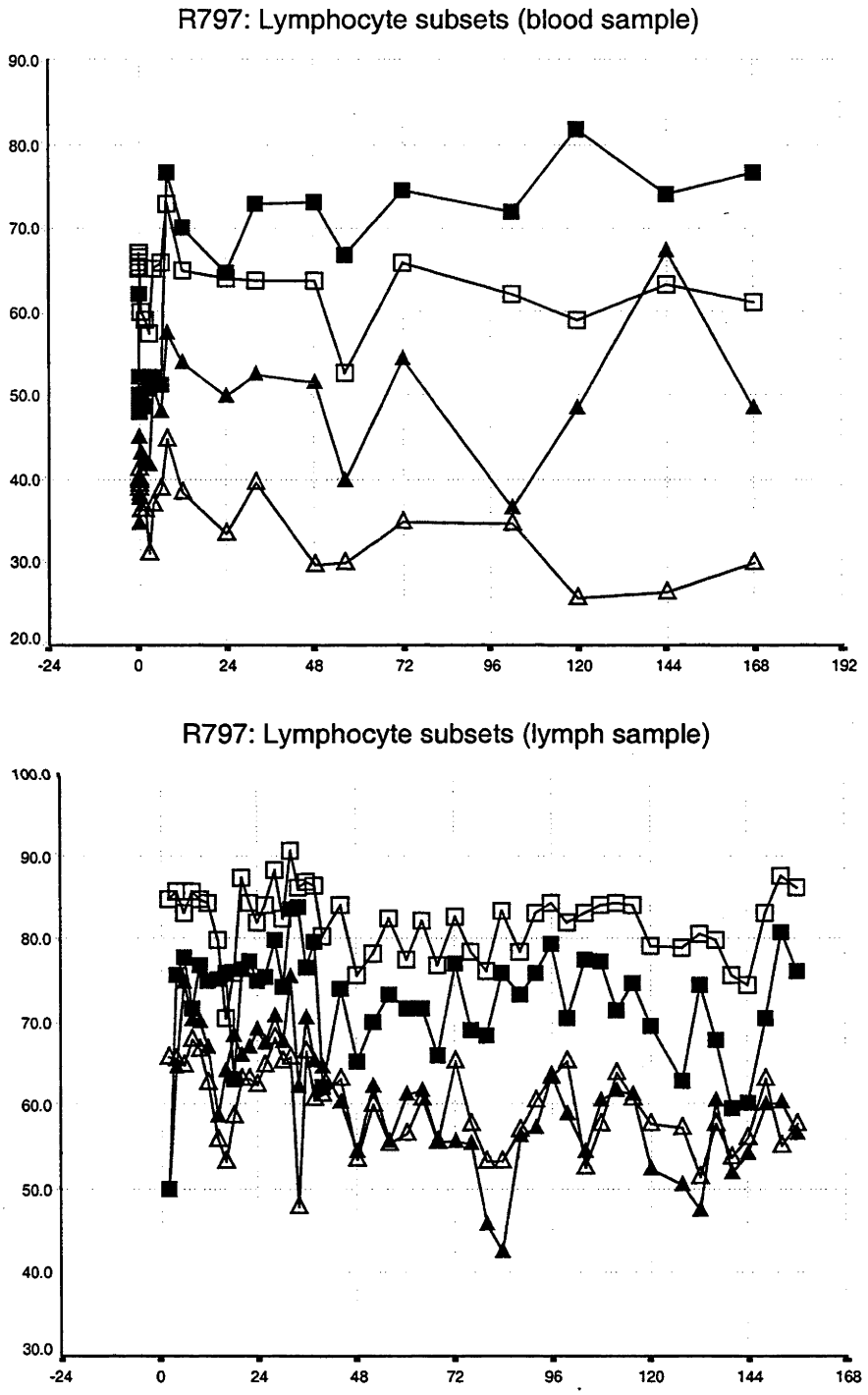

Figure 3.6J: Percentages of lymphocyte subsets in R890.

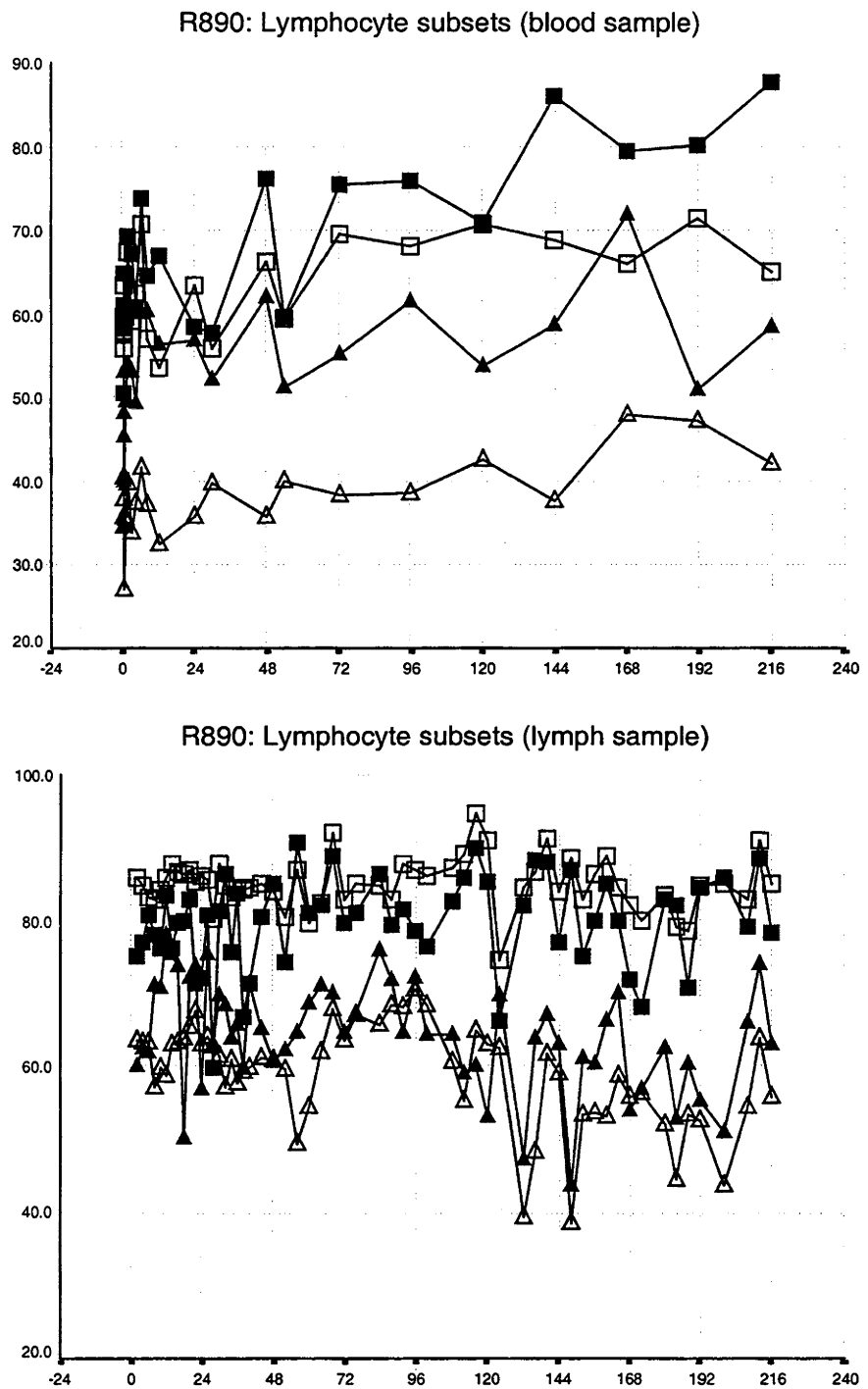

Statistical analysis was performed to summarise the findings of all the subset studies. The mean percentage of each lymphocyte subset in blood and efferent lymph (both in unlabelled and labelled populations) was determined from all of the data points available over the entire experimental time for each individual animal. Then, an overall mean percentage was calculated for each lymphocyte subset for all of the animals once more. Table 3.2 gives the mean percentage of each subset of the labelled population found in the blood and efferent lymph of each individual animal. Table 3.3 gives the mean percentage of each subset of the unlabelled population in blood and efferent lymph. The overall mean percentages (± standard deviations) for all animals are also presented at the bottom of each table. Figures 3.7A, 3.7B, 3.8A and 3.8B illustrate the mean percentage of each lymphocyte subset (found in blood and efferent lymph) for each individual animal in unlabelled and labelled populations respectively. Figures 3.9A, 3.9B, 3.10A and 3.10B indicate the overall mean percentages of each lymphocyte subset (found in blood and efferent) of all animals in unlabelled and labelled populations respectively.

In both labelled and unlabelled populations, the CD4 lymphocytes had a similar distribution (upper panels of Figures 3.7A, 3.8A, 3.9A and 3.10A and Table 3.2 - 3.3). The percentage of CD4 lymphocytes in the blood was invariably less than that in the lymph. Thus the overall mean percentage of CD4 lymphocytes in the blood (ie 46.85% and 34.86% in labelled and unlabelled populations respectively) was significantly ($p<0.05$) less than the overall mean percentage of CD4 lymphocytes in the efferent lymph (ie 62.64% and 56.33% in labelled and unlabelled populations respectively).

Measurement of the percentages of CD5 lymphocyte (in either the labelled or unlabelled population) gave results similar to those obtained with CD4 lymphocytes. The percentage of CD5 lymphocytes in the blood was always less than that in the lymph (lower panels of Figures 3.7A, 3.8A, 3.9A and 3.10A and Table 3.2 -3.3). The overall mean percentage of CD5 lymphocytes in the blood (ie 60.07% and 69.61% in labelled and unlabelled populations respectively) was significantly ($p<0.05$) less than the overall mean percentages of CD5 lymphocytes in the efferent lymph (ie 68.30% and 82.85% in labelled and unlabelled populations respectively).

By contrast, there were no significant ($p>0.05$) differences between the overall mean percentage of CD8 and CD45R lymphocytes in blood and efferent lymph in either labelled or unlabelled populations which were, respectively, shown in the upper and lower panels of Figures 3.7B, 3.8B, 3.9B and 3.10B and Table 3.2-3.3.

Table 3.2: Summary of lymphocyte subsets in the population of labelled lymphocytes in individual experiments.

Animal	Sample	% Lymphocyte subset in the labelled lymphocytes			
		CD4	CD5	CD8	CD45R
B857	Blood	36.47	-	14.20	-
	Lymph	59.32	-	17.98	-
R021	Blood	64.46	-	11.23	-
	Lymph	75.81	-	6.95	-
B045	Blood	42.43	-	7.39	-
	Lymph	57.52	-	5.54	-
R705	Blood	-	51.40	-	8.79
	Lymph	-	62.33	-	6.85
R632	Blood	-	65.89	-	2.54
	Lymph	-	66.51	-	4.79
R634	Blood	-	54.87	-	3.11
	Lymph	-	59.48	-	3.89
R798	Blood	-	58.15	-	6.81
	Lymph	-	68.74	-	6.57
R797	Blood	46.69	62.70	-	-
	Lymph	60.95	73.17	-	-
R890	Blood	53.80	68.00	-	-
	Lymph	64.27	79.73	-	-
	Mean Blood	46.85	60.07	11.82	5.57
	± SD	± 12.27	± 16.56	± 4.98	± 6.65
	Mean Lymph	62.64	68.30	12.97	5.83
	± SD	± 8.31	± 15.06	± 7.25	4.86

Table 3.3: Summary of lymphocyte subsets in the population of unlabelled lymphocytes in individual experiments.

Animal	Sample	% Lymphocyte subset in the unlabelled lymphocytes			
		CD4	CD5	CD8	CD45R
B857	**Blood**	25.98	-	30.88	-
	Lymph	48.57	-	33.74	-
R021	**Blood**	46.41	-	27.29	-
	Lymph	65.48	-	25.12	-
B045	**Blood**	37.11	-	18.98	-
	Lymph	47.74	-	18.84	-
R705	**Blood**	-	73.99	-	25.33
	Lymph	-	84.34	-	20.50
R632	**Blood**	-	72.75	-	21.14
	Lymph	-	82.30	-	25.43
R634	**Blood**	-	73.50	-	20.92
	Lymph	-	82.36	-	21.50
R798	**Blood**	-	70.07	-	25.16
	Lymph	-	80.46	-	28.86
R797	**Blood**	35.44	63.32	-	-
	Lymph	59.90	82.02	-	-
R890	**Blood**	38.20	63.07	-	-
	Lymph	58.97	84.99	-	-
	Mean Blood	34.86	69.61	27.12	23.35
	± sd	± 7.96	± 6.36	± 6.78	± 4.56
	Mean Lymph	56.33	82.85	28.72	24.12
	± sd	± 8.21	± 4.64	± 7.71	± 6.06

Figure 3.7A: The distribution of lymphocyte subsets in the labelled population in individual experiments.

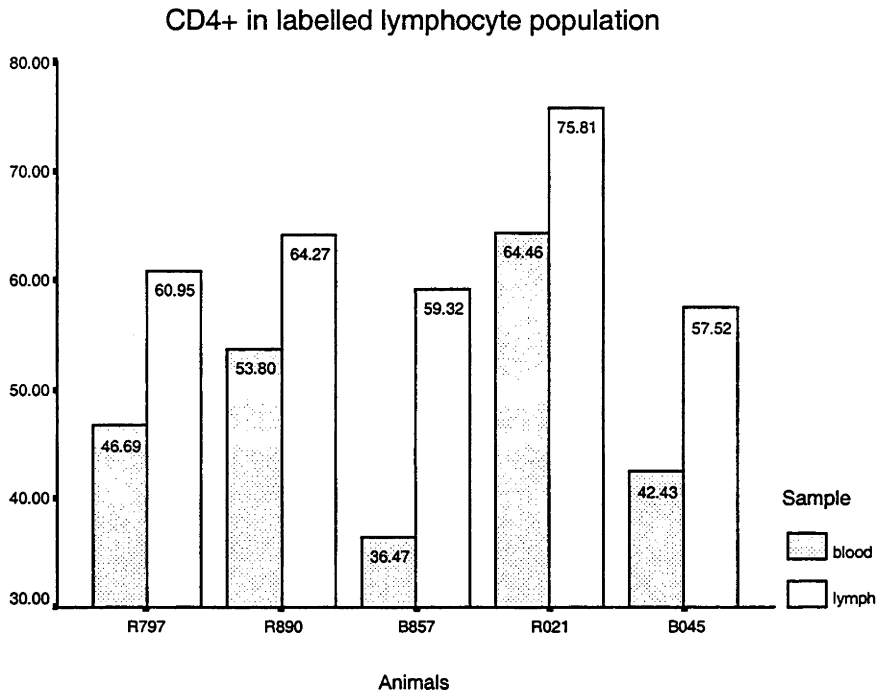

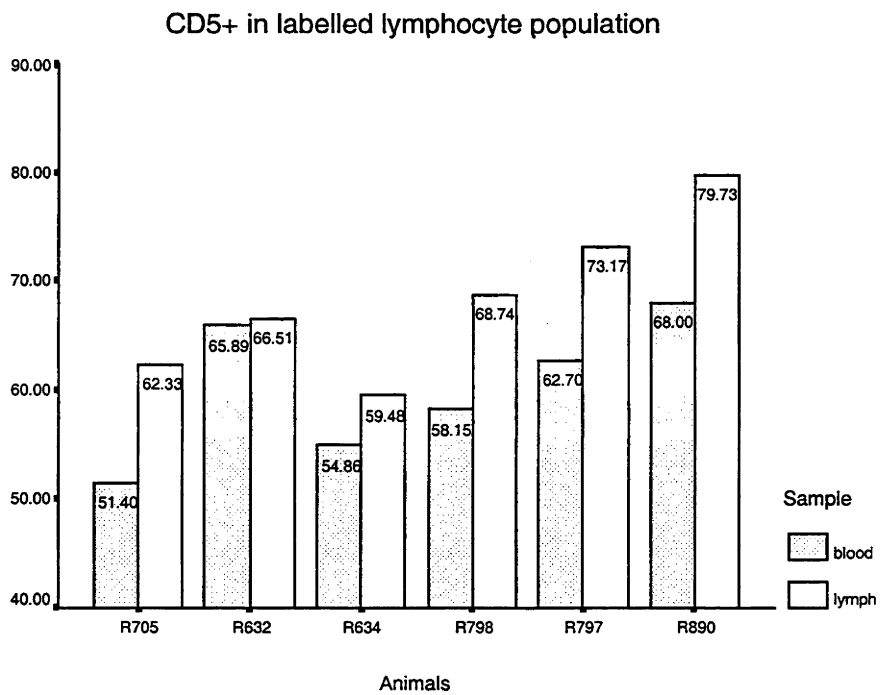

Figure 3.7B: The distribution of lymphocyte subsets in the labelled population in individual experiments.

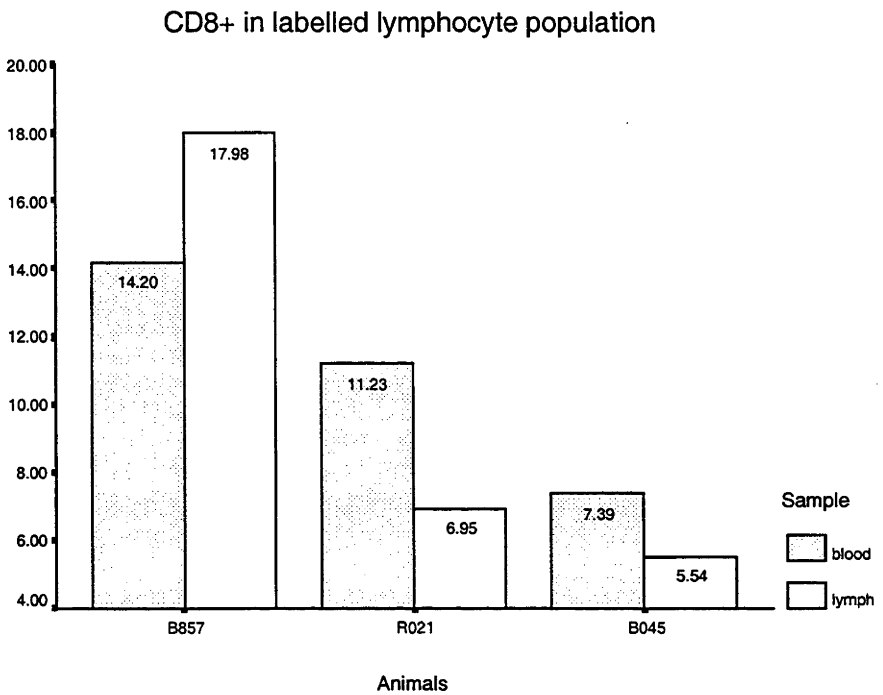

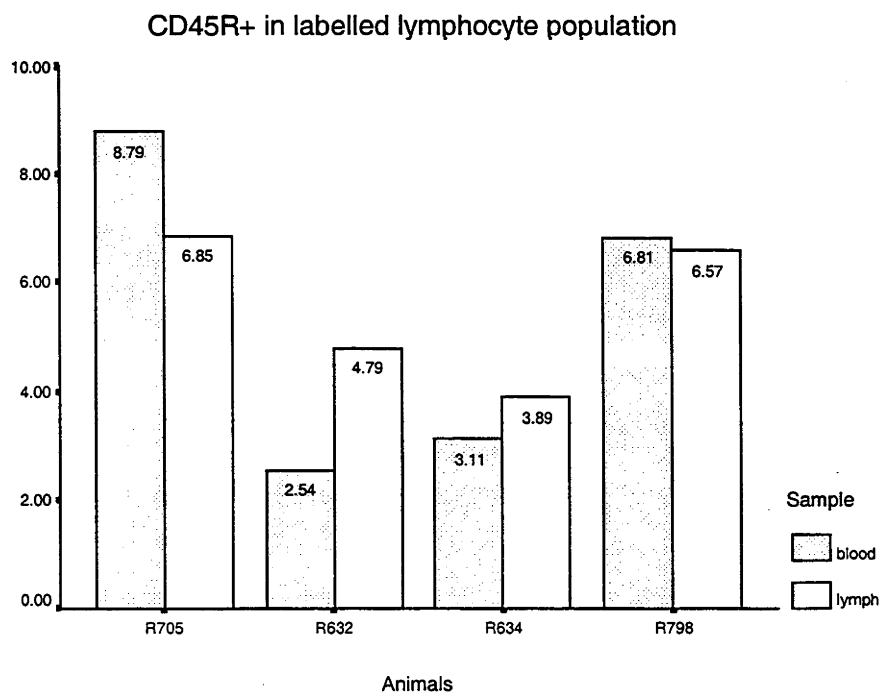

Figure 3.8A: The distribution of lymphocyte subsets in the unlabelled population in individual experiments.

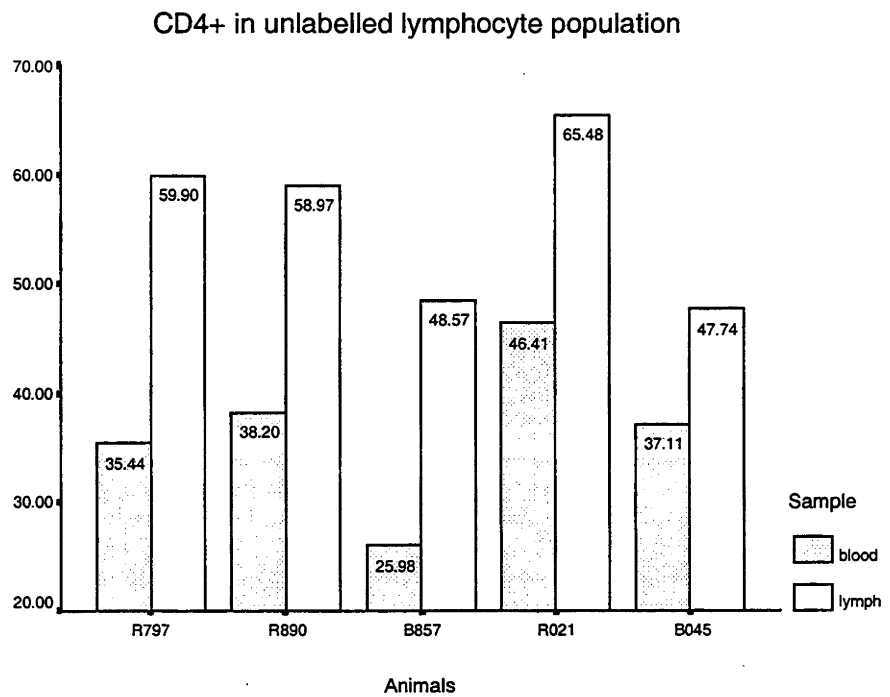

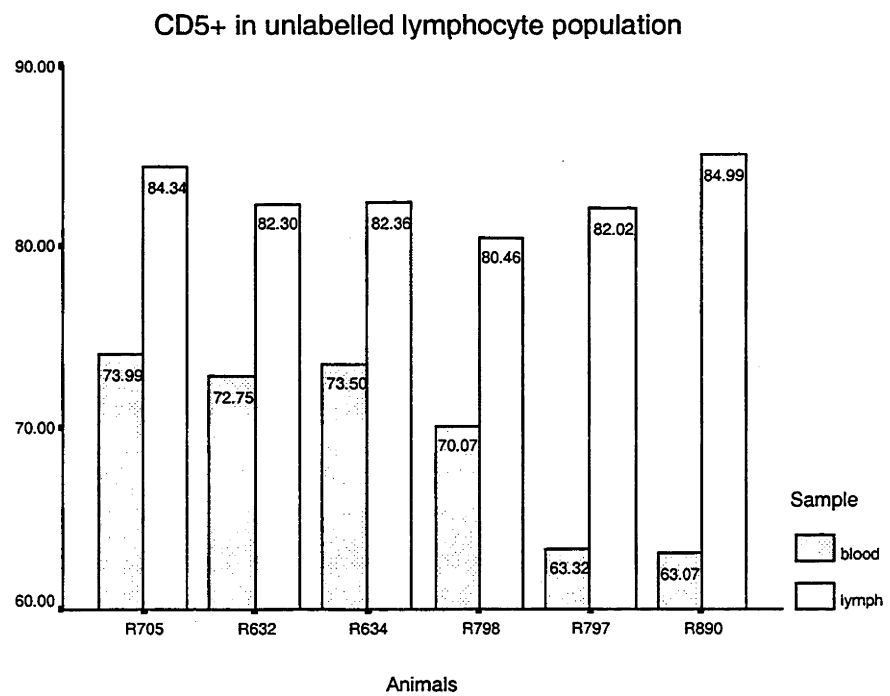

Figure 3.8B: The distribution of lymphocyte subsets in the unlabelled population in individual experiments.

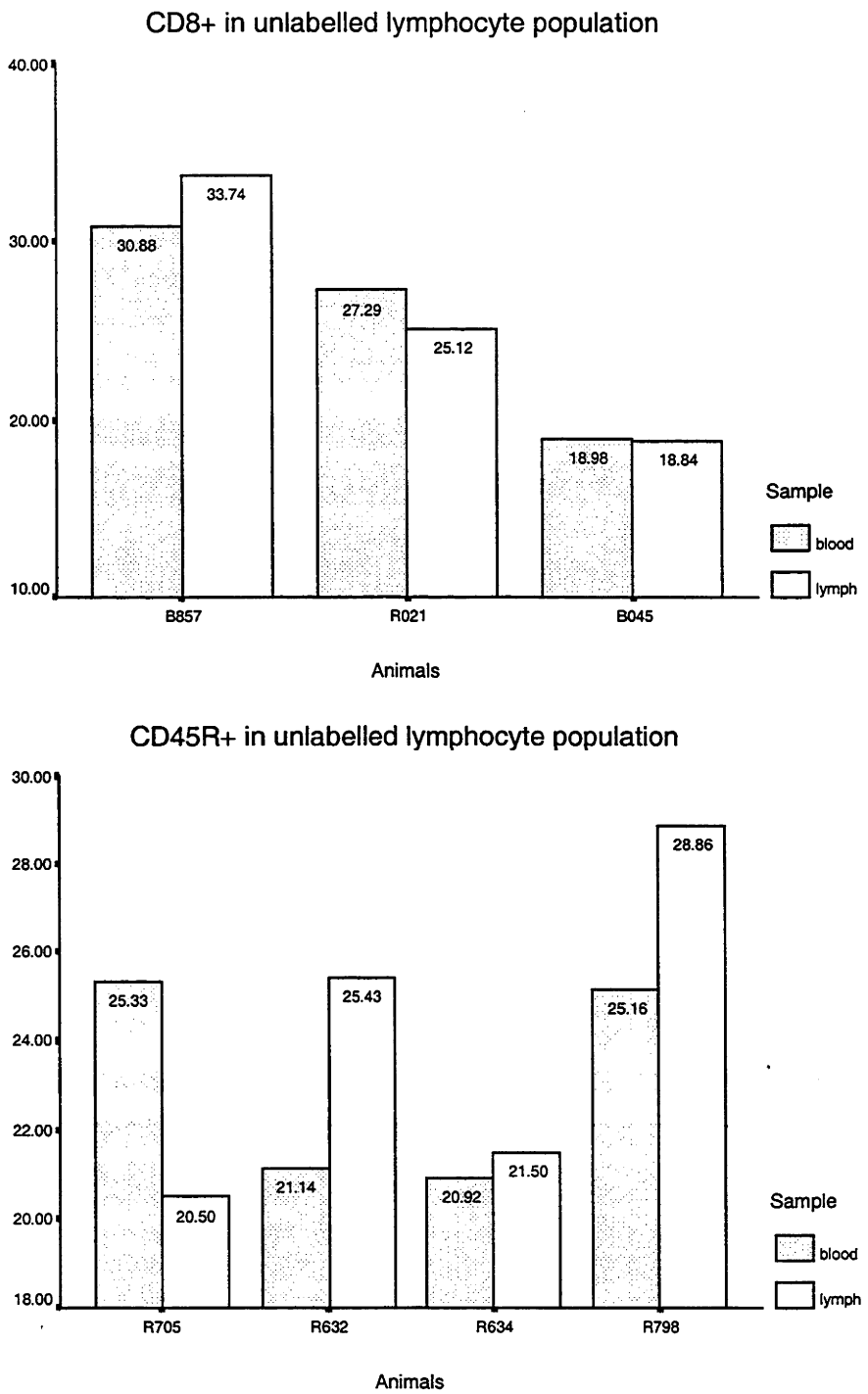

Figure 3.9A: The distribution of lymphocyte subsets in the labelled population in all experiments (aggregated).

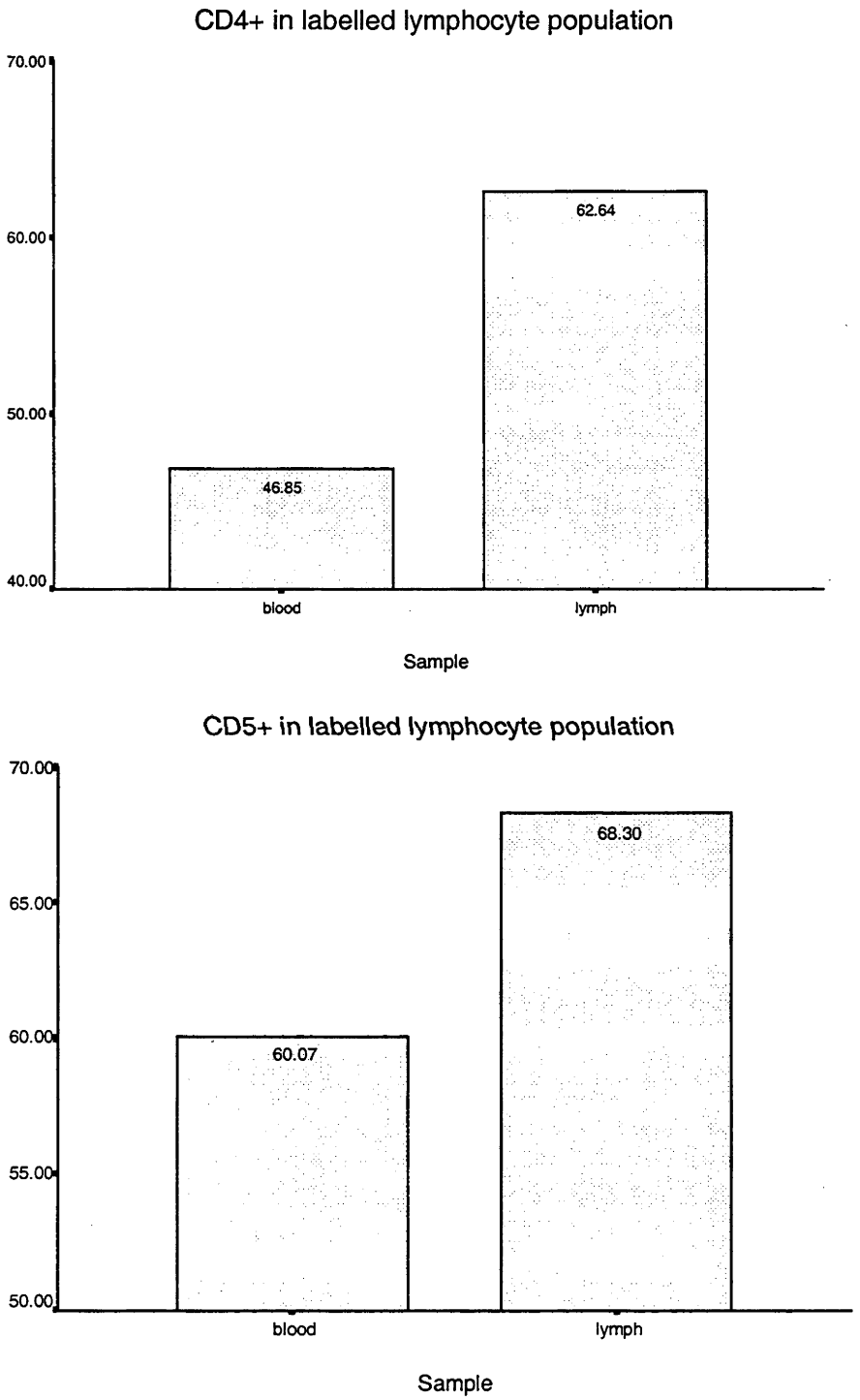

Figure 3.9B: The distribution of lymphocyte subsets in the labelled population in all experiments (aggregated).

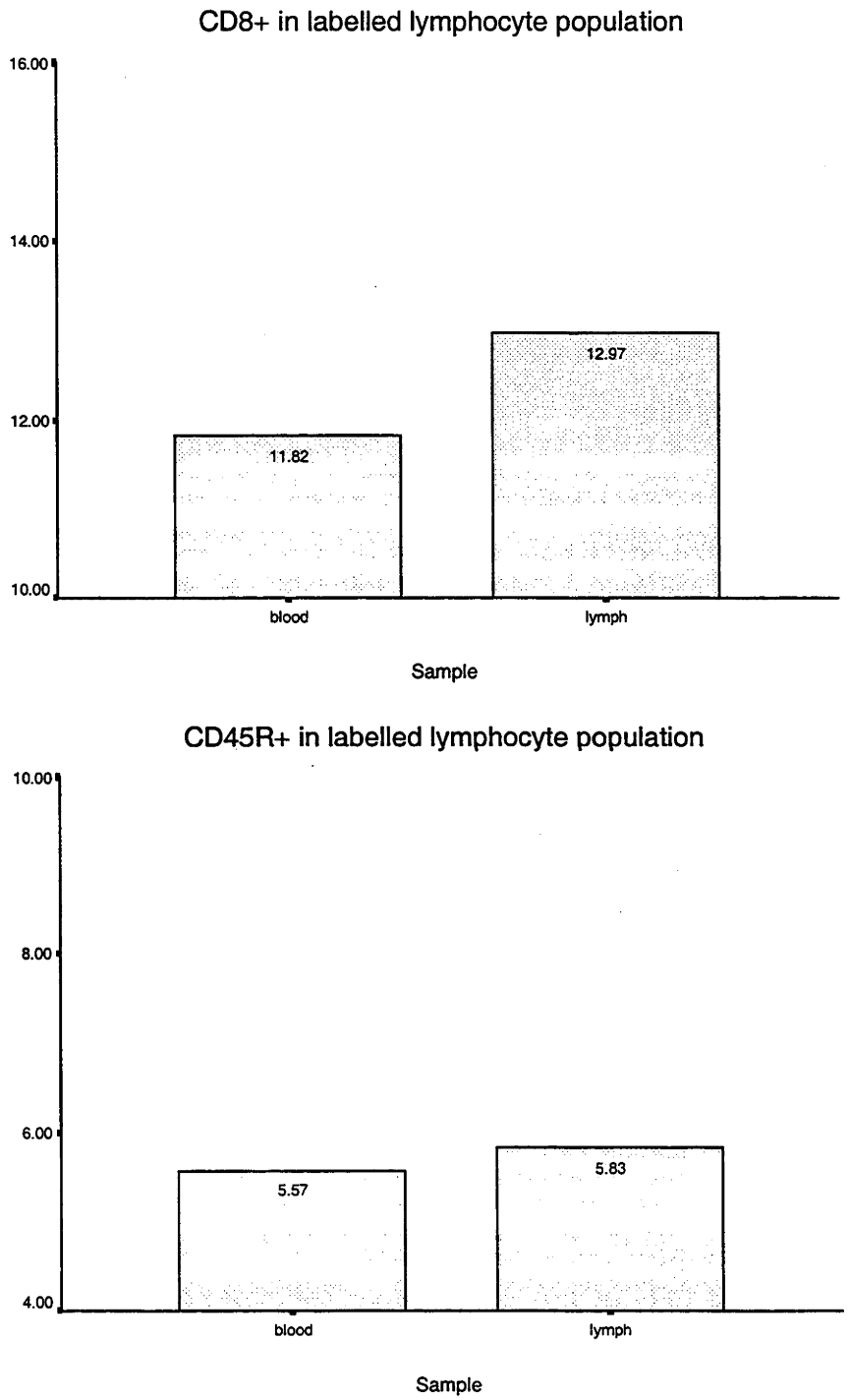

Figure 3.10A: The distribution of lymphocyte subsets in the unlabelled population in all experiments (aggregated).

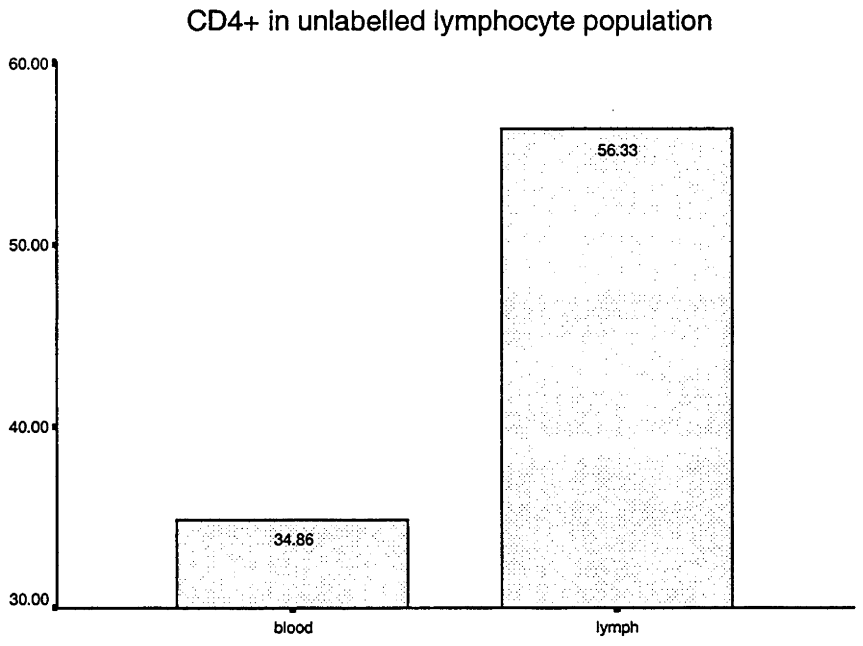

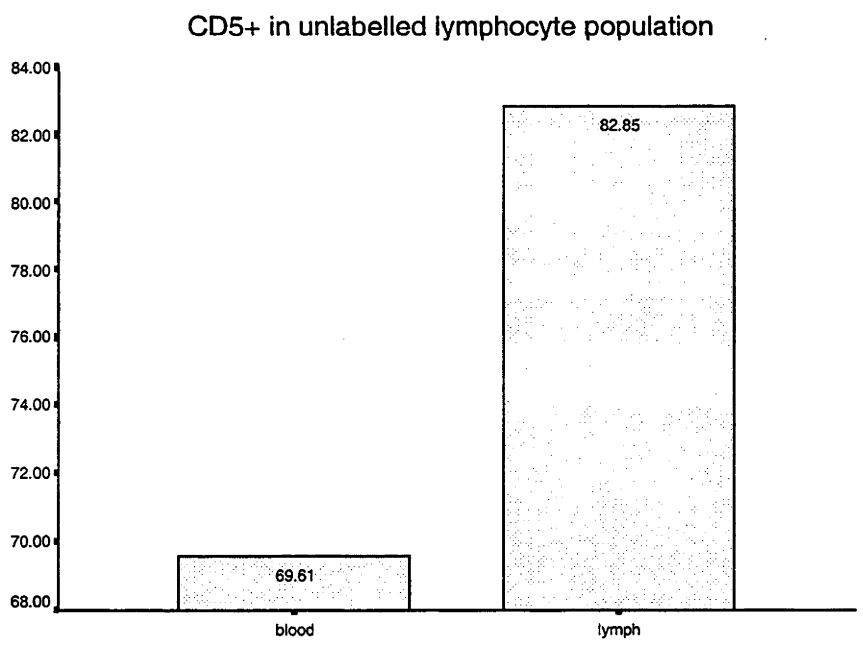

Figure 3.10B: The distribution of lymphocyte subsets in the unlabelled population in all experiments (aggregated).

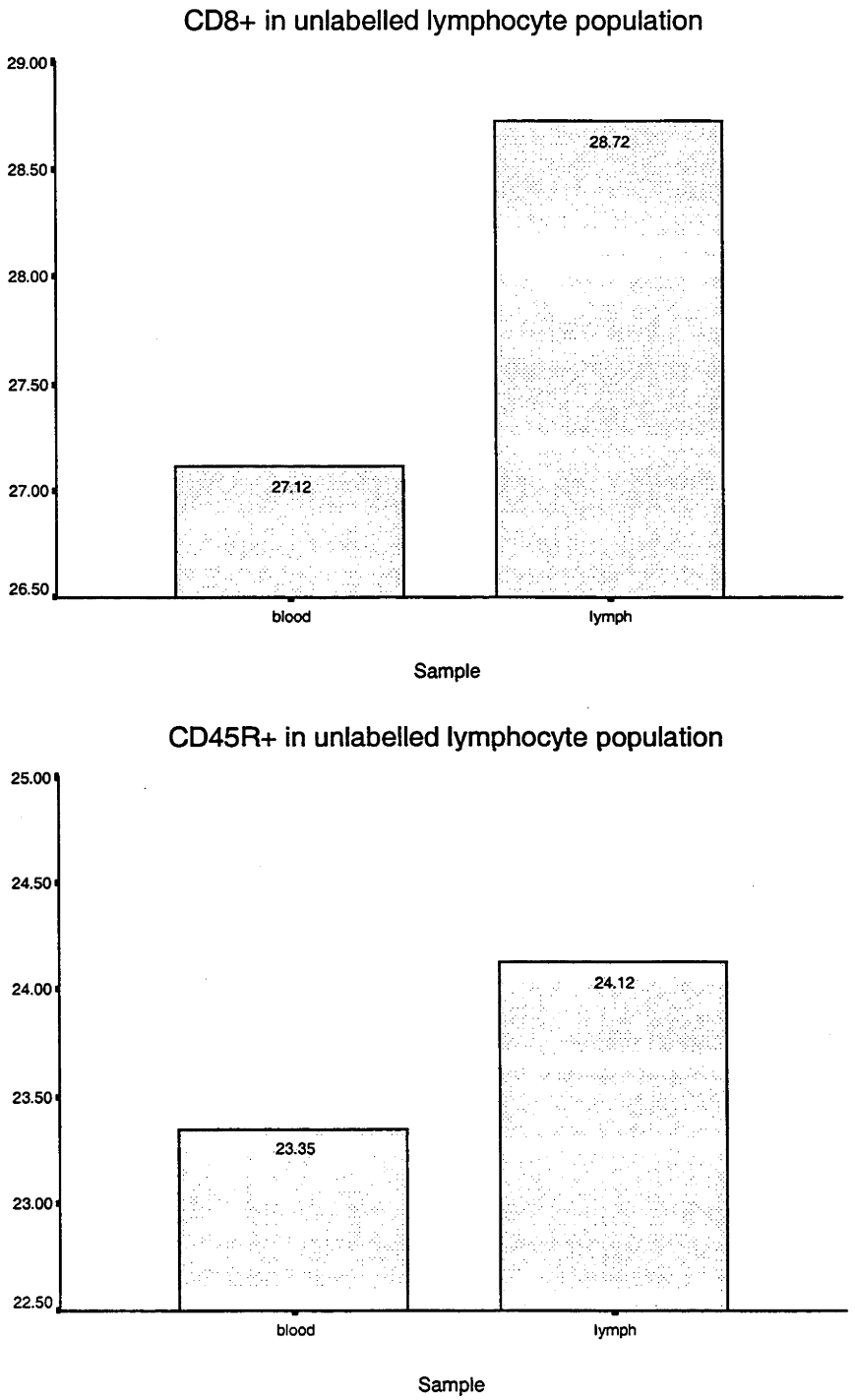

3.3.2 The relationship between lymphocyte subsets in the blood and efferent lymph and its interpretation

Under normal physiological conditions, it has been shown that 95% of the lymphocytes appearing in efferent lymph are derived from the blood (Hall and Morris, 1962; Hall and Morris, 1965b). The derivation of such a high proportion of lymphocytes from blood ensures that the levels of lymphocytes in blood, and any change in that level are very likely to affect those in the efferent lymph. Any description of the relationship between lymphocytes (and their subsets) found in the blood and in efferent lymph should assist in understanding lymphocyte migratory properties. There have been a number of previous studies describing the relationship between lymphocyte subsets found in blood and efferent lymph (Andrade *et al.*, 1998; Washington *et al.*, 1988; Abernethy *et al.*, 1990; Witherden *et al.*, 1990; Abernethy *et al.*, 1991).

Successful lymphocyte migration requires the operation of mechanisms of lymphocyte-endothelial interaction of the type already described in Chapter1 of this thesis. Lymphocyte-endothelial interactions are generally assumed to entail active participation by both lymphocytes and endothelial cells. The term "**extraction**" has often been used in lymphocyte recirculation studies to describe the efficiency of lymphocyte migration from blood (in the postcapillary venules) to the efferent lymph. However, this term should not be taken to imply that the lymphocytes in blood are passively "extracted" by the endothelial cells lining the postcapillary venules. Nevertheless, this term will be retained in this thesis to avoid any misinterpretation as it appeared in many original articles.

In one of these earlier studies, the differences between extraction rates of different lymphocyte subsets of lymphocytes from blood to lymph were reported (Washington *et al.*, 1988). In that study, using some additional assumptions and values from the literature, the authors calculated the number of lymphocytes delivered to and leaving the lymph node. Linear regression equations were then applied to derive a linear relationship between the number of lymphocytes in blood delivered to the lymph node and the numbers leaving in efferent lymph from the lymph nodes. These have been plotted on the x and y-axes respectively. Subsequently, the slopes were measured as a representation of extraction ratios. According to the linear equation in that study, higher slope values reflected a higher extraction rate. Using those defined extraction ratios, it was concluded that, under steady state conditions, CD4 lymphocytes were extracted from blood by the lymph node at a faster rate than other T lymphocyte subsets, including CD8 lymphocytes.

In some previous studies (Abernethy *et al.*, 1990; Witherden *et al.*, 1990; Abernethy *et al.*, 1991), a comparison of lymphocyte subset ratios (such as the CD4/CD8 ratio) between the starting (ie infused) and recirculated (ie labelled) populations was used to distinguish whether there were any migratory differences between different lymphocyte subsets. The hypothesis behind those studies is that if there were any differences between extraction rates of lymphocyte subsets, mediated by the endothelial venules in the lymph node, the subset ratios of the recirculated populations would differ from those of the starting populations. The results from those studies supported the finding that CD4 lymphocytes were extracted from blood more efficiently than any other T lymphocyte subset.

To obtain a parameter that could describe observations in the present study, the **Lymph /Blood (L/B) ratio** was defined as the percentage of a lymphocyte subset found in the efferent lymph divided by the percentage of the same lymphocyte subset occurring in the blood. As was the case with the extraction ratio utilised in a previous study (Washington *et al.*, 1988), the construction of the L/B ratio in the present study was intended to distinguish whether there were any differences between the migratory properties of different lymphocyte subsets. However, the L/B ratio has been defined lymphocytes only for the purposes of the present study as a parameter for describing the relationship between blood and lymph. Unlike the extraction ratio, it was not calculated from the actual numbers of lymphocytes found in blood and efferent lymph to describe the real number of lymphocytes actually delivered to or leaving a lymph node.

In this section, the calculation of the L/B ratio was based upon an assumption that, under normal conditions, all factors except the percentages of lymphocyte subsets involved in lymphocyte recirculation were uniquely invariable factors for each individual animal. These factors include blood and lymph flow rate, blood volume, concentrations of lymphocyte in blood and efferent lymph etc. Thus, the relationship between the number of lymphocyte subsets delivered to and leaving the lymph node (found in blood and efferent lymph respectively) would be in direct proportion to the relationship between the percentage of those lymphocyte subsets found in blood and lymph.

The hypothesis underlying use of the L/B ratio is that all of the lymphocyte subsets found in blood are actively available to be recruited by a lymph node. The applicability of this hypothesis to some lymphocyte subsets, such as gamma-delta T cells, may be subject to argument as there has been a report of the existence of a non-recirculating population of gamma-delta T cells

(Witherden *et al.*, 1990). However, only CD4, CD5, CD8 and CD45R lymphocytes were included in the present study. None of these subsets has been reported to be a non-recirculating population.

The differences observed in the present study between the percentages of lymphocyte subsets in labelled and unlabelled populations have been summarised in Figure 3.11A and 3.11B. In all lymphocyte subsets, except CD4, the percentages of the lymphocyte subset in the unlabelled population was significantly higher ($p<0.05$) than that in the unlabelled population in both blood and lymph samples. These significant differences were even greater in the case of CD8 and CD45R subsets than in that of the CD5 subset. By contrast, the percentages of the CD4 subset in the blood and lymph in the labelled population (ie 46.85% and 62.64% respectively) were significantly greater ($p<0.05$) than those in the unlabelled population (ie 34.86% and 56.33% respectively).

The L/B ratios were derived from the overall mean percentages of lymphocyte subsets in both labelled and unlabelled populations (Table 3.4). The values for the L/B ratio obtained in the case of CD8 and CD45R were very close to unity in both populations. The L/B ratios of labelled and unlabelled CD5 populations were slightly larger, namely 1.137 and 1.190 respectively. Nevertheless they still remained very close to each other. In contrast, the L/B ratios of CD4 cells were much greater than unity in both populations, namely 1.337 and 1.616 for labelled and unlabelled populations respectively.

Table 3.4: Summary of distribution of lymphocyte subsets (in overall experiments) in unlabelled and labelled lymphocytes and the L/B ratios.

	Labelled lymphocytes			Unlabelled lymphocytes		
	Blood	**Lymph**	**L/B Ratio**	**Blood**	**Lymph**	**L/B ratio**
CD4	46.85	62.64	1.337	34.86	56.33	1.616
CD5	60.07	68.30	1.137	69.61	82.85	1.190
CD8	11.82	12.97	1.097	27.12	28.72	1.059
CD45R	5.57	5.83	1.047	23.35	24.12	1.033

The values obtained for L/B ratios in the present study suggest that, of the lymphocyte subsets that were examined, CD4 lymphocytes were extracted from the blood with the greatest efficiency since the L/B ratios for them were invariably greater than other subsets. CD5 lymphocytes were extracted from the blood more efficiently than CD8 and CD45R lymphocytes. There was no significant difference in the efficiency with which CD8 and CD45R lymphocytes were extracted from the blood. These results recall previous reports that CD4

lymphocytes were extracted from the blood faster than CD5 and CD8 lymphocytes (Washington *et al.*, 1988; Abernethy *et al.*, 1990; Abernethy *et al.*, 1991).

The explanation for inequality of L/B ratios of CD4 lymphocytes in labelled and unlabelled populations, ie 1.337 and 1.616 respectively, is more complicated. The impact of tissue-specificity on the lymphocyte-endothelial cell recognition mechanism has been well established (Mackay *et al.*, 1988; Kimpton *et al.*, 1990; Mackay *et al.*, 1992; Washington *et al.*, 1994). In other words, recirculating lymphocytes may display a preference for recirculation through their tissue of origin. However, this was not the case in this study, as the labelled and unlabelled populations were derived from the same tissue, namely a peripheral lymph node. Some studies have reported on the effect of the type of lymphocyte subset (ie lymphocyte subset-specificity) on lymphocyte-endothelial recognition (Abernethy *et al.*, 1990; Abernethy *et al.*, 1991). Briefly, in those studies, some specific lymphocyte subsets (such as CD4) were always recruited from blood more efficiently than others, regardless of the sources of origin of those subsets. More importantly, it was found that those two factors (tissue-specificity and lymphocyte subset-specificity) influenced the lymphocyte-endothelial cell recognition mechanism independently.

L/B ratios in labelled and unlabelled populations reflect the influence of tissue-specific and lymphocyte subset-specific events respectively in the lymphocyte-endothelial cell recognition mechanism. The findings of the present study suggested that the lymphocyte subset-specific event is probably more important than the tissue-specific event in lymphocyte-endothelial cell recognition mechanisms of CD4 lymphocytes. This suggestion originated from the finding that the L/B ratio of CD4 lymphocytes in an unlabelled population (ie 1.616) was higher than in a labelled population (ie 1.337). On the other hand, lymphocyte subset-specific and tissue-specific events may be of equal importance in regulating the lymphocyte-endothelial cell recognition mechanism of CD5, CD8 and CD45R lymphocytes.

In the present study, only one lymphocyte CD molecule has been identified on the surface of each individual lymphocyte by the technique of monoclonal staining. However, there are undoubtedly some lymphocytes that present two or more CD molecules of interest (ie CD4, CD5, CD8 and CD45R) on their surfaces. For this reason the summations of the percentages of some lymphocyte subsets (such as CD4 and CD5) in the present study often exceeds 100% (Table 3.2, 3.3, and 3.4).

Figure 3.11A: A comparison of distribution of CD4 and CD5 lymphocyte (in overall experiments) in unlabelled and labelled populations of lymphocytes

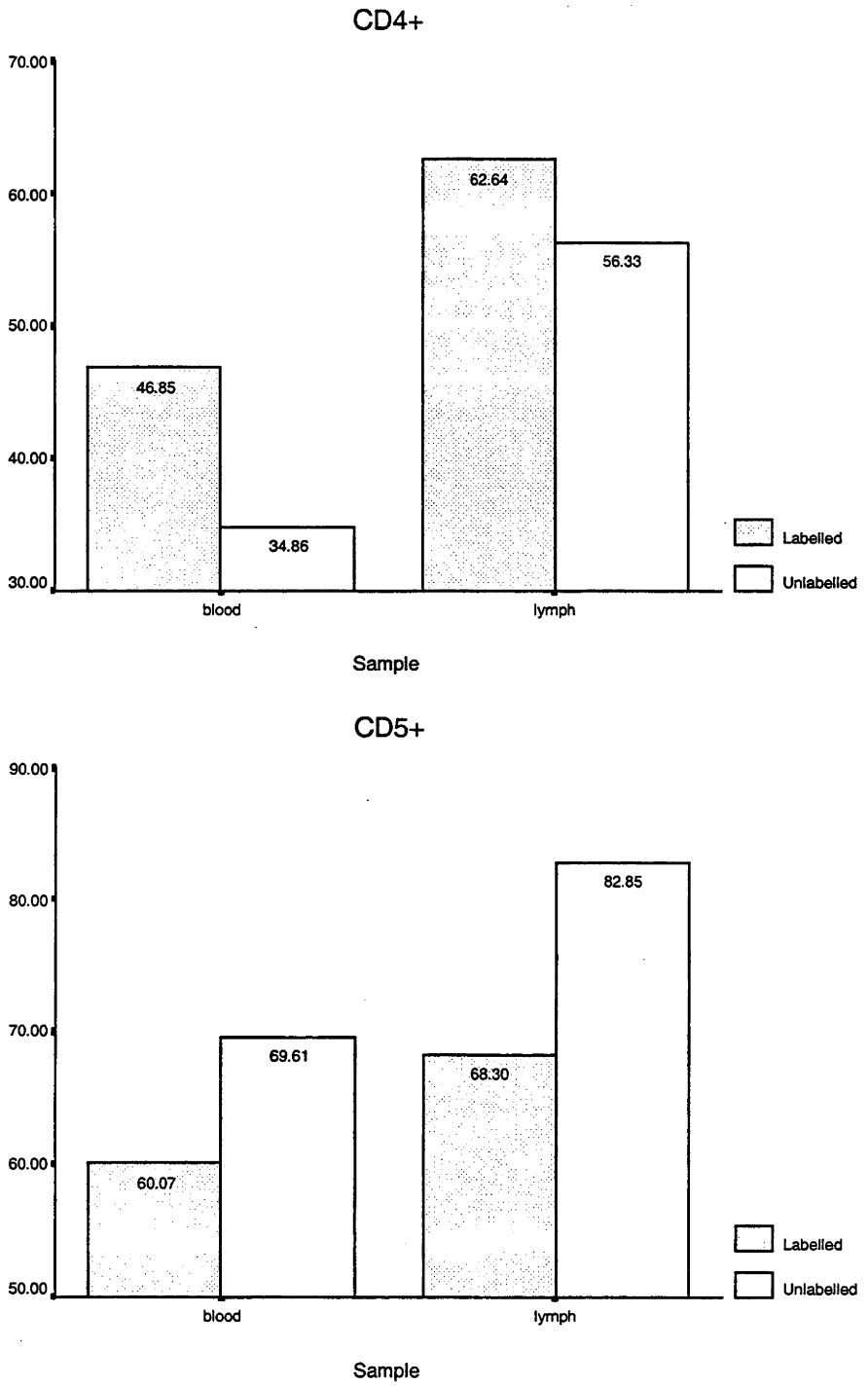

Figure 3.11B: A comparison of distribution of CD8 and CD45R lymphocyte (in overall experiments) in unlabelled and labelled populations of lymphocytes

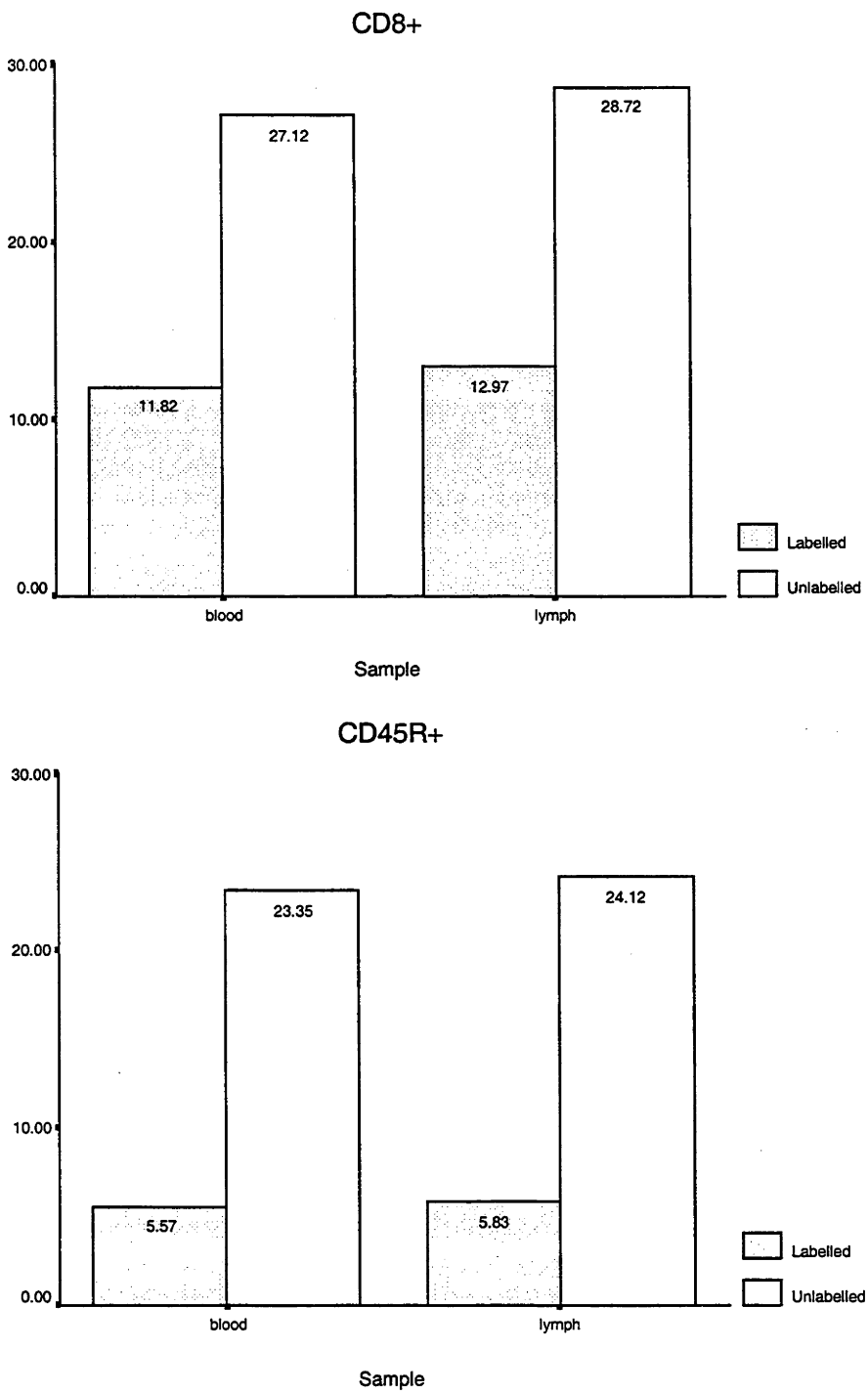

Chapter 4/
Compartmental models

4.1 Introduction

The concept of "compartment theory" was first thoroughly described in the late 1930s and has been used to explain biochemical and pharmacological processes from before 1940[28](Periti, 1964). Although a substantial number of tracer based studies were analysed during 1940-1960 in terms of compartment theory, no attempts were made to adopt a standard approach to compartmental analysis concepts. Most studies during that time involved the fields of physiology, biochemistry and pharmacology (Sheppard, 1962). Jacquez[29] defined a compartmental system as one which is made up of a finite number of macroscopic subunits called compartments, each of which consists of a homogenous and well-mixed material This definition has appeared in all editions of his books on the subject with slightly variations (Jacquez, 1972; Jacquez, 1985; Jacquez, 1996).

Currently, compartmental analysis is being widely used as a means of describing problems in a wide range of fields such as the biomedical, physical and social sciences. Researchers in pharmacokinetics, metabolic process and ecosystem modelling are among those who are most likely to gain more benefits from this type of analysis. Compartmental models were used to simulate the outputs and control the optimal level of anaesthetic agents administered intravenously (Young and Hsiao, 1994). In the treatment of kidney failure, the kinetics of waste products (such as urea) was efficiently described and explained using a two-compartmental model of urea kinetics (Grandi *et al.*, 1995). Parameters identified from the urea kinetics model have helped medical scientists to understand the real kinetics of urea in patients, to control urea at a steady level, and to develop advanced and alternative therapies for those who suffer from kidney failure.

---

[28] In 1964, PF Peritri commented about some previous works related to the compartment theory.
[29] John A Jacquez was one of the foremost scientists who made a great contribution to the compartmental analysis theory. His publication of the first edition of "Compartmental analysis in biology and medicine" in 1972 represented a major development of this type of analysis.

4.2 Compartmental models

This section will introduce some fundamental elements relating to compartmental models. Full details of both fundamental and advanced principles of compartmental analysis can be found in a number of sources (Jacquez, 1972; Godfrey, 1983; Jacquez, 1985; Jacquez, 1996). Several definitions relevant to this subject follow.

Compartment: Jacquez defined a compartment as "an amount of a material that acts kinetically like a distinct, homogeneous amount of material" (Jacquez, 1996). Sheppard described a compartment as "a quantity of a substance which has a uniform and distinguishable kinetic of transformation or transport" (Sheppard, 1948). Either a box or a circle is used to represent a compartment (Figure 4.1(a)).

The transfer coefficient is represented by an arrow defined as the "fraction of compartment from which the arrows originates, transferred per unit time" (Jacquez, 1985). From this definition, a material flow, ie rate of transfer, can be calculated from the product of the transfer coefficient and the compartment of origin. An arrow represents the direction of material flow while k_{ij} represents the transfer coefficient from compartment j to i. (Figure 4.1(b)).

Figure 4.1: Fundamental elements in compartmental models

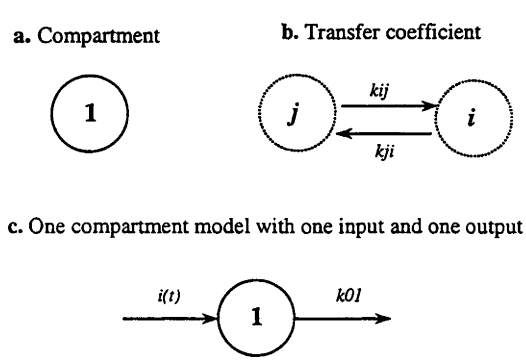

A compartment (a) and transfer coefficients (b) are represented by a circle and arrows respectively. A single compartmental model with one input and one output (c) is constructed by connecting two transfer coefficients with a compartment.

All of the following compartmental models are restricted to a particular class of linear systems defined as "***linear time-invariant***" models (ie, linear compartmental models with constant transfer coefficients). In other words, mass or material is linearly transferred from one compartment to another via constant

coefficient(s). More details about linear time-invariant systems can be found in Part II of Chapter 1 of this thesis.

Mathematical expressions for compartmental models: The mathematical equations used to represent compartmental models have been derived from balance equations applicable to physical and measurable parameters such as mass or heat. The conservation of mass is thus applicable to compartmental models.

When using compartmental models it is possible to formulate models in the form of mass or concentration. However, in this chapter, only balance equations concerned with the number of lymphocytes will be used in order to avoid any possible confusion in a mathematical context. For instance, the single compartmental model in Figure 4.1(c) represents a simple example of compartmental models. The mathematical model is a first order differential equation

$$\frac{dq_1(t)}{dt} = -k_{01}q_1(t) + i(t)\,. \tag{4.1}$$

where $q_1(t)$ is defined as the mass in the compartment and the subscript 1 identifies the particular compartment of interest. k_{01} is a positive constant value. The left-handed term of equation (4.1) describes the changing rate of $q_1(t)$, which is equal to the difference in rates of incoming, $i(t)$, and outgoing mass, $k_{01}q_1(t)$. The plus and minus signs indicate the direction of incoming and outgoing mass compared to the compartment that is being studied. In (4.1), the mass in the compartment 1 is increased and decreased by rates $i(t)$ and $k_{01}q_1(t)$ respectively.

Assuming that the external input rate is constant, $i(t) = I$, (4.1) can be solved to give

$$q_1(t) = q_1(0)e^{-f_{01}t} + \frac{I}{f_{01}}\left[1 - e^{-f_{01}t}\right] \tag{4.2}$$

where $q_1(0)$ is the constant value of the initial mass in the compartment (mass at time zero). From (4.2), it is clear that any changes that occur to f_{01} will produce a change in $q_1(t)$. Details for solving differential equations can be found in many sources (Kreyszig, 1993).

4.3 Lymphocyte migration: A view of compartmental modelling

Lymphocyte migration and related issues have been described in Chapter 1. This section summarises the events of lymphocyte migration in order to describe how a compartmental model is constructed.

Lymphocytes have a remarkable capacity to recognise specialised endothelial cells lining the capillary wall. Lymphocytes can attach to the wall, emigrate from the capillary through its wall and finally migrate into the surrounding lymphoid tissue. This property allows mature lymphocytes to travel through arterial and venous systems and return to their own sites of origin, the secondary lymphoid tissues. Figure 4.2 illustrates the sequence of events during lymphocyte migration. In general, lymphocytes that have successfully migrated through a lymph node have participated in all of the following processes

(1) **Delivery**: Lymphocytes circulate through the arterial system (via the arterial branches) and reach their site of migration, ie the postcapillary venules.
(2) **Adhesion:** Lymphocytes adhere to the endothelium of postcapillary venules using tissue-specific mechanisms of lymphocyte-endothelial cell reaction.
(3) **Emigration**: The physical configuration of lymphocytes changes allowing them to escape from the blood circulation via an inter-endothelial space.
(4) **Retention**: After successfully entering the lymphoid tissue, lymphocytes continue to migrate along pathways in the lymphoid tissue. Some lymphocytes migrate freely (ie mobile lymphocytes) while others bind themselves to the reticular mesh in lymphoid tissues (bound lymphocytes) in the course of immune responses. After a certain time, bound lymphocytes can detach (from the reticular mesh), become mobile and proceed with their migration until they reach their final destination, the efferent lymph vessel.

Previous studies have revealed the time scales of these stages during the process of lymphocyte migration in lymphoid tissue (Bjerknes *et al.*, 1986; Borgs and Hay, 1986). These time scales are of the order of seconds for delivery and adhesion and of minutes and hours for emigration and retention respectively. These time scales have influenced the form of construction of the compartmental model(s) to be described in the section 4.4.2 (lymph node model).

Figure 4.2: Diagram of lymphocyte migration

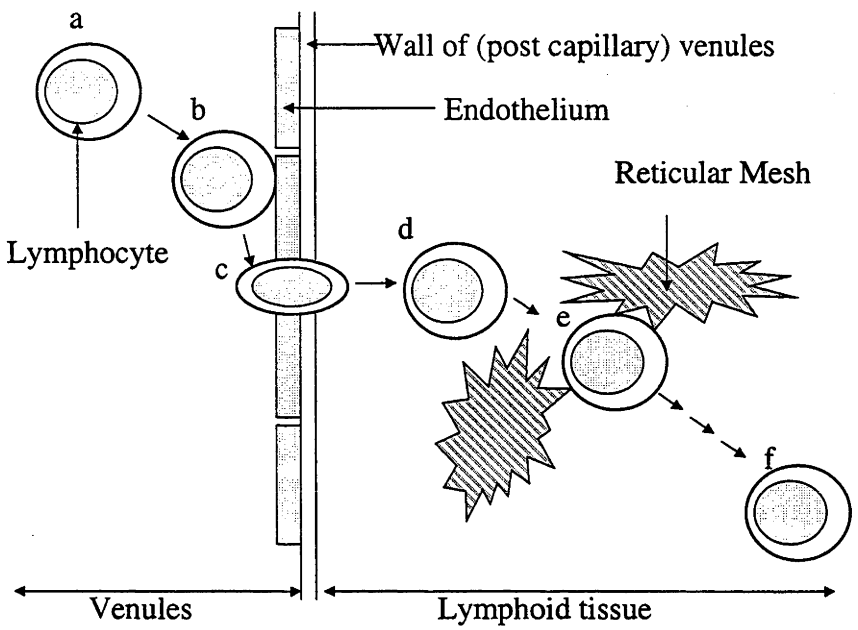

Figure 4.2 demonstrates the different stages of lymphocyte migration through lymphoid tissue in a lymph node. Lymphocytes travel along the blood vessel until they enter a postcapillary venule (a), then adhere to the endothelium (b) and migrate into the lymphoid tissue via an inter-endothelial space (c). In the lymphoid tissues, lymphocytes can be considered either to be mobile (d) or bound (to the reticular mesh) lymphocytes (e). Finally, lymphocytes migrate through the lymphoid tissue and reach the efferent lymph vessel (f) from which lymph samples can be collected. Note that, whilst in lymphoid tissues, lymphocytes in the mobile and bound stages are interchangeable (ie lymphocytes can attach, detach and reattach to the reticular mesh, and there are multiple steps before lymphocytes reach the efferent lymph vessel (f)).

4.4 Model construction

4.4.1 Blood model: a forcing function

Blood circulation plays an important role in almost all forms of biological transport in the body. These include carrying both cellular and non-cellular elements throughout the whole body. The driving force of blood circulation originating with the pumping action of the heart contributes a homogeneous mixture of all the fluid and cells present in the blood circulation, which is in agreement with the principle of the compartmental model. Given this unique characteristic of blood circulation, most medical and biological studies of compartmental models have been designed to present the blood (or plasma[30]) as the central compartment in the form of mamillary models[31], (ie multi-compartmental models in which a central compartment is connected to the others).

The transportation role of the blood circulation is most important in understanding lymphocyte recirculation and migration. Lymphocytes require the underlying force of the blood circulation to transport them to a migration site (ie postcapillary venules in a lymph node) before the whole process of emigration out of the blood stream can be completed. Even a mamillary model can be assumed to represent the kinetics of lymphocyte in the blood circulation. However, in the present study, to avoid solving successive unknown parameters in the final model, ***a forcing function*** was introduced as an alternative to represent lymphocyte kinetics in the blood compartment.

A forcing function is a known or defined mathematical function (in the time domain) that fully describes the kinetics of subjects of interest. The forcing or defined input function approach has been utilised to identify the unknown parameters in a number of complex systems in previous studies (Foster *et al.*, 1979; Miller *et al.*, 1981; Hirano and Yamada, 1983). In one of those studies (Foster *et al.*, 1979), a mechanistic model was used to explain zinc kinetics following a single intravenous injection of radioisotopically labelled zinc (^{69m}Zn). This zinc model comprised the plasma compartment (acting as the central compartment) connected with several peripheral compartments such as liver and red blood cells. At first, the ^{69m}Zn activity in plasma was fitted to a sum of exponentials and defined as a forcing function. This forcing function was used to

[30] Plasma is a cell-free fluid component of blood.
[31] A mamillary (or mechanistic) system is defined as a system in which a central compartment is surrounded by peripheral compartments which exchange material only with the central compartment and not with each other (Godfrey,1983).

provide a fractional input for the other compartments. In other words, the forcing function acts as an input-source function for the remainder of the model. The identification of unknown transfer coefficients was undertaken individually for each compartment. Subsequently, the final model was achieved in its entirety by assembling all the peripheral compartments together with the plasma compartment.

In the initial stage of present study, a search for a suitable forcing function for lymphocyte kinetics in the blood circulation was undertaken on a trial and error basis. As previously described in Chapter 3, after labelled lymphocytes are intravenously infused, they disappeared rapidly from the blood in the first few hours and the blood concentration gradually decreased to a relatively stable level after 24-48 hours. So a number of exponential functions[32], including a sum of two, three and four-term exponential functions, were selected and tested for their similarity as a forcing function by fitting each function individually to the actual data. Compared with two other functions, the sum of two-term exponentials in the form of

$$y(t) = A_1 e^{-\lambda_1 t} + A_2 e^{-\lambda_2 t} \qquad (4.3)$$

was selected where A_1, A_2, λ_1 and λ_2 are constant positive values. This choice was made on the basis of its general performance in relation to the quality of fitness and the reliability of identified parameters (data not shown). Having the sum of two-term exponentials as a satisfactory forcing function, the algorithm implemented in SAAMII allows one to connect this function to any other compartment(s) via (a) fraction coefficient(s). More detail will appear in section 4.6 (Fitting procedures).

Figure 4.3: Forcing function

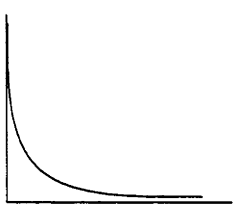

A schematic figure of a forcing function represents the lymphocyte kinetics in the blood circulation which follows the pattern of a sum of two-term exponentials. The full description of this was given in section 3.2.1of Chapter 3.

[32] Only some exponential functions with different terms were selected owing to the pattern of disappearance of labelled lymphocytes in blood. An exponential function is a function that has a power term of e (a real value of about 2.71828..).

4.4.2 Lymph node model

The single-compartmental model of the lymph node was associated with the forcing function described in section 4.4.1 and fitted the data obtained from some experiments. However, the results from this model could not clearly explain lymphocyte migration within the node as this single compartmental model assumes that all lymphocytes behave identically, ie one homogenous kinetic, which is unlikely to be the case in reality. Some previous studies have reported that different lymphocyte subtypes have different abilities to migrate in lymphoid tissue (Washington *et al.*, 1988; Abernethy *et al.*, 1990; Abernethy *et al.*, 1991), ie more than one kinetic system is required to explain lymphocyte kinetics in lymphoid tissue in its entirety. Thus a more complicated model would be more appropriate to explain this.

The multi-compartmental model in Figure 4.4(a) was initially constructed according to the physiology of lymphocyte migration as previously outlined in section 4.3. A full description of this model was given in Figure 4.4(a). However, to fit with the available experimental data, there was a need to modify this physiologically based model to another model, namely the modified multi-compartmental model (Figure 4.4(b)). There are n pairs (ie loops) of Compartment M and B in this model. The first Compartment M (M_1) receive lymphocytes (ie an input) from the blood whilst the last (M_n) deliver lymphocytes to the external system (ie as monitored in the efferent lymph). Compartment M and B represent, respectively, mobile (ie fast dynamics) and bound stages (ie slow dynamics) of migrating lymphocytes within the lymphoid tissue.

In this model, each Compartment B acts as a lymphocyte reservoir by receiving lymphocytes from the corresponding Compartment M, and storing and releasing them at a later stage. Lymphocytes in Compartment M could either bind to the reticular mesh (ie enter to corresponding Compartment B via k_{bm}) or migrate further to the next adjacent Compartment M via k_{mm}.[33] However, lymphocytes that reside in Compartment B can only leave the lymph node by passing through the corresponding Compartment M via k_{mb}, ie there is no real connection from Compartment B to the external system. This is relevant to the physiological reality since bound lymphocytes must detach themselves from the reticular mesh and become mobile lymphocytes before proceeding with migration.

[33] k_{mm} is defined as the transfer coefficient for lymphocytes transferred from Compartment $M_{(n-1)}$ to M_n and for lymphocytes transferred from the final M-Compartment to the external system. Where n is equal or greater than 2. However, this was defined will be used only in this thesis as it does not agree with the standard definition of compartmental model analysis.

The modified multi-compartmental model in Figure 4.4(b) was constructed by lumping together some parameters of the physiologically based model (Figure 4.4(a)). To achieve this, a few assumptions were made. First, all of the parameters that may be relevant to delivery (D), adhesion (A) and emigration (E) in physiologically based (ie true) models were aggregated into the entire modified multi-compartmental model. This assumption was dependent upon the knowledge that the time scale of those events, which is of the order of seconds for delivery and adhesion and of minutes for emigration (Bjerknes *et al.*, 1986), would have a minor impact upon the lymphocyte migration model as a whole (ie the entire migration process would take up to several hours). Second, among a pair (ie loop) of M and B compartments, there are three transfer coefficients to be identified (ie k_{mm} , k_{bm} , and k_{mb}). Subsequently, there will be 3 x n transfer coefficients for a model with n M-B loops. However, to make the fitting procedure simpler, all of those three transfer coefficients were assumed to be identical for all individual loops in the model (ie each individual loop represents identical lymphocyte kinetics). This may be relevant to the existence of anatomical segmentation of lymphoid tissue in that lymphocytes within each individual segment would probably have similar kinetic properties.

Brief descriptions of mathematical equations (ie mass balance equations) representing the first loop (ie Compartment M_1 and B_1) of the modified multi-compartmental model of the lymph node can be expressed as a set of differential equations as follows

$$\frac{dq_m(t)}{dt} = i(t) + k_{mb}q_b(t) - k_{bm}q_m(t) - k_{mm}q_m(t) \qquad (4.4)$$

and

$$\frac{dq_b(t)}{dt} = k_{bm}q_m(t) - k_{mb}q_b(t)\,. \qquad (4.5)$$

where $q_m(t)$ and $q_b(t)$, represent respectively the number of lymphocytes in Compartment M_1 and B_1. $i(t)$ is the external input of lymphocytes to Compartment M_1. In this case, this input is a fraction of the forcing function (previously defined in blood model, section 4.4.1) via k_{m1}. Given $i(t)$ is a constant value of I and an initial condition that $q_m(0) = q_b(0) = 0$ (ie there are no labelled lymphocytes in Compartment M_1 and B_1 at time zero) a set of solutions written in exponential equations can be solved from (4.4) and (4.5) as

$$q_m(t) = -\frac{(\lambda_2 + k_{mm} + k_{bm})\cdot I}{\lambda_1(\lambda_2 - \lambda_1)}\left[1 - e^{\lambda_1 t}\right] + \frac{(\lambda_1 + k_{mm} + k_{bm})\cdot I}{\lambda_2(\lambda_2 - \lambda_1)}\left[1 - e^{\lambda_2 t}\right] \qquad (4.6)$$

and $$q_b(t) = \frac{(\lambda_1 + k_{mm} + k_{bm})(\lambda_2 + k_{mm} + k_{bm}) \cdot I}{k_{mb}(\lambda_2 - \lambda_1)} \left(\frac{\left[1 - e^{\lambda_2 t}\right]}{\lambda_2} - \frac{\left[1 - e^{\lambda_1 t}\right]}{\lambda_1} \right) \quad (4.7)$$

where $$\lambda_1, \lambda_2 = \frac{-(k_{mm} + k_{bm} + k_{mb})}{2} \pm \frac{1}{2}\sqrt{(k_{mm} + k_{bm} + k_{mb})^2 - 4(k_{mm} \cdot k_{mb})} \quad (4.8)$$

Theoretically, the solution of the remainder of the model could be achieved by means of the same approach following (4.4) to (4.8). It is noted that taking time at infinity, the solution of equations gives a steady stage distribution of cells in the entire compartment. Subsequently, from (4.5), this leads to $\frac{dq_b(\infty)}{dt} = 0$ and

$$k_{bm} q_m(\infty) = k_{mb} q_b(\infty) \quad (4.9)$$

$$\frac{q_m(\infty)}{q_b(\infty)} = \frac{k_{mb}}{k_{bm}} \quad (4.10)$$

Equation (4.10) describes the relationship between two coefficients k_{mb}, k_{bm} and mass in Compartment M and B at the steady stage (ie time infinity).

Figure 4.4: Diagram of lymph node models

a) Physiologically based model

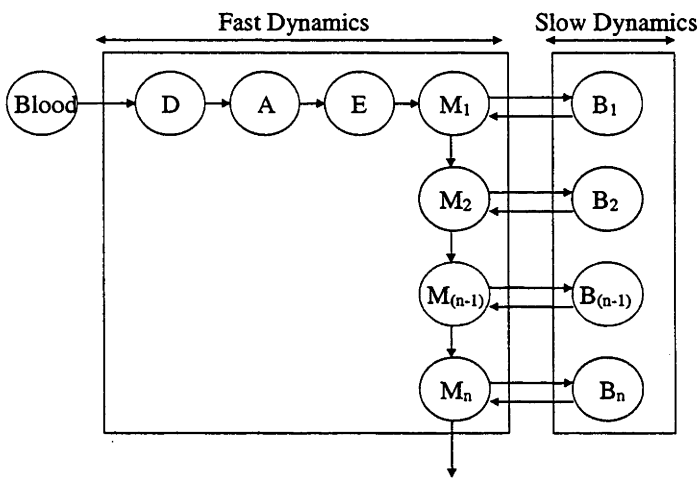

Figure 4.4(a) demonstrates a multi-compartmental model of the different stages of lymphocyte migration through the lymph node. D, A and E denote the delivery, adhesion, and emigration stages. There are serial compartments of the mobile and the bound stage. (M1,..,Mn and B1,..,Bn respectively). Each compartment of the mobile and bound stages is connected to each other. The fast dynamics compartment comprises all stages of D, A, E and M Meanwhile, the slow dynamics compartment comprises all stages of B.

b) Modified multi-compartmental model

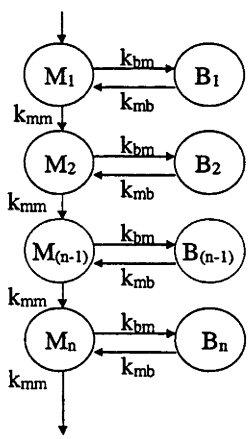

Figure 4.4(b): The modified multi-compartmental model represents lymphocyte kinetics within the lymph node. Compartment M and B represent, respectively, mobile (ie fast kinetics) and bound (ie slow kinetics) compartments in lymphoid tissue. The transfer coefficients k_{bm}, k_{mb} and k_{mm} were assumed to be of the same value for all individual loops of the entire model. More detail of the model was given in section 4.4.2 of this chapter.

4.4.3 Experimental model

In the experimental model, the forcing function (Figure 4.3) is considered as one single compartment acting as input-source (designated as Compartment 1). The final model for the whole experiment (Figure 4.5) is obtained by connecting the forcing function with the compartment M_1 of modified multi-compartmental model (Figure 4.4(b) by k_{m1}. Subsequently, the input to M_1 is provided by a fractional input from the forcing function (ie a product of k_{m1} and the forcing function).

Figure 4.5: Experimental model

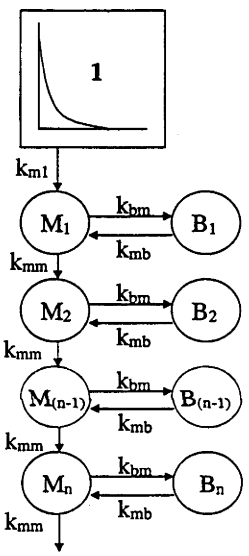

The experimental model is constructed by connecting the forcing function with the modified multi-compartmental lymph node model via a transfer coefficient k_{m1}. The sampling was assumed to have been taken from Compartment M_n of the modified multi-compartmental model.

4.5 Experimental data

Due to the very small levels and the substantial variations of CD8 and CD45R lymphocyte subsets in blood and efferent lymph, data relating to these subsets were discarded after preliminary consideration. The multi-compartmental model was trialed to fit with the remainder of data sets. However, only 7 (out of 21) data sets from the total population study were accepted in the final fitting procedure. Results from two other data sets from CD4 and CD5 subset studies (data not shown) were less satisfactory due to relatively high values of the standard variations of the identified parameters. Thus this section will present only the results of experimental data that were successfully processed through the entire procedure, namely 7 data sets of the total population.

4.6 Model fitting procedures: SAAMII

The experimental model was used to fit the actual data so as to identify the parameters of interest using a forcing or defined input function approach which has been utilised to examine a complex system in a number of studies (Foster *et al.*, 1979; Miller *et al.*, 1981; Hirano and Yamada, 1983). Briefly, a forcing function is a known or defined mathematical function in the time domain that fully describes the kinetics of a compartment of interest. One of those studies, a mechanistic[34] model was used to explain ^{69m}Zn kinetics following a single intravenous injection (Foster *et al.*, 1979). The ^{69m}Zn activity in plasma was fitted to a sum of exponentials and defined as a forcing function. Subsequently, this forcing function was used to provide a fractional input to other compartments (ie such as liver, red blood cells and so on). The identification of unknown parameters was undertaken individually for each compartment.

Similarly, the forcing function approach was adopted in the study of Foster. The two-compartmental model was fitted to the data of the present study by the following procedures.

1. The actual experimental data were normalised (ie non-dimensionalised) to reduce unnecessary parameters in the models. Details of data normalisation have been given in Appendix 1.
2. For the first step, normalised blood data were fitted to the forcing function. The parameters A_1, A_2, λ_1 and λ_2 were determined at this step.

[34] Mechanistic is another name for a mamillary system.

3. Input from Compartment 1 (ie forcing function), defined by a multiplication of the forcing function by the coefficient k_{m1}, was added to Compartment M_1 of the lymph node model.
4. All unknown parameters in the experimental model including k_{m1}, k_{mb}, k_{bm}, and k_{mm} were simultaneously searched for the best fit to the normalised lymph data. The algorithm implemented in ***SAAMII*** (SAAM Institute, Seattle, WA) was used to undertake the parameter identification procedure. When SAAMII fits a model to data, it invokes the optimizer. Through a series of iterations, SAAMII adjusts the value of the adjustable parameters to obtain a "best fit" between the calculated values and the data. The iterative process continues until SAAM II's convergence criteria (ie measures of the goodness of the fit) are satisfied or until the maximum number of specified iterations has been reached (SAAM-Institute, 1997). Once the fit is complete, the final parameter values are saved. The final parameters of which the standard deviations exceeded 50% of their own value were discarded from this analysis. Furthermore, all values in the correlation matrix[35] of those identified parameters must be less than 0.9.

[35]Lesser values in a correlation matrix indicate the higher independence of identified parameters. During fitting procedures, an identified parameter could be confounded with others. The correlation matrix can assist with decisions about final selection of identified parameters.

4.7 Results

Figure 4.6A-4.6D compare model outputs (in solid lines, ie s2) and actual data (normalised data of percentages of labelled lymphocytes in efferent lymph, presented as squared marks, ie lymph). By visual inspection, these model outputs appear to fit well with the actual data. Table 4.1 summarises all parameters (ie A_1, A_2, λ_1 and λ_2) used in the forcing function of individual data sets. Table 4.2 summarises all model parameters (ie k_{m1}, k_{mb}, k_{bm}, and k_{mm}) identified from the fitting procedures and two additionally defined parameters (ie $R_{b/m}$ and $R_{v/t}$). All details of these identified and defined parameters will be discussed in section 4.8 (discussion).

Figure 4.6A: Comparison of model outputs and actual data from R687

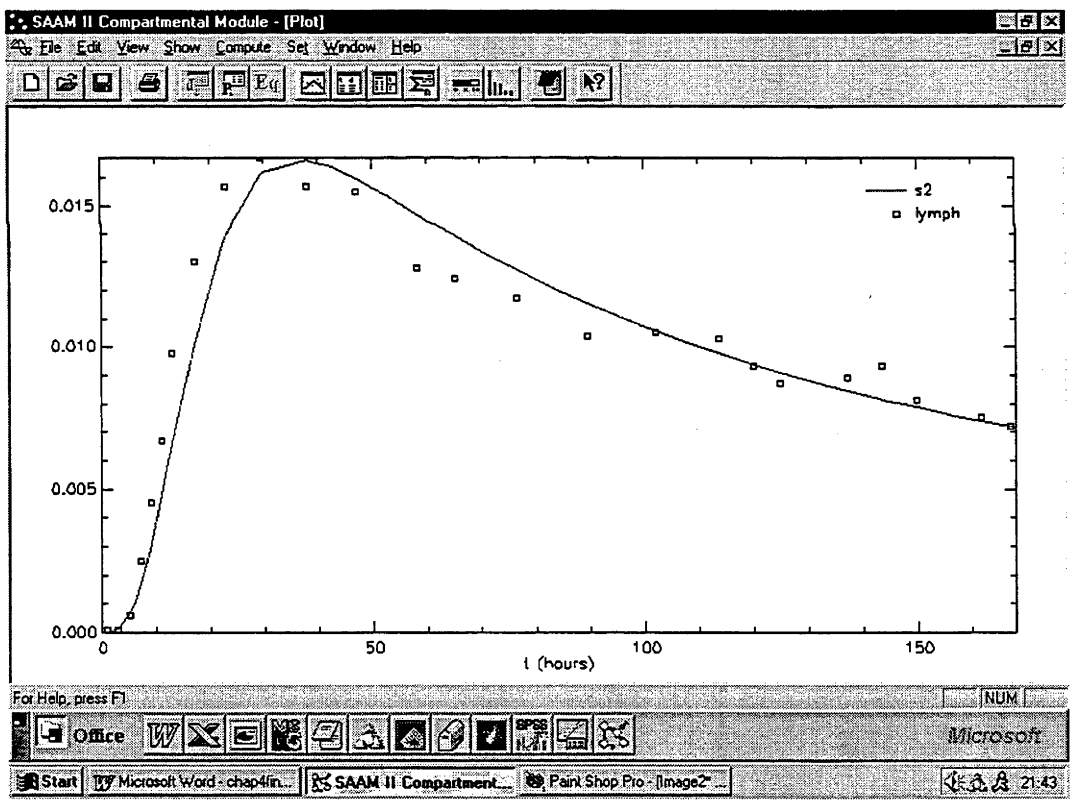

Figure 4.6B: Comparison of model outputs and actual data from R401 (upper panel) and R705 (lower panel)

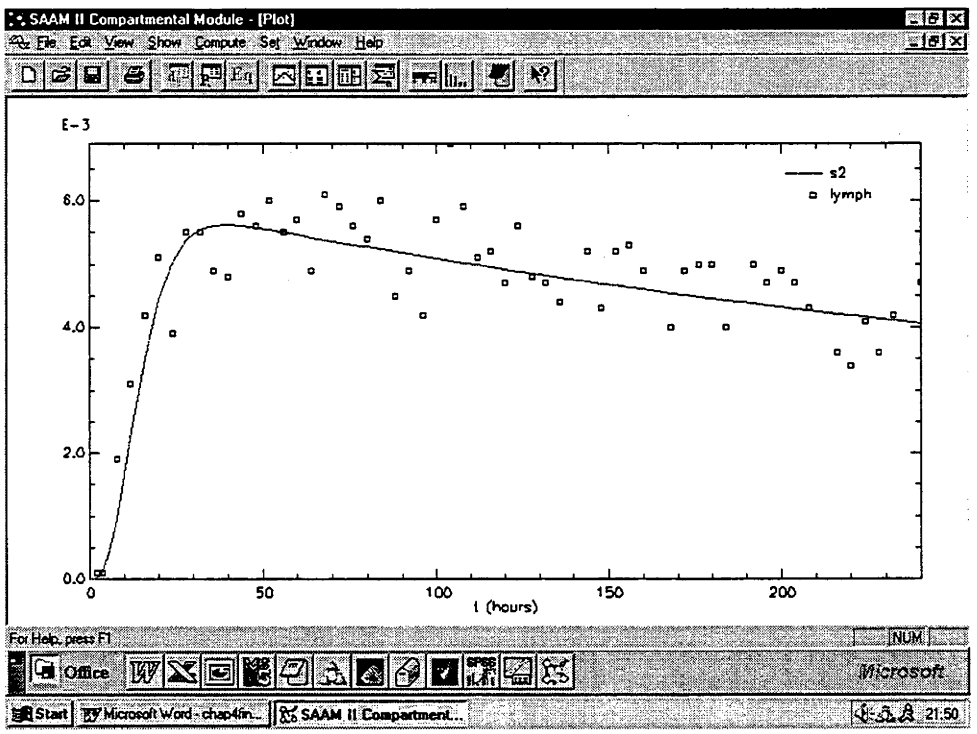

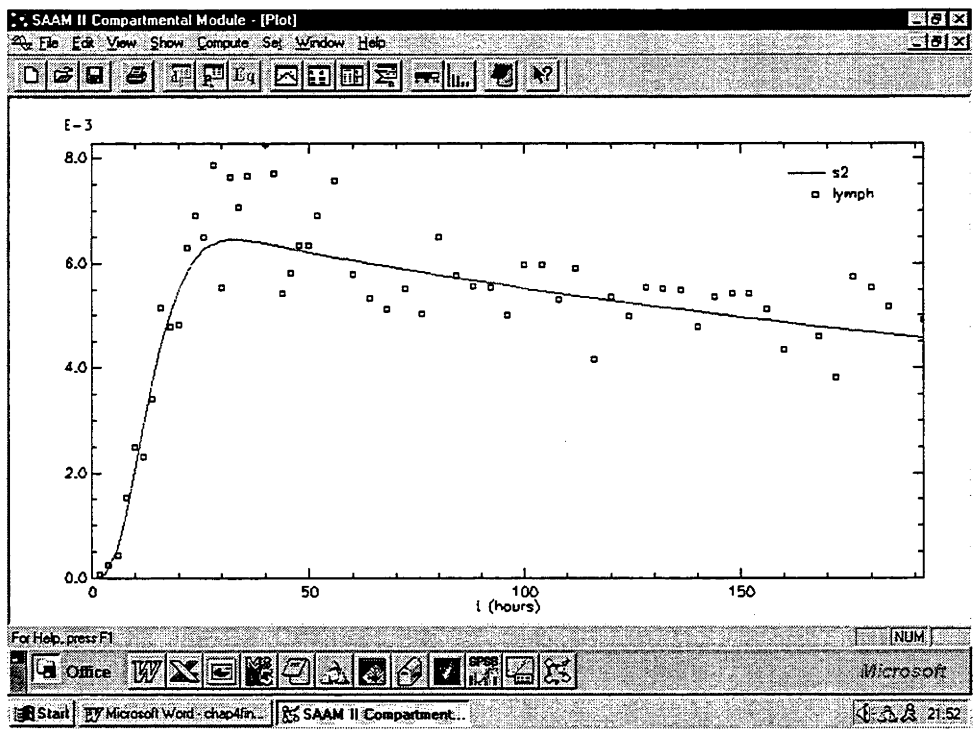

Figure 4.6C: Comparison of model outputs and actual data from R632 (upper panel) and R798 (lower panel)

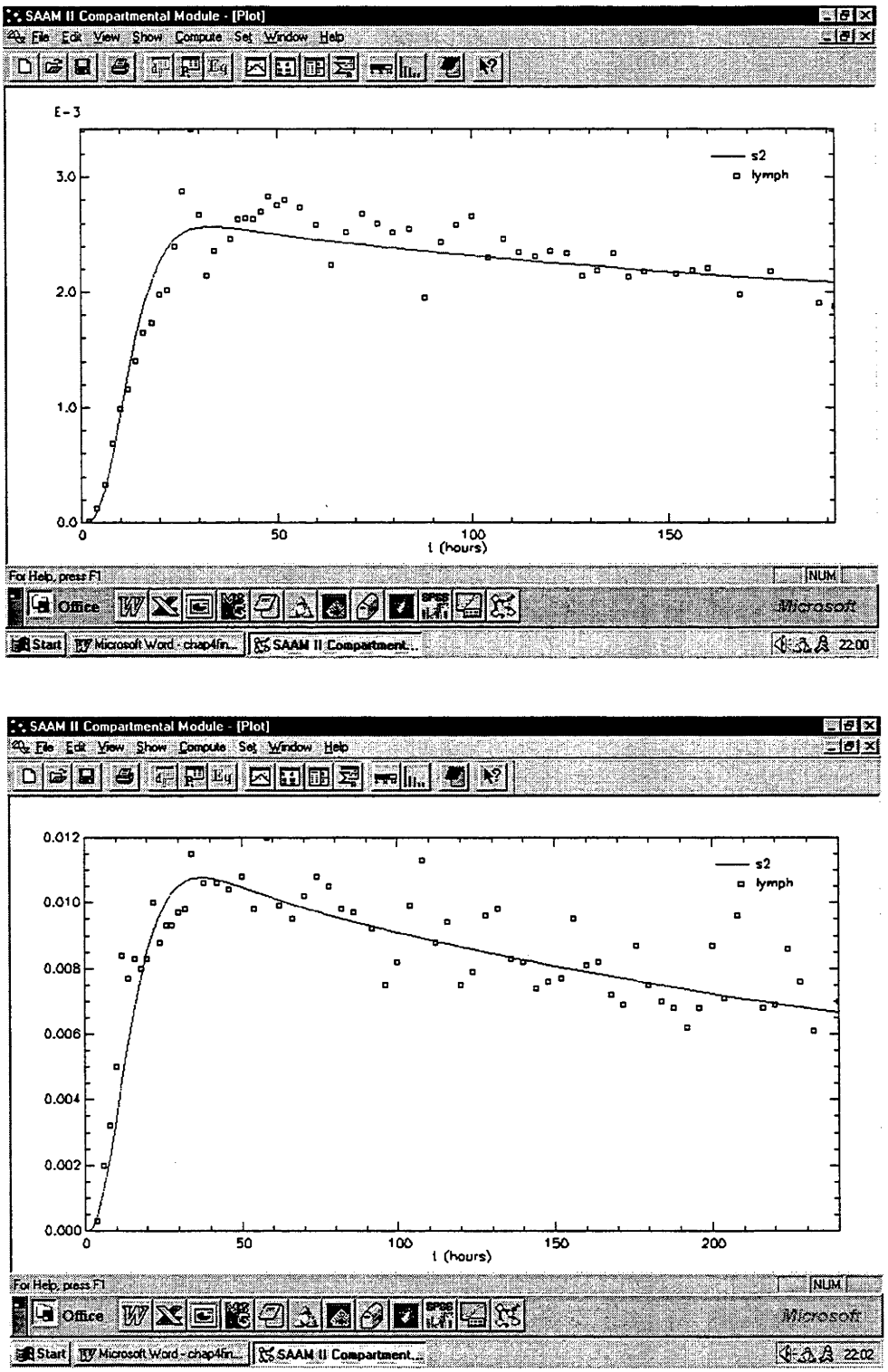

Figure 4.6D: Comparison of model outputs and actual data from Y044(1) (upper panel) and Y044(2) (lower panel)

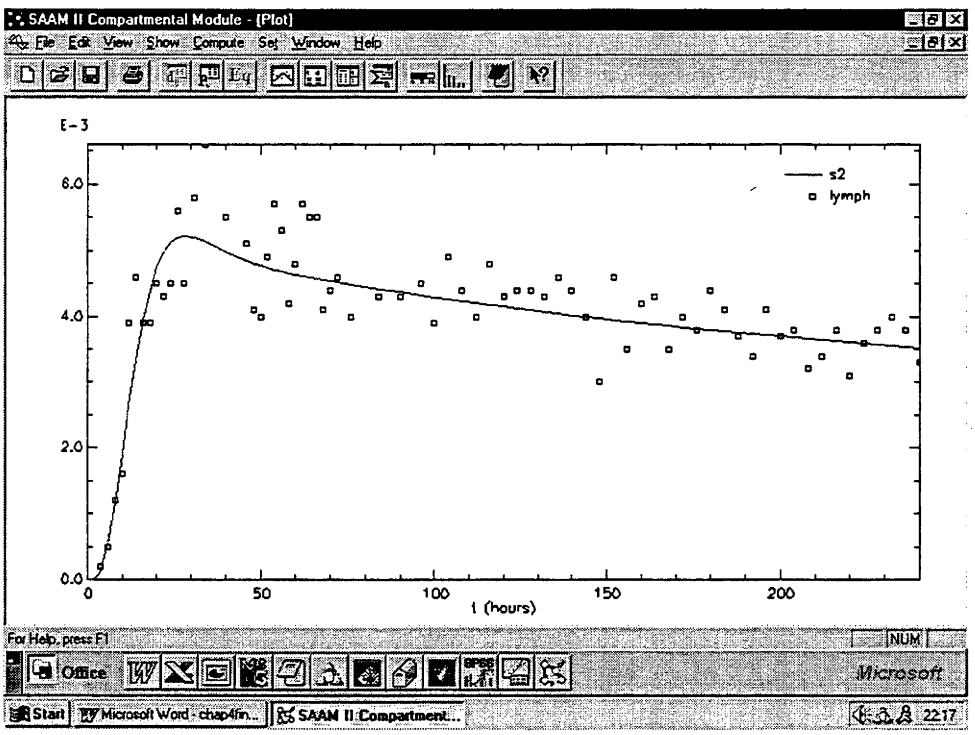

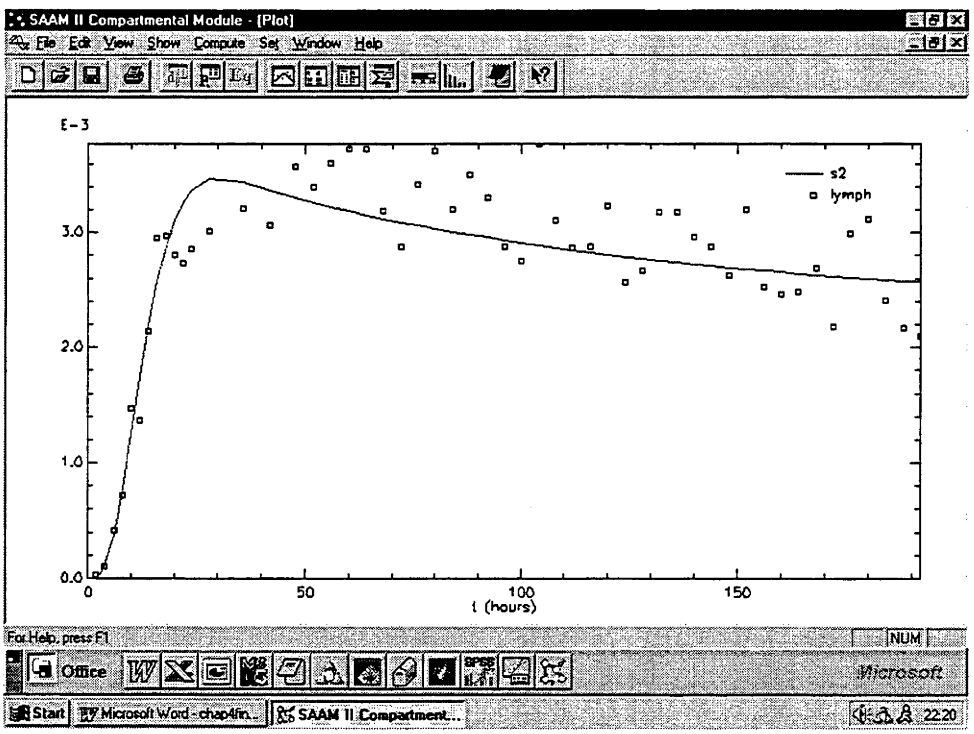

Table 4.1: Forcing function parameters

Animals	Parameters			
	A_1	λ_1	A_2	λ_2
R687	0.34441 ± 0.03167	0.01347 ± 0.00315	0.50402 ± 0.04317	0.99980 ± 0.27615
R401	0.38861 ± 0.03106	0.00325 ± 0.00095	0.53867 ± 0.04502	0.36785 ± 0.08859
R705	0.36148 ± 0.03808	0.00312 ± 0.00074	0.63693 ± 0.04614	0.26084 ± 0.05150
R632	0.25325 ± 0.04036	0.00313 ± 0.00154	0.72915 ± 0.04747	0.23589 ± 0.04043
R798	0.37687 ± 0.03293	0.00408 ± 0.00085	0.55312 ± 0.03607	0.17072 ± 0.02684
Y044(1)	0.22863 ± 0.03941	0.00557 ± 0.00206	0.62113 ± 0.04417	0.28802 ± 0.05370
Y044(2)	0.23548 ± 0.04369	0.00642 ± 0.00233	0.71884 ± 0.04530	0.25912 ± 0.03992

Table 4.2: Summary of model and defined parameters and their standard deviations

Animal	Model parameter			Defined parameters	
	k_{mm}	k_{bm}	k_{mb}	$R_{v/t}$ [a]	$R_{b/m}$ [b]
R687	0.14324 ± 0.00879	0.05936 ± 0.00707	0.00234 ± 0.00097	2.413 ± 0.287	25.368 ± 8.298
R401	0.15214 ± 0.00947	0.05376 ± 0.00723	0.00112 ± 0.00044	2.830 ± 0.461	48.000 ± 16.053
R705	0.15411 ± 0.00745	0.06034 ± 0.00736	0.00129 ± 0.00051	2.554 ± 0.366	46.775 ± 15.521
R632	0.11322 ± 0.00523	0.10761 ± 0.00752	0.00133 ± 0.00028	1.052 ± 0.107	80.910 ± 12.883
R798 [#]	0.08429 ± 0.00416	0.05165 ± 0.00348	0.00113 ± 0.00030	1.632 ± 0.135	45.708 ± 10.252
Y044(1)	0.11879 ± 0.00554	0.07949 ± 0.00713	0.00158 ± 0.00028	1.494 ± 0.170	50.310 ± 5.41
Y044(2)	0.09841 ± 0.00440	0.11257 ± 0.00596	0.00205 ± 0.00028	0.874 ± 0.046	54.912 ± 5.584
Mean ± SD	**0.12345 ±0.02721**	**0.07497 ±0.02573**	**0.00155 ±0.00047**	**1.836 ± 0.768**	**50.283 ± 16.425**

[a] $R_{v/t}$ is defined as the ratio of k_{mm} to k_{bm}. Subscripts v and t denote advection and attachment respectively. [b] $R_{b/m}$ is defined as the ratios of k_{bm} to k_{mb} Subscripts b and m denote bound and mobile stage lymphocytes respectively. [#] The modified multi-compartmental lymph node model with n=4 (ie three loop of B-M compartments) was used in all data sets, except in R798 where n=3 was used.

4.8 Discussion

Actual experimental data were used in the first attempt to solve unknown parameters in the experimental model. There were many obstacles to its use. A large number of unknown parameters were apparent. These unknown parameters were confounded in mathematical equations of the proposed model. Consequently, simultaneous solving of those parameters was not possible. Normalisation of data was performed using available and reliable information in order to eliminate unnecessary unknown parameters, ie parameters that were outside the field of interest.

In general, the normalisation procedures entailed scaling down only the magnitude of the actual data and not its pattern. Scaling down of the magnitude may interfere with only one unknown parameter in the experimental model namely k_{ml}. However, the primary goal of the present study is to define the migratory property of lymphocytes within lymphoid tissue, ie to identify parameters k_{mm} , k_{bm} , and k_{mb}. The delivery event k_{ml} (ie the transportation of lymphocytes through the blood circulation to the lymph node) is not the main interest of the present study.

By assuming that there exist two different kinetic forms of migrating lymphocytes (M stage and B stage lymphocytes), the modified multi-compartmental model constitutes a functional rather than an actual histological model. The histological correlates of the fast and slow kinetic compartments of this lymph node model remain to be fully determined. However, it is expected that the fast kinetic compartments may actually correspond to the large sinuses or porous spaces within lymphoid tissue where lymphocytes can easily mobilise without any distraction from cell-cell interactions. The kinetics of lymphocyte migration in M compartments would be simply explained by the dispersion phenomenon similar to those described in previous reports (Stekel *et al.*, 1997; Stekel, 1998). In contrast, the slow kinetic compartments may represent the dense cellular areas in lymphoid tissue (such as follicles) in which the most cell-cell interactions probably occurred.

Since cell-cell interactions play a crucial role in the immunological response as described in Chapter 1, any attempts to construct of theoretical models without taking account of cell-cell interaction would be unrealistic. Even the single compartmental model of the lymph node gave quite a good fit to the experimental data (data not shown). Since only one homogeneous kinetic was assumed in accord with the fundamental basis of compartmental analysis, this

single compartmental model could not describe the events of mixed kinetics (or mixed lymphocyte populations) within lymphoid tissue.

The physiologically based model of the lymph node represented in Figure 4.4(a) was assumed to be a true compartmental model on the basis of the available knowledge of the physiology and immunology of lymphocyte migration and its (cell-cell) interactions within lymphoid tissue. However, in the present study, there are still some mathematical constraints (ie identifiability of model) before such true models can be fitted to available data (ie percentages of labelled lymphocytes in blood and efferent lymph). The modified multi-compartmental model of the lymph node is necessarily undertaken as a means of reducing the number of parameters to be identified, and to make the model parameter identifiable with less error.

Owing to the strict criteria that were imposed for fitting procedures (ie convergence criteria, correlation values and rejection of parameters if their SD values exceeded 50% of their own values) as mentioned in section 4.6 of this chapter, only 7 data sets (all from total population studies) successfully satisfied the criteria and were accepted. None of the data sets from subset studies satisfactorily passed the fitting procedures. All parameters of the proposed forcing functions (A_1, A_2, λ_1 and λ_2) were identified before the entire fitting procedures were applied by fitting normalised blood data to the forcing function. However, the entire fitting procedures must be performed simultaneously when the final experimental model is to be used. In other words, the parameters k_{ml}, k_{mm}, k_{bm} , and k_{mb} in the experimental model must be solved simultaneously by using both normalised blood and lymph data. This made the fitting procedures more difficult in the context of a mathematical algorithm. Subsequently, a large number of data sets failed (according to the setting criteria) during the fitting procedures and were finally rejected. Thus the results of this analysis are confined to those data sets from the total population studies.

k_{mm} is the constant transfer coefficient (with a mean value of 0.12345 ± 0.02721 hour^{-1}) which describes the proportion of labelled lymphocytes leaving the M-compartment for the (next) adjacent M-compartment in an hour. k_{bm} is the constant transfer coefficient (with a mean value of 0.07497 ± 0.02573 hour^{-1}) describing the proportion of labelled lymphocytes leaving the M-compartment for the corresponding B-compartment (in the same loop) in an hour. On the other hand, in contrast to k_{bm}, k_{mb} (mean value of 0.00155 ± 0.00475 hour^{-1}) indicates the proportion of labelled lymphocytes leaving the B-compartment for the corresponding M-compartment (in the same loop) in an hour.

With reference to equation (4.10), $R_{b/m}$ is the parameter intentionally defined to demonstrate the relationship between lymphocytes in M and B compartments in a steady state. The mean value of $R_{b/m}$ (50.283 ± 16.425) indicates the proportion of the lymphocytes in B-compartments to those in M-compartments. This can be interpreted as indicating that, under normal physiological conditions, there were approximately 50 times more lymphocytes in bound form (ie lymphocytes which were engaged in cell-cell interactions) than those in mobile form (ie lymphocytes which were not currently undertaking cell-cell interactions). It can also be expected that the value of $R_{b/m}$ would increase during an immunological response since an increased proportion of migrating lymphocytes would be expected to enter the B-compartments.

Another parameter similar to $R_{b/m}$, $R_{v/t}$ is defined as the ratio of k_{mm} to k_{bm}. This parameter demonstrates the proportion (or probability) of lymphocytes continuing their migration via M-compartments relative to those entering the B-compartment (ie attachment to the reticular mesh). The mean value of $R_{v/t}$ found in this study was 1.818 ± 0.749. This can be interpreted to indicate that, under normal physiological conditions, a successfully migrating lymphocyte would have a higher likelihood of the order of 1.818 of migrating through the M-compartments (ie advection) rather than attachment to the reticular mesh. Like $R_{b/m}$, the value of $R_{v/t}$ would be expected to reduce during an immunological response due to the large proportion of migrating lymphocytes that would enter B-compartments to engage in cell-cell interactions.

4.9 Conclusion

Compartmental models are one of the classical models often used by biomedical scientists in many medically related fields. Fundamental knowledge (of the internal structure) of a model is often required, or assumed, to construct such models. This process is solely dependent upon the data available from the literature.

Some disadvantages of using compartmental models to represent lymphocyte migration have been recognised in this study. A large number of assumptions together with modification (ie normalisation) of actual data were required. The fitting procedures were generally rigid in this proposed model (ie the modified multi-compartmental model). This can lead to a large error in estimated parameters and, subsequently, to the failure of the fitting procedure in a large number of data sets.

Considering medical knowledge related to lymph node/ lymphocyte migration, the availability of experimental data and mathematical constraints on fitting procedures, the modified multi-compartmental model of the lymph node gave a partially satisfactory result. However, the proposed model may not itself be good enough to explain the actual events of lymphocyte migration. According to the assumptions of compartmental analysis in relation to rapid and effective mixing of mass in each compartment, this may be reasonable for lymphocyte kinetics in the blood circulation, but probably does not conform with lymphocyte migratory kinetics along pathways in lymphoid tissue.

Nevertheless, the findings from this study can probably provide some information essential for developing alternative models without the requirement for any additional assumptions or prior information. Providing all information findings from this study, mathematical models using partial differential equations (such as advection/ diffusion equations) may give better models to explain the complicated dynamic events of lymphocyte migration.

Chapter 5/
Prediction error models

5.1 Introduction

In this chapter, the prediction error approach to system identification in the time domain will be introduced. This approach was well established by Ljung (Ljung, 1987) and has been the basis of several subsequent reports (Yang and Khoo, 1994; Modarreszadeh *et al.*, 1995; Lai and Bruce, 1997; Berger and Malpas, 1998). This chapter will be restricted to consideration of linear time-invariant (LTI) systems with single input/ single output (SISO). The basic principles of linear systems and the related terminology have been described in part II of Chapter 1. This chapter will focus upon the principles of system identification and the form of analysis to be adopted will be functional system identification (see the section "functional and physical identification of system" in Chapter 1 for more details). Another approach, which combines system identification in the frequency domain together with structural modelling, will be presented in Chapter 6.

The term system identification refers to the process of mathematical modelling of systems in which the input and output signals have been observed on an experimental basis. Its applications in many fields are varied. For example, in engineering, knowledge of the characteristics of a system (ie an engine) will accelerate the implementation of any improvements or adjustments to be applied to that machine. A few studies have described very successful applications of system identification to the modelling of biomedical systems. An advanced approach to non-linear system identification has identified the configuration of retinal neurones in catfish (Marmarelis and Naka, 1973a; Marmarelis and Naka, 1973b). System identification using prediction error methods was successfully used to describe the physiology of the respiratory system and some disorders related to it (Modarreszadeh *et al.*, 1995; Lai and Bruce, 1997). In Berger's study, two inputs (ie the arterial blood pressure and the renal sympathetic nerve activity) and a single output (the renal blood flow) were recorded. The "autoregressive moving average with an exogenous input" (ARMAX) model was successfully applied to describe those input/output relationships (Berger and Malpas, 1998).

As a preliminary, the general concept of system identification will be introduced. A more specific and detailed description of this analysis will appear in the section on "system identification procedures" later in this chapter. The construction of a model using a system identification approach involves the following entities.

The data: It is a basic principle of system identification procedures that the data has been generated by observation of experiments specially undertaken to study the system. For example, the experimental design may include the application of some stimuli (ie input) to the system followed by simultaneous observation of both the stimuli and the response of the system (ie output). It is important to plan data collection to make it as informative as possible.

Model selection: A large number of models and model sets (ie families) may be utilised in the context of system identification. As an initial step, some sets of models are selected on the basis of their properties and their suitability for description of the system under study. Then, a number of candidate models are selected and their performances in relation to some (predetermined) identification criterion are assessed. It is a crucial step in system identification procedures to ensure that successful models have extracted sufficient information from the available data. Model selection involves choosing a particular model structure, a model order and a delay. This choice is often influenced by prior knowledge.

Model validation: Having a candidate model from the previous step, a final testing set is required to ensure that the selected model is good enough for one's purpose. This step is termed "model validation".

Models that meet all selection criteria and that pass validation tests can be considered as acceptable models (ie models that satisfy our requirements and are good enough to represent our studied system). In contrast, models that fail any of those tests may require revision.

The system identification loop described above can be represented schematically as shown in Figure 5.1.

Figure 5.1: The system identification loop

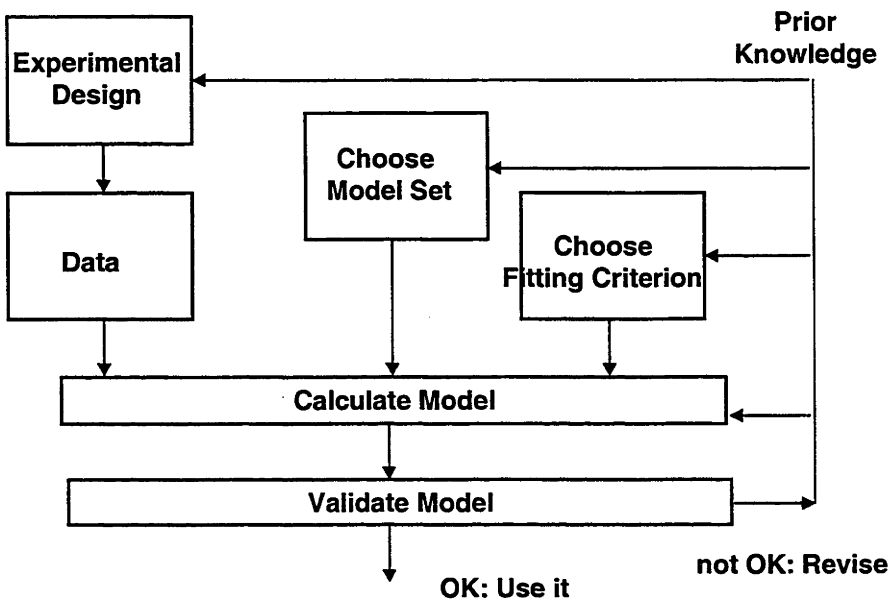

(From L.Ljung: System Identification, Theory for the user)

5.2 Prediction error models

This section summarises the fundamental concepts of ***prediction error models***. It is essential to select appropriate candidate models before proceeding to the next step in the system identification procedure. At the end of this section, four preliminary candidate models will be presented. The contents of this section unavoidably involve some advanced mathematics. However, the descriptions to be presented in this section will attempt to take account of the varying backgrounds of potential readers. The term "system" when it is used in this chapter will always be restricted to a single-input-single-output (SISO) time-invariant linear (LTI) system. Such a system obeys all the properties of the LTI system as described in Chapter 1. More details of prediction error models can be found in Ljung (Ljung, 1987; Ljung, 1991) and Söderström (Söderström and Stoica, 1989).

5.2.1 Impulse response

Generally, studies in biomedical systems entail the administration of certain material into the system under study as a short, rapid bolus, that is a unit impulse stimulus. For example a drug may be rapidly infused into the venous blood of an animal. The impulse response, generally, describes an (output) response by the system under study following the introduction of a unit impulse[36] stimulus to that system. In the present study, it is almost impossible to introduce such an ideal unit impulse into the system (ie the lymph node). In this system, the lymphocytes entering the lymph node via the blood represent the input (ie stimulus) to the lymph node. However, this stimulus will follow the pattern of an exponential decay function rather than being an ideal unit impulse stimulus, as previously explained in Chapter 3.

The response of a linear, time-invariant and causal[37] system to an input signal $u(t)$ can be described by a convolution integral[38] equation, which can be written as

---

[36] The **unit impulse** ($\delta(t)$) can be expressed by a Dirac function which has the property

$$\int_{-\infty}^{\infty} \delta(t)dt = 1.$$

[37] **Causality** is one of the fundamental properties of any physical system.

[38] **Convolution integration** is one form of mathematical integration. Convolution integration in time domain has a close relationship to a product in the Laplace domain.

$$y(t) = \int_{\tau=0}^{\infty} g(\tau)u(t-\tau)d\tau \tag{5.1}$$

where $y(t)$ and $u(t)$ are, respectively, the output from, and input to, the system (described in the time domain) and $g(\tau)$ is the impulse response. Such a system can be represented by Figure 5.2(a).

Given that the impulse response, the input to the system and some additional conditions are known, the output of this system can be calculated using (5.1). Thus the impulse response of the LTI system provides a complete characterisation of that system. In fact, all of the procedures contained in this chapter ultimately lead to identification of the impulse response of the system. In other words, information about lymphocyte migration within the lymph node system can be obtained by the identification and analysis of its impulse response.

In the discrete time domain, (5.1) can be written[39] as

$$y(t) = \sum_{k=1}^{\infty} g(k)u(t-k). \tag{5.2}$$

In (5.2), the sampling interval is assumed (without loss of generality) to be one time unit while k =1,2,3..

In reality, disturbance signals originating from many sources contaminate the signal of interest. Sources of disturbances are measurement noise, unmodelled dynamics, uncontrollable input sources, etc. By utilising the property of linearity of the LTI system, all significant noises can be lumped together to represent one disturbance term at the output of the system (Figure 5.2(b)).

$$y(t) = \sum_{k=1}^{\infty} g(k)u(t-k) + v(t) \tag{5.3}$$

where $v(t)$ is a disturbance signal. Note that the right hand side of (5.3) consists of the sum of two components. The former originates from the signal of interest and the latter originates from the disturbance signal. The disturbance signal $v(t)$ can also be modelled in the same manner as the signal of interest.

[39] (5.1) represents a continuous time signal which can be discretized to (5.2).

Figure 5.2: The linear time-invariant (LTI) system with single-input-single-output (SISO)

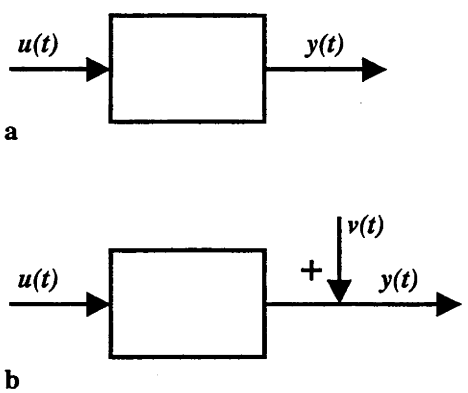

a) An LTI system with a single input, $u(t)$, and single output, $y(t)$.
b) An LTI system with a single input, $u(t)$, and single output, $y(t)$ with addition of a disturbance signal, $v(t)$.

Thus
$$v(t) = \sum_{k=0}^{\infty} h(k)e(t-k) \tag{5.4}$$

where $e(t)$ is a sequence of **independent**[40] and **identically distributed**[41] (**i.i.d**) random variables with a certain ***probability density function*** (***PDF***). To make the analysis simpler, $e(t)$ is assumed to be a zero mean ***Gaussian noise*** of variance σ^2, ie $\{e(t)\} = i.i.d, N(0, \sigma^2)$. Such signals are also known as ***"white noise"***. For the remainder of this chapter, $e(t)$ is assumed to be white noise.

If $v(t)$ in (5.3) is replaced with its equivalent from (5.4), we obtain

$$y(t) = \sum_{k=1}^{\infty} g(k)u(t-k) + \sum_{k=0}^{\infty} h(k)e(t-k). \tag{5.5}$$

Note that (5.5) completely describes the relationship between the output $y(t)$, the input $u(t)$ and the disturbance signal $e(t)$.

5.2.2 Transfer functions

To obtain an alternative expression of (5.5), the forward shift operator q is introduced

[40] "Independent" means that past information about the disturbance itself can not be used to infer knowledge about the value of the disturbance at present or in the future, ie E(e(t)| e(t-1), e(t-2))=E(e(t)).

[41] Identically distributed means $e(t)$ has the same PDF for all values of t.

$$qu(t) = u(t+1). \tag{5.6}$$

Also the backward shift operator q^{-1} can be defined as

$$q^{-1}u(t) = u(t-1). \tag{5.7}$$

From these shift operators, (5.5) can be rearranged as

$$y(t) = G(q)u(t) + H(q)e(t) \tag{5.8}$$

where

$$G(q) = \sum_{k=1}^{\infty} g(k)q^{-k} \tag{5.9}$$

$$H(q) = \sum_{k=0}^{\infty} h(k)q^{-k}. \tag{5.10}$$

Equations (5.8)-(5.10) represent a general model of a linear dynamic system. The transfer functions $G(q)$ and $H(q)$ are defined as the ***"deterministic transfer function"***[42] (ie ***the input-output dynamics***) and the ***"stochastic transfer function"*** (ie ***the noise dynamics***) respectively. Note that (5.8) has demonstrated a relationship between the output $y(t)$ and the known input $u(t)$ via input-output dynamics $G(q)$, and between the output $y(t)$ and white noise $e(t)$ via noise dynamics $H(q)$.

$G(q)$ and $H(q)$ can be represented as a ratio of polynomials

$$G(q,\theta) = q^{-nk}\frac{B(q)}{A(q)F(q)} \tag{5.11}$$

and

$$H(q,\theta) = \frac{C(q)}{A(q)D(q)}. \tag{5.12}$$

Where nk is defined as the ***system delay*** and

$$A(q) = 1 + a_1q^{-1} + ... + a_{n_a}q^{-n_a} \tag{5.13}$$

$$B(q) = b_0 + b_1q^{-1} + ... + b_{n_b}q^{-n_b} \tag{5.14}$$

$$C(q) = 1 + c_1q^{-1} + ... + c_{n_c}q^{-n_c} \tag{5.15}$$

$$D(q) = 1 + d_1q^{-1} + ... + d_{n_d}q^{-n_d} \tag{5.16}$$

$$F(q) = 1 + f_1q^{-1} + ... + f_{n_f}q^{-n_f}. \tag{5.17}$$

Here $a_1, a_2, ..a_{n_a}, b_0, b_1, ..b_{n_b}, c_1, c_2, ..c_{n_c}, d_1, d_2, ..d_{n_d}, f_1, f_2, ..f_{n_f}$ are, respectively, the parameters of $A(q), B(q), C(q), D(q), F(q)$ which need to be estimated. The vector θ defined as

$$\theta = [a_1..a_{n_a}b_0..b_{n_b}c_1..c_{n_c}d_1..d_{n_d}f_1..f_{n_f}]^T \tag{5.18}$$

contains the unknown parameters. Thus (5.8)-(5.12) can be rewritten in a polynomial format as (5.19).

---

[42] ***Deterministic*** and ***Stochastic*** describe the certainty and uncertainty concepts of activity respectively.

$$A(q)y(t,\theta) = q^{-nk}\frac{B(q)}{F(q)}u(t) + \frac{C(q)}{D(q)}e(t)\,. \tag{5.19}$$

Using the definition of q^{-nk}, (5.19) can be rearranged as

$$A(q)y(t,\theta) = \frac{B(q)}{F(q)}u(t-nk) + \frac{C(q)}{D(q)}e(t)\,. \tag{5.20}$$

5.2.3 Generalised prediction error models

Equations (5.19) and (5.20) are called ***generalised prediction error models*** (***PEM***). Subsequently, the predicted and simulated output models can be derived from the PEM.

$$\hat{y}(t,\theta) = H^{-1}(q,\theta)G(q,\theta)u(t) + \left[1 - H^{-1}(q,\theta)\right]y(t) \tag{5.21}$$

$$\tilde{y}(t,\theta) = G(q,\theta)u(t) \tag{5.22}$$

Equations (5.21) and (5.22) are the predicted and simulated output models whilst the signals $\hat{y}$ and $\tilde{y}$ are the predicted and simulated outputs respectively. The ***prediction error signal***, $\varepsilon(t)$, is defined as the difference between actual and model-predicted outputs.

$$\varepsilon(t) = y(t) - \hat{y}(t) \tag{5.23}$$

By substitution of (5.21) in (5.23), one obtains

$$\varepsilon(t) = H^{-1}(q,\theta)[y(t) - G(q,\theta)u(t)]\,. \tag{5.24}$$

Considering the prediction performance of models, a good (prediction) model would produce small prediction errors when applied to the data of interest. To identify an unknown system, the prediction error method has been applied to estimate the vector of unknown model parameters (θ) contained in the model equation by minimising a quadratic function[43] of the prediction error. The minimising algorithms of PEM are similar to those of the well known least mean square method.

$$V_N(\theta) = \frac{1}{2N}\sum_{t=1}^{N}\varepsilon^2(t|\theta) \tag{5.25}$$

[43] A ***quadratic function*** (or equation) is a mathematical equation which includes squared quantities. For example $y(x) = ax^2 + bx + c$ is a quadratic equation.

V_N is the ***quadratic function*** of $\varepsilon(t)$ called the ***prediction cost function***. Where N is length of data recorded. As can be seen in (5.25), given a similar PEM cost function, there is no discrimination between models with very different numbers of parameters. This could lead to the problem of "over-parameterisation" of models (ie there are too many (unnecessary) parameters in a model). To overcome this problem, ***Akaike's final prediction error (FPE)***, a modified version of the prediction cost function, is introduced.

$$\text{FPE} = \left(\frac{1+(d/N)}{1-(d/N)}\right) \cdot V_N(\theta) \tag{5.26}$$

by applying (5.23) to (5.25), one obtains

$$\text{FPE} = \left(\frac{1+(d/N)}{1-(d/N)}\right) \frac{1}{2N} \sum_{t=1}^{N} \varepsilon^2(t) \tag{5.27}$$

where d is the total number of estimated parameters of a model. In (5.27), the value of FPE depends on the number of estimated parameters (d) together with the size (ie length) of the data set (N). It can easily be seen from (5.27) that, given two models with an equal PEM cost, the FPE criterion will select the one with the fewer parameters.

Models can also be considered in terms of their simulation performances. Using the same approaches for the prediction error, the simulation cost function is computed by

$$\tilde{V}_N(\theta) = \frac{1}{2N} \sum_{t=1}^{N} [y(t) - \tilde{y}(t,\theta)]^2 \tag{5.28}$$

This simulation cost function, $\tilde{V}_N$, will be used to compare the models on the basis of their capacity for simulation.

5.2.4 Candidate models

The following four candidate models have been chosen for the purpose of identification of the lymph node system:

1. AutoRegressive with eXternal input (**ARX**) model is represented by

$$A(q)y(t) = q^{-nk} B(q)u(t) + e(t) \tag{5.29}$$

which can be rewritten as

$$y(t) = q^{-nk} \frac{B(q)}{A(q)} u(t) + \frac{1}{A(q)} e(t) \tag{5.30}$$

$\theta = [a_1 .. a_{n_a} b_0 .. b_{n_b}]^T$ is the vector of the ARX model parameters to be estimated.

2. AutoRegressive Moving Average with eXternal input (**ARMAX**) model is represented by

$$A(q)y(t) = q^{-nk}B(q)u(t) + C(q)e(t) \tag{5.31}$$

which can be rewritten as

$$y(t) = q^{-nk}\frac{B(q)}{A(q)}u(t) + \frac{C(q)}{A(q)}e(t) \tag{5.32}$$

$\theta = [a_1..a_{n_a}b_0..b_{n_b}c_1..c_{n_c}]^T$ is the vector of the ARMAX model parameters to be estimated.

3.**Output Error (OE)** model is represented by

$$y(t) = q^{-nk}\frac{B(q)}{F(q)}u(t) + e(t) \tag{5.33}$$

$\theta = [b_0..b_{n_b}f_1..f_{n_f}]^T$ is the vector of the OE model parameters to be estimated.

4. **Box-Jenkins (BJ)** model is represented by

$$y(t) = q^{-nk}\frac{B(q)}{F(q)}u(t) + \frac{C(q)}{D(q)}e(t) \tag{5.34}$$

$\theta = [b_0..b_{n_b}c_1..c_{n_c}d_1..d_{n_d}f_1..f_{n_f}]^T$ is the vector of the BJ model parameters to be estimated.

These four models have been used widely and many applications have been reported including identification in medical systems (Modarreszadeh *et al.*, 1995; Lai and Bruce, 1997; Berger and Malpas, 1998). Such candidate models offer a wide range of possible models which would be applicable to the lymph node system. This chapter will focus on only these four candidate models. Figure 5.3 illustrates all candidate models diagrammatically. In these diagrams, the deterministic (input-output dynamics) and stochastic transfer function (noise dynamics) are represented by solid and dotted rectangle boxes respectively.

The ARX is one of the models that is very often selected to represent a dynamic system because of its simplicity. The ARMAX is another model structure in the same family as ARX (ie this family has commonly parameterised input-output, and noise dynamics). Both ARX and ARMAX models contain a common polynomial part, $A(q)$, in both transfer functions (ie the input-output and the noise dynamics). In contrast, the OE and BJ models, which are in another family (ie the family of model structures with independently parameterised input-output and

noise dynamics.), do not contain a common polynomial part in their input-output and noise dynamics. In an OE model, the noise dynamics is fixed to $H(q)$=1 and is not estimated. It has been noted that independently parameterised model structures (such as OE and BJ models) give better simulation results. This can be explained by the fact that any misfit in the estimated noise model is reflected in a misfit of the input-output dynamics when using a model structure with common parameters in $G(q)$ and $H(q)$ (such as ARX and ARMAX).

Figure 5.3: The candidate models

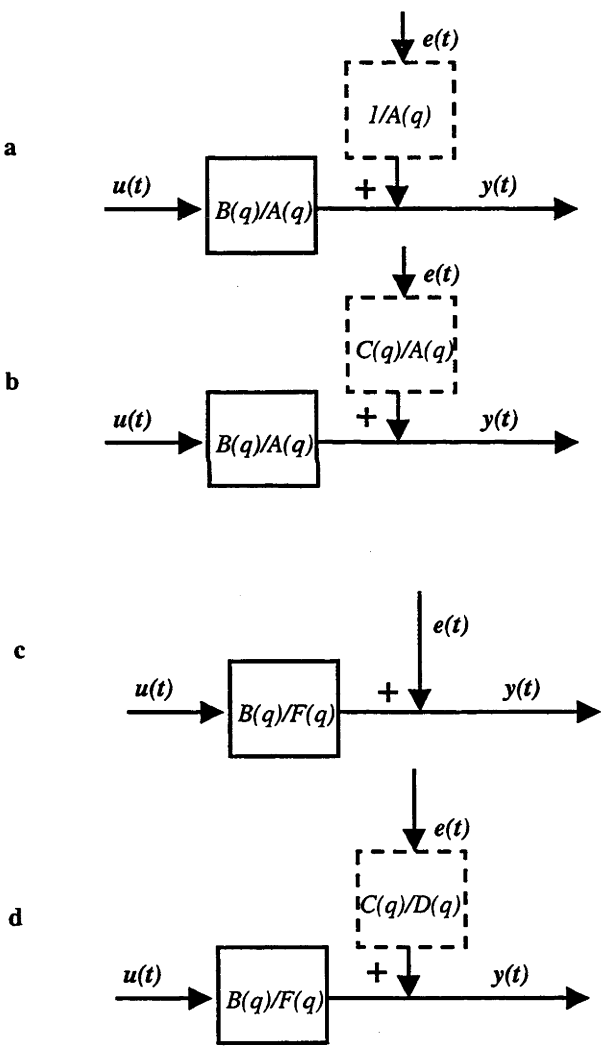

The figures demonstrate diagrams of candidate models where the deterministic (the input-output dynamics) and the stochastic transfer function (the noise dynamics) are represented by a solid and a dotted rectangle box respectively.

(a) ARX models
(b) ARMAX models
(c) OE models
(d) BJ models

5.3 System identification procedures

Previous lymphocyte recirculation and migration studies have been reviewed in Chapter 1. None of these studies appear to have considered the possibility of system identification modelling. The system identification adopted in this thesis has been strongly influenced by the work of Ljung (Ljung, 1987; Ljung, 1991), Modarreszadeh (Modarreszadeh *et al.*, 1995) and Lai (Lai and Bruce, 1997). In those studies, these researchers were able to identify the dynamics of the respiratory system in several conditions using PEM models (Modarreszadeh *et al.*, 1995; Lai and Bruce, 1997).

5.3.1 Lymph node system

The lymph node under investigation is assumed to be represented as a linear time invariant (LTI) system with single-input-single-output (SISO) as shown in the diagram in Figure 5.2(b). The system input $u(t)$ and output $y(t)$ represent the percentages of labelled lymphocytes in the venous blood and the efferent lymph of the studied lymph node respectively. Such an ideal lymph node model is in accord with the fact that, under normal physiological conditions, most lymphocytes (ie more than 95%) found in the efferent lymph are derived from blood rather than from other sources (Hall and Morris, 1962; Hall and Morris, 1965b). In this model, the inputs from other sources, such as from the afferent lymph, are ignored as they contribute less than 5% to the model output.

5.3.2 Experimental data

As mentioned in section 3.1 of Chapter 3, the present experiments can be categorised into two groups namely the total lymphocyte population and several subset (ie CD4, CD5, CD8 and CD45R) studies. To identify the lymph node system, it is essential that adequate experimental data are collected. In the present study, after some preliminary trials, any experiments that provided less than 100 hours of data (ie the experimental time was less than 100 hours) were discarded. The remainder of the experiments (15 out of 21 for the total population studies and 7 out of 11 for the subset studies) were subsequently incorporated into the whole system identification procedures.

5.3.3 Matlab as a tool

The system identification procedure and all of the graphic presentations in this chapter were performed by commands and algorithms implemented in ***Matlab***

and the ***Matlab System Identification Toolbox*** (Mathsoft Company-MA, USA). Matlab is a powerful interactive commercial program for numeric computation and data presentation. It has been widely used in solving complex problems in several fields including applied mathematics, physics, chemistry and engineering. The system identification toolbox of Matlab using an iterative Gauss-Newton algorithm has been satisfactorily implemented (Ljung, 1991). Details of this algorithm and the commands used in the present study are included in Appendix 2 to this thesis.

5.3.4 Determination of the system delay

The first step in the system identification procedure is to determine the system delay, nk, of selected candidate models. Selection of the appropriate value of the system delay will ensure a good performance from the final model. The following several methods can be used to determine the system delay.

- Generally, observation of a graph of the actual input-output data in the time domain, and of the time difference between the first appearance of the input and of the output may indicate an approximate value for the system delay. However, this procedure can not ensure reliability. Indeed, in the case of many data sets, this procedure would fail to provide clear indications for the identification of the system delay.
- Alternatively, the system delay can be detected by an impulse response estimation obtained from a correlation analysis of the input and the output. This can be undertaken in the Matlab environment (using the command **"cra"**). The determination of the system delay can be identified from visual observation of the identified impulse response.
- In this thesis, a more "ad hoc" searching procedure has been used for system delay determination. In general practice, a low order ARX model (na=0, nb=1, nk =d) has often been used as a prototype model to identify the system delay (d). Modarreszadeh et al used a low order Box-Jenkins model to obtain an optimal delay which gave a minimal FPE value (Modarreszadeh *et al.*, 1995). After several trials, a low order output error (OE) model (n_b=1, n_f=1, n_k =d) was selected as a good prototype model for the data in the present study. As the first step in using this, the prediction cost function (V_N) is calculated for this OE model with a delay of 1 (n_b=1, n_f=1, n_k =1). Then the value of the system delay is increased by 1 and the prediction cost function is re-calculated. The value of the system delay is defined over the range 0..10. Because a smaller value of the prediction cost function implies a better model, this function was used as an indication for determination of the

system delay. The prediction cost is depicted as a function of the system delay and the value of the system delay is selected at the region where an abrupt change of the prediction cost occurs (this can be observed by ***a knee*** in the graph that shows the prediction cost as a function of the system delay). Subsequently, the system delay is definitively selected and maintained as a constant value throughout the remaining steps of the identification procedure (in Section 5.3.5). The system delay could be also obtained by identifying a given range of ARX models (n_a, n_b, n_k) and the prediction cost versus n_k for a series values of n_a and n_b could be plotted using the command **"arxstruc"**. However, in the present study, OE models were chosen to determine the system delay on the basis of their established good simulation results.

5.3.5 Selection of model structures from candidate models

The four candidate models suggest a variety of parameters that have to be selected for the final model. In this step, a vector of model parameters, θ, is identified for each candidate model structure (ie ARX, ARMAX , OE and BJ model structures with a different number of parameters). The maximal order of each model parameter vector is, however, limited to the value of 3. For example, the vectors of OE and ARMAX model parameters are (n_b, n_f, n_k) and (n_a, n_b, n_c, n_k) respectively with n_a, n_b, n_c, $n_f \leq 3$. The system delay identified from Section 5.3.4 is used for the four candidate models. The individual value of the final prediction error (FPE) is calculated by means of (5.27) for the corresponding model structures. In a process similar to that used for the selection of the system delay, a graph representing the relationship between the FPE and the model dimension (ie the total number of identified parameters in each model) provides an indication of the model to be selected in each model structure.

In Matlab, the parameter estimation algorithm, which requires an iterative search for the minimum of (5.25) with a special start-up procedure, can be well implemented. The Gauss-Newton minimisation procedure is carried out until the norm of the Gauss-Newton direction is less than a certain level (ie tolerance) (Ljung, 1991). The four candidate models have been identified according to the prediction criterion (5.25) whereas a good fit to the actual data, ie a good simulation performance, has been the main goal in the present study. Therefore, the selection of the final model will be dependent upon the basis of the simulation criterion (5.28). Consequently, it would be expected that the final model will be either an OE or a BJ model as previously described in section 5.2.4.

5.3.6 Model validation

Because of the nature of the present study, most of the experimental data sets (after interpolation with a sampling period =1 hour) contain only about 100-240 data points. Such data sets are relatively small. The technique of ***"cross validation"***, a validation method that is performed on a data set that is different from the data set used to identify the model, can not be performed in the present study as it requires a considerable number of data points. Thus in the present study, model validation had to be undertaken on the same set of data that had been used to identify the four candidate models.

At this stage, the final four models have been selected according to the steps described in Sections 5.3.4-5.3.5. A validation test is required to ensure the adequacy of these models. In the present study, the ***residual analysis method*** has been selected as a validation test and will be performed on the final four models. Briefly, the ***residual*** (or error) is the difference between the actual output and the model output. The correlation of the residual with the input signal (cross correlation of the residual against the input, $R_{\varepsilon u}$) can reveal information (in the residual) that may help to explain the process, ie information that has not been used. $R_{\varepsilon u}$ is used for validation of the input-output dynamics. The correlation of the residual with itself (autocorrelation of the residual, $R_{\varepsilon\varepsilon}$) is used for the validation of the noise model. However, $R_{\varepsilon\varepsilon}$ is not of significance in this study since it is concerned only with simulation results, ie validation of the input-output dynamics. More details on residual analysis can be found in Ljung (Ljung, 1987; Ljung, 1991).

5.4 Results from the system identification procedure

5.4.1 System delay

The system delay was determined for individual experiments according to the procedures described in 5.3.3. Figure 5.4 demonstrates the relationship between the value of the system delay and the prediction cost function (V_N) for one of the experimental data sets (R798). By observation of the graph of prediction cost function versus the number of the system delay (Figure 5.4), the value of the prediction cost function V_N can be seen obviously to decline until the value of the delay n_k equals 5. Thus the system delay value of 5 was selected in this experiment. All of the system delays obtained from the 22 experimental data sets are summarised in Table 5.3-5.4.

Figure 5.4: The relationship between the system delay and prediction cost function

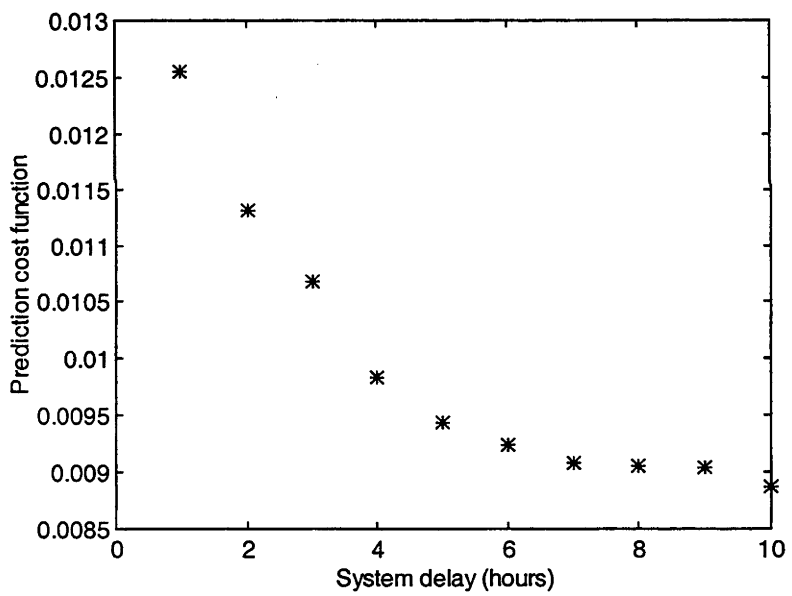

Figure 5.4 demonstrates a relationship between the system delay and prediction cost function for the OE model of R798. OE order 1,1,nk was used while the system delay ranges from 0 to 10. The prediction cost function significantly decreased until the system delay nk=5. A **"knee"** is described as an abrupt change in the value of the prediction cost function.

5.4.2 Comparison of different model structures

Selection of an appropriate model structure and orders is a difficult step and requires considerable background detail of the model structures. In general, even though a complicated (ie high order) model may explain the characteristics of our unknown system better than a less complicated (ie lower order) model, such attempts may lead to an over-parameterised problem. This is why the number of parameters is explicitly taken into account in a criterion of the type described in (5.27) which tends to select models of lower order than the criterion described in (5.25).

In this section, four candidate model structures, including ARX, ARMAX, OE and BJ, have been preselected to represent the lymph node system. Subsequently, 3 data sets (R705, R634 and R797) were randomly selected and searched for the "best" model for each candidate model structure. Details of this procedure have been given in sections 5.3.4 and 5.3.5. As mentioned in section 5.3.5, the final model in the present study will be chosen according to the simulation performance of selected models. The simulation cost function ($\tilde{V}_N$) is calculated for all the selected models (from each individual data set) and used to compare their simulation performances. The results of this study are shown in Table 5.1.

TABLE 5.1: A comparison of the different model structures and their simulation performances (Vsim).

Sheep	N	nk	Vsim			
			OE	BJ	ARX	ARMAX
R705	168	7	**0.0062** (1,2,nk)	0.0071 (1,1,0,2,nk)	0.0101 (3,1,nk)	0.0075 (2,1,2,nk)
R634	108	5	**0.0217** (1,2,nk)	0.0245 (1,0,1,2,nk)	0.0732 (3,1,nk)	0.0240 (2,1,2,nk)
R797	156	5	**0.0138** (1,2,nk)	0.0148 (1,0,1,2,nk)	0.0366 (3,1,nk)	0.0492 (2,1,2,nk)

Remarks: The orders of the models are given in parentheses. N and nk denote the number of data points and the value of the system delay used in the calculation. Vsim denotes the simulation cost function described in (5.28).

Among those four candidate models, the OE model gives the minimum value of $\tilde{V}_N$ in all 3 cases. This implies that the simulation performance of OE models is the best of the four candidate models. Indeed, as described before, ARX and

ARMAX models have a common polynomial $A(q)$ in input-output $G(q)$ and noise dynamics $H(q)$. Any misfit in the noise dynamics (for example, because $H(q)$ can not be modelled exactly) will be reflected by a misfit in the input-output dynamics. This misfit leads to poor simulation results. However, this is not the case for OE or BJ models which have independently parameterised $G(q)$ and $H(q)$. So, even if $H(q)$ can not be modelled exactly (for example, if $H(q)$ is fixed to 1 in the case of OE models), this does not necessarily lead to a misfit in $G(q)$ provided that the model structure used is flexible enough (ie n_b and n_f are large enough in the case of an OE model).

The OE model is to be preferred over the BJ model since only a correct modelling of $G(q)$ is of interest in the present study. The identification of an unnecessarily noise dynamic model would only lead to an increase in the variance of the identified parameters. Indeed, more parameters (including some which were unnecessary) could be identified with the same data set. Note that in validating an OE model (Figure 5.5), only the lower plot, (R_{eu}) should be considered since the noise dynamics $H(q)$ of the OE model (which is equal to one) is unsuitable for the description of the noise dynamic model.

Overall, the parameters obtained from the OE models have much smaller standard deviations (SD) than those obtained from the other models (Table 5.2). For example, in the BJ model of R705, the value of f_2 is 0.5303 while its SD is 0.1304 (ie almost 25% of its own value). An extreme example of this is in the ARMAX model of both R705 and R797. In these, the SD values of c_1 (ie 0.0617 and 0.0935, respectively) exceed their own c_1 values (ie 0.0190 and 0.0533, respectively. Such high SD values reflect a degree of uncertainty about the estimated parameters in that model which, indicates that, in practice, its use should be avoided. The relatively low SD of parameters estimated in the OE model provides further evidence supporting the selection of the low order OE model as the "final model" in the present study.

TABLE 5.2: A comparison of the parameters and their standard deviations estimated for the four candidate models.

Sheep	Model	Estimated parameters ± Standard deviations (SD)					
		b_0	c_1	d_1	f_1	f_2	
R705	OE	0.0122	-	-	-1.7928	0.8033	
		±0.0015	-	-	±0.0250	±0.0237	
	BJ	0.0263	0.6425	-	-1.5078	0.5303	
		±0.0071	±0.1210	-	±0.1363	±0.1304	
		a_1	a_2	a_3	b_0	c_1	c_2
	ARX	-1.5369	0.9796	-0.4092	0.0400	-	-
		±0.0704	±0.1157	±0.0678	±0.0082	-	-
	ARMAX	-1.8460	0.8539	-	0.0093	0.0190	-0.9286
		±0.0680	±0.0650	-	±0.0041	±0.0617	±0.0601
		b_0	c_1	d_1	f_1	f_2	
R634	OE	0.0233	-	-	-1.7489	0.7649	
		±0.0021	-	-	±0.0224	±0.0210	
	BJ	0.0257	-	-0.9006	-1.7115	0.7295	
		±0.0059	-	±0.0527	±0.0721	±0.0686	
		a_1	a_2	a_3	b_0	c_1	c_2
	ARX	-1.5935	0.9580	-0.3329	0.0476	-	-
		±0.0910	±0.1526	±0.0863	±0.0102	-	-
	ARMAX	-1.7986	0.8126	-	0.0200	-0.0677	-0.9322
		±0.0433	±0.0406	-	±0.0042	±0.0642	±0.0641
		b_0	c_1	d_1	f_1	f_2	
R797	OE	0.0186	-	-	-1.6867	0.6981	
		±0.0029	-	-	±0.0438	±0.0420	
	BJ	0.0155	-	-0.9504	-1.7813	0.7908	
		±0.0032	-	±0.0323	±0.0493	±0.0477	
		a_1	a_2	a_3	b_0	c_1	c_2
	ARX	-1.7245	1.0002	-0.2603	0.0247	-	-
		±0.0778	±0.1370	±0.0754	±0.0059	-	-
	ARMAX	-1.8998	0.9049	-	0.0083	0.0533	-0.6312
		±0.0662	±0.0643	-	±0.0045	±0.0935	±0.0901

5.4.3 Model validation

The OE model order (*1,2,nk*) was finally selected to model the lymph node system. Residual analysis was performed on all data sets and their final OE models. According to the OE model structure, the noise dynamic is assumed to be 1 (ie $H(q)$=1). Thus, the result of autocorrelation of the residuals ($R_{\varepsilon\varepsilon}$) is ignored and cross correlation between the input and the residual ($R_{\varepsilon u}$) is focused upon as an alternative. Cross correlation between the inputs and the residuals of each OE model should give a result close to zero for all lags. Any OE models giving an overall cross correlation exceeding the 99% confidence interval at any lag should be rejected. Typical results of the residual analysis of data sets of R705 are given in Figure 5.5 and demonstrate that each OE model is validated, ie there is no value of $R_{\varepsilon u}$ which exceeds the 99 % confidence interval.

Figure 5.5: Residual analysis

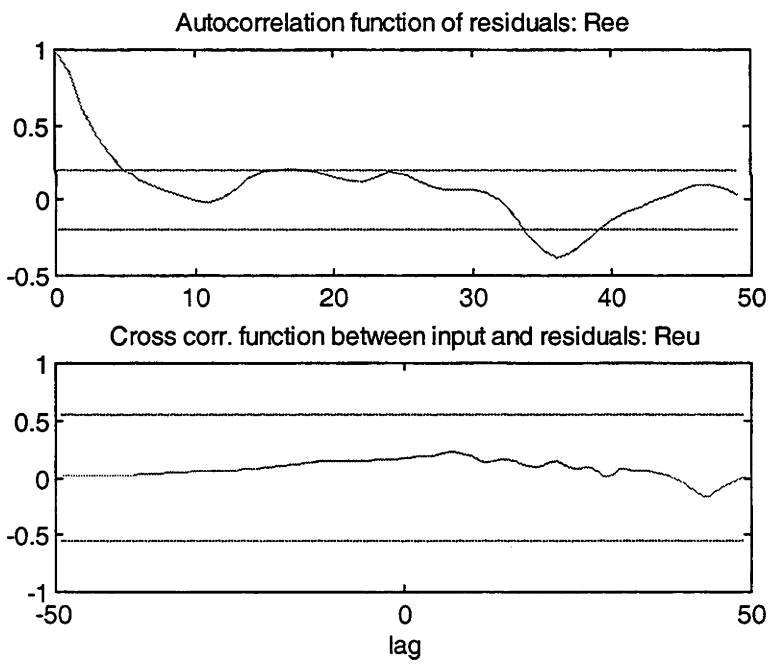

The lower panel illustrates the residual analysis of the data sets of R705, which indicates that the OE model is validated (ie there is no value of $R_{\varepsilon u}$ exceeding the 99 % confidence interval defined by a region between the two dotted lines). In the OE model, the noise dynamic, $H(q)$, is assumed to be 1. The autocorrelation of the residuals, $R_{\varepsilon\varepsilon}$, (upper panel) has to be ignored as it is evident that $H(q)$=1 is not a good noise model.

5.4.4 Comparison of the actual outputs and the model outputs

In this section, the actual input data have been applied to the final OE model identified from each data set to calculate a noise-free output simulation. Subsequently, the actual and the simulated model outputs are summarised in Figure 5.6A-5.6L. For all of the data sets (represented by dotted lines and circles), the simulated model outputs (represented by solid lines) show a reasonable fit to the actual outputs. The simulation cost function for these data sets (Table 5.3) is relatively low indicating a good fit for those models.

Figure 5.6A: Comparison of the actual outputs and the simulated model outputs

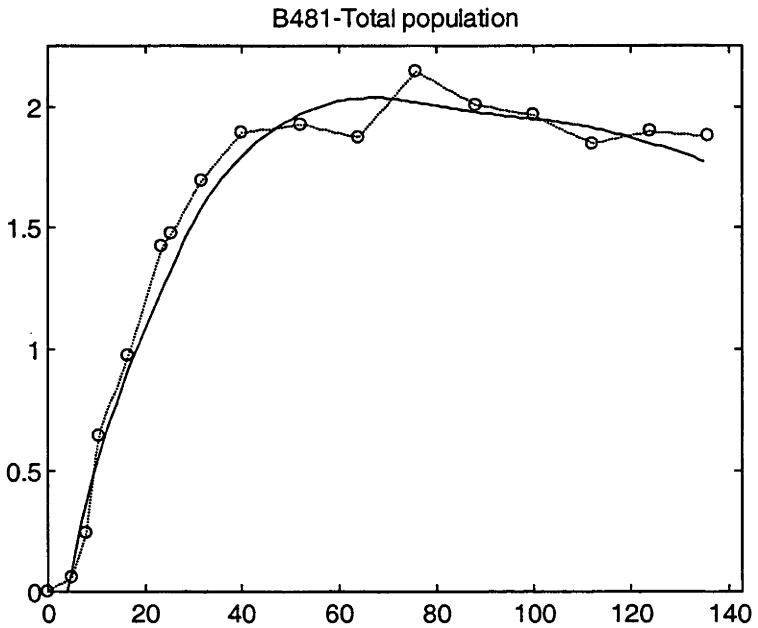

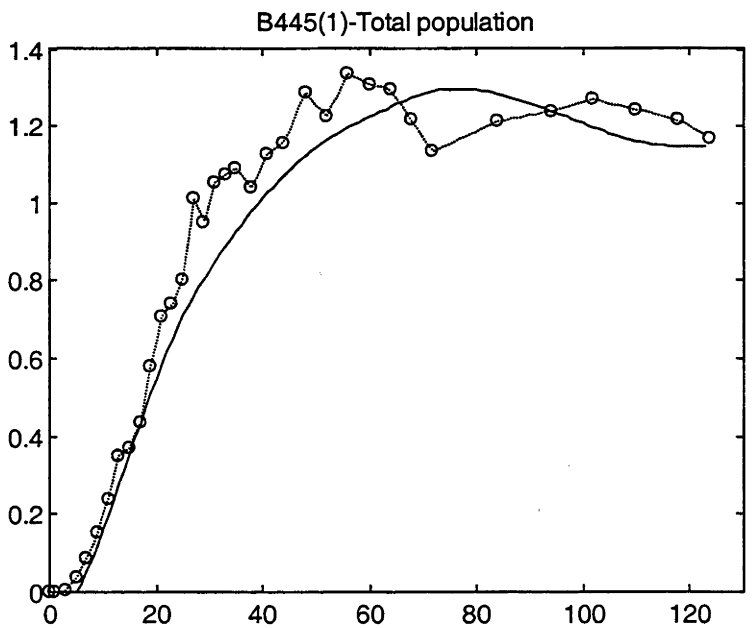

Figure 5.6B: Comparison of the actual outputs and the simulated model outputs

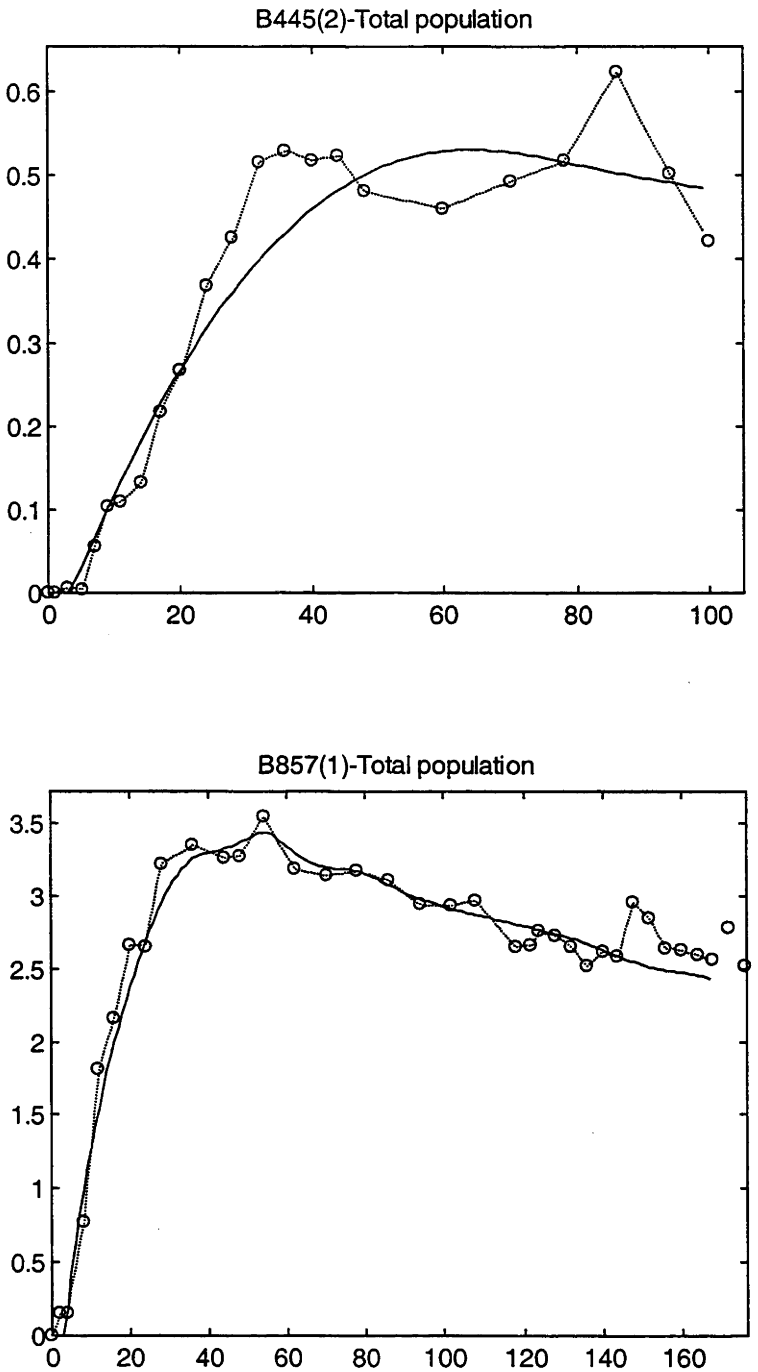

Figure 5.6C: Comparison of the actual outputs and the simulated model outputs

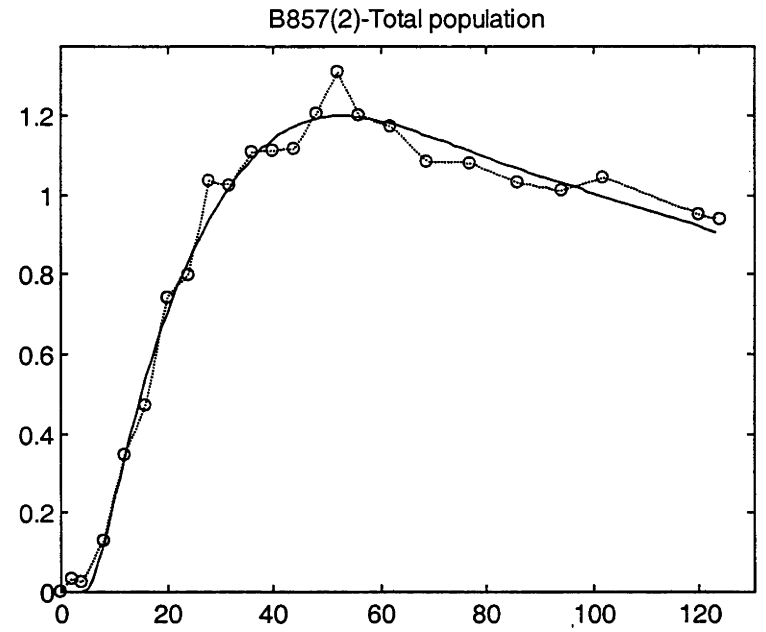

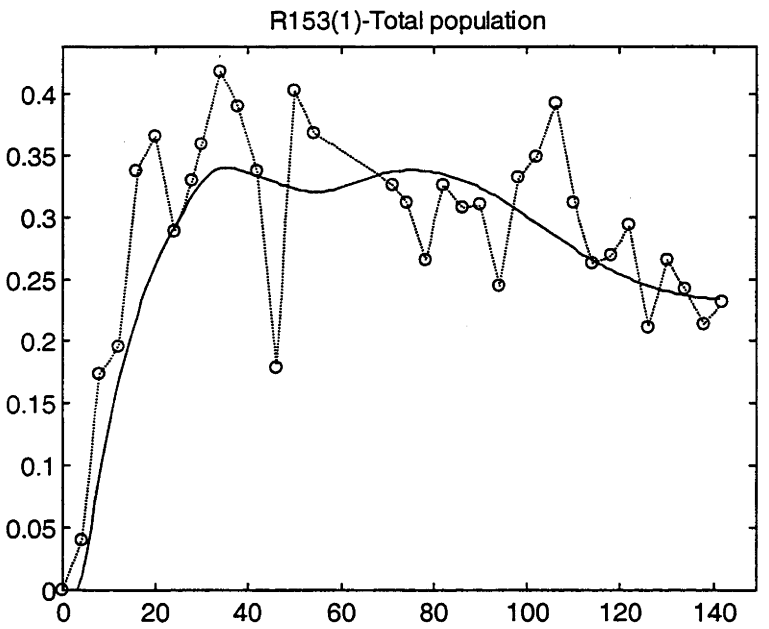

Figure 5.6D: Comparison of the actual outputs and the simulated model outputs

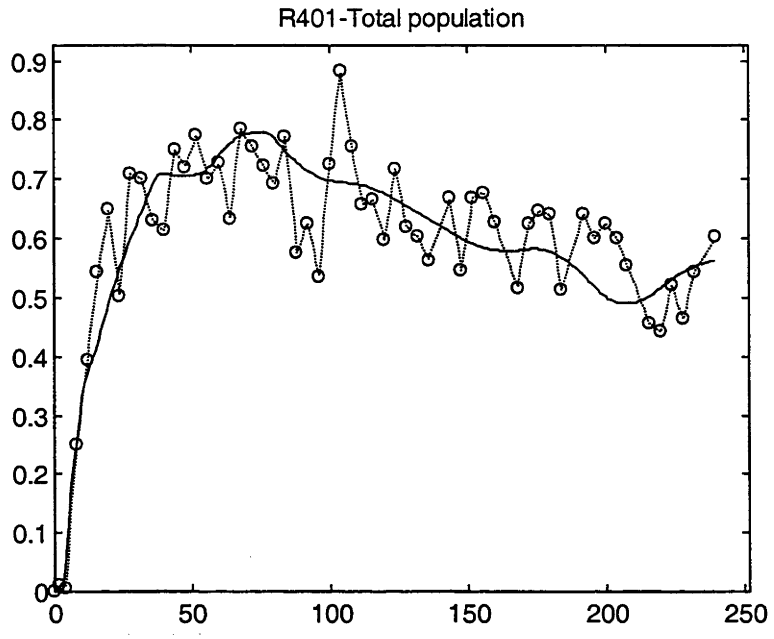

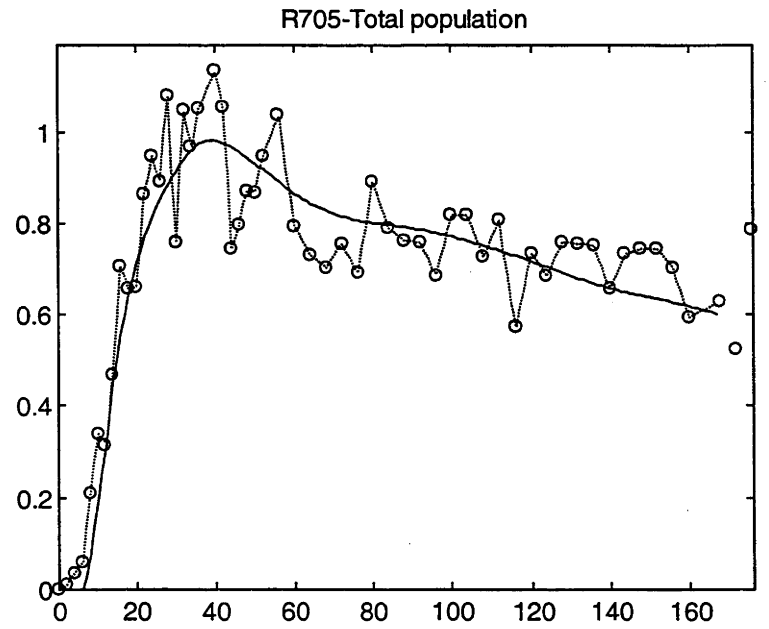

Figure 5.6E: Comparison of the actual outputs and the simulated model outputs

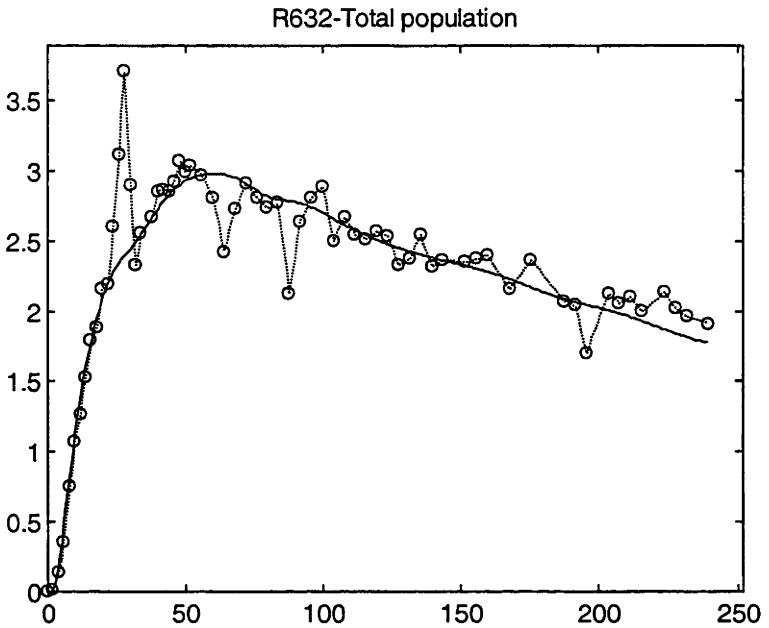

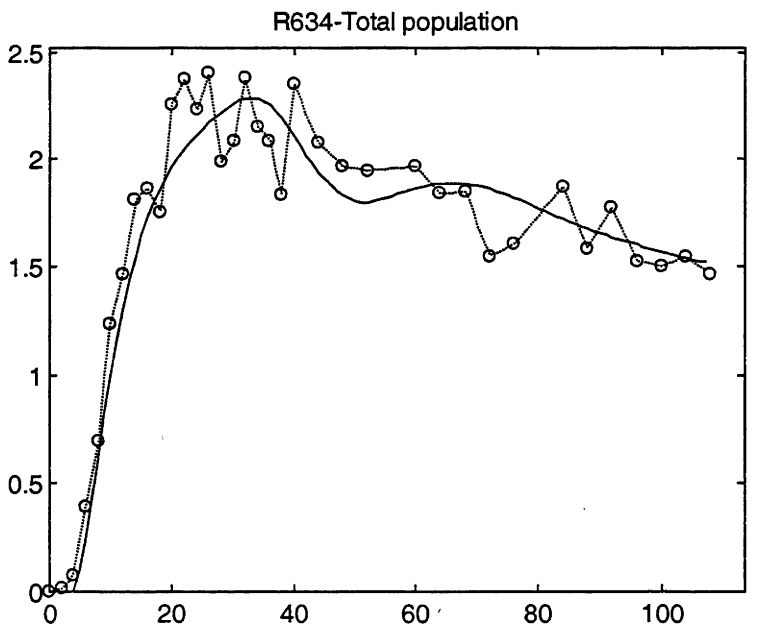

Figure 5.6F: Comparison of the actual outputs and the simulated model outputs

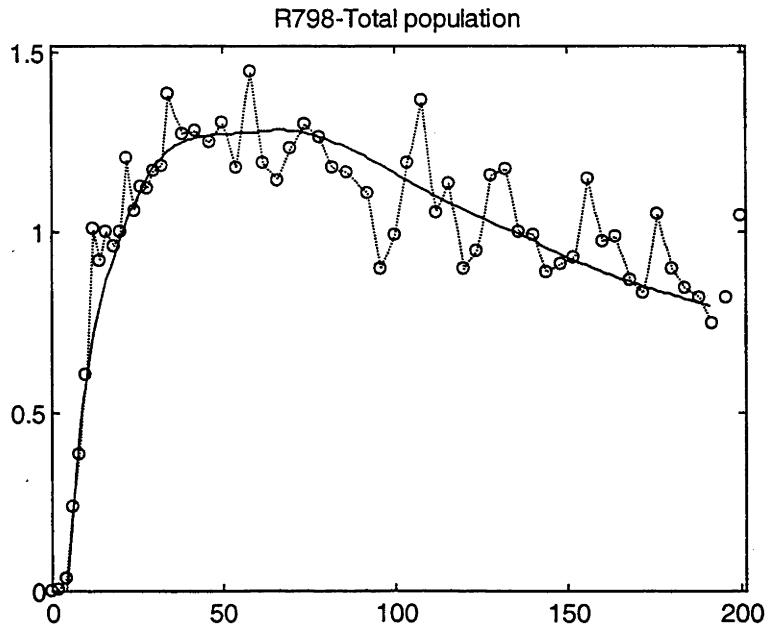

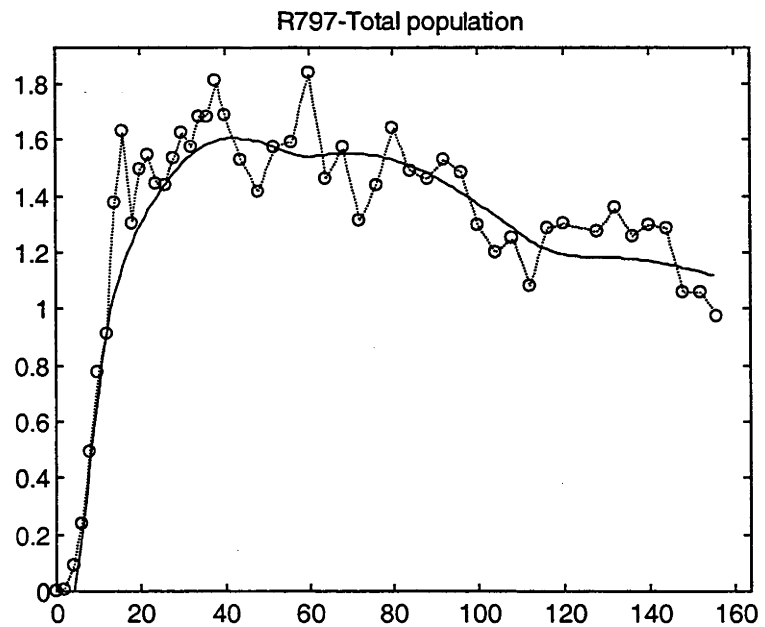

Figure 5.6G: Comparison of the actual outputs and the simulated model outputs

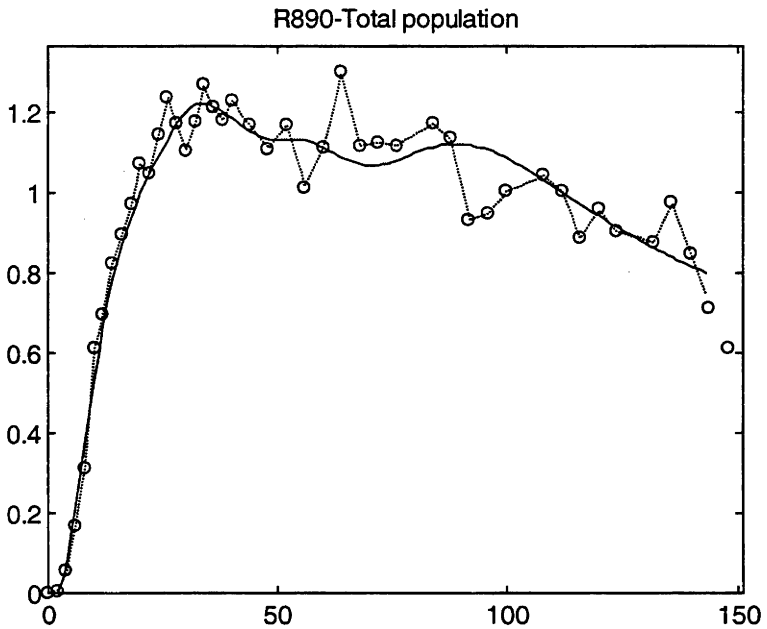

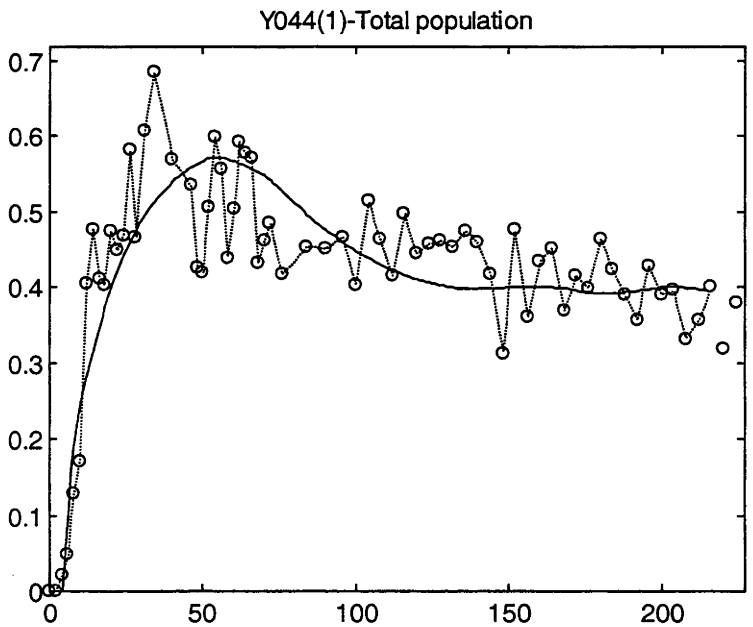

Figure 5.6H: Comparison of the actual outputs and the simulated model outputs

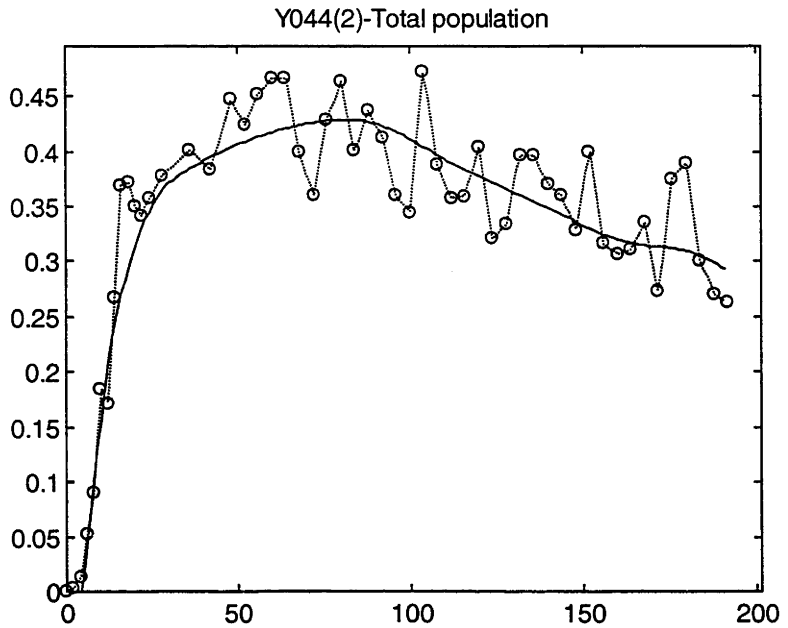

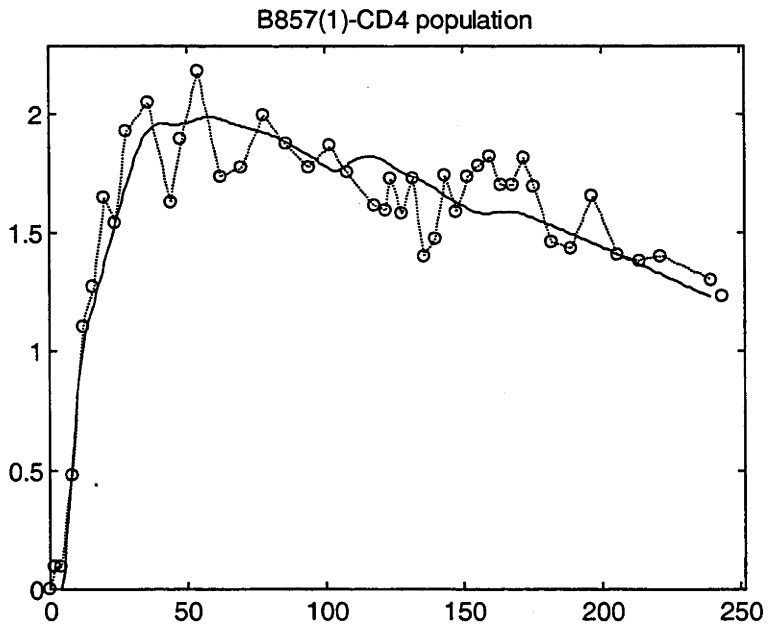

Figure 5.6J: Comparison of the actual outputs and the simulated model outputs

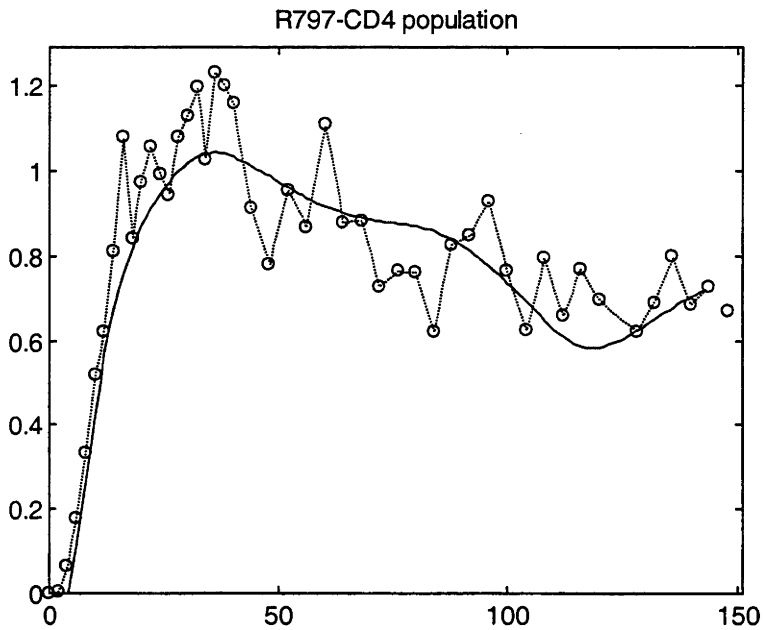

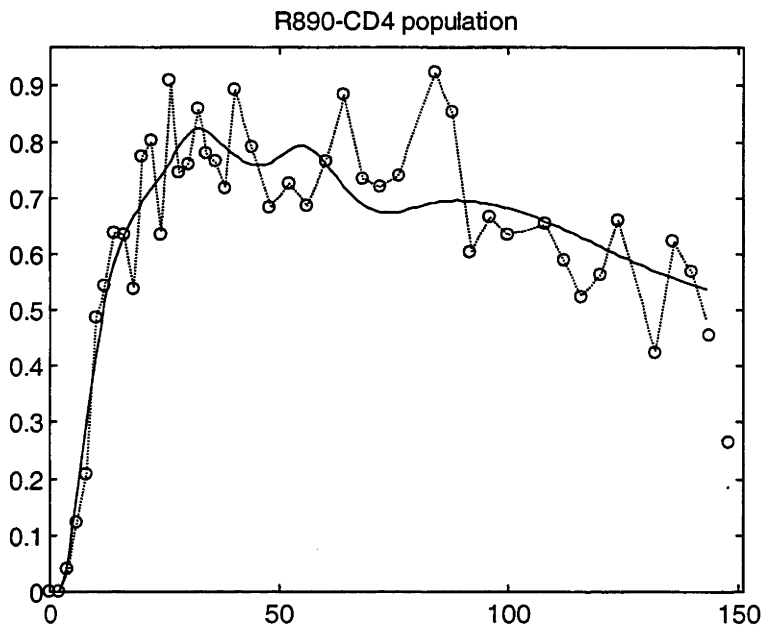

Figure 5.6K: Comparison of the actual outputs and the simulated model outputs

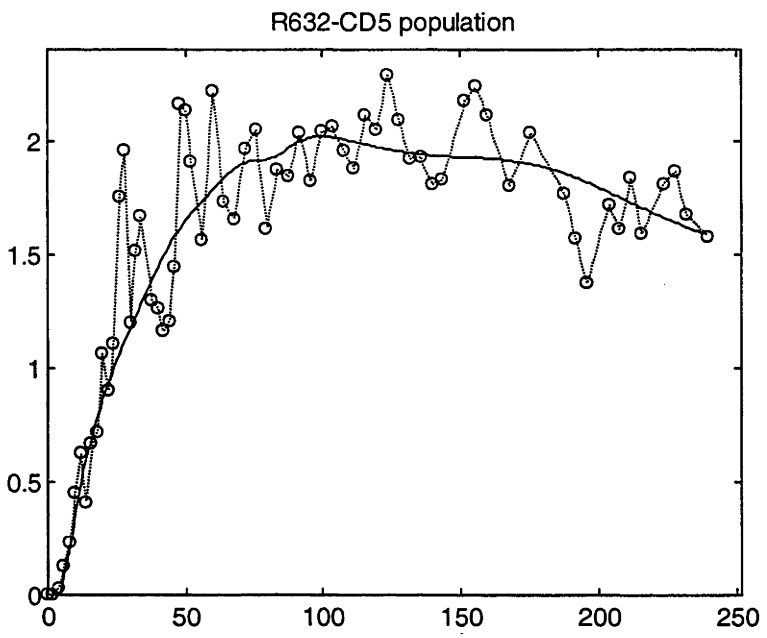

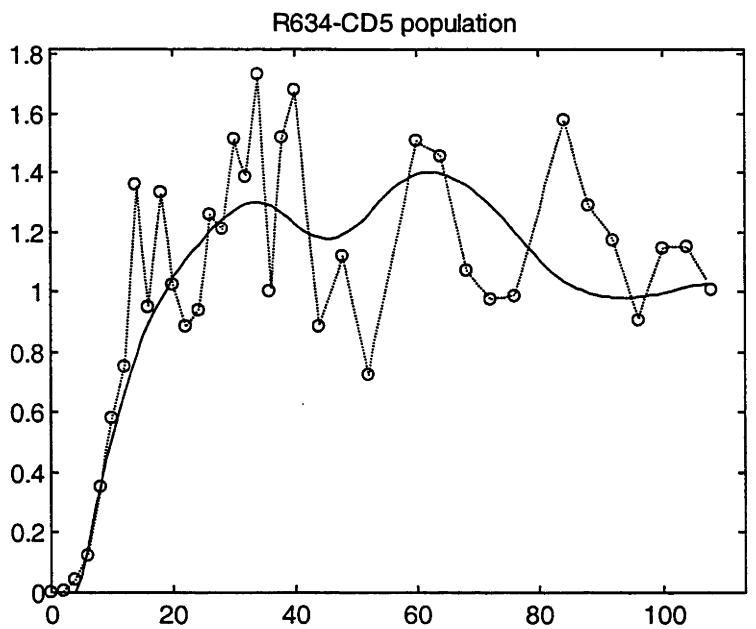

Figure 5.6L: Comparison of the actual outputs and the simulated model outputs

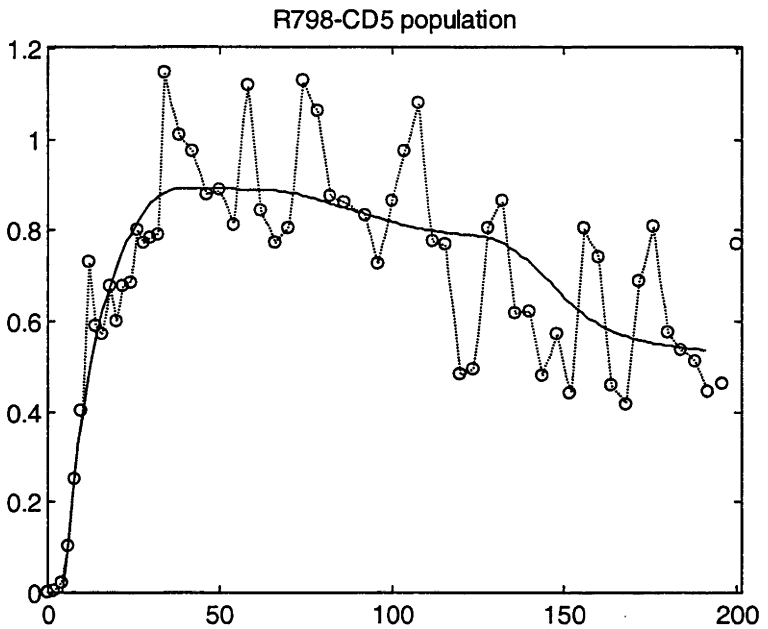

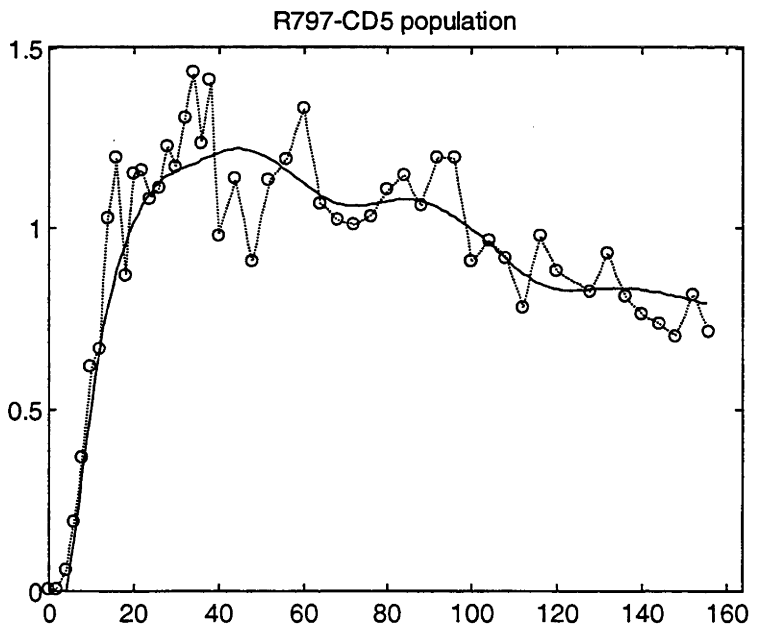

5.4.5 Summary of the estimated parameters

In undertaking this step, the OE model structure (*1,2,nk*), has been selected as the final model and will be used for identification in all of the remaining data sets. Selection of the final prediction error model and parameter identification were successfully achieved in 15 data sets of the total population studies and only 7 data sets of the subset studies (3 of the CD4 data sets and 4 of the CD5 data sets). Due to the very small levels and substantial variations in magnitude of CD8 and CD45R lymphocyte subsets in blood and efferent lymph, none of the data relating to these subsets could be successfully identified using the present procedures. All estimated parameters and their standard deviations are summarised in Table 5.3.

TABLE 5.3: Summary of the estimated parameters and their standard deviation for each data set.

Sheep	N	nk	Estimated parameters ± SD b_0	f_1	f_2	Vsim
	Total population study					
B481	136	5	0.0168 ± 0.0032	-1.5942 ± 0.0779	0.6026 ± 0.0763	0.0061
B445(1)	124	6	0.0059 ± 0.0008	-1.8676 ± 0.0165	0.8706 ± 0.0161	0.0091
B445(2)	100	4	0.0054 ± 0.0013	-1.8346 ± 0.0451	0.8374 ± 0.0445	0.0029
B857(1)	168	4	0.0535 ± 0.0251	-1.1125 ± 0.4007	0.1405 ± 0.3877	0.0161
B857(2)	124	5	0.0130 ± 0.0006	-1.8266 ± 0.0091	0.8338 ± 0.0087	0.0014
R153(1)	142	4	0.0093 ± 0.0019	-1.8175 ± 0.0326	0.8232 ± 0.0315	0.0023
R401	240	4	0.0477 ± 0.0191	-1.2855 ± 0.2841	0.3084 ± 0.2750	0.0043
R705	168	7	0.0122 ± 0.0015	-1.7928 ± 0.0250	0.8033 ± 0.0237	0.0062
R632	240	3	0.0167 ± 0.0016	-1.7989 ± 0.0187	0.8043 ± 0.0183	0.0400
R634	108	5	0.0233 ± 0.0021	-1.7489 ± 0.0224	0.7649 ± 0.0210	0.0217
R798	192	5	0.0396 ± 0.0162	-1.2514 ± 0.2970	0.2771 ± 0.2865	0.0095
R797	156	5	0.0186 ± 0.0029	-1.6867 ± 0.0438	0.6981 ± 0.0420	0.0138
R890	144	3	0.0156 ± 0.0008	-1.8430 ± 0.0087	0.8512 ± 0.0084	0.0044
Y044(1)	216	5	0.0355 ± 0.0285	-1.0651 ± 0.7233	0.0857 ± 0.0769	0.0034

Y044(2)	192	5	0.0102 ± 0.0018	-1.6723 ± 0.0556	0.6789 ± 0.0545	0.0010
	CD4 population study					
B857(1)	240	5	0.0512 ± 0.0105	-1.5951 0.0798	0.6119 ± 0.0764	0.0161
R797	144	5	0.0240 ± 0.0043	-1.7313 0.0426	0.7438 ± 0.0405	0.0108
R890	144	3	0.0305 ± 0.0036	-1.7763 0.0273	0.7898 ± 0.0258	0.0061
	CD5 population study					
R632	240	5	0.0142 ± 0.0034	-1.8047 ± 0.0443	0.8092 ± 0.0432	0.0351
R634	108	5	0.0342 ± 0.0147	-1.6314 ± 0.1537	0.6557 ± 0.1436	0.0523
R798	192	5	0.0453 ± 0.0258	-1.4030 ± 0.3322	0.4320 ± 0.3158	0.0151
R797	156	5	0.0228 ± 0.0033	-1.7310 ± 0.0359	0.7450 ± 0.0340	0.0098

5.5 Analysis of the simulated unit impulse response

If the model characteristics (transfer functions) are provided, certain types of input can be applied to simulate their outputs. In this section, the input-output dynamics transfer function $G(q)$ of the OE model $(1,2,nk)$ was used to simulate the unit impulse response by applying the unit impulse input. Consequently, some unique features (such as delay, gain, etc) can be extracted from the unit impulse responses.

5.5.1 Simulation of unit impulse responses

As previously mentioned, the system can be completely described by its unit impulse response. Having established a satisfactory model from section 5.4, simulation will be performed to observe the unit impulse responses after a defined unit impulse input. Generally, the unit impulse input could be applied directly as a test input in a variety of systems under study and followed by observation of the output (ie unit impulse response). As a consequence of lymphocyte recirculation in the blood, the pattern of disappearance of labelled lymphocytes from venous blood followed an exponential decay rather than being an ideal unit impulse input. This result was presented in section 3.2.1 in Chapter 3 of this thesis. Subsequently, since the ideal unit impulse input could not be applied in the present study, a simulation of the response to a unit impulse has been undertaken as an alternative after identification of a model of the system under study.

The final models in Table 5.3 were used to represent the lymph node system in the corresponding experiments. The unit impulse response was computed and graphic representations obtained from Matlab. The time scale for the unit impulse response is given as 160 hours, which covers all of the important features of unit impulse responses in this study (Figure 5.7A – 5.7L). Details of the simulation procedure and Matlab commands can be found in Appendix 2.

The general pattern of the unit impulse response comprised two main components (Figure 5.7A – 5.7L). The first component was the rapidly rising portion following the system delay. This was characterised by a period during which the unit impulse responses ranged from zero, to the highest (ie peak) response. The peaks were observed in a range of approximately 0.025 to 0.120. The peak values of the unit impulse response obtained from the CD4 population study were generally higher than those obtained from the others (lower panel of Figure 5.7H, and Figure 5.7J). The second component of the response, which

occupied a longer period compared with the first one, was the gradual decline from the peak. In the present study, almost all of the peaks in unit impulse responses (21 out of 22) were observed within the first 20 hours. Only the peak from B445(1) was observed later than 20 hours (Figure 5.7A - lower panel). The unit impulse responses slowly declined and converged to zero in 13 out of 22 cases (Figure 5.7A – 5.7L) over the course of the observation time (ie 160 hours).

Figure 5.7A: Simulated unit impulse responses

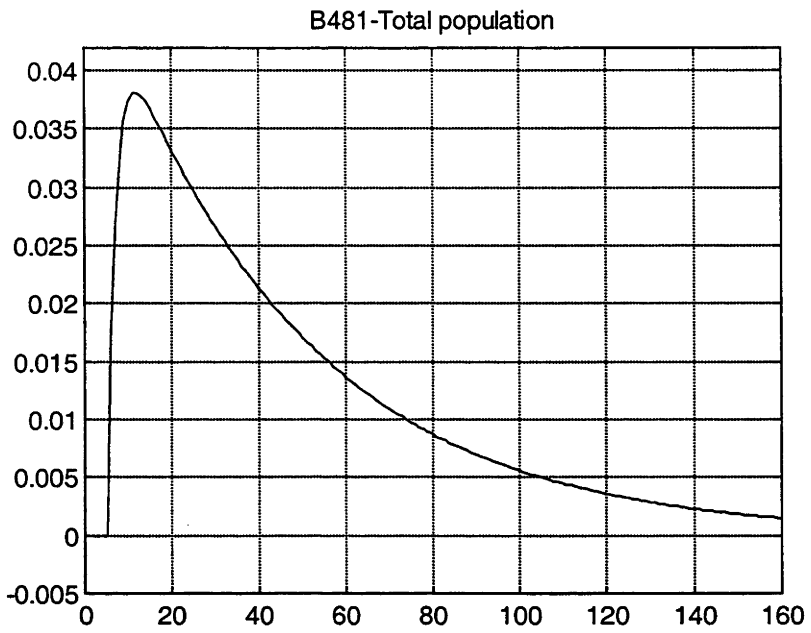

Figure 5.7B: Simulated unit impulse responses

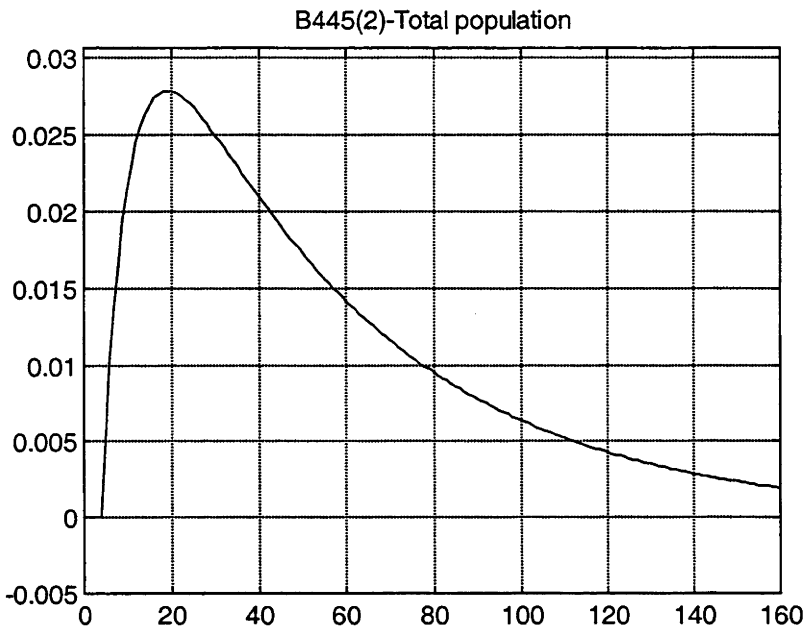

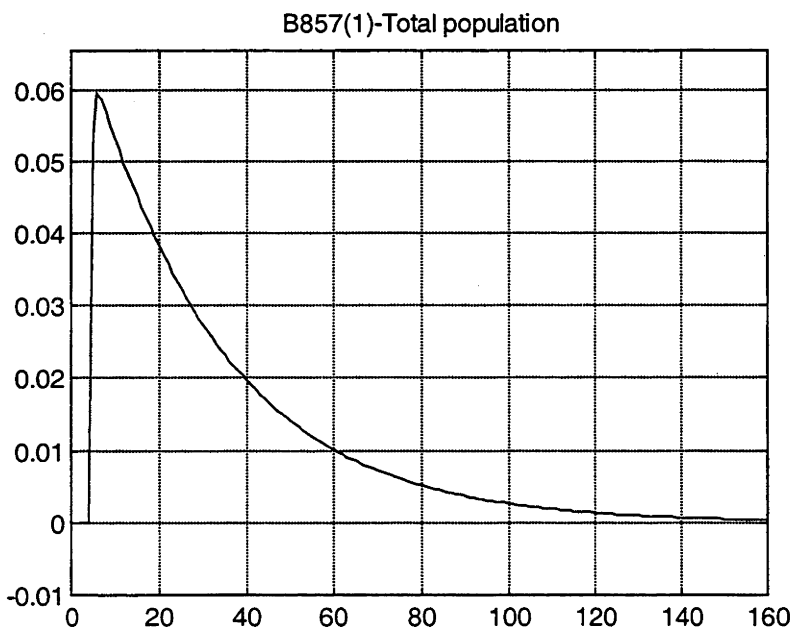

Figure 5.7C: Simulated unit impulse responses

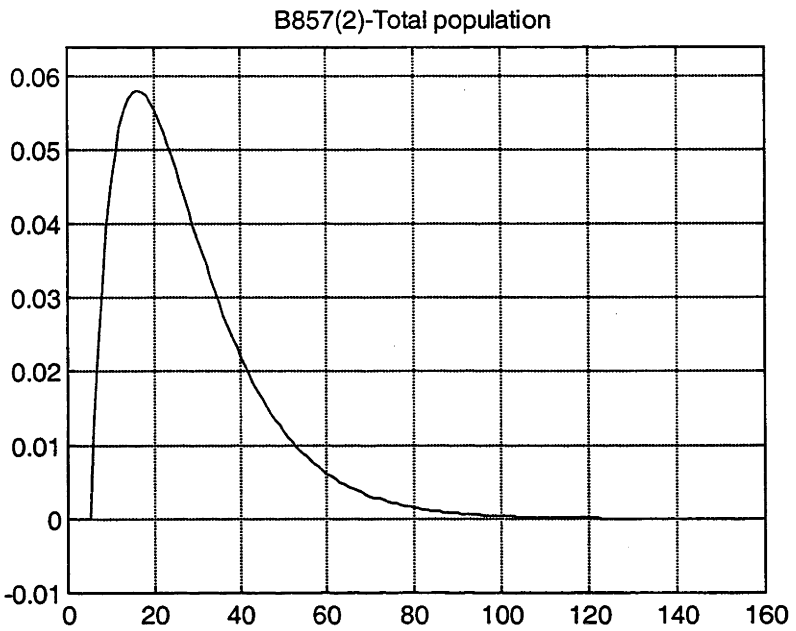

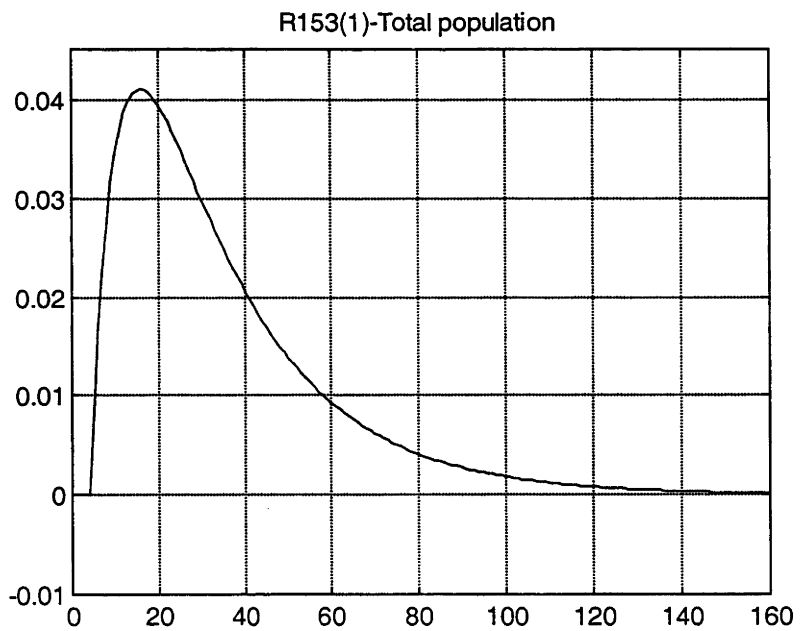

Figure 5.7D: Simulated unit impulse responses

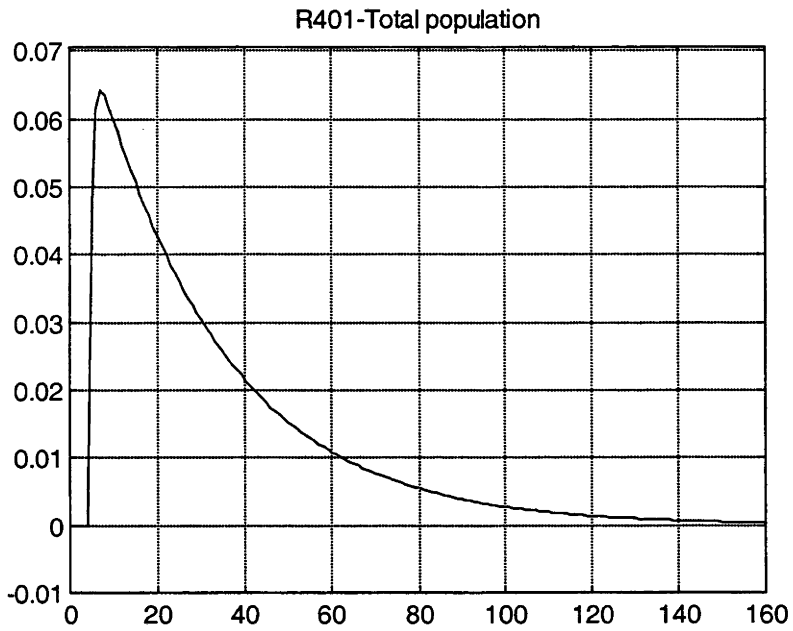

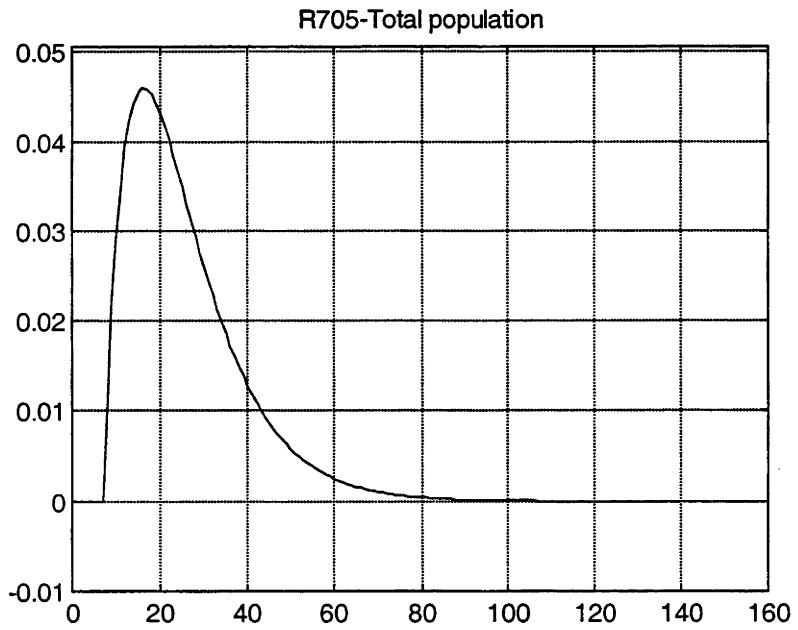

Figure 5.7E: Simulated unit impulse responses

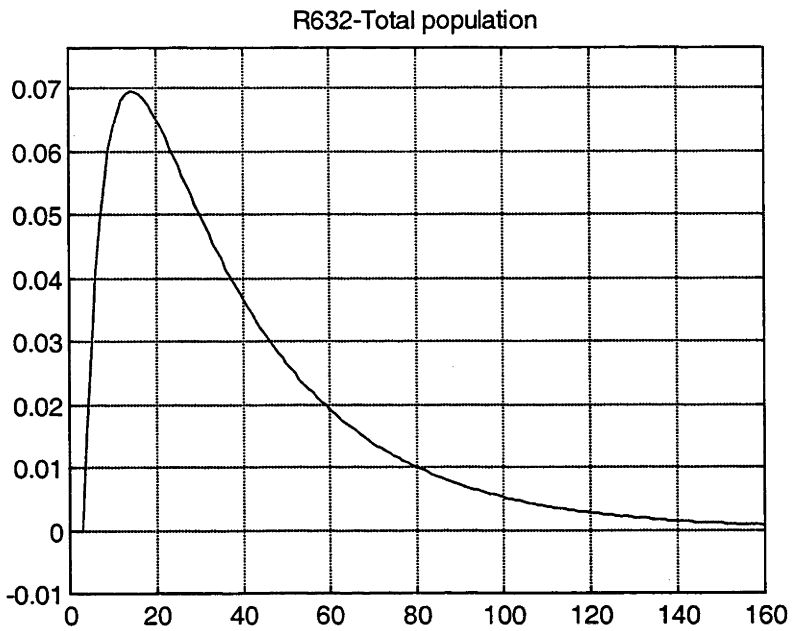

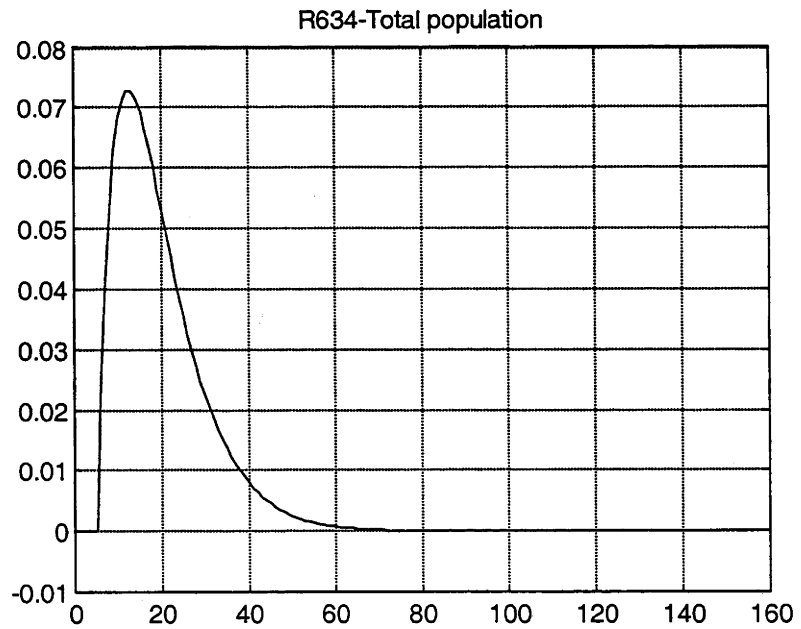

Figure 5.7F: Simulated unit impulse responses

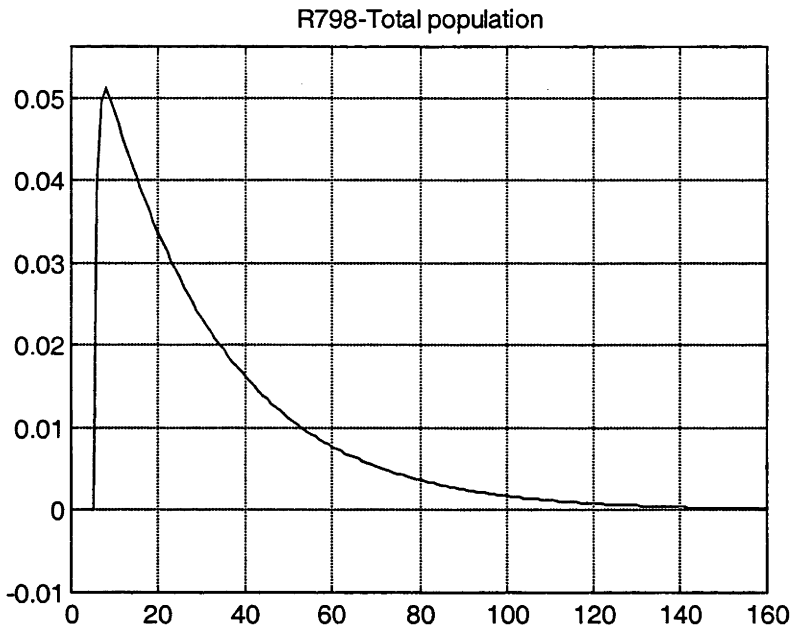

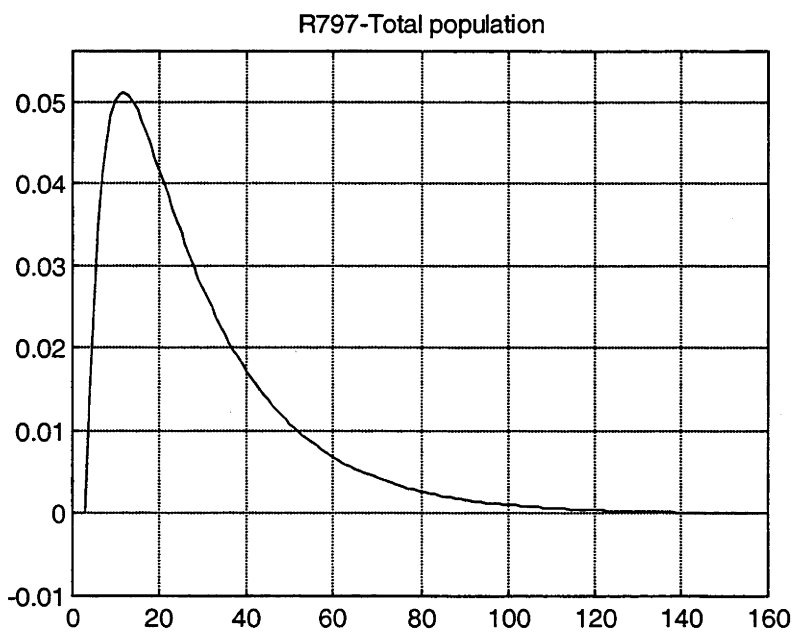

Figure 5.7G: Simulated unit impulse responses

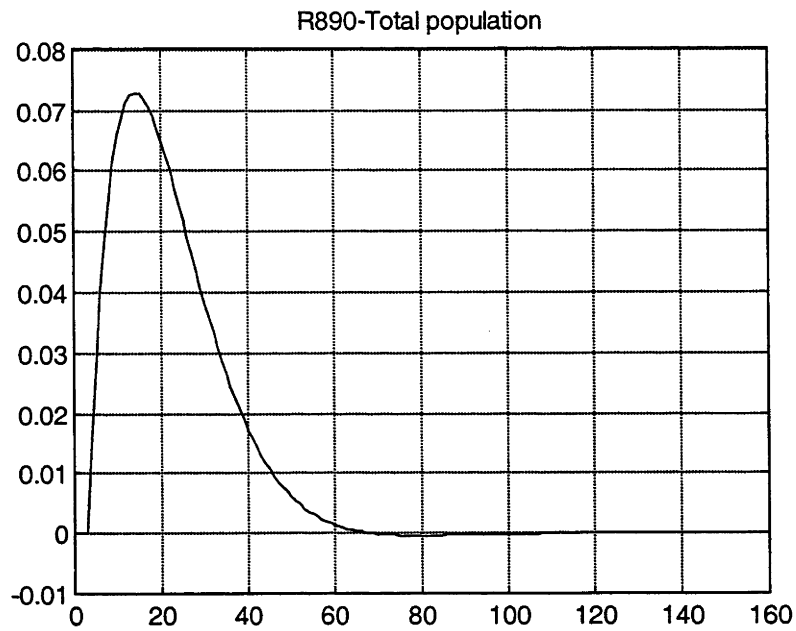

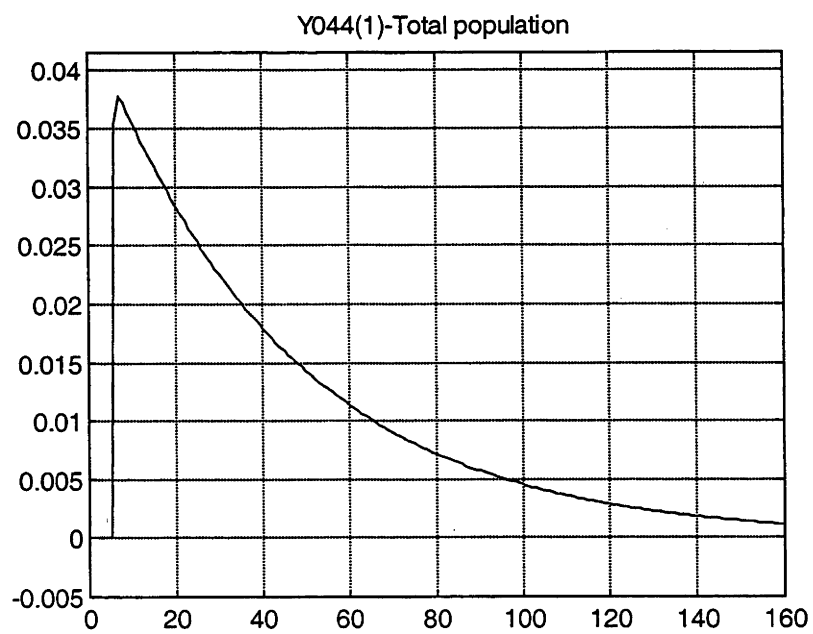

Figure 5.7H: Simulated unit impulse responses

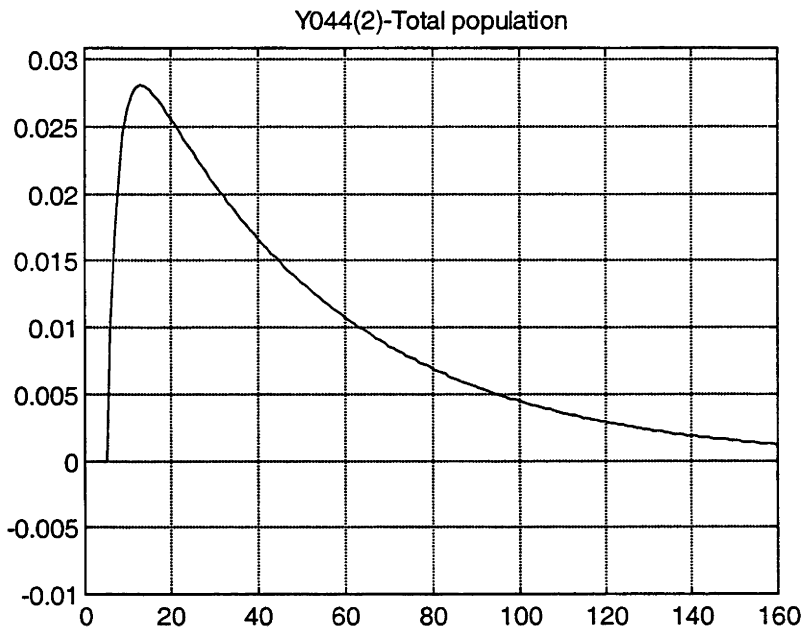

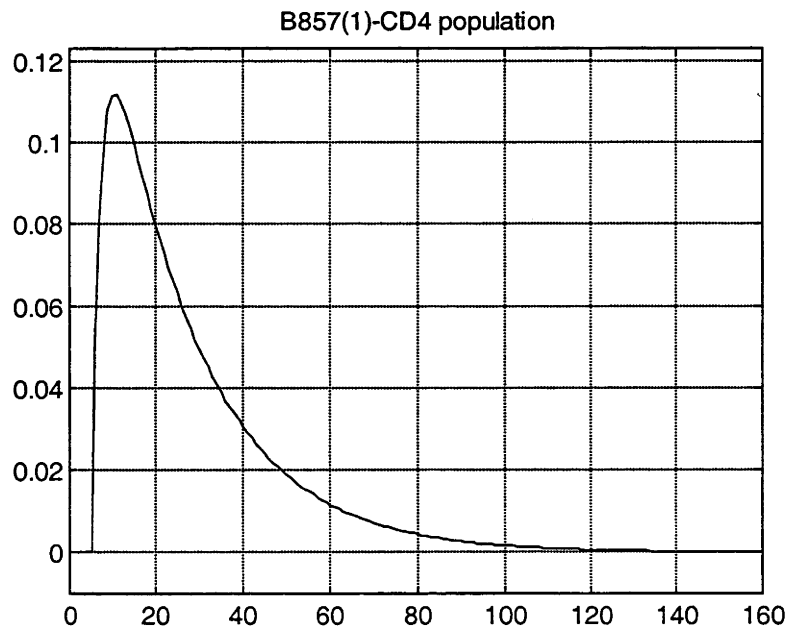

Figure 5.7J: Simulated unit impulse responses

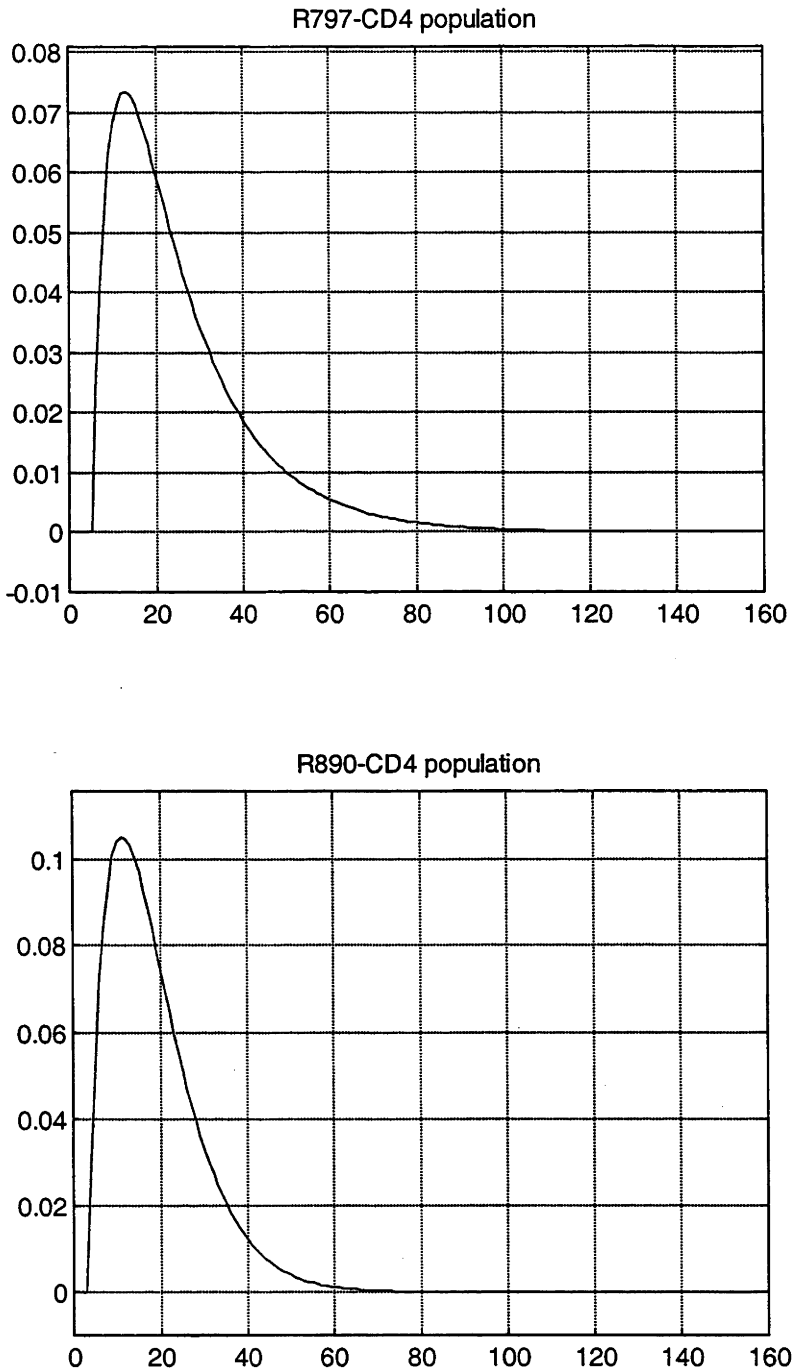

Figure 5.7K: Simulated unit impulse responses

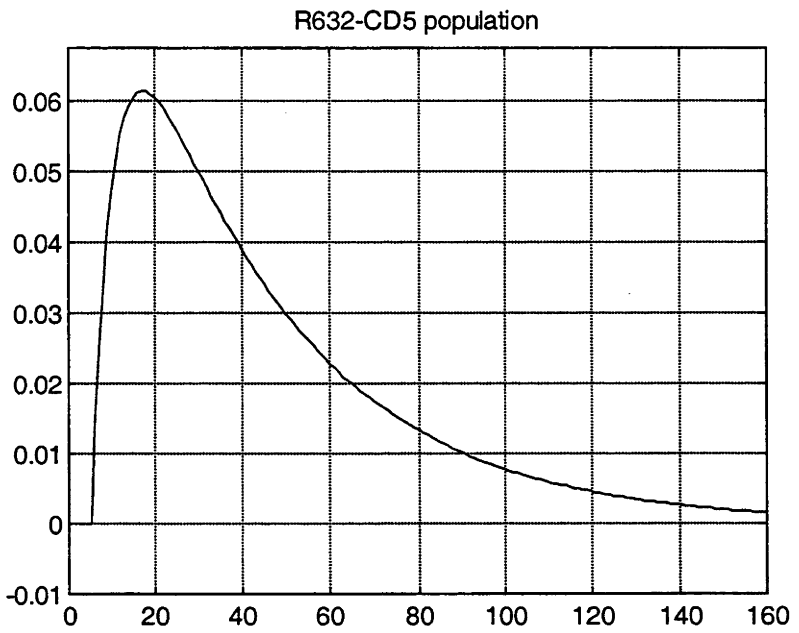

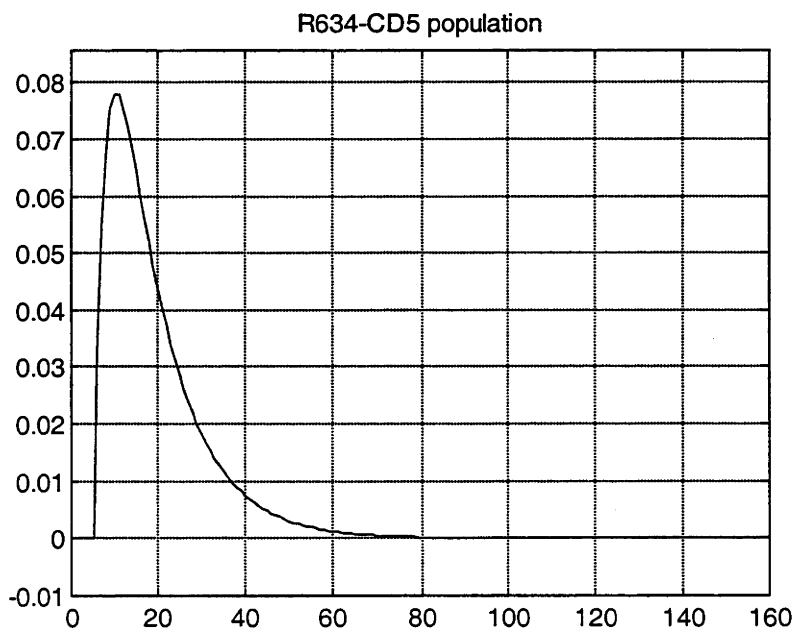

Figure 5.7L: Simulated unit impulse responses

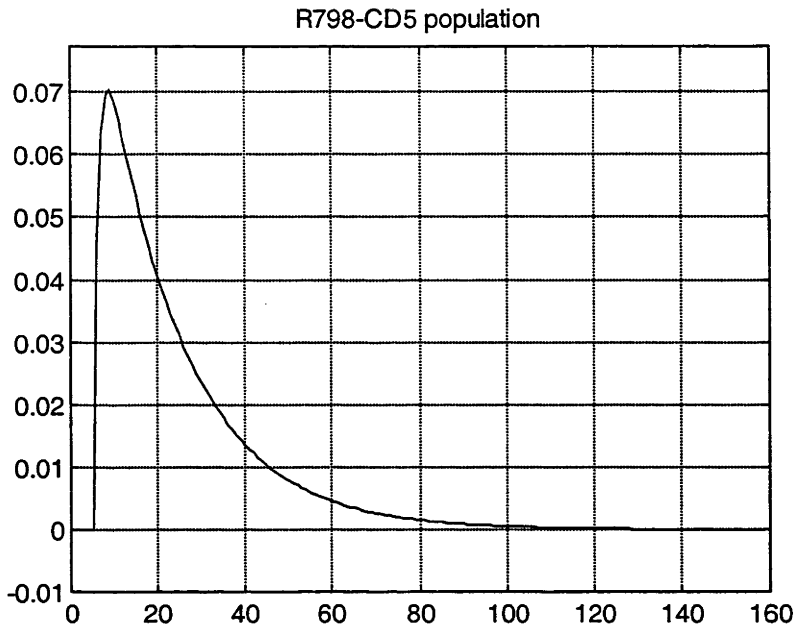

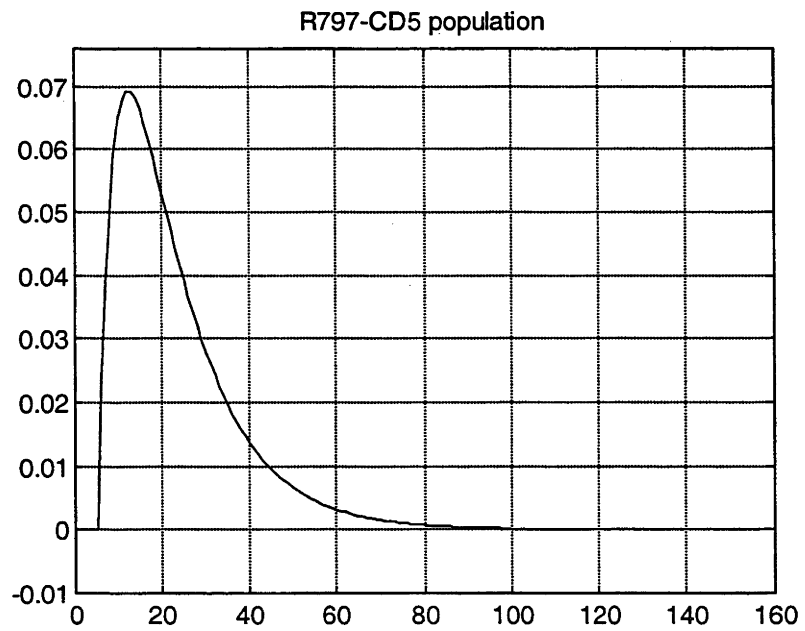

5.5.2 Feature extraction from the simulated unit impulse response

In this section, making use of the final OE models in Table 5.3, the unit impulse responses are simulated under noise-free conditions. The unit impulse responses are computed by Matlab and used to extract the following features:

- **The system delay (nk)** is the time duration before any influence of the input on output is observed.
- **Peak** is the maximal value of the unit impulse response.
- **Peak time (T_{peak})** is the time at which the peak value is observed.
- **Rising time (T_{rise})**is the peak time minus the system delay.
- **MTT_{75}** is the mean (transit) time at which the integral of the unit impulse response attains 75% of its final integral value.
- **Response Time (T_{resp})** is the time at which the integral of the unit impulse response reaches 95% of its final integral value.
- **Gain** is the integral of a unit impulse input from time zero to time infinity.

Table 5.4 summarises these features including system delay (nk) and the simulation cost function (Vsim) in each individual data set.

Figure 5.8: Feature extraction from a simulated unit impulse response.

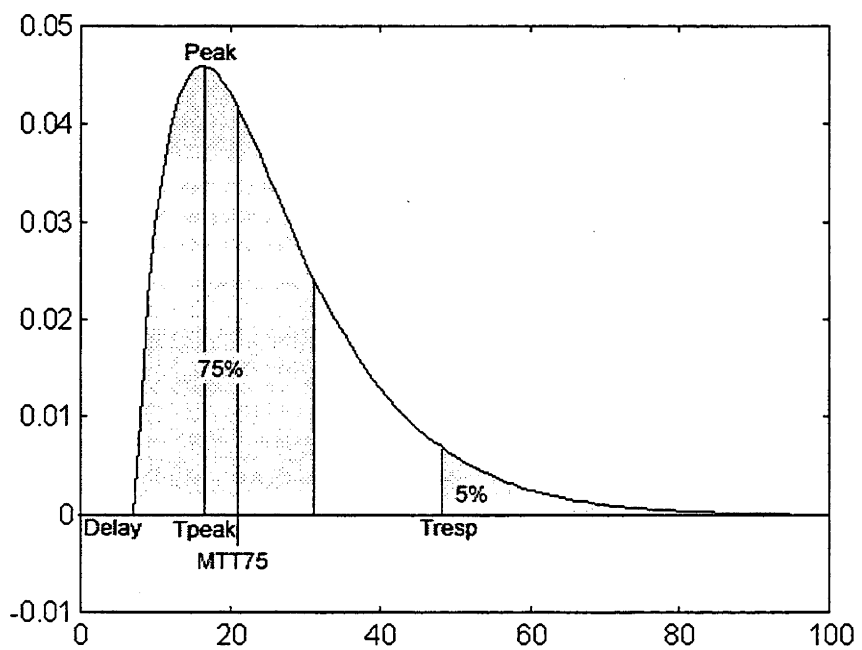

TABLE 5.4: Summary of characteristics of the unit impulse response in individual studies

Animal	nk	Peak	T_{peak}	T_{rise}	MTT_{75}	T_{resp}	Gain	Vsim
	Total population study							
B481	5	0.0381	10.71	5.71	25.93	118.90	1.9237	0.0061
B445(1)	6	0.0357	21.40	15.40	29.74	109.61	1.9514	0.0091
B445(2)	4	0.0279	18.01	14.01	31.38	126.62	1.7979	0.0029
B857(1)	4	0.0625	4.56	0.56	17.20	90.32	1.8999	0.0161
B857(2)	5	0.0580	15.05	10.05	18.27	58.28	1.7886	0.0014
R153(1)	4	0.0411	14.89	10.89	20.79	82.97	1.6291	0.0023
R401	4	0.0642	6.25	2.25	17.14	88.65	2.0733	0.0043
R705	7	0.0460	15.17	8.17	17.67	50.41	1.1668	0.0062
R632	3	0.0695	13.35	10.35	21.56	95.91	3.0753	0.0400
R634	5	0.0730	11.41	6.41	13.11	37.90	1.4502	0.0217
R798	5	0.0510	7.05	2.05	17.14	84.26	1.5331	0.0095
R797	5	0.0513	11.28	6.28	17.76	75.91	1.6285	0.0138
R890	3	0.0730	13.11	10.11	14.65	42.00	1.9216	0.0044
Y044(1)	5	0.0406	5.50	0.50	23.94	116.51	1.6732	0.0034
Y044(2)	5	0.0281	12.12	7.12	26.93	120.37	1.4835	0.0010
Mean	**4.67**	**0.0502**	**11.91**	**7.51**	**20.77**	**86.38**	**1.8001**	**0.0094**
± SD	**± 1.05**	**±0.0157**	**± 4.68**	**± 4.71**	**± 5.62**	**± 29.44**	**±0.4248**	**±0.0103**
	CD4 population study							
B857(1)	5	0.1120	9.63	4.63	15.65	67.86	3.0384	0.0161
R797	5	0.0735	11.78	6.78	15.58	57.23	1.9219	0.0108
R890	3	0.1055	10.22	7.22	11.95	37.69	2.2677	0.0061
Mean	**4.33**	**0.0970***	**10.54**	**6.21**	**14.39***	**54.26***	**2.4093***	**0.0110**
± SD	**± 1.15**	**±0.0206**	**± 1.11**	**± 1.39**	**± 2.12**	**± 15.30**	**±0.5716**	**±0.0050**
	CD5 population study							
R632	5	0.0614	16.06	11.06	26.35	110.44	3.1207	0.0351
R634	5	0.0781	9.40	4.40	11.86	40.36	1.4058	0.0523
R798	5	0.0704	7.64	2.64	13.46	59.53	1.5614	0.0151
R797	5	0.0692	11.47	6.47	14.50	49.85	1.6279	0.0098
Mean	**5.00**	**0.0698***	**11.14**	**6.14**	**16.54**	**65.05**	**1.9289**	**0.0281**
± SD	**± 0.00**	**±0.0068**	**± 3.63**	**± 3.63**	**± 6.63**	**± 31.26**	**±0.7999**	**±0.0195**

* Denotes statistically significantly differences (p value less than 0.05)

5.6 Discussion

In Chapter 1, a number of earlier lymphocyte recirculation and lymphocyte migration studies were reviewed. The interpretation of those studies was dependent upon the results of actual observation. In this chapter, system identification procedures have been systematically applied to actual observations to describe the details of lymphocyte migration.

The system identification prediction error method has been successfully applied to many problems including the identification of medical systems, many details of which were not known, such as the abnormal movement of the eyeball (Rey and Galiana, 1991) and the mechanism of muscle contraction (Hunt *et al.*, 1998). In the present chapter, system identification of the lymph node was introduced as a means of studying its function. The technique used in this chapter has been shown to have some advantages over the one used in Chapter 4 (Compartmental models) as it is dependent only upon the initial assumption of a linear dynamics system for the lymph node and the experimental results (ie a stimulus-response relationship) rather than on prior information or any additional assumptions.

In the present study, four candidate model structures were proposed and the selection of the final model was systematically undertaken using selection criteria. The OE model was selected from among the four candidate models (ARX, ARMAX, OE and BJ) to represent the lymph node model because of its good simulation performance (represented by the lowest value of the simulation cost function, Table 5.1). The identified parameters for the OE model showed relatively low standard deviations in their values, compared with those applicable to other models, reflecting the reliability of these identified parameters. Moreover, a validation test (residual analysis) was performed to ensure the adequacy of the selected OE models.

The existence of non-linear effects was suggested by this analysis. In most experiments, the simulation of system outputs using actual input data indicated that there were large systematic errors after 144-196 hours (results not shown). No simple explanation is apparent for these events. The migration of lymphocytes could be linearly represented only during a certain time range, ie until approximately 144 hours after stimulation. It is possible that the lymph node system is composed of several linear dynamic subsystems so that the final output represents the combined effect of output of each individual subsystem. Alternatively, the lymph node as an entity may behave as a non linear system.

However, for the purpose of this thesis, the assumption that a linear system will suffice to explain functioning of the lymph node under normal physiological conditions will be retained.

In section 5.5, a unit impulse was applied to the present, known system dynamics to elicit a noise-free unit impulse response. Information contained in the patterns of a unit impulse response was extracted for some defined parameters. Using this technique, Modarreszadeh was able to report a number of physiological parameters related to the findings of his ventilation studies (Modarreszadeh *et al.*, 1995).

The overall features of the unit impulse response suggest that different kinetic stages are applicable to migrating lymphocytes. The first, rapidly rising component of the unit impulse response, represented by the steeper slope and shorter time period to reach the peak, describes a faster rate of lymphocyte appearance in efferent lymph (ie output) compared with the second, gradually declining component. The occurrence of this declining component may imply a slow release (or wash out) of migrating lymphocytes from the lymphoid tissue of the lymph node. The rapidly rising component may imply a relatively fast intake (or recruitment) of migrating lymphocytes into the tissue.

Generally, the system delay is the time period required before a change in the input will be reflected by a change in the output. In the present study, the system delay would represent the minimum time required for a lymphocyte to escape from the blood circulation and to reappear in the efferent lymphatic vessel of the lymph node. In other words, any lymphocyte that migrates via the shortest path through the lymphoid tissue would require a certain time equal to the system delay time to reappear in the efferent lymph. This study did not show any significant differences between system delays obtained from studies of different lymphocyte populations (ie 4.67 ± 1.05, 4.33 ± 1.15 and 5.00 ± 0.00 hours for total, CD4 and CD5 populations respectively). The similarity of these values for system delay suggests that all lymphocyte phenotypes may share a common shortest path in lymphoid tissue.

It is obvious that there is a considerable difference in the time spent during the first and second kinetic components. Generally, the time spent in the declining component is much longer (approximately 10 times) than that in the rapidly rising component. For all unit impulse responses, the time required to reach their peaks, T_{rise} (7.51 ± 4.71, 6.21 ± 1.39 and 6.14 ± 3.63 hours for total, CD4 and CD5 populations respectively) is much less than that required to complete their

responses, T_{resp} (86.38 ± 29.44, 54.26 ± 15.30 and 65.05 ± 31.26 hours for total, CD4 and CD5 populations respectively).

The peak (ie maximal value of unit impulse response) values are 0.0502 ± 0.0157, 0.0970 ± 0.0206 and 0.0698 ± 0.0068 for total, CD4 and CD5 populations respectively. The peak values of the unit impulse response obtained from the CD4 population study are significantly higher than those obtained from the other populations. However, there are no significant differences in T_{peak} (ie the time required for lymphocytes to reach their maximal level in the efferent lymph). These times are 11.91 ± 4.68, 10.54 ± 1.11 and 11.14 ± 3.63 hours, respectively, for total, CD4 and CD5 lymphocyte populations. These findings from the present study differ from others, which reported that migrating lymphocytes reached their peak concentration in the efferent lymph of peripheral lymph nodes at approximately 24-48 hours (Frost *et al.*, 1975; Trevella and Morris, 1980; Reynolds *et al.*, 1982). These reports were based on actual experimental data without any adjustment for the effect of continual recirculation throughout the experiment. The observed timing of peak values would be subject to interference for the reasons mentioned above.

It is assumed that gain, which is the integral of a unit impulse response from time zero to time infinity (ie this is equivalent to the whole area under the curve of a unit impulse response), is the total outcome of a unit impulse response. Generally, if inputs of the same quantity and quality are given to different systems, the system with a higher gain will yield a higher output. In other words, the system gain describes how well the system will respond to the given unit impulse input. Similarly, the gain of the lymph node system in the present study would describe the response (ie level of labelled lymphocytes) in the efferent lymphatic corresponding to the unit impulse input given. In all unit impulse responses, average gain values are always larger than 1 (1.8001 ± 0.4248, 2.4093 ± 0.5716 and 1.9289 ± 0.7999 hours for total, CD4 and CD5 lymphocyte populations respectively). Among all the lymphocyte populations of interest, the significantly higher value of the average gain in the CD4 lymphocyte population indicates that the lymph node gives a larger CD4 lymphocyte response (ie more output or frequency of labelled CD4 lymphocytes in the efferent lymph) under the same conditions (ie after the same unit impulse input). However, there are no significant differences between average gain values calculated for the total and CD5 lymphocyte populations. This finding confirms previous reports (Washington *et al.*, 1988; Witherden *et al.*, 1990; Abernethy *et al.*, 1990; Abernethy *et al.*, 1991) of the existence of a subset-specific event for migrating lymphocytes (ie CD4 lymphocytes are extracted from the blood circulation better than the other

subpopulations). Moreover, it agrees with the results obtained for the values of L/B ratios described earlier in Section 3.3.2 of Chapter 3 of this thesis.

As a derivative from the definition of gain, MTT_{75} is another parameter intentionally defined (as the mean time at which the integral of the unit impulse response attains 75% of its final value) to denote the mean transit time of the majority (ie 75%) of migrating lymphocytes from the unit impulse response. It has been shown that MTT_{75} values are 20.77 ± 5.62, 14.39 ± 2.12 and 16.54 ± 6.63 hours for total, CD4 and CD5 populations respectively. This can be interpreted as indicating that at least 75% of migrating lymphocytes, regardless of their phenotypes, would spend less than 24 hours in migrating through the lymphoid tissue (ie only 25%, or less, would spend more than 24 hours). Furthermore, CD4 lymphocytes spend significantly less time than do the total population and CD5 lymphocytes. However, there is no significant difference between MTT_{75} of total population and CD5 lymphocytes. The time spent during the migratory process may reflect cell-cell interactions within lymphoid tissue. If so, this finding may imply that CD4 lymphocytes have fewer, or a similar number of interactions and require less time than total population and CD5 lymphocytes.

Other evidence, provided by T_{resp}, supports the hypothesis that CD4 lymphocytes spent less time in the lymphoid tissue. This parameter is defined to monitor the completeness of a unit impulse response (ie by cut off at 95% of the total outcome). T_{resp} values obtained for the CD4 lymphocyte population (54.26 ± 15.30 hours) are significantly less than those obtained from either the total or CD5 lymphocyte population (86.38 ± 29.44, and 65.05 ± 31.26 hours respectively). Not surprisingly, similarly to the results of MTT_{75}, T_{resp} for total and CD5 lymphocyte populations are not significantly different.

5.7 Conclusion

Theoretical modelling of biomedical systems should permit major breakthroughs in current medical research and can provide valuable information. For this study, a peripheral lymph node was assumed to be a linear dynamic system with a single input and a single output. Given experimental data (the input-output relationship) together with implementation of the prediction error method of system identification, many characteristics of the studied system could be determined from its unit impulse response.

A comprehensive detailed description of lymph node system structure is yet to be attained. Nevertheless, the use of prediction error models should assist in gaining a better understanding of the problems of lymphocyte migration. Lymphocyte migration models, constructed from data collected under normal physiological conditions, will be necessary to interpret events occurring in pathological conditions.

Chapter 6/
Structured models

6.1 Introduction

The differences between the concepts of functional and physical models were introduced in part II of Chapter 1. To recapitulate briefly, physical models are models constructed by connecting known models of subsystems together. Thus, these models can describe the actual configuration of the systems which are being studied. However, the construction of such models requires considerable prior knowledge of the particular systems. For example, the physical model developed to describe the lymph node in Chapter 4 (Compartmental models) required some knowledge of lymph node structure and function together with assumptions from previous studies relating, to the number of lymphocytes residing in the lymph nodes (as seen in detail in section 4.3-4.4 of Chapter 4).

The prediction error models and the analysis of the unit impulse responses in the time domain presented in Chapter 5 are other attempts to describe the lymph node system. The results of this analysis have given an indication of the pattern of lymphocyte migration in both the whole population and subsets of lymphocytes. However, it still has not provided sufficient information about the actual structure of a lymph node model to permit description of this process.

In this chapter, the procedure that has been developed for building structured models of dynamic systems will be introduced, as briefly foreshadowed in the concluding section of Chapter 5. This procedure is based on a combination of system modelling in the frequency and time domains. The procedure presented, allows the construction of structured models of the dynamic systems under study without requiring any a priori knowledge about the configuration of these systems. It employs exclusively a posteriori information about them obtained from measurements performed on them. This technique has been successfully applied, and the results reported, in pharmacokinetic studies (Durisova *et al.*, 1995).

6.2 System modelling in the frequency domain

System modelling in the frequency domain is an alternative approach to the time domain approaches presented in Chapter 3 (Compartmental models) and Chapter 4 (Prediction error models) for identification of unknown systems. System modelling in the frequency domain has some advantages over approaches in the time domain for modelling complex systems, which require high-order models, (Durisova and Dedik, 1994). Frequency domain methods have been widely utilised in technical fields. However, during recent years these methods have increasingly also been employed to explore unknown systems in biomedical fields. For example, in pharmacokinetic studies, the frequency responses of biological systems have been utilised to implement frequency domain analysis (Dedik and Durisova, 1994; Dedik and Durisova, 1995; Durisova *et al.*, 1995).

In this section, some general descriptions of the system transfer function and of frequency responses will be introduced. More comprehensive details of their applications in modelling attempts will be presented in the following sections of this chapter. Briefly, the frequency response method is based on an approximation to the frequency response of a dynamic system. The system frequency response can be obtained either by measurements made on the system in the frequency domain (ie for technical systems), or it can be calculated from the measured input-output of the system in the time domain. Models in the form of a ratio of two frequency dependent polynomials are used to model the system frequency response (Schoukens and Pintelon, 1991). All of the relevant fundamental principles applicable to a linear system and some of the terminology have been referred to in detail in part II of Chapter 1.

6.2.1 System transfer function

Under some specified initial conditions a linear time invariant (LTI) system with single-input-single-output (SISO) can be represented by a model in the form of differential equation (6.1) (Schoukens and Pintelon, 1991).

$$y(t)+b_1\frac{dy(t)}{dt}+b_2\frac{d^2y(t)}{dt^2}+\ldots+b_{m-1}\frac{d^{m-1}y(t)}{dt^{m-1}}+b_m\frac{d^my(t)}{dt^m}= G\cdot\left(a_0u(t)+a_1\frac{du(t)}{dt}+a_2\frac{d^2u(t)}{dt^2}+\ldots+a_{n-1}\frac{d^{n-1}u(t)}{dt^{n-1}}+a_n\frac{d^nu(t)}{dt^n}\right) \quad (6.1)$$

where $y(t)$ and $u(t)$ are the system output and input, respectively. The polynomial coefficients $b_1, b_2, \ldots, b_{m-1}, b_m, a_0, a_1, a_2, \ldots, a_{n-1}, a_n$ are real values, and G is a real value representing the system gain. The leading coefficient of the left-hand side of equation (6.1) is 1. Generally, the order n is less than m for all practical systems not containing a system shunt[44], and the value of m determines the model order. ***The Laplace transformation*** of the function $f(t)$ is defined by

$$L\{f(t)\} = f(s) = \int_{-\infty}^{\infty} e^{-st} f(t)dt \tag{6.2}$$

for the variable s whose real part >0. If both sides of (6.1) are Laplace transformable functions, (6.1) can be presented in the Laplace domain as follows

$$\begin{aligned} &Y(s)(1 + b_1 s + b_2 s^2 + \ldots + b_{m-1} s^{m-1} + b_m s^m) = \\ &U(s) \cdot G(a_0 + a_1 s + a_2 s^2 + \ldots + a_{n-1} s^{n-1} + a_n s^n) \end{aligned} \tag{6.3}$$

by using the Laplace transformation under zero initial conditions. $Y(s)$ and $U(s)$ are the Laplace transforms of $y(t)$ and $u(t)$, respectively. (6.3) can be re-written as follows

$$H(s) = \frac{Y(s)}{U(s)} = G \cdot \left(\frac{a_0 + a_1 s + a_2 s^2 + \ldots + a_{n-1} s^{n-1} + a_n s^n}{1 + b_1 s + b_2 s^2 + \ldots + b_{m-1} s^{m-1} + b_m s^m} \right). \tag{6.4}$$

The function $H(s)$ is ***the transfer function*** of the system having output Y and input U. This transfer function may be represented as

$$H(s) = \hat{H}(s) \cdot G \,. \tag{6.5}$$

Here $\hat{H}(s)$ is ***the normalised transfer function***, representing the system's dynamic properties. The ***system gain***, G represents the system's static property. By substituting $A(s)$ and $B(s)$, respectively, for the numerator and denominator polynomials of (6.4) and (6.5), the following equations can be obtained

$$\hat{H}(s) = \frac{A(s)}{B(s)} \tag{6.6}$$

[44] The shunt is an element which bridges the system and establishes a direct path for a signal (mostly a fraction of the signal) through the system.

and $$H(s) = G\frac{A(s)}{B(s)}. \qquad (6.7)$$

The system transfer function directly expresses the relationship between the system output and input in the Laplace domain. In other words, the system transfer function contains all the information about the system available from the system output and input. Furthermore, (6.6) and (6.7) show that the system's dynamic properties are represented by the ratio of the polynomials $A(s)$ to $B(s)$.

6.2.2 System frequency response

The system frequency response in the form of equation (6.8) can be formally obtained using the system transfer function given by (6.4) and replacing the Laplace variable s with the product $i\omega$.

$$H(\omega) = G \cdot \left(\frac{a_0 + a_1 i\omega + a_2 (i\omega)^2 + \ldots + a_{n-1}(i\omega)^{n-1} + a_n (i\omega)^n}{1 + b_1 i\omega + b_2 (i\omega)^2 + \ldots + b_{m-1}(i\omega)^{m-1} + b_m (i\omega)^m} \right) \qquad (6.8)$$

where ω is the radial frequency and i is the imaginary unit. As previously mentioned in Chapter 5, the unit impulse response of an LTI system could completely describe the characteristics of that system in the time domain (Ljung, 1987). Furthermore, when the known transfer function of any LTI system is provided, the output of that system can be identified for any specified input (such as the unit impulse or the unit step function).

By analogy with the system transfer function, the system frequency response contains all the information available in input-output measurements of the system (Schoukens and Pintelon, 1991). Thus, identification of the model of the system frequency response can be the first step in obtaining the necessary information about the system. Subsequently, this information can be employed in the preparation of a structured model of this system.

6.3 Fundamental systems

Generally, almost all real world dynamic systems are composite systems. Thus the system transfer functions of those systems can be generated by combining the transfer functions of their fundamental systems, which will be introduced below.

6.3.1 Ideal linear dynamic system

This refers to a system the output of which is identical to the input (Figure 6.1(a)). The frequency response of this system is the point (1,0) in the complex plane[45]. A straight line is used in Figure 6.1a as the symbol to represent this system. The transfer function of the ideal linear dynamic system is given by

$$H(s) = 1 . \tag{6.9}$$

6.3.2 Proportional linear dynamic system

This refers to a system the output of which is equal to a proportion G of the input (Figure 6.1(b)). The frequency response of this system is the point (G,0) in the complex plane. A circle is used in Figure 6.1b as the symbol to represent this system. The transfer function of the proportional linear dynamic system is given by

$$H(s) = G . \tag{6.10}$$

6.3.3 Ideal linear dynamic system with time delay

This refers to a system the output of which is equal to the input with a positive time shift (Figure 6.1(c)). The frequency response of this system is a circle with a radius of 1 in the complex plane. A triangle is used in Figure 6.1c as the symbol to represent this system. The transfer function of the ideal linear dynamic system with time delay τ is given by

$$H(s) = e^{-\tau \cdot s} . \tag{6.11}$$

[45] The expression the "complex plane" refers to a two-dimensional perpendicular plane the x-and y-axes of which represent the real and imaginary values, respectively.

6.3.4 First-order linear dynamic system

This refers to a system the frequency response of which converges to the points (1,0) and (0,0) in the complex plane, for frequency values converging from zero to infinity (Figure 6.1(d)). A rectangle is used in Figure 6.1d as the symbol to represent this system. The transfer function of a first-order linear dynamic system with time constant T is given by

$$H(s) = \frac{1}{1 + T \cdot s}. \tag{6.12}$$

The meaning of the time constant T is as follows: If the input in the form of a unit step function is being introduced into a linear first-order dynamic system starting from zero initial conditions, the output of this system will reach the steady-state level at time T, subject to the hypothetical condition that the increase of the output over the time interval [0, T] is equal to that at time zero.

Figure 6.1: Fundamental systems and their representations

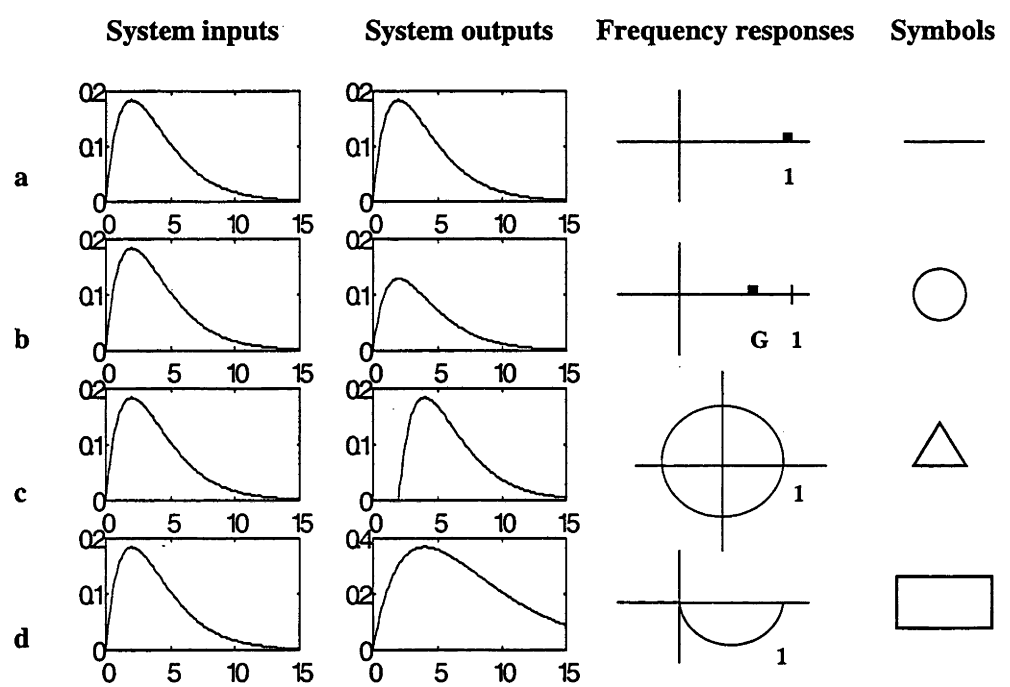

6.4 Building of a structured model of the lymph node system

6.4.1 Experimental data

In this section, requirements similar to those previously mentioned in section 5.3.2 of Chapter 5, in relation to sufficient experimental data, apply to construction of a structured model. Consequently, any experiments that contained less than 100 hours of data were discarded. The remainder of the experiments (17 out of 21 of the total population studies and 8 out of 11 of the subset (ie CD4, CD5, CD8 and CD45R) studies) were subsequently incorporated into the procedures for building a structured model.

6.4.2 Definition of the lymph node system

The lymph node system H_N was defined by its transfer function $H_N(s)$

$$H_N(s) = \frac{C_{ef}(s)}{C_{vb}(s)}. \qquad (6.13)$$

in the Laplace domain, where C_{ef} and C_{vb} were the measured concentration profiles of labelled lymphocytes in the efferent lymph and venous blood respectively. This definition is based on the deterministic circulatory model, introduced in a previous study (Dedik and Durisova, 1996). The definition of the system H_N, given by equation (6.13), represents an abstract mathematical expression of the relationship between the concentrations of labelled lymphocytes in the efferent lymph and in the venous blood. The lymph node system H_N is schematically shown in Figure 6.2.

Figure 6.2: Schematic representation of lymph node system

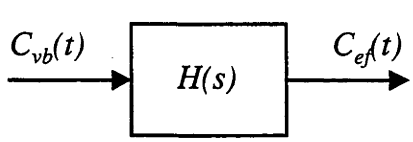

The lymph node system is considered to be a linear time-invariant system with single-input-single-output and is represented by a rectangle. Incoming and outgoing arrows represent the system input $C_{ef}(t)$ and output $C_{vb}(t)$ respectively. $H(s)$ defines the system transfer function in the Laplace domain.

6.4.3 Modelling of the lymph node system in the frequency domain

To model the lymph node system H_N in the frequency domain, the frequency response method (Schoukens and Pintelon, 1991) was used. The calculated frequency response of the lymph node system H_N was obtained as the ratio of the Fourier transforms of the output C_{ef} to those of the input C_{vb} of this system. The Fourier transforms were determined as sums of the Fourier transforms of straight lines approximating the measured input and output profiles between two adjacent measured points and as the Fourier transforms of exponential functions approximating these profiles in time intervals from the last sampling time to infinity. The model of the calculated frequency response of the lymph node system H_N was obtained in the form of equation (6.13), using the Levy method (Levy, 1959). To decide on optimal model numerator and denominator polynomial degrees n and m, the Complex Criterion (CC) (Dedik and Durisova, 1994) and the Akaike information criterion (AIC) (Akaike, 1976) in the complex and the time domain, respectively, were applied. The unit impulse response of the lymph node system H_N was estimated as the response of the optimal model of the calculated frequency response to the input in the form of the unit impulse. All of the calculations were performed employing the software package CXT (**Comple**X **T**ools for Linear Dynamic System Analysis) (Dedik and Durisova, 1995; Dedik and Durisova, 1996), http://www.cpb.uokhsc.edu/pkin/pkin.html.

6.4.4 Modelling of the lymph node system in the time domain

In general, the parameters of models of system frequency responses do not permit direct physical interpretations, especially in the case of complex systems, ie the type of systems that must be modelled by high-order models. In this section, a procedure for building structured models of complex systems containing time delays will be described. The procedure is based on the combination of system modelling in the frequency and time domains, and consists of the following steps:

1. Either the shape of the normalised calculated frequency response or of the unit impulse function (or of both these functions) can indicate the presence of time delays in the structure of the system. Correspondingly, if system time delays exist, the whole frequency band of the normalised calculated frequency response can be separated into two frequency bands, ie the low and high frequency band.

2. In the low frequency band, any influences of the system time delays on the normalised calculated frequency response can not be identified by the naked

eye. Thus the normalised calculated frequency response of the system in this frequency band can be approximated by low-order auxiliary models consisting of sub-models of the fundamental systems (mentioned in section 6.3) without time delays. The auxiliary models, outputs of which are similar to the measured output of the studied system, can be regarded as suitable auxiliary models of this system.

3. The system time delays can be estimated in either the frequency or the time domain. Using the normalised calculated frequency response in the high-frequency band, the system delays (τ_j) can be estimated by $\tau_j = \pi / (\omega_{2,j} - \omega_{1,j})$. Where $j \in [1, k]$, $\omega_{2,j}$ and $\omega_{1,j}$ are the frequencies in which the real or imaginary parts of the normalised calculated frequency response of the system attain a local maximum and a local minimum, respectively. k is the number of the local maxima and minima. In the time domain, the system time delays (τ_j) can be estimated as the time points of onset of peaks of the unit impulse response.

4. Various structured models of the system under study can be created and described by sets of differential equations in the time domain, in such a way that these models consist of suitable auxiliary models selected in the low- frequency band and of models of the ideal systems with time delays selected in the high-frequency band. The solutions of these models, corresponding to the measured input of the studied system, can be fitted to the measured output of the system, using the Gauss-Newton method in the time domain. The unit impulse response of these models can be determined by applying a unit impulse input to them.

5. A group of structured models can be selected according to the following criteria:

a) All the selected models must have estimates of the standard uncertainties of type A (ISO TN 1297)[46] that are less than 50% of the corresponding parameter estimates.
b) The model outputs and the unit impulse responses estimated from the structured models must be similar to the output and the unit impulse response of the frequency model of the studied system.

6. Eventually, the structured model with the minimum AIC value can be selected in that group and considered to be the final structured model of the studied system.

[46] A new name for the standard error, according to the terminology adopted by "Guide to the Expression of Uncertainty in Measurement", ISO, Berne, 1993.

6.4.5. Candidate structured models of the lymph node system

With respect to the AIC values, standard errors, and all of the common statistical criteria of goodness of models, the following two different structured models, namely a positive feedback model and a parallel model, were selected as optimal models for description of the lymph node system.

A) Positive feedback model: The positive feedback model illustrated in Figure 6.3 consists of two simple first-order linear systems in serial connection and a positive feedback loop. The model parameters are: the gains G_1, G_2, G_3, the time constants T_1, T_2 and the time delay τ_1. However, this feedback model could not be readily explained within a physiological context (see more detail in discussion of this chapter). Interpretation based on data available in the present and previous studies did not support the existence of the feedback loop in the model of the lymph node system. For this reason an alternative model was constructed which had the capacity to explain more of the physiological details of lymphocyte migration.

Figure 6.3: Positive feedback model

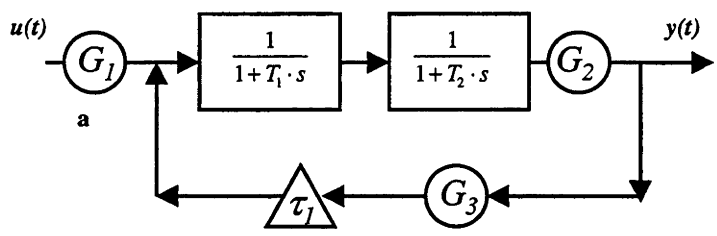

The first proposed model contains a feedback loop with two first order linear models in serial cascade (two rectangles). $u(t)$ and $y(t)$ are, respectively, the input and output of the system. G_1, G_2, G_3, T_1, T_2 and τ_1 are model parameters to be identified. The circle and triangle represent the proportional linear system and ideal linear system with time delay respectively.

B) Parallel model: The parallel model given in Figure 6.4 consists of two models representing simple first-order linear systems in serial connection and an additional parallel unit. This parallel unit consists of several branches, where each branch contains one time delay and one gain parameter. The parameters of this model are analogous to those employed in the positive feedback model. With respect to the number of the branches identified as an optimum for a given experiment, the models obtained are correspondingly named as 2, 3 and 4-

branch parallel models. The parallel model can be considered as more relevant for physiological application than the previous feedback model (see more detail in the discussion of this chapter).

Figure 6.4: Parallel model

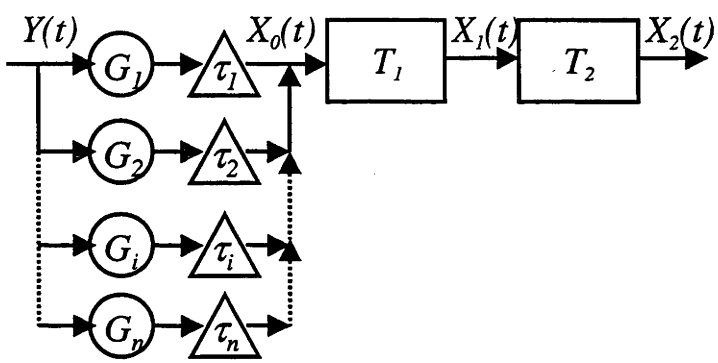

The second proposed model contains a parallel loop with two first order linear models in serial cascade (two rectangles). $Y(t)$ and $X_2(t)$ are, respectively, the input and output of the system. G_1, G_2, G_i, G_n, T_1, T_1, T_2, τ_1, τ_2, τ_i and τ_n are model parameters to be identified. The circle and triangle represent a proportional linear system and an ideal linear system with time delay respectively.

6.4.6 Mathematical descriptions of the parallel model

Using the transfer functions of the fundamental systems described in section 6.3 and Laplace domain algebra (Kreyszig, 1993) the transfer functions of the parallel model of the lymph node system shown in Figure 6.4 can be obtained in the form of (6.14).

$$H(s) = \frac{\sum_{i=1}^{n} G_i e^{-\tau_i s}}{(1+T_1 s)(1+T_2 s)} \tag{6.14}$$

In the time domain, this parallel model can be described by differential equations (6.15-6.17).

$$x_0(t) = \sum_{i=1}^{n} G_i Y(t-\tau_i) \tag{6.15}$$

$$T_1 \frac{dx_1(t)}{dt} = x_0(t) - x_1(t) \tag{6.16}$$

$$T_2 \frac{dx_2(t)}{dt} = x_1(t) - x_2(t) \tag{6.17}$$

Using equations (6.15)-(6.17), the unit impulse response of the parallel model can be obtained in the form of (6.18).

$$x_2(t) = w(t) = \frac{1}{|T_1 - T_2|} \sum_{i=1}^{n} G_i \left| e^{-\left(\frac{t-\tau_i}{T_1}\right)} - e^{-\left(\frac{t-\tau_i}{T_2}\right)} \right| \tag{6.18}$$

where T1≠T2 and

$$x_2(t) = w(t) = \frac{\sum_{i=1}^{n} (t - \tau_i) G_i e^{-\left(\frac{t-\tau_i}{T}\right)}}{T^2} \tag{6.19}$$

where T1=T2=T.

By analogy with the system time constant T which represents dynamic properties of linear first-order dynamic systems, the mean time T_m can be used to characterise the dynamic properties of linear low- and/or high-order dynamic systems. The general formula for the mean time T_m is given by (6.20) (Durisova *et al.*, 1995).

$$T_m = \frac{-\lim_{s \to 0} \frac{dH(s)}{ds}}{-\lim_{s \to 0} H(s)} \tag{6.20}$$

In pharmacokinetics the value T_m has been described as the ***mean residence time***. With respect to the physiology of lymphocyte migration, within the lymph node system this value can be named the ***mean transit time***, MTT.

Using the model transfer function of the lymph node system given by (6.14) and the formula given by (6.20), MTT_i can be derived for the branch i in the form of (6.21)

$$MTT_i = T_1 + T_2 + \tau_i \tag{6.21}$$

where MTT_i represents the average time spent by the lymphocytes in travelling through the branch i.

Similarly, the average mean transit time, $\overline{MTT}$, representing the average time taken by the whole lymphocyte population in travelling through the lymph node, can be determined according to (6.22)

$$\overline{MTT} = \frac{1}{\sum_{i=1}^{n} G_i} \left[\sum_{i=1}^{n} (T_1 + T_2 + \tau_i) \cdot G_i \right] \tag{6.22}$$

6.5 Results

Due to the low frequency and large variations in the magnitude of CD8 and CD45R lymphocyte subsets in blood and efferent lymph, data about these subsets were preliminary discarded. This section will present only the results of experimental data which was successfully passed through the entire process. This included 13 data sets and 7 data sets of the total population and subset studies (3 of CD4 data sets and 4 of CD5 data sets).

6.5.1 Unit impulse responses of lymph node systems estimated by the CXT program

In section 5.5.1 of Chapter 5, the unit impulse responses computed in the time domain were presented. In this section, unlike the methods used in Chapter 5, the optimal model of the calculated system frequency response for each experiment was determined and, subsequently, the unit impulse response of this model was estimated using the CXT program. The time scale for the unit impulse response was given as 160 hours, which covers all the important features of unit impulse responses in this study (Figure 6.5A – 6.5K). It is obvious that most of these unit impulse responses contained several peaks (ie they did not decrease monotonously like those observed in Chapter 5). The magnitude of the first peak, which ranged between 0.003 and 0.012, was always greater than that of any of the others (if there were more than one). In almost all of these experiments, except for the R632-CD5 population study (Figure 6.5J-upper panel), peak values were observed within the first 20 hours. The findings in relation to the range of peak values and times at which peaks were observed were similar to those found in the unit impulse responses in Chapter 5.

In all of the unit impulse responses, there were other peaks (ie or elevations) of lesser magnitude compared with the first. These were observed at approximately 60-80 hours in most cases. The magnitude of first, second and third peaks was of descending value. For example, in B481 (Figure 6.5A-upper panel), the first peak is recognised at approximately 15 hours while the second and third peaks are recognised at around 70 and 125 hours, respectively. Figure 6.5A - 6.5K summarise the unit impulse responses corresponding to each individual experiment.

Figure 6.5A: Summary of unit impulse responses of individual experiments.

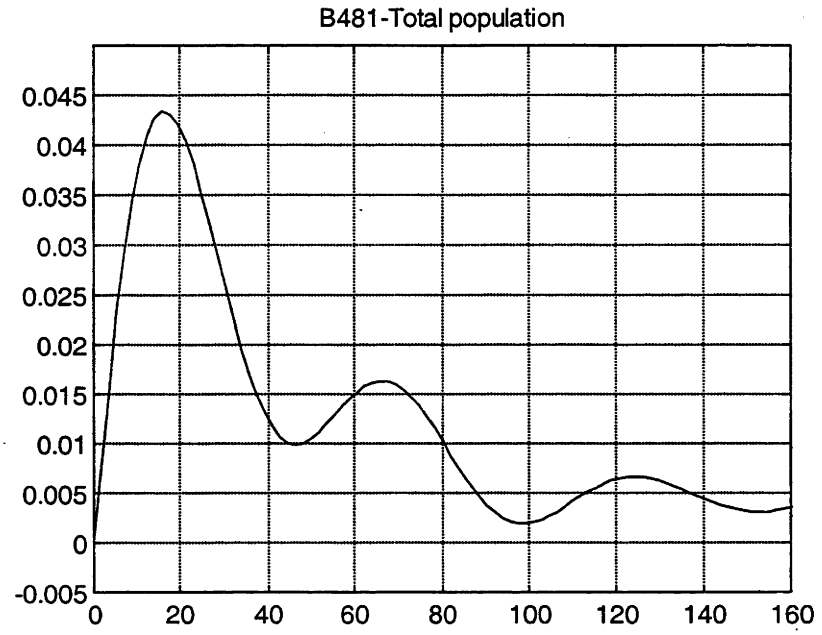

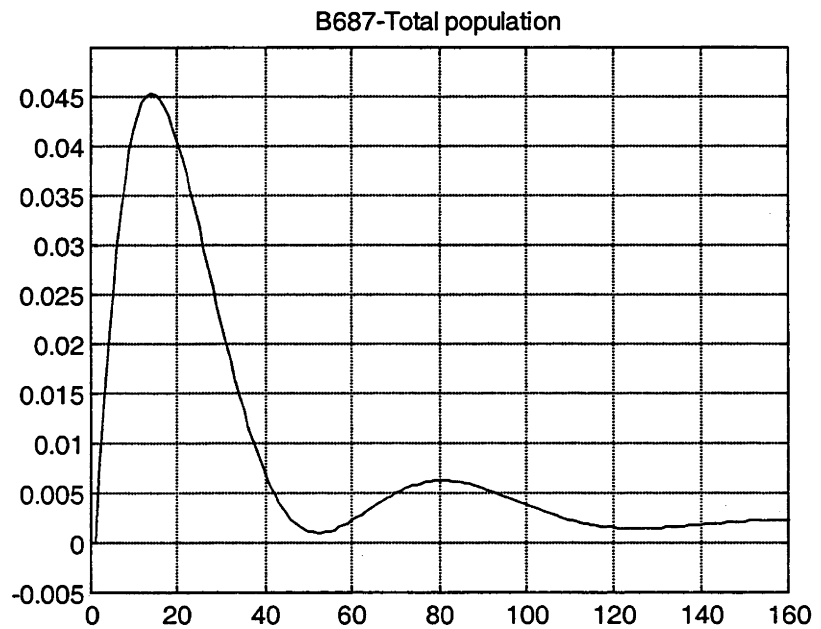

Figure 6.5B: Summary of unit impulse responses of individual experiments.

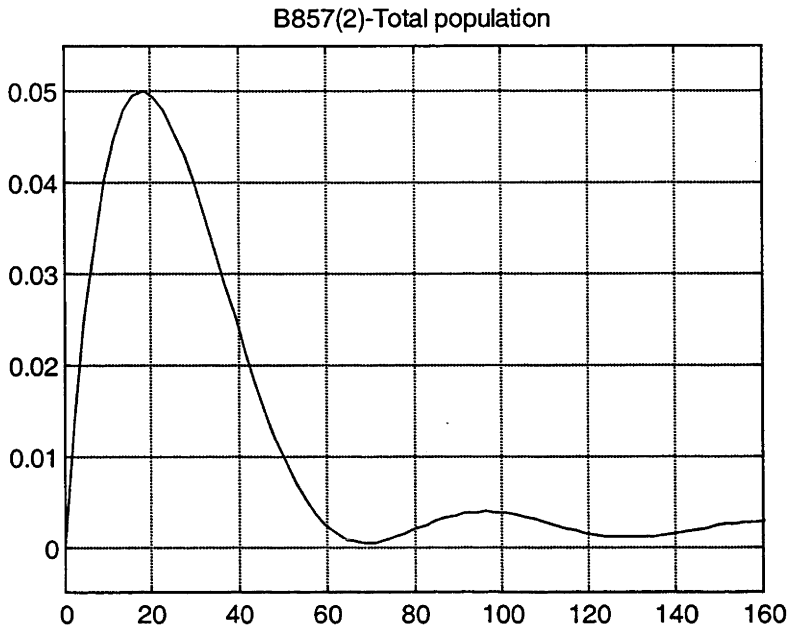

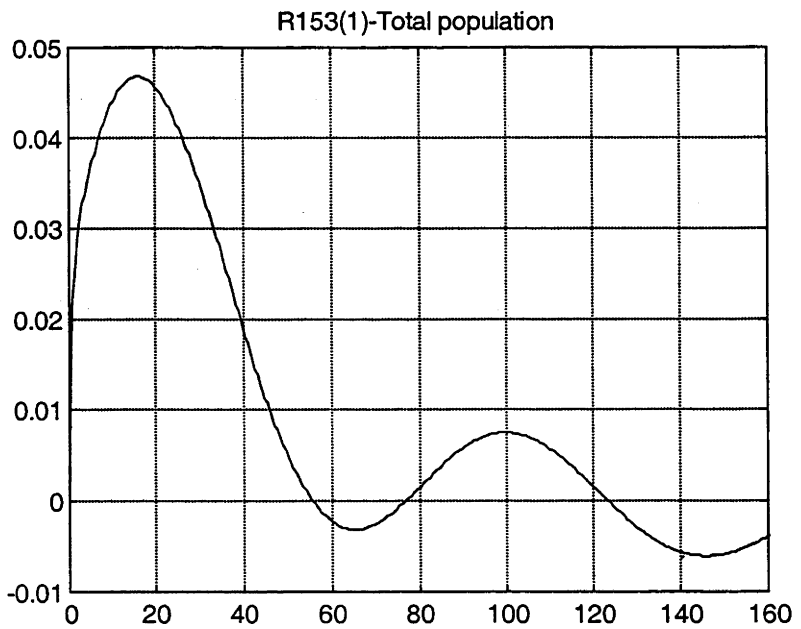

Figure 6.5C: Summary of unit impulse responses of individual experiments.

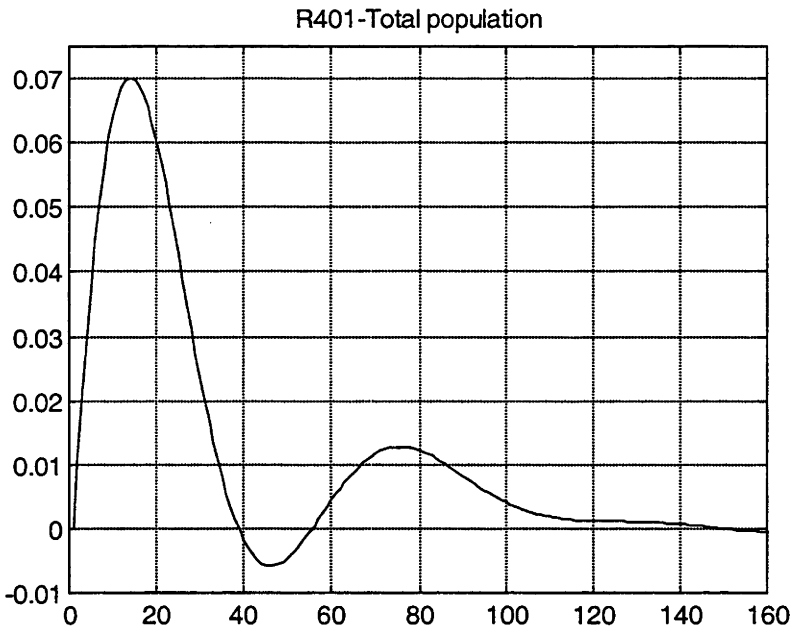

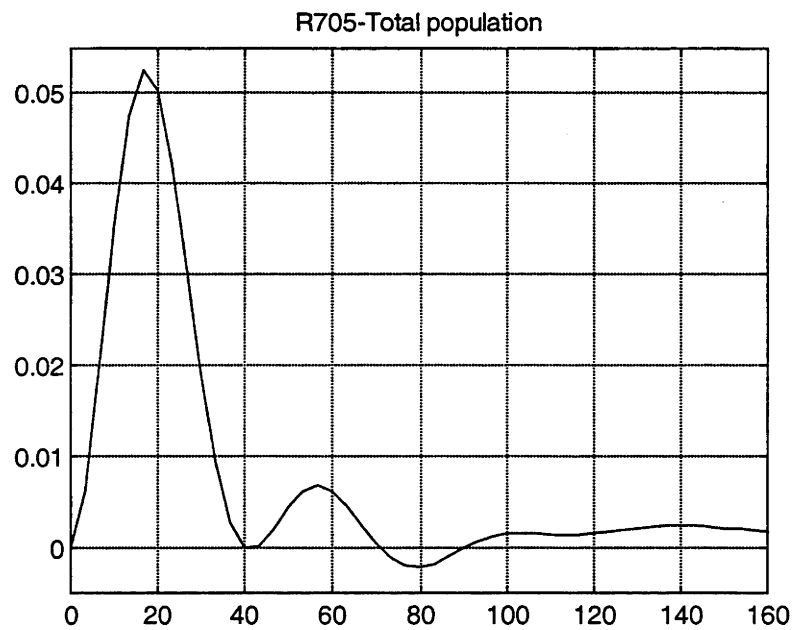

Figure 6.5D: Summary of unit impulse responses of individual experiments.

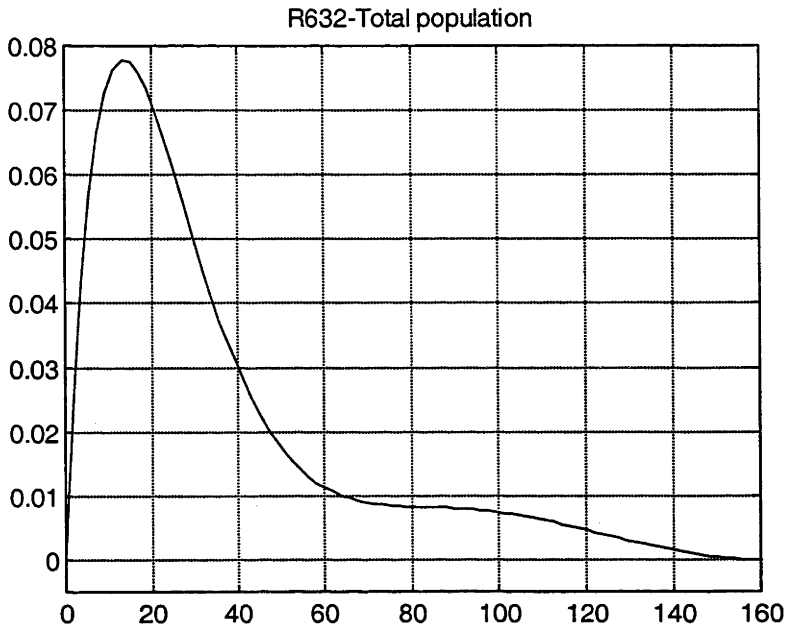

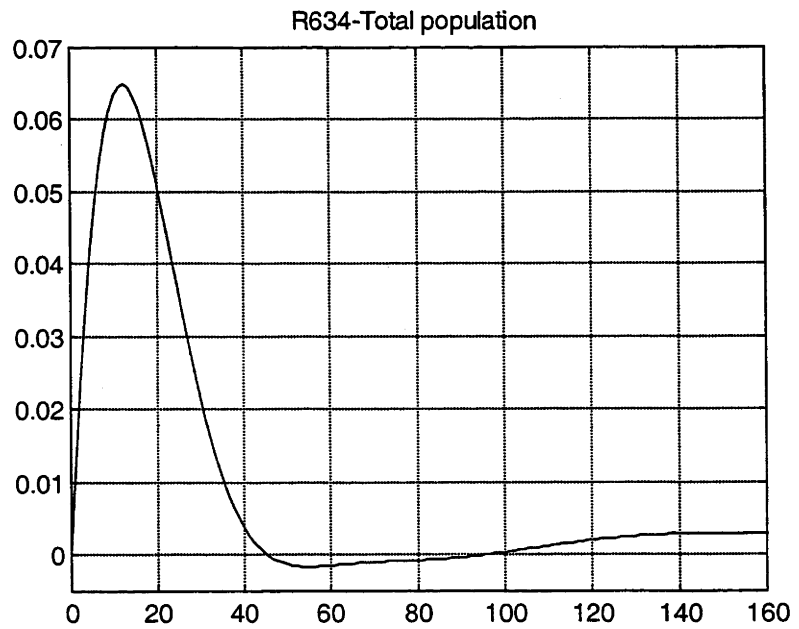

Figure 6.5E: Summary of unit impulse responses of individual experiments.

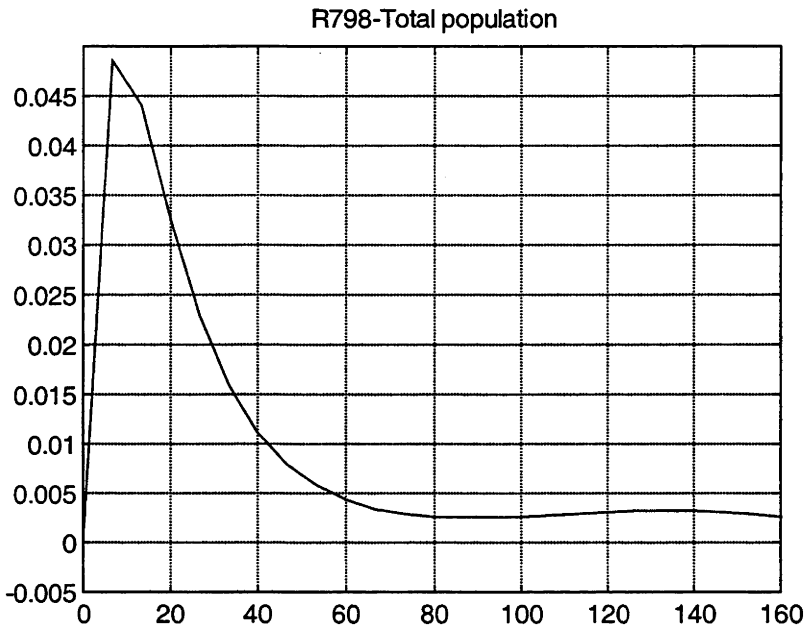

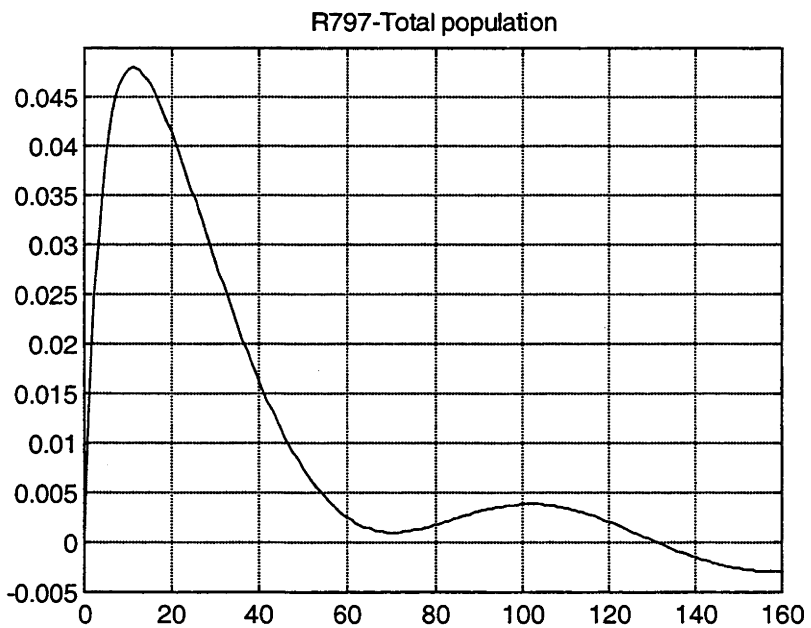

Figure 6.5F: Summary of unit impulse responses of individual experiments.

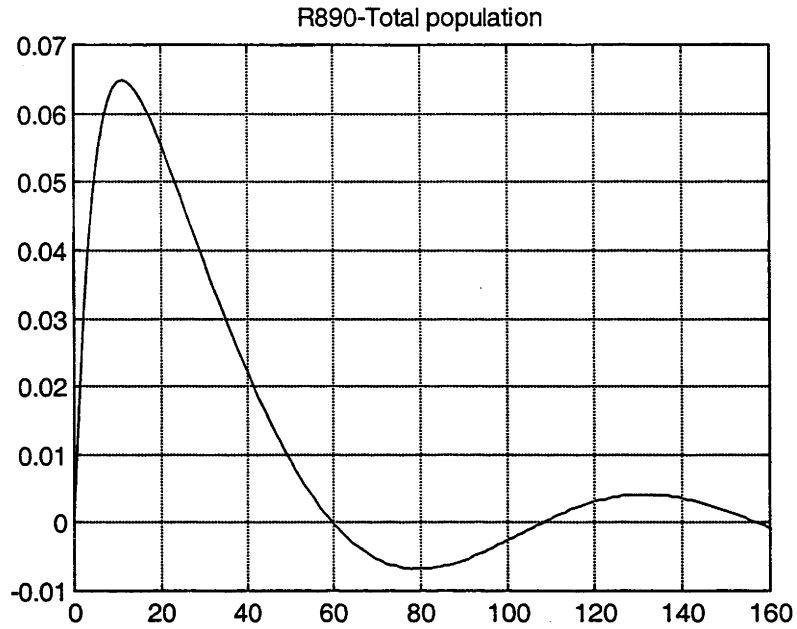

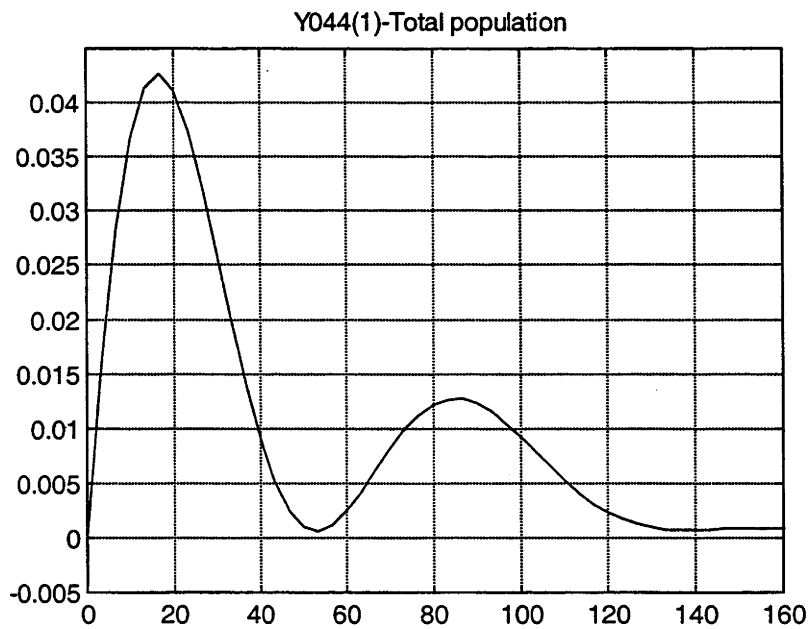

Figure 6.5G: Summary of unit impulse responses of individual experiments.

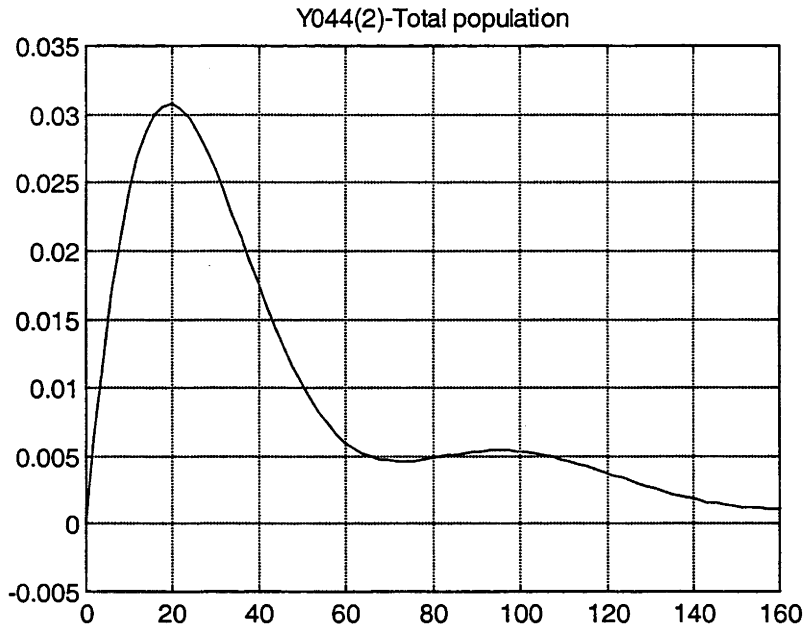

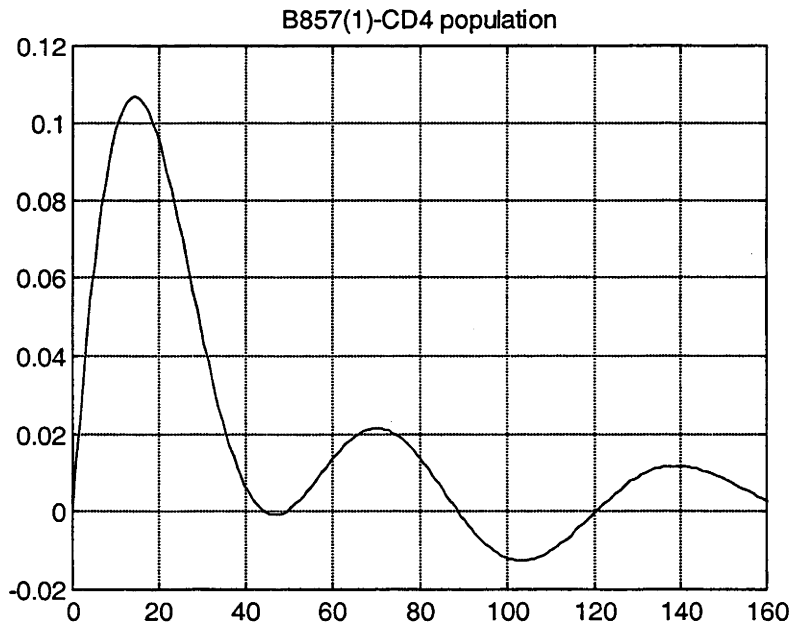

Figure 6.5H: Summary of unit impulse responses of individual experiments.

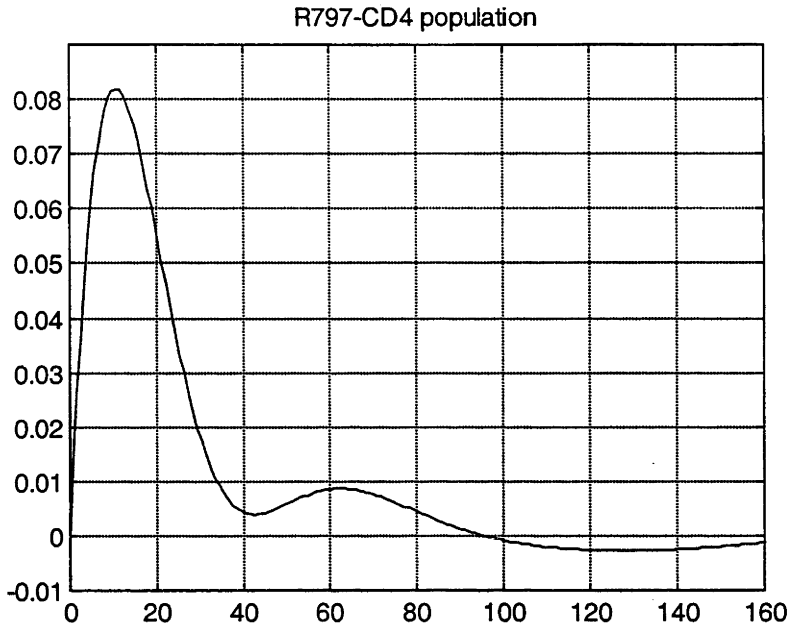

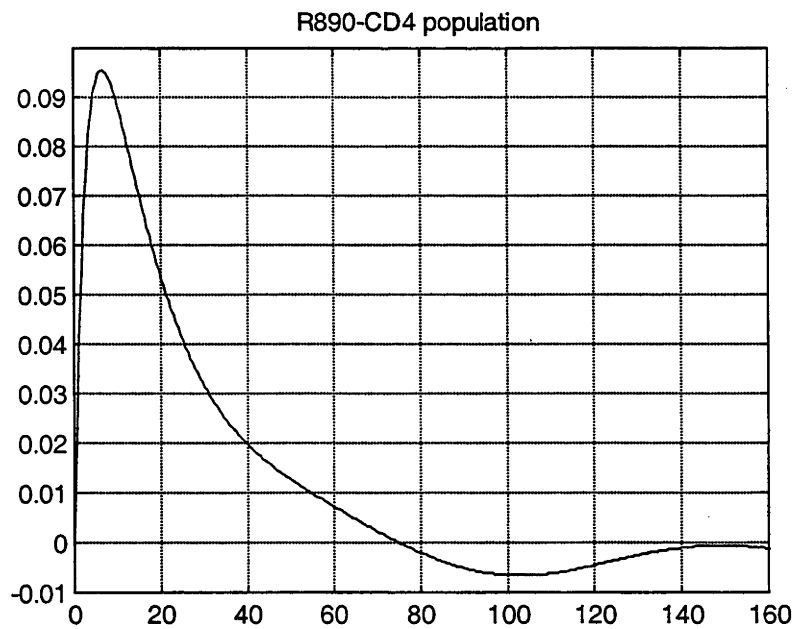

Figure 6.5J: Summary of unit impulse responses of individual experiments.

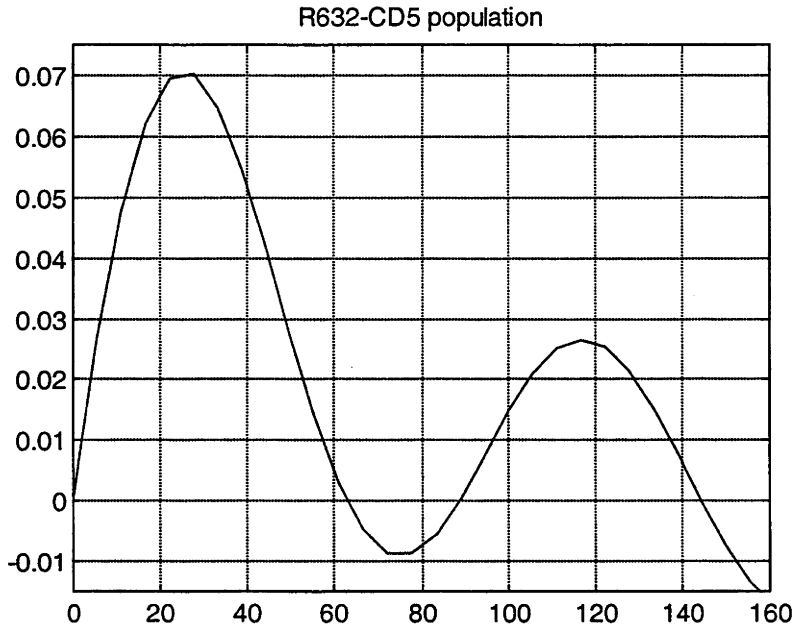

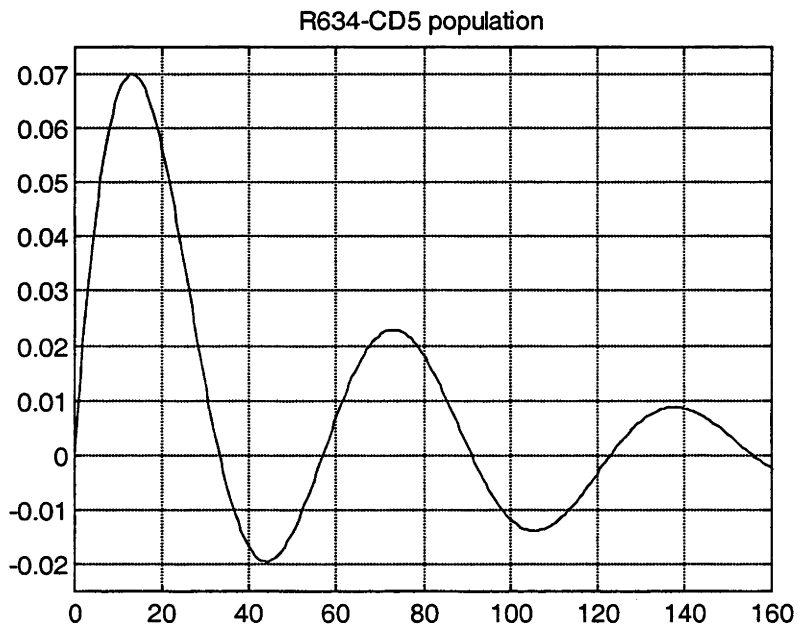

Figure 6.5K: Summary of unit impulse responses of individual experiments.

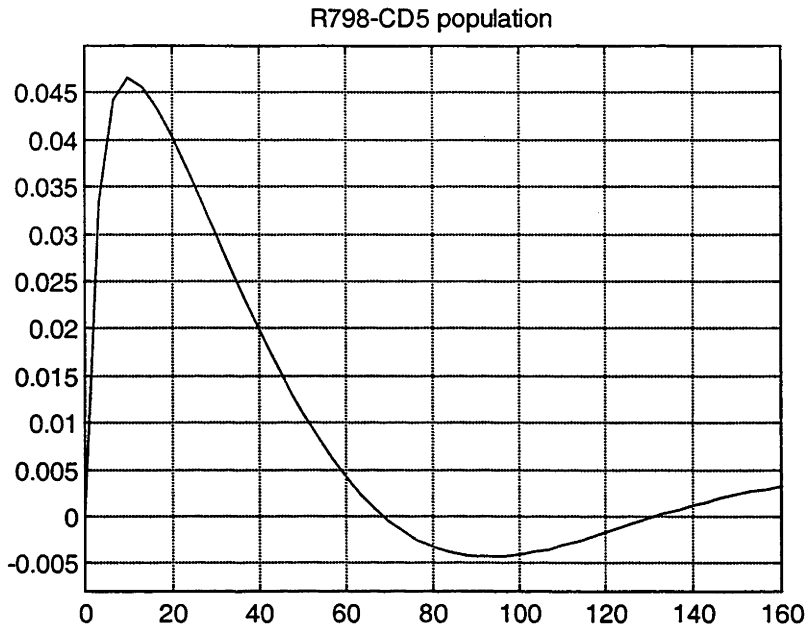

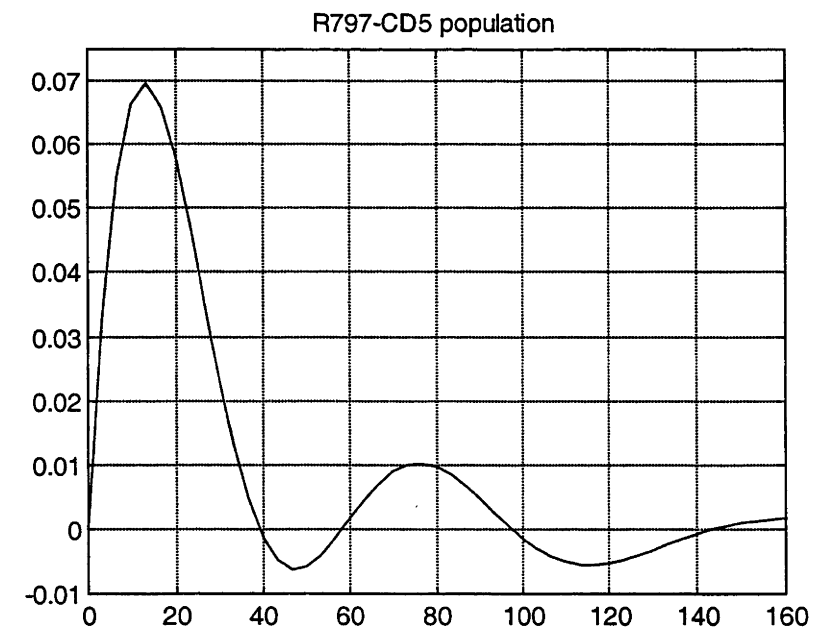

6.5.2 Comparison of outputs of parallel models with different numbers of branches

For each experiment, the outputs of parallel models with different numbers of branches have been calculated and their AIC values compared (Table 6.1). The minimum value of the AIC indicated the final model for each experiment, as previously described in section 6.4.4 (Modelling of the lymph node system in the time domain).

Table 6.1: Interval estimates of parameters of parallel models of lymph node systems and AIC values from each individual experiment.

	AIC			
	1-branch	**2-branch**	**3-branch**	**4-branch**
		Total population study		
B481	-24.80	-30.26	**-36.23**	-30.36
B687	-38.12	-71.75	-80.00	**-91.37**
B857(2)	**-67.90**	-66.98	N/A	N/A
R153(1)	N/A	**-84.35**	-81.34	N/A
R401	N/A	-56.96	**-57.72**	N/A
R705	-22.61	**-44.17**	-42.02	-37.87
R632	N/A	45.12	**43.38**	48.05
R634	**13.20**	21.07	N/A	N/A
R798	10.81	-1.55	-10.94	**-11.55**
R797	0.73	-3.17	**-9.69**	N/A
R890	**-59.21**	-53.25	N/A	N/A
Y044(1)	N/A	-72.85	**-103.91**	N/A
Y044(2)	**-131.69**	-117.50	-99.99	N/A
		CD4 population study		
B857(1)	N/A	**-5.21**	-2.69	N/A
R797	-15.31	**-20.23**	N/A	N/A
R890	**-45.89**	-42.96	N/A	N/A
		CD5 population study		
R632	**92.48**	96.71	94.14	N/A
R634	**34.99**	36.38	N/A	N/A
R798	**26.14**	31.28	N/A	N/A
R797	-14.47	**-15.94**	N/A	N/A

The value of AIC in bold type indicates the final model selected from that experiment. N/A denotes not applicable (ie the singular matrix was obtained in the Gauss-Newton procedure).

6.5.3 Comparison between experimental outputs and final structured parallel models

Outputs can be calculated from the final structured parallel model (ie either 2, 3 or 4-branch model) that has been obtained from the previous section. The calculated outputs show a good fit with the actual data (ie experimental outputs). Figure 6.6A-6.6K summarises all the calculated outputs (presented by solid lines) from the final model compared with the actual experimental data (presented by dotted lines and circles). The fitting results were fairy good in most cases.

Figure 6.6A: Comparison of actual and calculated outputs from the selected branch model

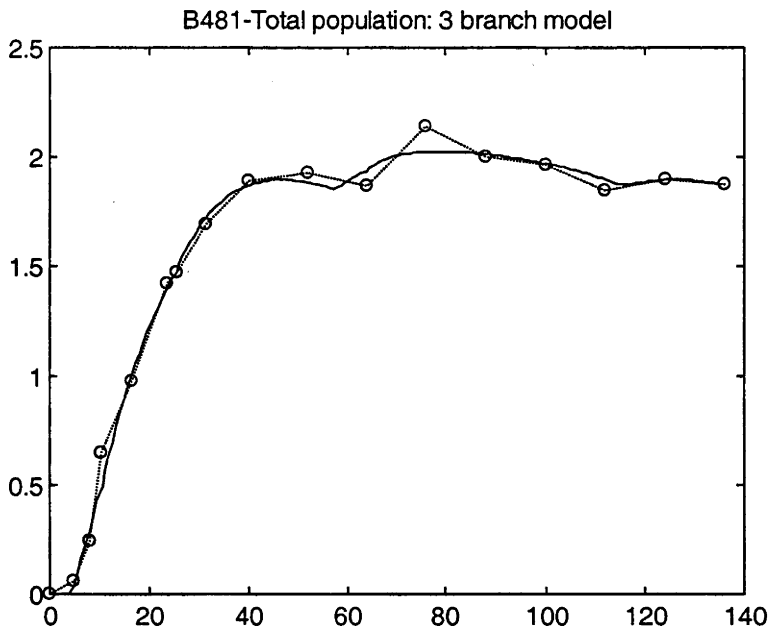

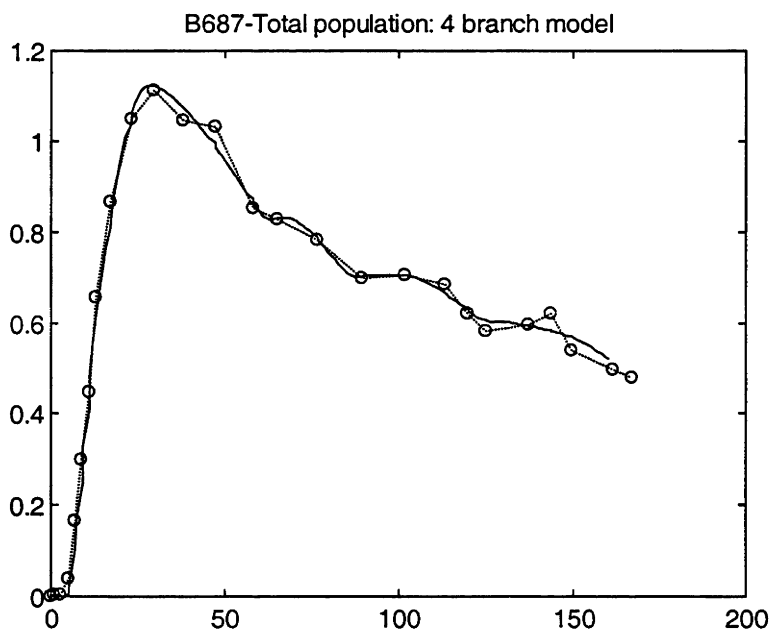

Figure 6.6B: Comparison of actual and calculated outputs from the selected branch model

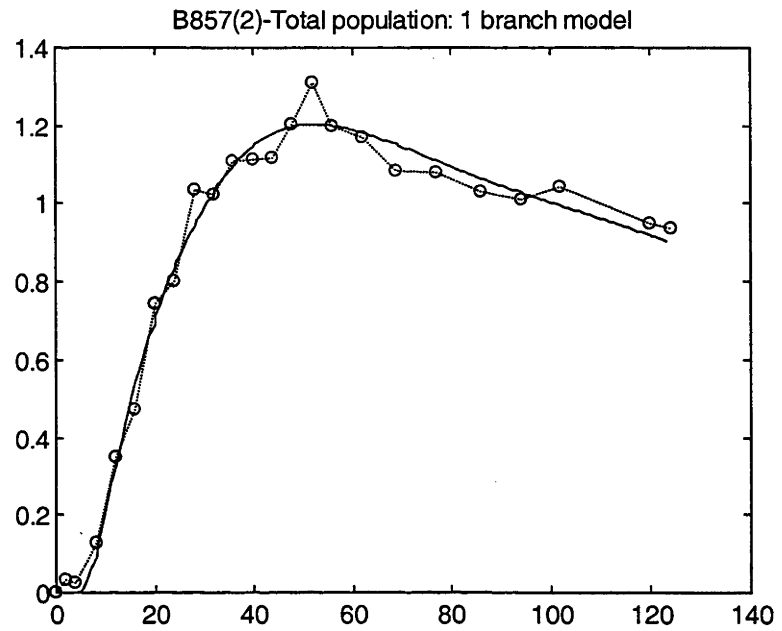

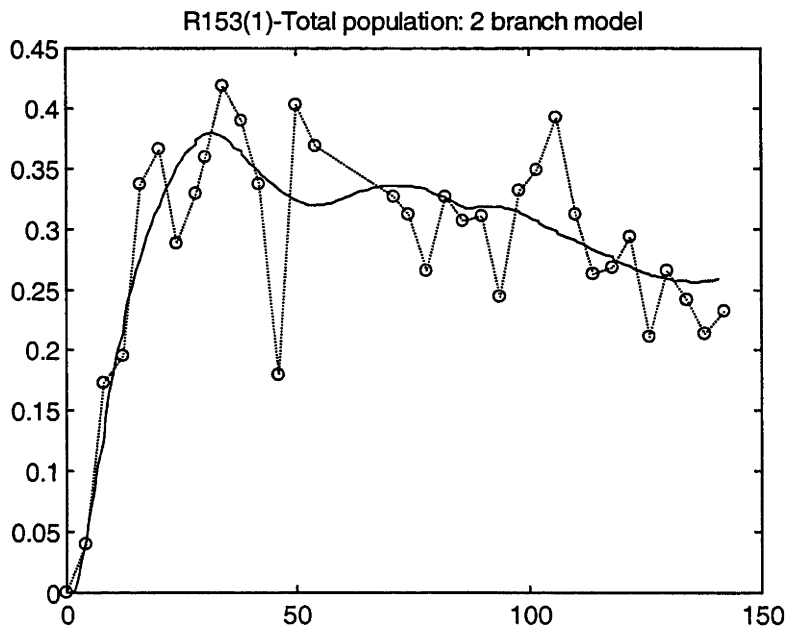

Figure 6.6C: Comparison of actual and calculated outputs from the selected branch model

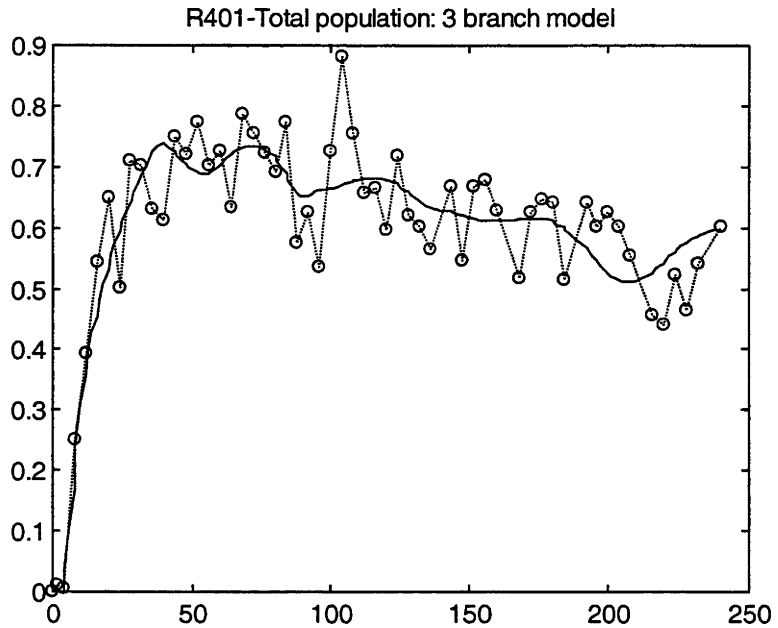

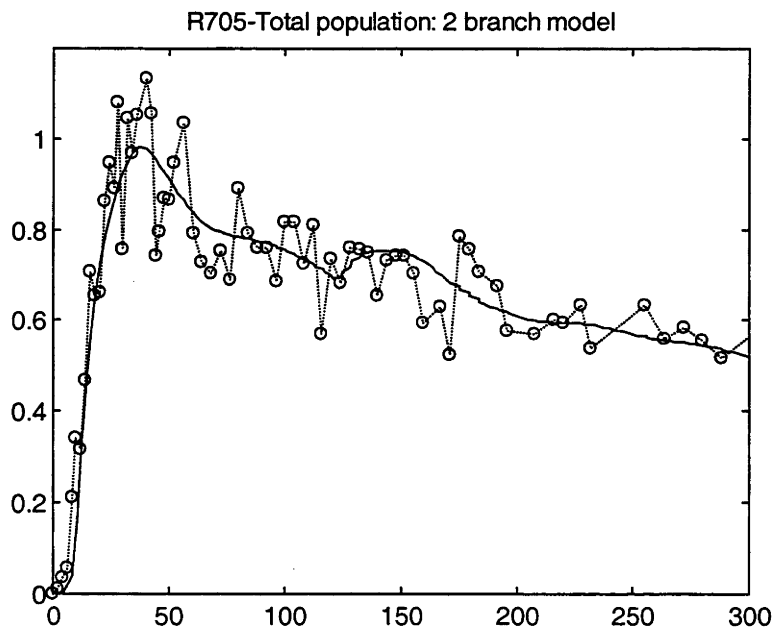

Figure 6.6D: Comparison of actual and calculated outputs from the selected branch model

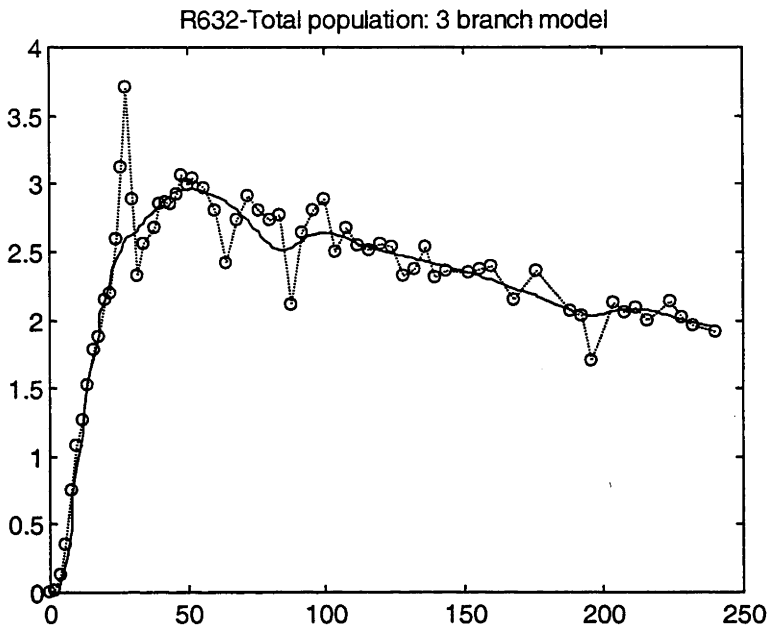

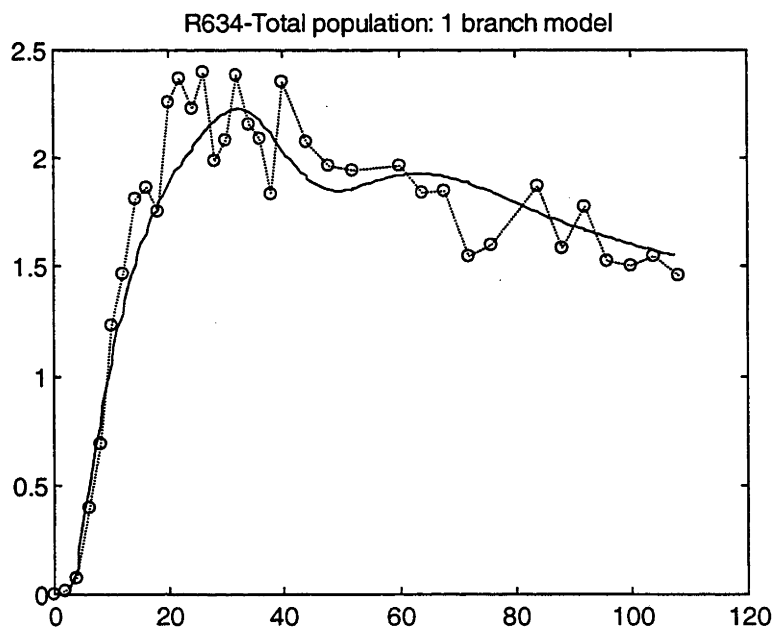

Figure 6.6E: Comparison of actual and calculated outputs from the selected branch model

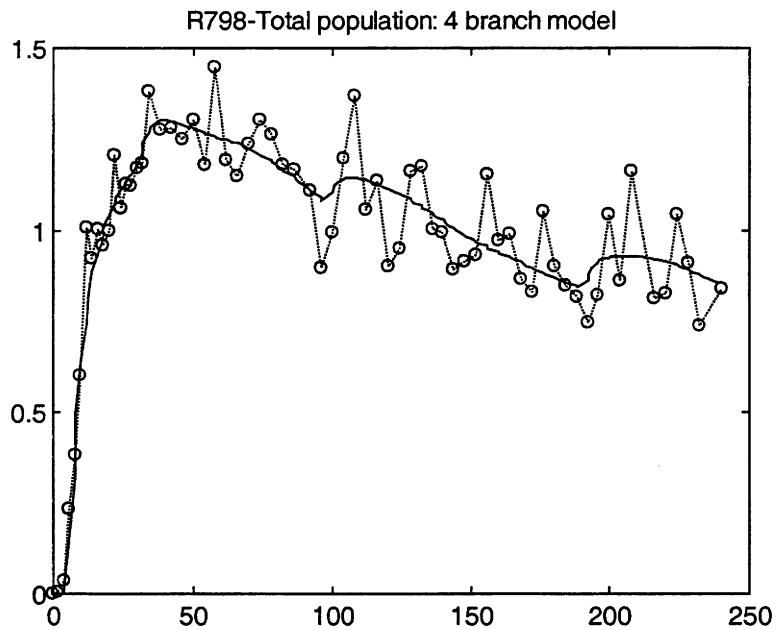

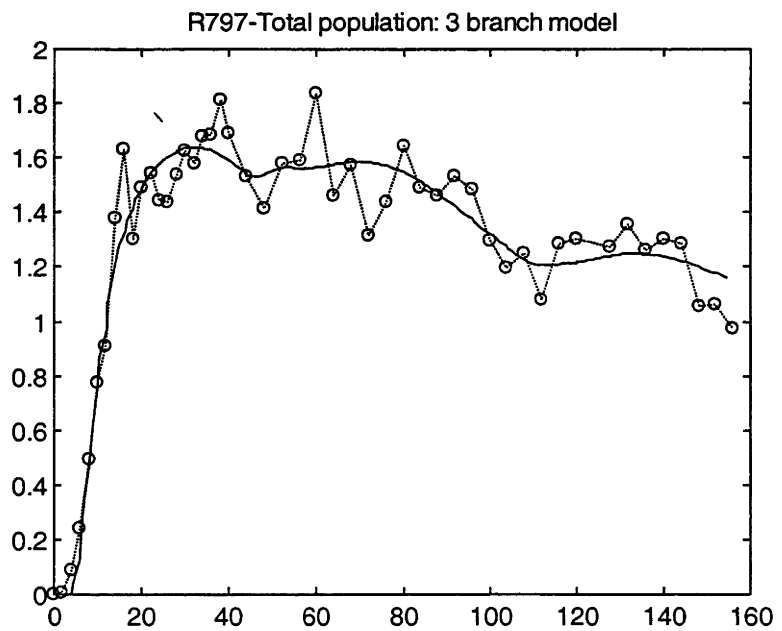

Figure 6.6F: Comparison of actual and calculated outputs from the selected branch model

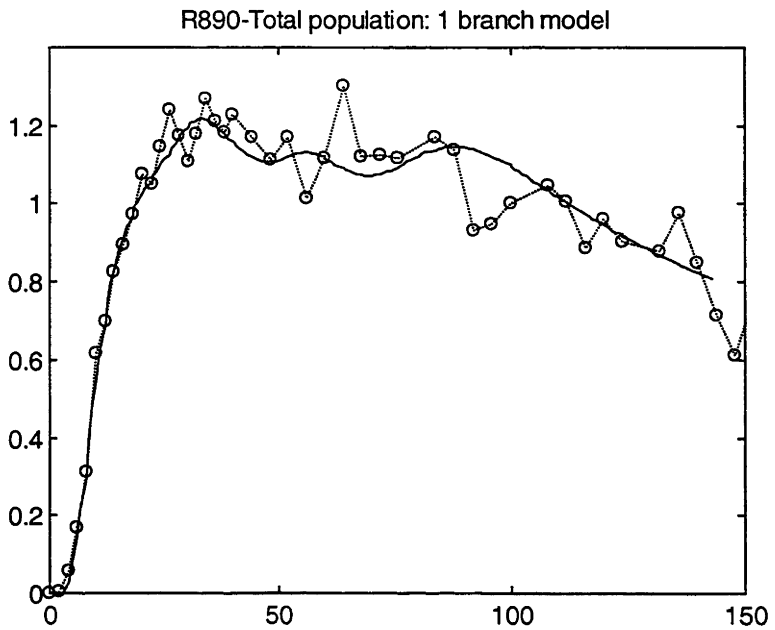

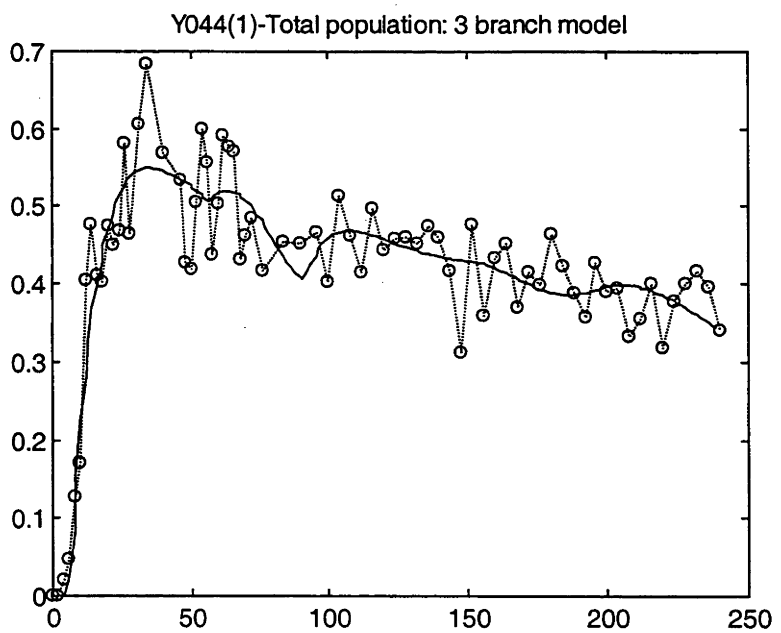

Figure 6.6G: Comparison of actual and calculated outputs from the selected branch model

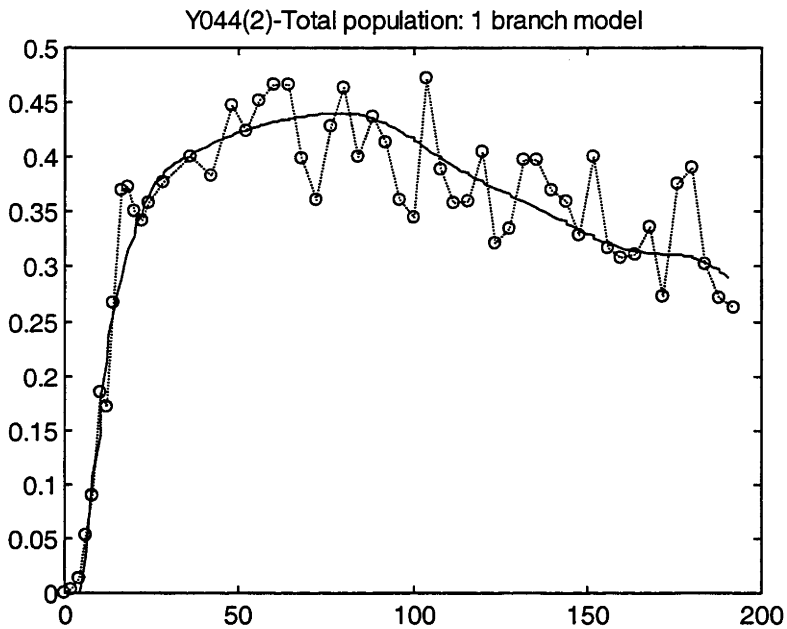

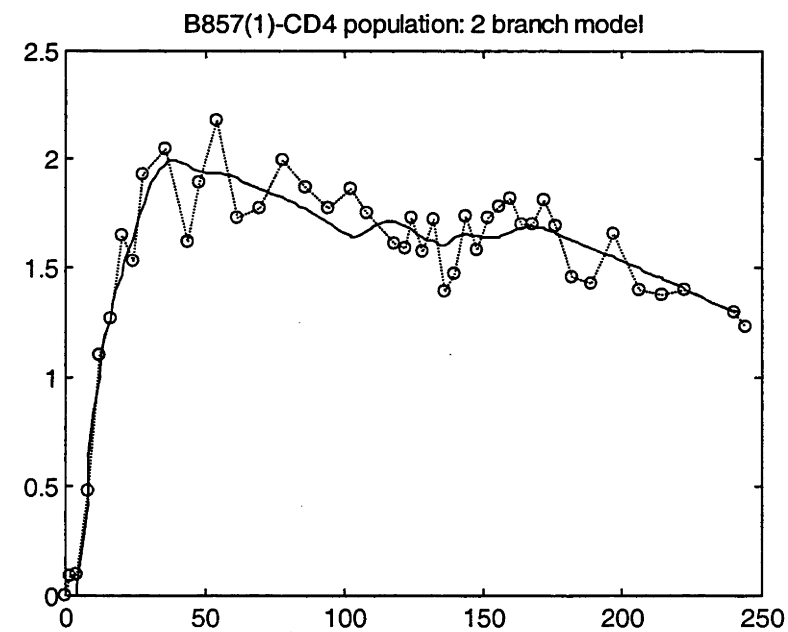

Figure 6.6H: Comparison of actual and calculated outputs from the selected branch model

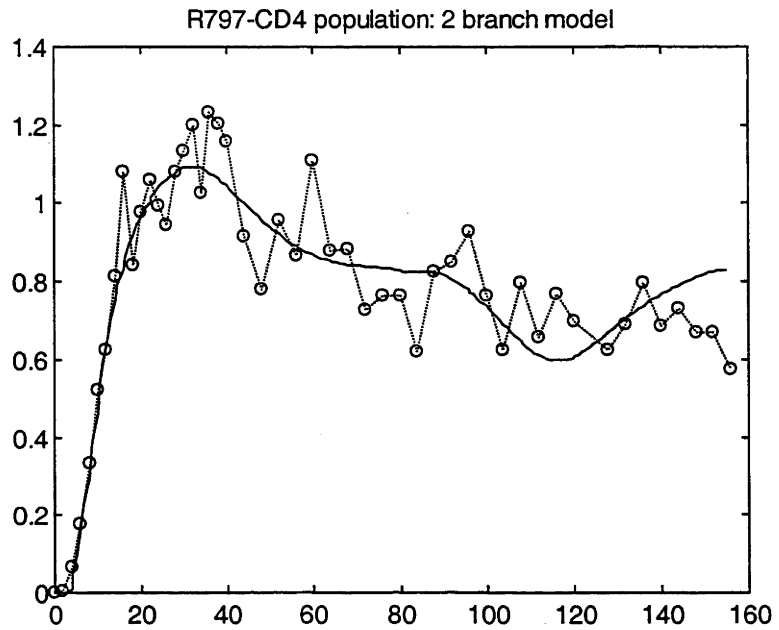

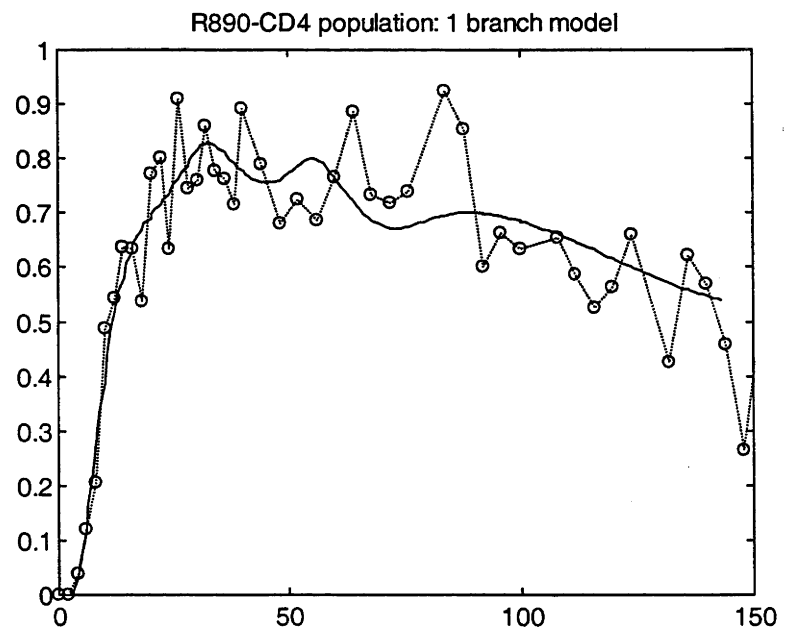

Figure 6.6J: Comparison of actual and calculated outputs from the selected branch model

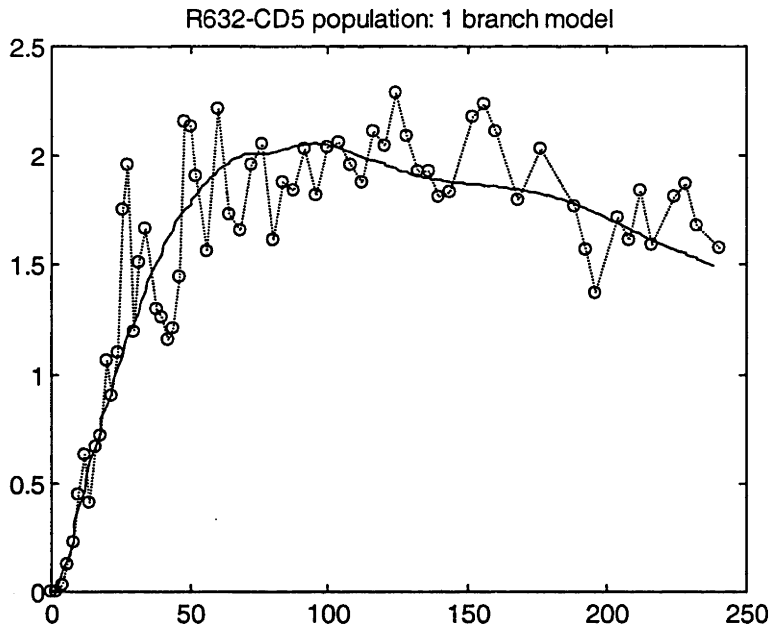

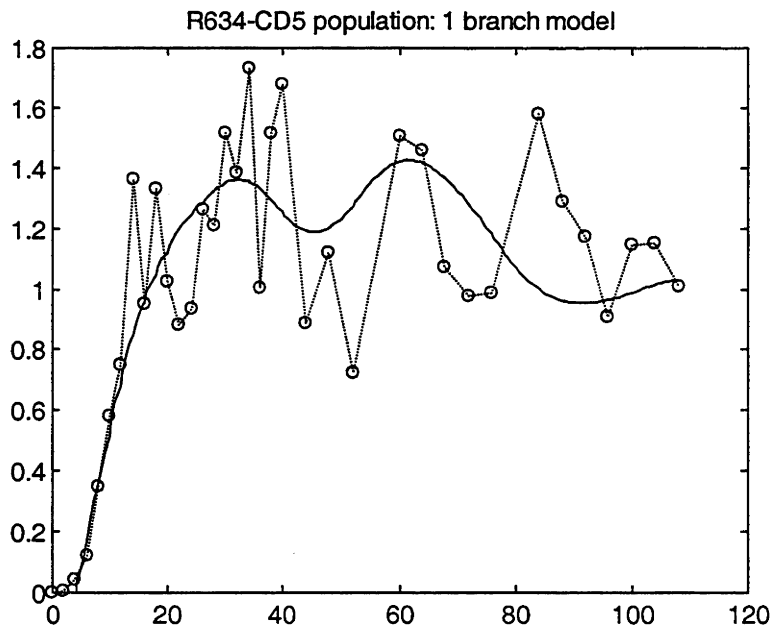

Figure 6.6K: Comparison of actual and calculated outputs from the selected branch model

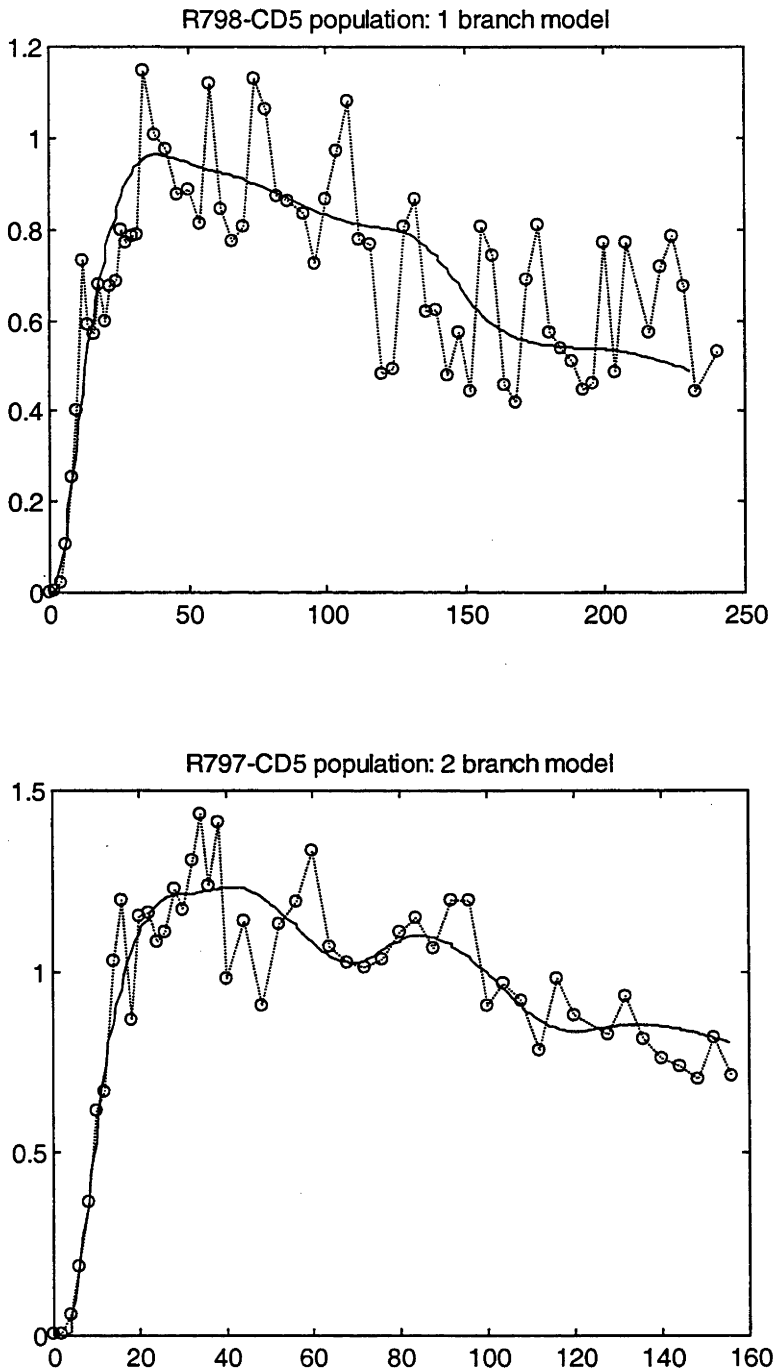

6.5.4 Estimation of parameters in selected parallel models

One of the parallel models providing the minimum AIC value was selected as an optimal model for each individual experiment. Table 6.2A-6.2C demonstrates the interval estimates of the parameters of those selected parallel models.

Table 6.2A: Summary of interval estimates of parameters of selected parallel models in total population studies.

Sheep	B481	B687	B857(2)	R153(1)	R401	R705	R632
Selected model	3-branch	4-branch	1-branch	2 branch	3 branch	2-branch	3-branch
T_1	4.354	9.815	11.319	13.347	2.718	8.540	12.346
	± 2.929	± 2.349	± 0.074	± 8.231	± 2.954	± 0.348	± 0.318
T_2	20.313	4.883	11.319	8.325	17.988	8.540	12.346
	± 6.819	± 2.090	± 0.074	± 12.314	± 4.734	± 0.348	± 0.318
τ_1	3.574	4.291	4.326	1.043	2.578	4.466	2.499
	± 1.540	± 0.550	± 0.797	± 2.361	± 2.127	± 0.833	± 0.971
G_1	1.467	1.191	1.784	1.589	1.856	1.150	2.744
	± 0.109	± 0.023	± 0.023	± 0.087	± 0.075	± 0.022	± 0.045
τ_2	56.683	60.711	-	84.984	87.358	120.753	83.465
	± 3.683	± 3.971		± 10.057	± 11.000	± 6.159	± 4.245
G_2	0.397	0.150	-	0.200	0.223	0.154	0.352
	± 0.080	± 0.045		± 0.094	± 0.099	± 0.029	± 0.053
τ_3	114.290	84.700	-	-	133.861		194.968
	± 10.075	± 5.908			± 35.491		± 13.583
G_3	0.214	0.104	-	-	0.073		0.177
	± 0.119	± 0.043			± 0.089		± 0.091
τ_4	-	122.900	-	-	-		-
	-	± 7.735					-
G_4	-	0.086	-	-	-		-
	-	± 0.023					-
Gain	**2.078**	**1.531**	**1.784**	**1.789**	**2.152**	**1.304**	**3.273**
AIC	**-36.23**	**-91.37**	**-67.90**	**-84.35**	**-57.72**	**-44.17**	**43.38**

Table 6.2B: Summary of interval estimates of parameters of selected parallel models in total population studies.

Sheep	R634	R798	R797	R890	Y044(1)	Y044(2)
Selected model	1-branch	4-branch	3 branch	1 branch	3 branch	1 branch
T_1	10.822 ± 1.210	1.496 ± 2.841	8.037 ± 0.390	8.280 ± 0.215	2.736 ± 1.435	40.467 ± 19.354
T_2	5.511 ± 1.971	15.583 ± 2.925	8.037 ± 0.390	8.280 ± 0.215	17.521 ± 3.995	1.910 ± 0.043
τ_1	1.934 ± 0.851	3.633 ± 1.935	3.181 ± 0.927	2.933 ± 0.569	4.412 ± 1.799	3.869 ± 0.012
G_1	1.482 ± 0.051	1.228 ± 0.148	1.416 ± 0.051	1.937 ± 0.026	1.244 ± 0.090	1.552 ± 0.012
τ_2	-	27.899 ± 12.400	44.065 ± 1.234	-	54.895 ± 3.314	-
G_2	-	0.189 ± 0.132	0.204 ± 0.049	-	0.209 ± 0.077	-
τ_3	-	95.848 ± 7.954	107.530 ± 20.792	-	89.743 ± 6.269	-
G_3	-	0.173 ± 0.046	0.074 ± 0.050	-	0.285 ± 0.049	-
τ_4	-	188.472 ± 8.163	-	-	-	-
G_4	-	0.151 ± 0.052	-	-	-	-
Gain	**1.482**	**1.741**	**1.694**	**1.937**	**1.738**	**1.552**
AIC	**13.20**	**-11.55**	**-9.69**	**-59.21**	**-103.91**	**-131.69**

Table 6.2C: Summary of interval estimates of parameters of selected parallel models in subset studies.

Sheep	R857(1) CD4	R797 CD4	R890 CD4	R632 CD5	R634 CD5	R798 CD5	R797 CD5
Selected Model	2 branch	2 branch	1 branch	1 branch	1 branch	1 branch	2 branch
T_1	3.783 ± 2.571	7.815 ± 0.392	7.353 ± 0.409	17.913 ± 3.050	6.111 ± 0.547	9.831 ± 0.767	7.110 ± 0.368
T_2	15.255 ± 5.609	7.815 ± 0.392	7.353 ± 0.409	17.913 ± 3.050	6.111 ± 0.547	9.831 ± 0.767	7.110 ± 0.368
τ_1	3.066 ± 1.375	2.559 ± 1.670	2.509 ± 0.978	0.440 ± 2.582	3.326 ± 1.747	0.593 ± 3.011	2.769 ± 0.949
G_1	2.872 ± 0.055	1.864 ± 0.054	2.281 ± 0.051	3.073 ± 0.059	1.407 ± 0.070	1.595 ± 0.043	1.600 ± 0.043
τ_2	134.238 ± 7.589	80.495 ± 16.212	-	-	-	-	69.763 ± 22.035
G_2	0.300 ± 0.068	0.123 ± 0.068	-	-	-	-	0.062 ± 0.053
τ_3	-	-	-	-	-	-	-
G_3	-	-	-	-	-	-	-
τ_4	-	-	-	-	-	-	-
G_4	-	-	-	-	-	-	-
Gain	**3.172**	**1.987**	**2.281**	**3.073**	**1.407**	**1.436**	**1.662**
AIC	**-5.21**	**-20.23**	**-45.89**	**92.48**	**34.99**	**26.14**	**-15.94**

6.5.5 Estimation of mean transit times and percentages of lymphocytes travelling along each path of selected parallel models

The percentages of lymphocytes travelling along the individual branches of the parallel models, and the values for the mean transit times MTT_i corresponding to these branches are listed in Table 6.3. For example, the majority of the lymphocytes, about 71% in the 3-branch model and 78% in the 4-branch model, corresponding to experiments B481 and B687, travel along branch 1, with mean transit times of approximately 28 and 19 hours respectively. The remainder of the lymphocytes travel with different mean transit times.

Table 6.3: Summary of MTT_i of individual branches and mean MTT ($\overline{MTT}$) of a parallel model of the lymph node

	Branch1		Branch2		Branch3		Branch4		$\overline{MTT}$	Gain
	%	MTT_1	%	MTT_2	%	MTT_3	%	MTT_4		
					Total population studies					
B481	70.62	28.24	19.10	81.35	10.28	138.96	-	-	**49.79**	**2.078**
B687	77.80	18.99	9.81	75.41	6.80	99.40	5.59	137.60	**36.64**	**1.531**
B857(2)	100	26.96	-	-	-	-	-	-	**26.96**	**1.784**
R153(1)	88.82	22.72	11.18	106.66	-	-	-	-	**32.10**	**1.789**
R401	86.25	23.28	10.36	108.06	3.39	154.57	-	-	**36.52**	**2.152**
R705	88.19	21.55	11.81	137.83	-	-	-	-	**35.28**	**1.304**
R632	83.84	27.19	10.75	108.16	5.41	219.66	-	-	**46.31**	**3.273**
R634	100.00	18.27	-	-	-	-	-	-	**18.27**	**1.482**
R798	70.53	20.71	10.86	44.98	9.94	112.93	8.67	205.55	**48.54**	**1.741**
R797	83.59	19.26	12.04	60.14	4.37	123.60	-	-	**28.74**	**1.694**
R890	100.00	19.49	-	-	-	-	-	-	**19.49**	**1.937**
Y044(1)	71.58	24.67	12.03	75.15	16.41	110.00	-	-	**44.73**	**1.738**
Y044(2)	100	46.25	-	-	-	-	-	-	**46.25**	**1.552**
Mean	86.25	24.43	11.99	88.64	8.09	137.02	7.13	171.58	**36.12**	**1.850**
± SD	±11.39	± 7.36	± 2.77	±28.79	± 4.51	±40.92	± 2.18	±48.05	**±10.69**	**±0.488**
					CD4 population studies					
R857(1)	90.54	22.10	9.46	153.28	-	-	-	-	**34.51**	**3.172**
R797	93.81	18.19	6.19	96.13	-	-	-	-	**23.01**	**1.987**
R890	100.00	17.22	-	-	-	-	-	-	**17.22**	**2.281**
Mean	94.78	19.17	7.83	124.71	-	-	-	-	**24.91**	**2.480**
± SD	± 4.80	± 2.58	± 2.31	±40.41	-	-	-	-	**± 8.80**	**±0.617**
					CD5 population studies					
R632	100	36.27	-	-	-	-	-	-	**36.27**	**3.073**
R634	100	15.55	-	-	-	-	-	-	**15.55**	**1.407**
R798	100	20.25	-	-	-	-	-	-	**20.26**	**1.436**
R797	96.27	16.99	3.73	83.98	-	-	-	-	**19.49**	**1.662**
Mean	99.07*	22.27	3.73	83.98	-	-	-	-	**22.89**	**1.895**
± SD	± 1.87	± 9.54	-	-	-	-	-	-	**± 9.15**	**±0.794**

*Denote statistical differences (p value less than 0.05)

6.6 Discussion

Modelling of lymphocyte migration in the time domain was described in Chapter 3 (Compartmental models) and Chapter 5 (Prediction error models). However, in some situations, such as those applying in complex systems, system modelling in the time domain could not explain clearly the system characteristics. In this chapter, an alternative approach has been introduced, using the frequency response method in combination with the Gauss-Newton method. System modelling in the frequency domain has been employed to identify such complex systems. The applications of frequency domain analysis have been reported in many fields including pharmacokinetics, where almost all the systems can be considered complex (Durisova *et al.*, 1995).

In all the experiments, the normalized calculated frequency responses of the lymph node system H_N contained several loops, indicating that this system was complex and might include time delays or feedback loops (Durisova *et al.*, 1995). On the basis of this finding, the first proposed structured model was constructed with two linear dynamic systems in serial connection and a positive feedback loop (ie feedback model). This model achieved an acceptable level of performance in relation to all the modelling criteria (results not shown). The explanation of the feedback loop in this model, however, contrasted with both: 1) accurate experimental data about lymphocyte pathways in lymphoid tissue; 2) the selected experimental setting. In the experiments, all lymphocytes that reappeared in the efferent lymph were discarded. This ensures that no fraction of the lymphocyte output would be aggregated with the input, ie no lymphocytes from efferent lymph of the lymph node under study were returned to the blood circulation.

With the reference to the positive feedback model (Figure 6.3), if there had been a real positive feedback in the lymph node system H_N, it could be an indication that some lymphocytes reaching the terminal end of the system (ie in efferent lymph) were able to return to the proximal end of system (ie postcapillary venule) by some mechanism intrinsic to the cell itself. This suggestion was not supported by any studies of lymphocyte migration and recirculation. Furthermore, it is unlikely that migrating lymphocytes would have the ability to migrate back to the postcapillary venule by using only their intrinsic motive capabilities to overcome the more powerful driving force of pressure gradients in lymphatic vessels (Zweifach and Prather, 1975). In Chapter 3, the two-compartmental models were assumed to represent the lymph node. Although, there was a two-way

connection between the fast and slow compartments in the lymph node model, neither was functioning as a genuine feedback to the system input.

A parallel model with a variable number of branches was selected as the optimum structured model. For each individual experiment, the final model was selected from the minimum AIC value among the available candidate models (ie 1, 2, 3 and 4 branch parallel model). Application of the parameters identified from the Gauss-Newton method, as presented in Table 6.3 has shown that there would be a variable degree of distribution of both the number of lymphocytes and the mean transit time (MTT_i) in each branch. As seen in equation (6.22), the values of the gain obtained from each branch were expressed as proportions of the number of lymphocytes travelling in each branch to the total number of lymphocytes travelling in all the branches, ie in the whole lymph node system.

Similarly to the results from Chapter 5, the selected parallel models in this chapter have shown that migrating lymphocytes possess several different sets of dynamic properties, ie lymphocyte dynamics in lymphoid tissue are not homogeneous. Furthermore, the mean transit times and percentages of lymphocytes entering the corresponding path (ie branch) were successfully quantified. From Table 6.3, it was indicated that a large number of the lymphocytes would spend a shorter mean transit time, while a minority would require a longer mean transit time in each individual path. The overall mean transit times for the total lymphocyte population study were 24.43 ± 7.36, 88.64 ± 28.79, 137.02 ± 40.92 and 171.58 ± 48.05 hours for branches 1 to 4 respectively. The corresponding percentages of lymphocytes entering branches 1 to 4 were 86.25 ± 11.39, 11.99 ± 2.77, 8.09 ± 4.51 and 7.13 ± 2.18 % respectively. In other words, about 86 % of the total lymphocyte population would require just over 24 hours to migrate through the lymphoid tissue. This conclusion is similar to that in Chapter 5, namely that at least 75% of migrating lymphocytes would need less than 24 hours to migrate through the lymphoid tissue, while the remainder would take more than 24 hours.

In the subset studies (Table 6.3), the overall mean transit times for the CD4 lymphocyte population were 19.17 ± 2.58 and 124.71 ± 40.71 hours for branches 1 and 2 respectively. The percentages of CD4 lymphocytes entering these two branches are 94.78 ± 4.80 and 7.83 ± 2.31 %. The results for the CD4 population were only interpreted for 1 and 2 branch models. The overall mean transit times for the CD5 lymphocyte population (obtained from 1 and 2 branch models) were 22.27 ± 9.54 and 83.98 ± 0 hours whilst the percentages of CD5 lymphocytes in each branch were 99.07 ± 1.87 and 3.73 ± 0 % for branch 1 and 2 respectively.

There were no significant differences of the overall mean transit times and percentages in these subset studies compared with those in the total population study, with exception of the mean percentage of CD5 lymphocytes in branch 1. However, the final models selected in CD4 and CD5 subset studies were only 1 or 2 branch models. In contrast, in the total population study, 1, 2, 3 and 4-branch models were selected respectively in 4, 2, 5 and 2 data sets from a total of 13 data sets (Table 6.1 and 6.3).

If the number of branches reflects genuinely different kinetics (ie degree of cell-cell interactions) of migrating lymphocytes occurring within the lymphoid tissue, this may be interpreted as indicating that there is a considerable homogeneity of kinetics between CD4 and CD5 lymphocytes in the present study. For example, one simple model, such as a 1-branch model may explain the entire kinetics of CD4 or CD5 lymphocytes (in many cases). In other words, it may be concluded from this study that the kinetics of CD4 and CD5 lymphocytes within lymphoid tissue are relatively homogeneous under normal physiological conditions. In fact, in the total population study, most of the selected models (9 out of 13) contained more than 1 branch which is in agreement with the nature of a large number of lymphocyte phenotypes (ie representing several different kinetics) in the total lymphocyte population.

Unlike the results from Chapter 5 which showed significant differences in MTT_{75}, T_{resp} and gain between CD4 subpopulations and total populations (see Table 5.4 of Chapter 5 for more detail), there were no significant differences in the average values of mean MTT ($\overline{MTT}$) and gain (Table 6.3). However, the gain value of CD4 lymphocytes found in this chapter reflected the same trend as that observed in Chapter 5 in which gain in the CD4 population was higher than in the total and CD5 populations. The average mean transit times were 36.12 ± 10.69, 24.91 ± 8.80 and 22.89 ± 9.15 hours, and the average values of gain were 1.850 ± 0.488, 2.480 ± 0.617 and 1.895 ± 0.794 for total, CD4 and CD5 lymphocyte populations respectively.

In the challenged lymph node, the term "shut down" (Hall and Morris, 1965a; Smith and Morris, 1970) has been applied to describe an abrupt drop in lymphocyte output in the lymph during the first 24 hours after exposure of the lymph node to an antigen. From the information generated by structured models, a number of explanations could be formulated for this shut down. Firstly, a rearrangement of lymphocyte distribution may have occurred between branches. For instance, after challenge, the majority of the migrating lymphocytes may not travel via branch 1 as found in the present study. The results of lymph node

challenge experiments reported from other laboratories have clearly defined the time scale of this shut down phenomenon (Hay *et al.*, 1974; Cahill *et al.*, 1976). The lymphocyte output dropped dramatically within 24 hours after challenge, then suddenly overshot by 48 hours.

6.7 Conclusion

In this chapter, the application of a combination of frequency and time domain modelling techniques was used with the goal of obtaining the optimum structured model of lymphocyte migration. From the biomedical point of view, structured models gave a clear picture of the lymph node configuration. Unlike the compartmental model approach used in Chapter 4, this approach does not require any prior information about the lymph node in order to construct suitable models. It requires only the information contained in input-output measurements which is the same requirement for the prediction error identification approach in Chapter 5.

The structured model approach presented here permits modelling of unknown and complex systems with suitable environments. Mathematical constraints have been overcome by two step techniques, ie the modelling of the normalised calculated system frequency response in the frequency domain and the modelling of the measured system output in the time domain.

The minimisation of mathematical errors by setting criteria, assures the mathematical correctness of the final structured models in addition to providing maximum information about the system. This information allows an improved understanding about lymphocyte migration within the lymphoid tissue under normal physiological conditions. To understand this process fully, further work which would contribute to an improvement of this model is required. Ultimately, a model, which can explain some specific conditions of lymphocyte migration, such as the response of an antigenically challenged lymph node, would be of considerable value in facilitating further developments in lymphocyte and immunological studies.

Chapter 7/
General discussion

Introduction

In this study, events associated with lymphocyte migration in peripheral lymphoid tissue have been experimentally examined. The experimental data was used to describe the kinetics of lymphocyte migration within lymphoid tissue and to construct three different classes of theoretical models. This thesis presents three novel models of lymphocyte migration derived from original data collected specially for the purpose of modelling. It demonstrates the variety of information obtainable from different models. With current advances in engineering, mathematics and related technology, theoretical modelling of biological and medical problems has been increasingly utilised to provide more comprehensive information that can not be acquired by means of ordinary investigations. The use of such an approach to the study of biomedical problems, accompanied by rapid progress in computer technology, is likely to represent a new trend in research studies in many fields.

The life history and functions of lymphocytes remained the subject of much speculation until the definitive demonstration of their recirculation, and of their significance in immune responses, by Gowans (Gowans, 1959). Lymphocytes are shown to able to escape from the blood circulation into tissues. The majority of this emigration takes place from small postcapillary venules in lymphoid tissue. After moving between the specialised endothelial cells that line these venules, lymphocytes spend variable times within lymphoid organs (ie lymph nodes and spleen) before leaving via efferent lymphatic vessels that ultimately drain into large lymphatics which terminate by re-entering the blood circulation. This recirculation pattern ensures that lymphocytes with a full range of immunological reactivities are continually available throughout lymphoid tissues of the body. With this remarkable property of lymphocytes, immune surveillance and dissemination of immunological memory throughout the body are assured.

Lymphocyte recirculation and migration are highly dynamic processes involving complicated cellular interactions in a large number of organs and tissues. From a physiological point of view, it is unlikely to be profitable to attempt to investigate such a highly dynamic process by means of *in vitro* studies. For example, the

study of lymphoid tissue might reveal the nature of a specific pattern of lymphocyte distribution in that tissue at fixed time points. However, it can not reflect the dynamic process of lymphocyte recirculation that requires a certain time period.

The extent to which the lymphatic system is accessible to experimental investigation will be dependent on the species of experimental animal selected. The technique of thoracic duct cannulation is probably the only method available to access the lymphatic system of small laboratory species. Consequently, the data obtained from small animal models has been largely restricted to the central components of the lymphatic system rather than including information relating to the peripheral lymphatic systems where lymphocyte migration as distinct from lymphocyte recirculation can be examined. The depletion of the number of circulating lymphocytes in small animals as a result of thoracic duct drainage is likely to impose unsatisfactory conditions for the study of lymphocyte migration. Ideally, study of migration requires maintenance of the number of circulating lymphocytes at the most stable level attainable. Lymphocyte depletion in small animals rapidly follows drainage of central lymph. In one study, the total number of lymphocytes in thoracic duct lymph declined sharply and exponentially within the first 48 hours. The number of T and B lymphocytes in blood dropped to approximately 10 and 25% of their initial value respectively after 24 hours thoracic duct drainage. As a result, approximately half of the total lymphocyte pool was drained away within a week (Westermann *et al.*, 1994).

The physiological process of lymphocyte migration is complex and dynamic. The differential migration and life span of different lymphocyte subsets is an inherent feature of the normal function of the mammalian immune system. Adequate assessment of the processes involved requires the presence of an intact blood and lymphatic circulatory system and the ability to isolate individual tissues. The use of large animal species such as the sheep permits access, by surgical intervention, to peripheral lymphatic vessels (Hall and Morris, 1962; Hall and Morris, 1965b). Such a sheep model provides an invaluable experimental means of studying these processes.

Experiments performed with sheep permit a longer period for data collection from each individual animal. On the other hand, data about lymphocyte migration through the peripheral lymphoid tissues of small animals has been restricted to series of single point observations from large numbers of animals on the basis of which the underlying kinetics have been indirectly inferred. Lymphocyte depletion, which is invariably a complication of lymphatic cannulation in rodent

models, is not a major concern in sheep. Since the number of lymphocytes drained from an isolated peripheral node is a relatively small proportion of the total population of circulating lymphocytes, it is possible to track recirculating lymphocytes labelled with suitable fluorescent tracers for a long period *in vivo* (Abernethy *et al.*, 1985; Young *et al.*, 1993; Andrade *et al.*, 1996).

In studies of lymphocyte recirculation, the intravenous injection of labelled lymphocytes into sheep followed by observation of the level of those labelled lymphocytes in both venous blood and efferent lymph has been recognised as the most suitable method. This was employed in the present study. The interpretations from previous studies depended upon results obtained from actual observations. However, few attempts have been made to apply mathematical descriptions to explain lymphocyte migration (Ottaway, 1981; Farooqi and Mohler, 1989). The present study appears to be the first specially planned for the purpose of modelling and applying a mathematically systematic approach to identify quantitative information describing the events of lymphocyte migration.

Modelling

During recent decades, biomedical scientists have increasingly focused on the applications of modelling methods which have been previously confined to technical fields such as engineering and mathematics. Many studies have reported the successful implementation of such modelling techniques to complicated biomedical problems (Modarreszadeh *et al.*, 1995; Berger and Malpas, 1998). As noted above, one of the aims of this project was to explore the efficiency of three different modelling methods in explaining the behaviour of lymphocytes migrating within lymphoid tissue under normal conditions. The present experiments, taking account of the modelling restrictions inherent in *in vivo* experiments (such as nature of data originated from sampling techniques), were planned to generate information in the form of simultaneous input-output data and so to avoid unnecessary assumptions.

The collection of novel data in the present study was considered to have advantages over previous studies as the experiments were planned in advance for the purpose of subsequent modelling. The data consisted of two main components (ie simultaneous blood and efferent lymph data) which can be quantitatively described and modelled. In contrast with the present study, previous modelling studies of lymphocyte migration and recirculation (Ottaway, 1981; Farooqi and Mohler, 1989; Stekel, 1997; Stekel *et al.*, 1997; Stekel, 1998), utilised retrospective data which had not been collected specifically for the

primary goal of modelling. A necessary feature of these studies was the incorporation of a considerable number of assumptions and also of the use of data from literature that was required for the process of construction of those models. This thesis has reported complete sets of simultaneous data on lymphocyte recirculation. The data sets obtained from the present study should provide information not only for the present study, but also for further studies.

Compartmental models

The multi-compartmental model developed to represent the lymph node system in this thesis was based on the principle of mass balance equations which are a set of ordinary differential equations. The presence of a well mixed mass occupying a compartment and the linearity of the whole model were the major assumptions required in developing this model. The construction of such a model presupposes the availability of considerable information about lymph node function and lymphocyte migration.

A physiological model was initially proposed based on available knowledge. As a result of previous studies, it is known that the time required for a lymphocyte to be delivered to the postcapillary venules and cross the venule wall (delivery, adhesion and emigration stages) are fast dynamic events (Bjerknes *et al.*, 1986; Borgs and Hay, 1986). Consequently, the modified multi-compartmental model constructed by aggregating some parameters (in the fast dynamic components) was reasonable. The multi-compartmental model mimics the actual (physiological) events of lymphocyte migration and demonstrates fine details of each step in lymphocyte migration in a manner analogous with real events.

A lymphocyte that has successfully migrated (ie has entered the efferent lymph) has experienced the events either of advection (ie migration along a fast dynamic path) or attachment (ie to the reticular mesh), or both, throughout its journey within lymphoid tissue. Application of the multi-compartmental model suggested, by $R_{w/t}$, that overall, a lymphocyte might have a higher chance of traversing the fast (advection) rather than the slow route (ie of attachment to the mesh). This increased likelihood was calculated to be of the order of approximately 1.82 to 1 under normal conditions. This implies that the events involved in lymphocyte migration through lymphoid tissue are exclusively non-random. In other words, a lymphocyte may attach to the mesh, spend a period of time there (which is sufficient for its interactions with other cells) and then detach from the mesh. Thus cell-cell interaction could play an important role in regulating the number of cells attached to the mesh, and as a consequence, the time required for

migration of the whole lymphocyte population. It would be predicted that the value of $R_{w/t}$ would be reduced if conditions were changed (such as during the early stages of an immunological response) since a larger proportion of migrating lymphocytes should attach to the mesh to ensure that adequate cell-cell interactions occurred during the most intense phase of the immunological response.

Another finding (ie $R_{b/m}$) from the compartmental model also suggested that the population of lymphocytes bound in the mesh was much larger (about 50 times so) than that of unbound (ie mobile or fast dynamic) lymphocytes. This implies that the majority of lymphocytes in lymphoid tissue are in an immunologically active stage (ie having an interaction with other cells). Furthermore, it suggests that lymphoid tissue has a capacity to reserve a large number of lymphocytes in bound form rather than merely constituting no more than a path for migrating lymphocytes.

Since only 7 of 21 data sets could be successfully fitted with this multi-compartmental model, information derived from it should remain subject to some reservations. Nevertheless, inferences drawn from it may provide some basis for further developments of similar kinds of models such as Partial Differential Equation (PDE) models and for devising experiments to test some of the inferences drawn from it.

Prediction error models

Prediction error models were comprehensively examined in Chapter 5. The output error (OE) model was finally selected on account of its better performance in simulation compared with that of the other three candidate models. Unlike the conditions applicable to compartmental models, no assumptions concerning structural models of lymph nodes were required for an OE model. The final models were systematically tested under strict criteria and validation tests. The unit impulse responses calculated from selected OE models provided invaluable information about lymphocyte migration.

Review of the relevant literature dealing with lymphocyte recirculation and migration suggests that this exercise may be the first attempt to examine the kinetics of lymphocyte migration using this approach. If the technique of system identification using a prediction error model had not been available, it would not have been possible to arrive at the results that were obtained solely by using ordinary observations of actual experimental data.

The information derived from this study differed from those in the existing literature in some points. It was previously reported that the peak time of appearance of labelled lymphocytes in efferent lymph was about 24-48 hours (Frost *et al.*, 1975; Trevella and Morris, 1980; Reynolds *et al.*, 1982). However, such studies did not consider the effect of recirculated labelled lymphocytes on the observed data. By contrast with previous reports, in this study, the peak time was estimated at only about 11.91 ± 4.68 hours for the total lymphocyte population.

The time required for migration by the majority (ie 75%) of lymphocytes (MTT_{75}) and for the completion of the entire response (T_{resp}) could be calculated from the unit impulse response of the final model. The results of this calculation demonstrated some remarkable advantages of this modelling approach over the traditional method of dealing with observations of this type. According to MTT_{75} and T_{resp}, it was predicted that even though 75% of migrating lymphocytes would have reappeared in the efferent lymph in the time indicated by MTT_{75}, there would still be some lymphocytes that required the time indicated by T_{resp} to finish their migration. This finding reflects the heterogeneity of the kinetics of migrating lymphocytes within a single population. This aspect of migration has not been effectively quantified by previous studies.

However, the value of the gain calculated in this way, which represents the total outcome (or efficiency) after applying a unit impulse to a system, is in agreement with the conclusions of previous reports (Washington *et al.*, 1988; Witherden *et al.*, 1990). Compared with other subsets, lymphocytes expressing CD4 have shown a significantly higher gain. This can be explained if it is postulated that subset-specificity occurs in lymphocyte migration. Moreover, results from T_{resp} have shown that CD4 lymphocytes spent significantly less time within lymphoid tissue. From this, it could be concluded that CD4 lymphocytes have a greater capacity than other lymphocyte populations to enter lymphoid tissue and migrate through it at significantly higher speed.

The system delays identified from the prediction error model were of the order of 3-7 hours for the total lymphocyte population. The system delay time generally describes the time required for a system to process an output from input. Thus the system delay time in this prediction error model may be defined as the time lag between the disappearance of labelled lymphocytes from blood (ie input signal) and their reappearance in the efferent lymph (ie output signal). In other words, any arbitrary lymphocyte in the blood circulation (at the point of entry to the postcapillary venules) would spend at least 3-7 hours (ie a time equal to the

system delay time) in adhering to and crossing the wall of postcapillary venules, migrating through lymphoid tissue and reappearing in the efferent lymph.

With reference to the stages of lymphocyte migration previously described in section 4.3 of Chapter 4 (Compartmental models), it should be noted, firstly, that every migrating lymphocyte must cross the venule wall. Secondly, once within lymphoid tissue, cells can either migrate freely (ie mobile lymphocytes) or bind to the reticular mesh (ie bound lymphocytes). However, the path that proceeds through D (delivery), A (adhesion), E (emigration) and the mobile stages (M1, M2,.., Mn) is the shortest common path. In other words, a migrating lymphocyte, if it is to be successful, must take this common path since direct connections are not possible between the bound stages. This implies that, once a lymphocyte has attached to the reticular mesh in lymphoid tissue, it is necessary that it detaches from the reticular mesh (to become a mobile lymphocyte) before it can proceed with its migration in lymphoid tissue. Thus this system delay time is applicable only to the shortest time required for a lymphocyte to migrate along this common (and shortest) path. Any lymphocytes which bind to the reticular mesh will necessarily spend additional time apart from the system delay time.

Furthermore, the results of applying the prediction error method have revealed that the system delay was much less than the time that the majority of lymphocytes spent in lymphoid tissues (ie MTT_{75}, which is 20.77 ± 5.62 hours for the total lymphocyte population). This suggests that ***most lymphocytes***, while migrating through lymphoid tissue, bound to the reticular mesh at least at some stage before they left the lymph node. If the majority of lymphocytes migrating through lymphoid tissue remained in the mobile stage for the entire duration of their migration process within lymphoid tissue, a high frequency of lymphocytes should reappear in the efferent lymph after approximately 3-6 hours. However, this would not be in agreement with the experimental observations which reveal that only a small number of lymphocytes appear in efferent lymph within the first 6 hours in all experiments (Figure 3.5 A-3.5W- lower panels).

The period of time that a lymphocyte spends in a bound state and the number of bindings (ie the frequency with which a mobile lymphocyte became a bound lymphocyte and vice versa) remain in doubt. None of the models developed in the present study were informative in relation to these two points. However, as a simple approximation, it may be hypothesized that the entire binding period for the majority of migrating lymphocytes resembled the differences between MTT_{75} and the system delay, namely about 16.1, 10.06 and 11.54 hours for total, CD4 and CD5 lymphocyte populations respectively. This binding period should reflect

the total time required for the establishment of immune reactions by lymphocytes in lymphoid tissue under normal physiological conditions and could reasonably be expected to increase if circumstances required a longer reaction time.

Structured models

Like the prediction error models, the structured models in Chapter 6 have been systematically constructed under strict criteria without the incorporation of any assumptions concerning the actual structure of the lymph node. The development of a structured model was based on a combination of modelling in the frequency and time domains.

The findings that there were likely to be different mean transit times (MTT) and percentages of cells in each individual branch of parallel models have strongly supported the findings of the prediction error models in Chapter 5 insofar as these relate to the heterogeneity of kinetics of migrating lymphocytes. Furthermore, it was found that the majority of migrating lymphocytes require a shorter time period to migrate through lymphoid tissue, which is in agreement with findings of the prediction error models. The substantially homogeneous kinetics of the major lymphocyte subsets (CD4 and CD5) was implied by the finding of fewer branches in the final models selected for those lymphocytes.

Overall, the structured models of the lymph node system presented in Chapter 6 are original when compared with the literature in three main ways:

1 Modelling method. While the common modelling methods (e.g. the compartment modelling methods applied in Chapter 4 of this thesis and the methods introduced by Stekel, (Stekel *et al.*, 1997; Stekel, 1998) utilise abstract prior information about model structures, the method of building structured models employed in Chapter 6 is exclusively dependent upon a posteriori knowledge provided by real experimental measurements.

2 Inherent model characteristics. In biomedical studies, compartmental models are frequently used in such a way that the analytical solutions of these models (poly-exponential functions) are fitted to the measured profiles. In contrast, the models described in Chapter 6 represent real relationships between the measured concentration time profiles of labelled lymphocytes in the venous blood and efferent lymph, taking into account both of these measured profiles. The models of the lymph node systems were optimised and successfully constructed in the form of differential equations (while the inputs and outputs of

these models were the measured profiles of labelled lymphocytes in venous blood and efferent lymph respectively) with systematic procedures under set criteria.

3 Applicability of the models. The structured models presented in Chapter 6 can be employed not only to describe lymphocyte migration qualitatively and/or quantitatively, but also to test statistically for changes in lymphocyte migration under different situations, eg under physiological and several pathological conditions.

Conclusion

Lymphocyte recirculation and migration permit immune recognition of foreign antigens and dissemination of immunological memory throughout the body. Study of lymphocyte migration in the peripheral lymphoid tissue was a major concern in the present study because of its essential role in the immune response. A large (ie sheep) model was employed to study lymphocyte migration because it offered many advantages over small animal models. Experiments were planned to obtain informative data for construction of suitable models.

Theoretical models have been increasingly recognised by biomedical researchers to have application to biomedical problems. In this thesis, three different approaches, namely compartmental models, prediction error models and structured models, have been developed to describe the dynamic of lymphocyte migration within lymphoid tissue under normal conditions. The contents of this thesis present experimental observations of lymphocyte migration using three different modelling approaches which have not been previously reported. The information obtained from each individual model shows some degree of variation which will provide more comprehensive descriptions of the entire complicated events of lymphocyte migration. The information given in this thesis should help to contribute to the future development of understanding of lymphocyte migration.

One of the major questions raised by the study of lymphocyte migration is that of the manner in which the immune response will affect the kinetics of migration of lymphocytes. Clear evidence of lymphocyte migratory response to antigenic challenge manifest by the rapid drop in the number of lymphocytes (ie "shut down") found in efferent lymph has been reported (Hall and Morris, 1965a; Smith and Morris, 1970). This event implies the existence of a non-linear phenomenon as the basis for immune responses. This was reflected by the unstable levels of

lymphocytes in efferent lymph after antigenic challenge and this could not be explained in a simple quantitative manner by any of the models presented in this thesis. Nevertheless, the results obtained from models in this thesis suggest some information that may imply how such a non-linear response can be explained, not by current knowledge of biology or medicine, but by a modelling approach. The rearrangement of lymphocytes migrating through different branches in the parallel model in Chapter 6 or an increase of MTT_{75} in Chapter 5, expected to occur after the challenge, are some possible explanations that could be derived from the current models in this thesis.

Future experiments that could provide a more comprehensive range (ie examination of as many lymphocyte subsets as possible) of informative data relating either to normal physiological, or to some special, conditions (such as antigenic challenge) would be valuable for developing future models. All information presented in this thesis should be considered as fundamental knowledge to guide the development of more complicated lymphocyte migration models. Non-linear models, rather than the models available in this thesis, may be the ultimate models to explain the events occurring in response to challenge.

Theoretical models of lymphocyte migration should help to understand more about the real kinetics of lymphocyte migration than can be inferred from current knowledge. The more advanced model can be utilised as a tool to study not only the kinetics of a certain subpopulation but also the mixed kinetics of the entire lymphocyte population. It is likely that, with more understanding about lymphocyte migration and the validation of current models, future models should be capable of explaining a chaos phenomenon such as the immunological reactions of the entire range of lymphocytes throughout the body. Such ideal models should be potentially applicable to clinical situations and would be the ultimate aim of this study.

Appendix 1/
Data normalisation

The equations described in the models In Chapter 4 are dependent upon mass balance equations (ie the actual number of lymphocytes) which is according to the principle of compartmental analysis. However, it is unlikely that ideal data could be obtained because of many restrictions applying to *in vivo* experiments. Data normalisation was undertaken and aimed to achieve an appropriate physiologically reasonable relationship between actual data obtained in the blood and efferent lymph and to reduce the number of unknown parameters which may interfere with the fitting procedures. During data normalisation, some available values from the literature and from a few experimental trials were used which is unavoidable.

Blood data:

d_0 is the total number of labelled lymphocytes injected into the blood circulation at time *0* hours. N_B is the total number of lymphocytes in the blood pool assumed to be a constant value during the entire experimental period. $N_B^+(t)$ is the number of labelled lymphocytes in the blood circulation at time *t* hours. Then, $P_B^+(t)$ is a percentage of the number of labelled lymphocytes relative to total lymphocytes in blood at time *t* hours,

$$P_B^+(t) = \frac{N_B^+(t) \cdot 100}{N_B}. \qquad \text{(A1.1)}$$

If a perfect mixing of labelled lymphocytes in the venous blood is assumed, the maximal value of $P_B^+(t)$ occurred immediately after labelled lymphocytes were injected into the blood circulation,

$$P_{B\,\max}^+ = \frac{d_0 \cdot 100}{N_B}. \qquad \text{(A1.2)}$$

$P_{B\,\max}^+$ is the maximal value of $P_B^+(t)$, assumed to occur at time zero of each experiment, ie $P_B^+(0) = P_{B\,\max}^+$. Dividing (A1.1) by (A1.2) leads to

$$\frac{P_B^+(t)}{P_{B\,\max}^+} = \frac{N_B^+(t)}{d_0}. \qquad \text{(A1.3)}$$

Introducing the dimensionless blood fraction, $F_B^+(t)$

$$F_B^+(t) = \frac{N_B^+(t)}{d_0} \qquad \text{(A1.4)}$$

into (A1.3) and (A1.4), gives

$$F_B^+(t) = \frac{P_B^+(t)}{P_{B\,\max}^+} = \frac{N_B^+(t)}{d_0}. \qquad \text{(A1.5)}$$

Efferent lymph data:

Define N_L to be the total number of lymphocytes in our studied lymph node, assumed to be a constant value for the entire experimental period. Then

$$P_L^+(t) = \frac{N_L^+(t)\cdot 100}{N_L} \qquad \text{(A1.6)}$$

where $N_L^+(t)$ is the number of labelled lymphocytes in the lymph node at time *t* hours and $P_L^+(t)$ is a percentage of lymphocytes in a lymph sample[47] at time *t* hours which are labelled. Rearranging (A1.6) gives

$$N_L^+(t) = \frac{P_L^+(t)\cdot N_L}{100} \qquad \text{(A1.7)}$$

Similarly to the dimensionless blood fraction, by dividing (A1.7) by d_0, produces the dimensionless lymph fraction, $F_L^+(t)$ as follows

$$F_L^+(t) = \frac{N_L^+(t)}{d_0} = \frac{P_L^+(t)}{100}\cdot\frac{N_L}{d_0}. \qquad \text{(A1.8)}$$

There is still another difficulty. In (A1.8), N_L is an unknown value. The total number of lymphocytes in the lymph node, N_L, varied depending upon the size of the lymph node which can be estimated by

[47] We assumed a linear relationship between percentages of labelled lymphocytes in the efferent lymph and in the lymph node. Thus, $P_L^+(t)$ is assumed to represent the percentages of labelled lymphocytes in the lymph node since direct sampling from lymph node could not be experimentally undertaken.

$$N_L = Wt \times D \tag{A1.9}$$

D represents the density, that is the average number of lymphocytes in one gram of peripheral lymphoid tissue (Cells/ gram). Seven pre-scapular lymph nodes were removed from 5 animals and the total content of lymphocytes was individually counted. The value of D was concluded as an approximate value of $275.13 \pm 7.72 \times 10^6$ (cells per gram). According to a previous report (Hall, 1964), the lymphocyte output per unit time ($Flux_L$) was related to the size (weight) of that lymph node by

$$Flux_L = 3.0 \times 10^7 \cdot Wt \tag{A1.10}$$

Wt is the weight of the lymph node in grams. While, the unit of $Flux_L$ is lymphocytes/ hour. From (A1.9) and (A1.10), we obtain

$$N_L = \frac{D \cdot Flux_L}{3.0 \times 10^7}. \tag{A1.11}$$

By replacing D=275.13x10^6 in (A1.11)

$$N_L \cong 9.171 \cdot Flux_L \tag{A1.12}$$

From (A1.12), by giving a known average lymphocyte output ($Flux_L$) for each animal, the average total number of lymphocytes in that lymph node can be determined. A constant value K_L is defined as

$$K_L = \frac{N_L}{100 \cdot d_0}. \tag{A1.13}$$

Introducing K_L into (A1.8)

$$F_L^+(t) = K_L \cdot P_L^+(t) \tag{A1.14}$$

From (A1.12) and (A1.13)

$$K_L = \frac{9.171 \cdot Flux_L}{100 \cdot d_0} \cong 0.0917 \cdot \frac{Flux_L}{d_0} \tag{A1.15}$$

For each individual experiment, the lymphocyte output in lymph per hour ($Flux_L$) and percentages of labelled lymphocyte in both blood and lymph ($P_B^+(t)$ and $P_L^+(t)$) were monitored. Individual d_0 was counted before injection. All this information including equation (A1.4), (A1.14) and (A1.15), $P_B^+(t)$ and $P_L^+(t)$

can be transformed (normalised) to the dimensionless $F_B^+(t)$ and $F_L^+(t)$ respectively. Table A1.1 summarises all parameters used in data normalisation for data

Table A1.1: Summary of parameters used in the data normalisation.

Animals [a]	Parameters			
	d_0 [b]	P^+_{max} [c]	$Flux_L$ [d]	K_L [e]
B481	3.95	5.5031	19.93	0.0046
B687	1.08	3.7254	18.21	0.0155
B445(1)	1.99	4.4892	14.10	0.0065
B445(2)	1.52	3.3823	16.28	0.0098
B882	1.69	3.8713	21.75	0.0118
B857(1)	1.33	4.4476	13.46	0.0093
B857(2)	0.52	1.6383	12.17	0.0215
R021(1)	0.92	3.3333	16.36	0.0163
B045	0.55	0.6867	10.12	0.0169
R021(2)	0.59	1.3900	13.84	0.0215
R401	1.61	1.1963	13.78	0.0078
R705	1.92	2.4283	15.30	0.0073
R632	1.80	4.5027	15.36	0.0078
R634	1.54	4.1973	15.42	0.0092
R798	1.64	2.6928	14.78	0.0083
R797	2.52	4.2660	21.54	0.0078
R890	0.60	1.9758	8.70	0.0133
Y044(1)	1.08	2.0116	11.26	0.0096
Y044(2)	1.40	1.8083	12.15	0.0080

[a] **Animals** were coded according to their tagged numbers. [b] d_0 is a unit of 10^9 cells.
[c] $P+_{max}$ were assumed to be represented by the maximum percentages of labelled lymphocytes obtained from individual blood data of each experiments. [d] $Flux_L$ were calculated from the average number of lymphocytes per hour for the whole experimental time. (x10^7 cells per hour) [e] K_L was calculated from equation (A1.15).

Appendix 2/
Matlab algorithms and commands

The system identification procedure described in Chapter 5 was performed using commands implemented in Matlab and the Matlab System Identification Toolbox (Mathsoft Company, MA, USA). Matlab is a powerful interactive program for numeric computation and data presentation. It has been widely used in complex numerical problems in almost all fields including problems in applied mathematics, physics, chemistry and engineering. The system identification algorithm in Matlab has been well implemented (Ljung, 1991) and reported in many references (Modarreszadeh *et al.*, 1995; Lai and Bruce, 1997).

The algorithms were written in several Matlab M-files in order to execute the system identification procedures. Most of these algorithms require commands implemented in the Matlab System Identification Toolbox. Only a set of unique commands with brief explanations, not all the commands used in Chapter 5, will be presented in this appendix. More details of the Matlab commands can be obtained from the system identification Matlab manual (Ljung, 1991).

1. **Data Importation:** The command ***"load"*** was used to retrieve the actual data that were saved in an ASCII file to the Matlab environments.
2. **Data manipulation:** A simple linear interpolation was performed to obtain a constant discrete data signal (with a fixed sampling period of 1 hour) from the actual data. The command ***"interp1"*** was used to perform a linear 1-dimension interpolation in all data sets.
3. **Selection of system delay:** Given the interpolated input-output data from step 2, the prediction cost function (V_N) of the OE model order (1,1,nk) was calculated by the command "***oe***". Then the relationship between the cost function and the system delay was plotted by the command ***"plot"*** to provide an indication (ie an abrupt change in prediction cost function or "***a knee***") of the system delay to be selected.
4. **Selection of model structure:** A parameter vector, θ, for each candidate model structure was constructed by the command **"struc"** (and its modifications) and tested to obtain the corresponding final prediction error (FPE). Commands **"arx"**, **"armax"**, **"oe"**, and **"bj"** were used to compute

the prediction error estimates of the ARX, ARMAX, OE and BJ models respectively. Then the relationship between the FPE and the model dimension (ie the total number of identified parameters in each model) was plotted by the command ***"plot"*** to provide an indication of the model order to be selected.

5. **Calculation for information of model characteristics:** Following selection of the final model structure and the corresponding interpolated data from previous steps, the transfer functions $H(q)$ and $G(q)$ of the final model of each data set were automatically calculated and saved as a specially formatted matrix named "a theta matrix" under the Matlab environment[48]. This theta matrix contains important characteristics of those two transfer functions (such as information about the model structure, the estimated parameters and their estimated accuracy) which are necessary for the step of validation and simulation.
6. **Model validation:** Given a theta matrix and the input signal, the cross correlation of the inputs and the residuals and the autocorrelation of the residuals were performed and presented by the command ***"resid"***.
7. **Simulation of the output from the actual input:** The deterministic $H(q)$ and stochastic transfer functions $G(q)$ of the final model had been already determined at step 5 and saved in the theta matrix. With this theta matrix, it is possible to simulate any particular output from a given input. In this step, the actual input was applied to the calculated transfer functions to produce the simulated output by the command ***"idsim"***. The plot of the simulated and actual outputs was obtained by the command ***"plot"***.
8. **Simulation of the unit impulse/ unit step response:** The commands used in this step were the same as those used in step 7. However, the unit impulse input, defined by a vector of [1 0 0 ..], was selected as the input to the system. Subsequently, the output (ie the unit impulse response) was presented by the command ***"plot"***.

[48] "Matlab environment" is often referred as a working situation which the (main) Matlab program and all of its accessories (ie toolboxes) can be worked and mutually interacted.

References

Abernethy N. J., Chin W., Lyons H. and Hay J. B. (1985) A dual laser analysis of the migration of XRITC-labeled, FITC-labeled, and double-labeled lymphocytes in sheep. *Cytometry* **6**, 407-413.

Abernethy N. J. and Hay J. B. (1992) The recirculation of lymphocytes from blood to lymph: physiological considerations and molecular mechanisms. *Lymphology* **25**, 1-30.

Abernethy N. J., Hay J. B., Kimpton W. G., Washington E. and Cahill R. N. (1991) Lymphocyte subset-specific and tissue-specific lymphocyte-endothelial cell recognition mechanisms independently direct the recirculation of lymphocytes from blood to lymph in sheep. *Immunology* **72**, 239-245.

Abernethy N. J., Hay J. B., Kimpton W. G., Washington E. A. and Cahill R. N. (1990) Non-random recirculation of small, CD4+ and CD8+ T lymphocytes in sheep: evidence for lymphocyte subset-specific lymphocyte- endothelial cell recognition. *Int Immunol* **2**, 231-238.

Akaike H. (1976) Canonical correlation analysis of time series and the use of an information criterion. In *System Identification: Advances and case studies* (Edited by Mehera R. K. and Lainiotis D. G.), p. 27-93. Academic Press, London.

Akcahuseyin E., van Duyl W. A., Vincent H. H., Vos M. C. and Schalekamp M.A. (1998) Continuous arterio-venous haemodiafiltration: hydraulic and diffusive permeability index of an AN-69 capillary haemofilter. *Med Biol Eng Comput* **36**, 43-50.

Andrade W. N., Johnston M. G. and Hay J. B. (1996) A method for tracking the migration of blood lymphocytes. *Immunol Invest* **25**, 455-467.

Andrade W. N., Johnston M. G. and Hay J. B. (1998) The relationship of blood lymphocytes to the recirculating lymphocyte pool. *Blood* **91**, 1653-1661.

Andrew W. and Andrew N. V. (1949) Lymphocyte in normal epidermis of rat and of man. *Anat Rec* **104**, 217-241.

Baykal A., Ranjan R. and Thakor N. V. (1997) Estimation of the ventricular fibrillation duration by autoregressive modeling. *IEEE Trans Biomed Eng* **44**, 349-356.

Berger C. S. and Malpas S. C. (1998) Modelling of the dynamic relationship between arterial pressure, renal sympathetic nerve activity and renal blood flow in conscious rabbits. *J Exp Biol* **201**, 3425-3430.

Bjerknes M., Hazel C. and Ottaway C. A. (1986) Dynamics of Lymphocyte-Endothelial Interactions in Vivo. *Science* **231**, 402-405.

Bloom W. (1937) Transformation of lymphocytes into granulocytes in vitro. *Anat Rec* **69**, 99-121.

Borgs P. and Hay J. B. (1986) A quantitative lymphocyte localization assay. *J Leukoc Biol* **39**, 333-342.

Boroujerdi M. A., Umpleby A. M., Jones R. H. and Sonksen P. H. (1995) A simulation model for glucose kinetics and estimates of glucose utilization rate in type 1 diabetic patients. *Am J Physiol* **268**, E766-74.

Bradley L. M., Malo M. E., Fong S., Tonkonogy S. L. and Watson S. R. (1998) Blockade of both L-selectin and alpha4 integrins abrogates naive CD4 cell trafficking and responses in gut-associated lymphoid organs. *Int Immunol* **10**, 961-968.

Bradley L. M., Watson S. R. and Swain S. L. (1994) Entry of naive CD4 T cells into peripheral lymph nodes requires L- selectin. *J Exp Med* **180**, 2401-2406.

Bunting C. H. and Huston J. (1921) Fate of lymphocyte. *J Exp Med* **33**, 593.

Burnet F. M. (1959) *The clonal selection theory of acquired immunity.* University Press, Cambridge.

Butcher E. C. (1991) Leukocyte-endothelial cell recognition: three (or more) steps to specificity and diversity. *Cell* **67**, 1033-1036.

Cahill R. N., Frost H. and Trnka Z. (1976) The effects of antigen on the migration of recirculating lymphocytes through single lymph nodes. *J Exp Med* **143**, 870-888.

Chin G. W. and Cahill N. P. (1984) The appearance of fluorescein-labelled lymphocytes in lymph following in vitro or in vivo labelling: the route of lymphocyte recirculation through mesenteric lymph nodes. *Immunology* **52**, 341-347.

Chin W. and Hay J. B. (1980) A comparison of lymphocyte migration through intestinal lymph nodes, subcutaneous lymph nodes, and chronic inflammatory sites of sheep. *Gastroenterology* **79**, 1231-1242.

Dedik L. and Durisova M. (1994) Frequency response method in pharmacokinetics. *J Pharmacokinet Biopharm* **22**, 293-307.

Dedik L. and Durisova M. (1995) CXT: a programme for analysis of linear dynamic systems in the frequency domain. *Int J Biomed Comput* **39**, 231-241.

Dedik L. and Durisova M. (1996) CXT-MAIN: a software package for determination of the analytical form of the pharmacokinetic system weighting function. *Comput Methods Programs Biomed* **51**, 183-192.

Durisova M. and Dedik L. (1994) Comparative study of human pentacaine pharmacokinetics in time and frequency domain. *Methods Find Exp Clin Pharmacol* **16**, 219-232.

Durisova M., Dedik L. and Balan M. (1995) Building a structured model of a complex pharmacokinetic system with time delays. *Bull Math Biol* **57**, 787-808.

Ebert R. H., Sanders A. G. and Florey H. W. (1940) Observation on lymphocytes in chambers in rabbit's ear. *Brit J Exp Path* **21**, 212-218.

Ehrich W. E. (1946) Role of lymphocyte in circulation of lymph. *Ann N.Y. Acad Sci* **46**, 823-857.

Farooqi Z. H. and Mohler R. R. (1989) Distribution models of recirculating lymphocytes. *IEEE Trans Biomed Eng* **36**, 355-362.

Ford W. L. and Simmonds S. J. (1972) The tempo of lymphocyte recirculation from blood to lymph in the rat. *Cell Tissue Kinet* **5**, 175-189.

Fossum S., Smith M. E. and Ford W. L. (1983) The recirculation of T and B lymphocytes in the athymic, nude rat. *Scand J Immunol* **17**, 551-557.

Foster D. M., Aamodt R. L., Henkin R. I. and Berman M. (1979) Zinc metabolism in humans: a kinetic model. *Am J Physiol* **237**, R340-349.

Frost H., Cahill R. N. and Trnka Z. (1975) The migration of recirculating autologous and allogeneic lymphocytes through single lymph nodes. *Eur J Immunol* **5**, 839-843.

Gallatin W. M., Weissman I. L. and Butcher E. C. (1983) A cell-surface molecule involved in organ-specific homing of lymphocytes. *Nature* **304**, 30-34.

Godfrey K. (1983) *Compartmental models and their application.* Academic Press Inc.(London).

Gowans J. L. (1957) The effect of the continuous re-infusion of lymph and lymphocytes on the output of the thoracic duct of unanesthetized rats. *Brit J Exp Path* **38**, 67-78.

Gowans J. L. (1959) The recirculation of lymphocytes from blood to lymph in rats. *J Physiol* **146**, 54-69.

Gowans J. L. and Knight E. J. (1964) The route of re-circulation of lymphocytes in the rat. *Proc Roy Soc Lond Biol* **159**, 257-282.

Grandi F., Avanzolini G. and Cappello A. (1995) Analytic solution of the Variable-Volume Double-Pool urea kinetics model applied to parameter estimation in hemodialysis. *Comput Biol Med* **25**, 505-518.

Hall J., Scollay R. and Smith M. (1976) Studies on the lymphocytes of sheep. I. Recirculation of lymphocytes through peripheral lymph nodes and tissues. *Eur J Immunol* **6**, 117-120.

Hall J.G. (1964) The function of lymphatic system in immunity, Ph.D.Thesis, Australian National University, 65.

Hall J. G. and Morris B. (1962) The output of cells in lymph from the popliteal node of sheep. *Quart J Exp Physiol* **47**, 360-369.

Hall J. G. and Morris B. (1965a) The immediate effect of antigens on the cell output of a lymph node. *J Exp Pathol* **46**, 450-454.

Hall J. G. and Morris B. (1965b) The origin of the cells in the efferent lymph from a single lymph node. *J Exp Med* **121**, 901-910.

Hay J. B., Cahill R. N. and Trnka Z. (1974) The kinetics of antigen-reactive cells during lymphocyte recruitment. *Cell Immunol* **10**, 145-153.

Hirano K. and Yamada H. (1983) Studies on the absorption of practically water-insoluble drugs following injection VII: plasma concentration after different subcutaneous doses of a drug in aqueous suspension in rats. *J-Pharm-Sci* **72**, 602-607.

Hunt K. J., Munih M., Donaldson N. N. and Barr F. M. (1998) Investigation of the Hammerstein hypothesis in the modeling of electrically stimulated muscle. *IEEE Trans Biomed Eng* **45**, 998-1009.

Imhof B. A. and Dunon D. (1995) Leukocyte migration and adhesion. *Adv Immunol* **58**, 345-416.

Issekutz T., Chin W. and Hay J. B. (1980) Measurement of lymphocyte traffic with indium-111. *Clin Exp Immunol* **39**, 215-221.

Jacquez J. A. (1972) *Compartmental Analysis in Biology and Medicine: Kinetics of distribution of tracer-labeled materials.* American Elsevier Publishing Company, New York, NY.

Jacquez J. A. (1985) *Compartmental Analysis in Biology and Medicine*, Ann Arbor, MI.

Jacquez J. A. (1996) *Compartmental Analysis in Biology and Medicine.* BioMedWare, Ann Arbor, MI.

Kimpton W. G., Washington E. A. and Cahill R. N. (1989) Recirculation of lymphocyte subsets (CD5+, CD4+, CD8+, T19+ and B cells) through fetal lymph nodes. *Immunology* **68**, 575-579.

Kimpton W. G., Washington E. A. and Cahill R. N. (1990) Non-random migration of CD4+, CD8+, gamma delta + T19+, and B cells between blood and lymph draining ileal and prescapular lymph nodes in the sheep fetus. *Int Immunol* **2**, 937-943.

Kreyszig E. (1993) *Advanced Engineering Mathematics.* John Wiley & Sons.

Lai J. and Bruce E. N. (1997) Ventilatory stability to transient CO2 disturbances in hyperoxia and normoxia in awake humans. *J Appl Physiol* **83**, 466-476.

Lawrence M. B. and Springer T. A. (1991) Leukocytes roll on a selectin at physiologic flow rates: distinction from and prerequisite for adhesion through integrins. *Cell* **65**, 859-873.

Lepault F., Gagnerault M. C., Faveeuw C. and Boitard C. (1994) Recirculation, phenotype and functions of lymphocytes in mice treated with monoclonal antibody MEL-14. *Eur J Immunol* **24**, 3106-3112.

Levy E. C. (1959) Complex curve fitting. *IRE Trans Automat Contr* **4**, 37-43.

Ljung L. (1987) *System Identification: Theory for the User*. Prentice Hall International, New Jersey.

Ljung L. (1991) *System Identification Toolbox User's Guide*. Mathworks.

Lyons B. A. and Parish C. R. (1994) Determination of lymphocyte division by flow cytometry. *J Immunol Methods* **171**, 131-137.

Mackay C. (1995) Lymphocyte migration. A new spin on lymphocyte homing. *Curr Biol* **5**, 733-736.

Mackay C. R., Andrew D. P., Briskin M., Ringler D. J. and Butcher E. C. (1996) Phenotype, and migration properties of three major subsets of tissue homing T cells in sheep. *Eur J Immunol* **26**, 2433-2439.

Mackay C. R., Kimpton W. G., Brandon M. R. and Cahill R. N. (1988) Lymphocyte subsets show marked differences in their distribution between blood and the afferent and efferent lymph of peripheral lymph nodes. *J Exp Med* **167**, 1755-1765.

Mackay C. R., Maddox J. F. and Brandon M. R. (1986) Three distinct subpopulations of sheep T lymphocytes. *Eur J Immunol* **16**, 19-25.

Mackay C. R., Marston W. L., Dudler L., Spertini O., Tedder T. F. and Hein W. R. (1992) Tissue-specific migration pathways by phenotypically distinct subpopulations of memory T cells. *Eur J Immunol* **22**, 887-895.

Mann J. D. and Higgins G. M. (1950) Lymphocytes in the thoracic duct, intestinal and hepatic lymph. *Blood* **5**, 177-190.

Marchesi V. T. and Gowans J. L. (1964) The migration of lymphocytes through the endothelium of venules in lymph nodes: an electron microscope study. *Proc Roy Soc Lond Biol* **159**, 283.

Marmarelis P. Z. and Marmarelis V. Z. (1978) Analysis of Physiological Systems: The White-Noise Approach. Plenum Press, New York.

Marmarelis P. Z. and Naka K. I. (1973a) Nonlinear analysis and synthesis of receptive-field responses in the catfish retina. I. Horizontal cell leads to ganglion cell chain. *J Neurophysiol* **36**, 605-618.

Marmarelis P. Z. and Naka K. I. (1973b) Nonlinear analysis and synthesis of receptive-field responses in the catfish retina. II. One-input white-noise analysis. *J Neurophysiol* **36**, 619-633.

Martonen T. B. (1993) Mathematical model for the selective deposition of inhaled pharmaceuticals. *J Pharm Sci* **82**, 1191-1199.

McGeown J. G. and Crockard A. D. (1993) Lymphocyte subsets recirculate from blood to lymph at different rates in conscious sheep. *Pflugers Arch* **422**, 533-535.

Medawar J. (1940) Observations on lymphocytes in tissue culture. *Brit J Exp Path* **21**, 205-211.

Miller J. F. A. P. and Mitchell G. F. (1969) Cell to Cell Interaction in the Immune Response. *Transplant Proc* **1**, 535-538.

Miller S. C., Himmelstein K. J. and Patton T. F. (1981) A physiologically based pharmacokinetic model for the intraocular distribution of pilocarpine in rabbits. *J-Pharmacokinet-Biopharm* **9**, 653-677.

Modarreszadeh M., Bruce E. N., Hamilton H. and Hudgel D. W. (1995) Ventilatory stability to CO2 disturbances in wakefulness and quiet sleep. *J Appl Physiol* **79**, 1071-1081.

Ottaway. (1981) A method for the quantitative analysis of lymphoid cell migration experiments. *Immunol Lett* **2**, 283-290.

Parker R. S., Doyle F. J., 3rd and Peppas N. A. (1999) A model-based algorithm for blood glucose control in type I diabetic patients. *IEEE Trans Biomed Eng* **46**, 148-157.

Pederson N. C. and Morris B. (1970) The role of the lymphatic system in the rejection of homografts: a study of lymph from renal transplants. *J Exp Med* **131**, 936-969.

Periti P. F. (1964) Comment on the applicability of compartment theory to interacting biochemical systems. *Experientia* **20**, 294.

Rebuck J. W. and Crowley J. H. (1955) A method of studying leukocytic functions in vivo. *Ann N.Y. Acad Sci* **59**, 757-794.

Rey C. G. and Galiana H. L. (1991) Parametric classification of segments in ocular nystagmus. *IEEE Trans Biomed Eng* **38**, 142-148.

Reynolds J., Heron I., Dudler L. and Trnka Z. (1982) T-cell recirculation in the sheep: migratory properties of cells from lymph nodes. *Immunology* **47**, 415-421.

Reynolds J. D., Chin W. and Shmoorkoff J. (1988) T and B cells have similar recirculation kinetics in sheep. *Eur J Immunol* **18**, 835-840.

Rippley R. K. and Stokes C. L. (1995) Effects of cellular pharmacology on drug distribution in tissues. *Biophys J* **69**, 825-839.

SAAM-Institute. (1997) *SAAM II User Guide*, Seattle, WA.

Schoefl G. I. (1972) The migration of lymphocytes across the vascular endothelium in lymphoid tissue. A reexamination. *J Exp Med* **136**, 568-588.

Schoukens J. and Pintelon R. (1991) *Identification of Linear Systems: A Practical Guide for Accurate Modelling*. Pergamon Press, London.

Seldinger S. I. (1953) Catheter replacement of needle in percutaneous arteriography: new technique. *Acta Radiol*, 368-376.

Sheppard C. W. (1948) The theory of transfers within a multi-compartment system using isotopic tracers. *J Appl Phys* **19**, 70-76.

Sheppard C. W. (1962) *Basic principles of the tracer method : an introduction to mathematical tracer kinetics.* John Wiley & Sons, New York.

Shimizu Y., Newman W., Tanaka Y. and Shaw S. (1992) Lymphocyte interactions with endothelial cells. *Immunol Today* **13**, 106-112.

Sjövall H. (1936) Experimenttle Untersuchungen über das Blut und die blutbildenden Organe-besonders das lymphatische Gewebe-des Kaninchens bei wieder-holten Aderlässen. *Acta Path Microbiol Scand* **Supp 27**, 1-308.

Smith J. B. and Morris B. (1970) The response of the popliteal lymph node of the sheep to swine influenza virus. *Aust J Exp Biol Med Sci* **48**, 33-46.

Smith M. E. and Ford W. L. (1983) The recirculating lymphocyte pool of the rat: a systematic description of the migratory behaviour of recirculating lymphocytes. *Immunology* **49**, 83-94.

Smith M. E., Martin A. F. and Ford W. L. (1980) Migration of lymphoblasts in the rat. Preferential localization of DNA- synthesizing lymphocytes in particular lymph nodes and other sties. *Monogr Allergy* **16**, 203-232.

Söderström T. and Stoica P. (1989) *System Identification.* Prentice Hall International, Cambridge.

Sprent J. (1973) Circulating T and B lymphocytes of the mouse. I. Migratory properties. *Cell Immunol* **7**, 10-39.

Sprent J. and Basten A. (1973) Circulating T and B lymphocytes of the mouse. II. Lifespan. *Cell Immunol* **7**, 40-59.

Springer T. A. (1990) Adhesion receptors of the immune system. *Nature* **346**, 425-434.

Springer T. A. (1994) Traffic signals for lymphocyte recirculation and leukocyte emigration: the multistep paradigm. *Cell* **76**, 301-314.

Stamper H. B., Jr. and Woodruff J. J. (1976) Lymphocyte homing into lymph nodes: in vitro demonstration of the selective affinity of recirculating lymphocytes for high-endothelial venules. *J Exp Med* **144**, 828-833.

Stekel D. J. (1997) The role of inter-cellular adhesion in the recirculation of T lymphocytes. *J Theor Biol* **186**, 491-501.

Stekel D. J. (1998) The simulation of density-dependent effects in the recirculation of T lymphocytes. *Scand J Immunol* **47**, 426-430.

Stekel D. J., Parker C. E. and Nowak M. A. (1997) A model of lymphocyte recirculation. *Immunol Today* **18**, 216-221.

Tanaka Y., Adams D. H. and Shaw S. (1993) Regulation of leukocyte recruitment by proadhesive cytokines immobilized on endothelial proteoglycan. *Curr Top Microbiol Immunol* **184**, 99-106.

Trevella W. and Morris B. (1980) Reassortment of cell populations within the lymphoid apparatus of the sheep. *Ciba Found Symp* **71**, 127-144.

Ursino M. and Innocenti M. (1997) Mathematical investigation of some physiological factors involved in hemodialysis hypotension. *Artif Organs* **21**, 891-902.

Washington E. A., Katerelos M., Cahill R. N. and Kimpton W. G. (1994) Differences in the tissue-specific homing of alpha beta and gamma delta T cells to gut and peripheral lymph nodes. *Int Immunol* **6**, 1891-1897.

Washington E. A., Kimpton W. G. and Cahill R. N. (1988) CD4+ lymphocytes are extracted from blood by peripheral lymph nodes at different rates from other T cell subsets and B cells. *Eur J Immunol* **18**, 2093-2096.

Westermann J., Matyas J., Persin S., van der Meide P., Heerwagen C. and Pabst R. (1994) B- and T-lymphocyte subset numbers in the migrating lymphocyte pool of the rat: the influence of interferon-gamma on its mobilization monitored through blood and lymph. *Scand J Immunol* **39**, 395-402.

Westermann J., Puskas Z. and Pabst R. (1988) Blood transit and recirculation kinetics of lymphocyte subsets in normal rats. *Scand J Immunol* **28**, 203-210.

Weston S. A. and Parish C. R. (1992) Calcein: A novel marker for lymphocytes which enter lymph nodes. *Cytometry* **13**, 739-749.

Wexler A. S., Ding J. and Binder-Macleod S. A. (1997) A mathematical model that predicts skeletal muscle force. *IEEE Trans Biomed Eng* **44**, 337-348.

Witherden D. A., Kimpton W. G., Washington E. A. and Cahill R. N. (1990) Non-random migration of CD4+, CD8+ and gamma delta+T19+ lymphocytes through peripheral lymph nodes. *Immunology* **70**, 235-240.

Woodruff E. A., Martin J. F. and Omens M. (1997) A model for the design and evaluation of algorithms for closed-loop cardiovascular therapy. *IEEE Trans Biomed Eng* **44**, 694-705.

Yang F. and Khoo M. C. (1994) Ventilatory response to randomly modulated hypercapnia and hypoxia in humans. *J Appl Physiol* **76**, 2216-2223.

Young A. J., Hay J. B. and Mackay C. R. (1993) Lymphocyte recirculation and life span in vivo. *Curr Top Microbiol Immunol* **184**, 161-173.

Young S. T. and Hsiao K. N. (1994) A phamacokinetic model to study administration of intravenous anaesthetic agents. *IEEE Eng Med Biol* **April/ May**, 263-268.

Zhao Y., Chien S. and Skalak R. (1995) A stochastic model of leukocyte rolling. *Biophys J* **69**, 1309-1320.

Zweifach B. W. and Prather J. W. (1975) Micromanipulation of pressure in terminal lymphatics in the mesentery. *Am J Physiol* **228**, 1326-1335.